Functional analyses of thiol-switches and their impact on the mycothiol redox potential in actinomycetes

Inaugural-Dissertation

to obtain the academic degree

Doctor rerum naturalium (Dr. rer. nat.)

submitted to the Department of Biology, Chemistry and Pharmacy

of **Freie Universität Berlin**

by

QUACH NGOC TUNG

from Hanoi, Vietnam

Year of submission: 2019

1st. Reviewer: **Prof. Dr. Haike Antelmann**

Institut für Biologie – Mikrobiologie, Freie Universität Berlin

2nd. Reviewer: **Prof. Dr. Christiane Wolz**

Interfakultäres Institut für Mikrobiologie und Infektionsmedizin, Universität Tübingen

Date of defense: 19.02.2020

TABLE OF CONTENTS

Zusammenfassung der Dissertation

In ihrem natürlichen Lebensraum oder während Infektionen sind Bakterien häufig reaktiven Sauerstoffspezies (ROS) und reaktiven Chloridspezies (RCS) ausgesetzt, die oxidativen Stress und die Induktion anti-oxidativer Abwehrmechanismen verursachen. ROS und HOCl können alle Makromoleküle der Zelle schädigen, einschließlich Proteine, Nukleinsäuren und Lipide. Zur Bekämpfung von ROS und zur Erhaltung des reduzierten Zustands des Zytoplasmas, produzieren Bakterien niedermolekulare Thiole (LMW) als wichtige Antioxidantien zur Neutralisierung von ROS. Gramnegative Bakterien und Eukaryoten nutzen Glutathion als LMW-Thiol. Gram-positive Firmicutes und Actinomycetes kodieren jedoch nicht die Enzyme für die GSH-Biosynthese und produzieren stattdessen alternative LMW-Thiole, wie Bacillithiol (BSH) bzw. Mycothiol (MSH). Die verschiedenen Funktionen des LMW-Thiols BSH in *Bacillus subtilis* und *Staphylococcus aureus* sind in **Kapitel 1** dieser Dissertation zusammengefasst.

Unter oxidativem Stress sind die LMW-Thiole GSH, BSH und MSH an post-translationalen Modifikationen mit Proteinthiolen beteiligt, die als Protein-*S*-Glutathionylierungen, *S*-Bacillithiolierungen bzw. *S*-Mycothiolierungen bezeichnet werden. Protein-*S*-Thiolierungen schützen Proteinthiole vor irreversibler Überoxidation zu Cys-Sulfonsäuren und sind an der Redoxregulation von Proteinen beteiligt. In *S. aureus* wurden zuvor etwa 57 Proteine gefunden, die unter HOCl-Stress *S*-bacillithioliert waren, einschließlich GapDH als Haupttarget. Die Reduktion von *S*-bacillithiolierten Proteinen wird durch Bacilliredoxine (Brx) katalysiert, die von BSH und der NADPH-abhängigen BSSB-Reduktase (YpdA) im Brx/BSH/YpdA-Redoxweg regeneriert werden, wie in **Kapitel 2** beschrieben. Durch NADPH-gekoppelte Elektronentransfer-Assays konnte ich zeigen, dass YpdA als BSSB-Reduktase fungiert, deren Aktivität vom redox-aktiven Cys14 abhängig ist. Ich zeigte ferner, dass der Brx/BSH/YpdA-Weg die De-Bacillithiolierung von *S*-bacillithioliertem GapDH *in vitro* katalysieren kann. Interessanterweise wurde gezeigt, dass YpdA an der Entgiftung von *S*-thioallyliertem BSH, das als Allylmercaptobacillithiol (BSSA) bezeichnet wird, unter Allicin-Stress beteiligt ist. Dies wird in **Kapitel 3** dargestellt. Somit bewirken YpdA und Brx die Regenerierung des Pools von reduzierten LMW-Thiolen und Protein-Thiolen in *S. aureus* unter Allicin-Stress.

In Eukaryoten wurden Glutaredoxine mit redox-sensitiven GFP2 (Grx-roGFP2) fusioniert, um dynamische Änderungen des GSH-Redoxpotentials bei hoher räumlich-zeitlicher Auflösung zu messen. In Actinomyceten wurden verwandte Mycoredoxine genutzt, um Mrx1-roGFP2-Biosensoren für Messungen des MSH-Redoxpotentials (E_{MSH}) in

Mycobacterium tuberculosis (*Mtb*) zu konstruieren, wodurch eine Heterogenität des E_{MSH} während Makrophagen-Infektionen und in Antibiotika-resistenten *Mtb*-Isolaten aufgedeckt wurde. Eine Übersicht über Anwendungen der Redox-Biosensoren bei pathogenen Bakterien unter oxidativem Stress und Infektionen ist in **Kapitel 4** zu finden. Die meisten dieser Redox-Biosensoren werden auf Plasmiden ektopisch exprimiert, was zu unterschiedlichen Expressionsniveaus von roGFP2-Fusionen führen kann.

Ein Ziel dieser Doktorarbeit war die Konstruktion eines stabil integrierten Mrx1-roGFP2-Biosensors zur Quantifizierung von E_{MSH}-Veränderungen in *Corynebacterium glutamicum*, der in **Kapitel 5** beschrieben wird. Der Mrx1-roGFP2-Biosensor wurde in die Genome des *C. glutamicum* Wildtyps und in Mutanten integriert, denen Redoxregulatoren und antioxidative Enzyme fehlten. Es wurden E_{MSH}-Änderungen während des Wachstums und unter oxidativem Stress gemessen. Biosensor-Messungen ergaben, dass *C. glutamicum* Wildtyp-Zellen während der gesamten Wachstumskurve ein stark reduzierendes E_{MSH} mit basalen E_{MSH}-Spiegeln von -296 mV aufrechterhalten. Aufgrund des H_2O_2-resistenten Phänotyps von *C. glutamicum* reagiert Mrx1-roGFP2 schwach auf 20-40 mM H_2O_2, wird jedoch durch niedrige NaOCl-Dosen schnell oxidiert. Wir beobachteten weiterhin die basalen E_{MSH}-Veränderungen und die H_2O_2-Reaktion von Mrx1-roGFP2 in *mshA*-, *mtr*-, *sigH*-, *oxyR*-, *mpx*-, *tpx*- und *katA*-Mutanten, die in der Redoxregulation und der Entgiftung von Antioxidantien beeinträchtigt sind. Während der Biosensor in *mshA*- und *mtr*-Mutanten konstitutiv oxidiert wurde, war in der *sigH*-Mutante eine geringere Basal-Oxidation zu beobachten. Die Katalase KatA wurde als wichtiges H_2O_2-Entgiftungsenzym bestätigt, das für eine schnelle Reduktion des Biosensors nach Entgiftung von H_2O_2 erforderlich ist. Im Gegensatz dazu hatten die Peroxiredoxine Mpx und Tpx nur einen geringen Einfluss auf die Entgiftung von H_2O_2. Weitere Live-Imaging-Experimente mit konfokaler Laser-Scanning-Mikroskopie dokumentierten die stabile Expression und Fluoreszenz des Biosensors auf Einzelzell-Ebene. Zusammenfassend wurde der stabil integrierte Mrx1-roGFP2-Biosensor erfolgreich als neuartiges Redox-Tool zur Messung dynamischer E_{MSH}-Veränderungen in *C. glutamicum* während des Wachstums, unter oxidativem Stress und in verschiedenen Mutanten-Hintergründen eingesetzt, um die Funktionen von MSH, SigH und KatA für das intrazelluläres E_{MSH} aufzudecken.

Wir waren weiterhin daran interessiert, neue Thiol-basierte Redox-Regulatoren zu identifizieren, die durch HOCl über Thioloxidation in Actinomyceten reguliert werden und vor oxidativem Stress schützen. Frühere Redox-Proteomik-Studien ergaben, dass der MarR-Typ Regulator MSMEG_4471 (HypS) unter HOCl-Stress stark oxidiert ist. Als weiteres Ziel

dieser Arbeit habe ich die Funktion und den Regulationsmechanismus von HypS in *Mycobacterium smegmatis* charakterisiert, der in **Kapitel 6** beschrieben wird. RNA-seq-Transkriptomik- und qRT-PCR-Analysen der *hypS*-Mutante ergaben, dass *hypS* autoreguliert ist und die Transkription des co-transkribierten *hypO*-Gens reprimiert, das für einen Multidrug-Efflux-Transporter kodiert. Die DNA-Bindeaktivität von HypS an das 8-5-8 bp-Inverted Repeat im Promoter des *hypSO*-Operons wurde unter NaOCl-Stress gehemmt. Die DNA-Bindung des HypSC58S-Mutantenproteins war jedoch nicht unter NaOCl-Stress *in vitro* beeinträchtigt, was auf eine wichtige Rolle von Cys58 beim Redox-Sensing von NaOCl-Stress hinweist. Es wurde gezeigt, dass HypS durch die Bildung von Cys58-Cys58‘-intermolekularen Disulfiden zwischen den HypS-Untereinheiten unter HOCl-Stress inaktiviert wird, was zu einer Derepression der *hypO*-Transkription führt. Die Ergebnisse zu den Phänotypen der *hypS*-Mutante zeigten, dass das HypR-Regulon Resistenz gegenüber HOCl-, Rifamipicin- und Erythromycin-Stress verleiht. So wurde HypS als neuer redox-sensitiver Repressor identifiziert, der Resistenz von Mykobakterien gegenüber HOCl-Stress und Antibiotika vermittelt.

Zusammenfassend haben die Ergebnisse meiner Doktorarbeit zu einem tieferen Verständnis der Rolle von Redoxregulatoren und antioxidativen Enzymen auf die MSH-Homöostase unter basalen Wachstumsbedingungen und oxidativem Stress in Actinomyceten beigetragen. Ich habe ferner einen neuen Redox-Regulator charakterisiert, der Resistenz gegenüber HOCl und Antibiotika verleiht und ein zukünftiges Target für Antibiotika zur Bekämpfung lebensbedrohlicher Tuberkulose-Infektionen sein könnte.

Summary of the dissertation

In their natural habitat or during infections, bacteria are frequently exposed to reactive oxygen species (ROS) and reactive chloride species (RCS), which cause an oxidative stress response and the induction of antioxidant defense mechanisms. ROS and HOCl can damage all macromolecules of the cell, including proteins, nucleic acids and lipids. To cope with ROS and to restore the reduced state of the cytoplasm, bacteria produce low molecular weight (LMW) thiols as important antioxidants and scavengers of ROS. Gram-negative bacteria and eukaryotes utilize glutathione as major LMW thiol. However, Gram-positive firmicutes and actinomycetes do not encode the enzymes for GSH biosynthesis and instead produce alternative LMW thiol, such as bacillithiol (BSH) and mycothiol (MSH), respectively. The various functions of the LMW thiol BSH in *Bacillus subtilis* and *Staphylococcus aureus* are summarized in **chapter 1**.

Under oxidative stress, the LMW thiols GSH, BSH and MSH were shown to form post-translational modifications with protein thiols, termed as protein *S*-glutathionylations, *S*-bacillithiolations and *S*-mycothiolations, respectively. Protein *S*-thiolations protect protein thiols from irreversible overoxidation to Cys sulfonic acids and function in redox regulation of proteins. In *S. aureus*, about 57 proteins were previously found *S*-bacillithiolated under HOCl stress including GapDH as major target. The reduction of *S*-bacillithiolated proteins is catalyzed by bacilliredoxins (Brx) which are regenerated by BSH and the NADPH-dependent BSSB reductase (YpdA) in the Brx/BSH/YpdA redox pathway as described in **chapter 2**. Using NADPH-coupled electron transfer assays I showed that YpdA acts as BSSB reductase which depends on the redox-active Cys14. I further revealed that the Brx/BSH/YpdA pathway can catalyze de-bacillithiolation of *S*-bacillithiolated GapDH *in vitro*. Interestingly, YpdA was shown to be involved in detoxification of *S*-thioallylated BSH, termed as allylmercaptobacillithiol (BSSA), under allicin stress which is presented in **chapter 3**. BrxA catalyzed reduction of *S*-thioallylated GapDH to regenerate in part GapDH activity. Thus, YpdA and Brx function to restore the pool of reduced LMW thiols and protein thiols in *S. aureus* under allicin stress.

In eukaryotes, glutaredoxins have been fused to redox-sensitive GFP2 (Grx-roGFP2) to measure dynamic changes in the GSH redox potential at high spatio-temporal resolution. In actinomycetes, related mycoredoxins have been used to construct Mrx1-roGFP2 biosensors for measurements of the MSH redox potential in *Mycobacterium tuberculosis* (*Mtb*), revealing heterogeneity of the MSH redox potential (E_{MSH}) during macrophage infections and in antibiotics resistant *Mtb* isolates. An overview of redox biosensor

applications in pathogenic bacteria under oxidative stress and infections is presented in **chapter 4**. Most of these redox biosensors are expressed ectopically on plasmids, resulting in different expression levels of roGFP2 fusions.

The first main goal of this PhD thesis was to construct a stable integrated Mrx1-roGFP2 biosensor for quantification of E_{MSH} changes in *Corynebacterium glutamicum*, which is described in **chapter 5**. The Mrx1-roGFP2 biosensor was integrated in the genomes of *C. glutamicum* wild type and mutants lacking redox regulators and antioxidant enzymes to measure E_{MSH} changes during the growth and under oxidative stress. Biosensor measurements revealed that *C. glutamicum* wild type cells maintain a highly reducing intrabacterial E_{MSH} throughout the growth curve with basal E_{MSH} levels of -296 mV. Due to its H_2O_2 resistant phenotype, Mrx1-roGFP2 responds weakly to 20-40 mM H_2O_2, but is rapidly oxidized by low doses of NaOCl. We further monitored basal E_{MSH} changes and the H_2O_2 response of Mrx1-roGFP2 in *mshA*, *mtr*, *sigH*, *oxyR*, *mpx*, *tpx* and *katA* mutants which are compromised in redox-signaling and the antioxidant defense. While the probe was constitutively oxidized in the *mshA* and *mtr* mutants, a small oxidative shift in basal E_{MSH} was observed in the Δ*sigH* mutant. The catalase KatA was confirmed as major H_2O_2 detoxification system required for fast biosensor re-equilibration upon return to non-stress conditions. In contrast, the peroxiredoxins Mpx and Tpx had only little impact on E_{MSH} and H_2O_2 detoxification. Further live imaging experiments using confocal laser scanning microscopy documented the stable biosensor expression and fluorescence at the single cell level. In conclusion, the stable integrated Mrx1-roGFP2 biosensor was successfully applied as novel redox tool to monitor dynamic E_{MSH} changes in *C. glutamicum* during the growth, under oxidative stress and in different mutant backgrounds revealing major roles of MSH, SigH and KatA for intracellular E_{MSH}.

We were further interested to identify novel thiol-based redox regulators that sense HOCl via thiol-oxidation in actinomycetes and confer protection under oxidative stress. Previous redox proteomics studies identified the novel MarR-type regulator MSMEG_4471 (HypS) as highly oxidized under HOCl stress. As second main goal of this PhD thesis, I have characterized the function and redox-regulatory mechanism of HypS in *Mycobacterium smegmatis* which is described in **chapter 6**. RNA-seq transcriptomics and qRT-PCR analyses of the *hypS* mutant revealed that *hypS* is autoregulated and represses transcription of the co-transcribed *hypO* gene which encodes a multidrug efflux pump. DNA binding activity of HypS to the 8-5-8 bp inverted repeat sequence upstream of the *hypSO* operon was inhibited under NaOCl stress. However, the HypSC58S mutant protein was not impaired in

DNA-binding under NaOCl stress *in vitro*, indicating an important role of Cys58 in redox sensing of NaOCl stress. HypS was shown to be inactivated by Cys58-Cys58' intersubunit disulfide formation under HOCl stress, resulting in derepression of *hypO* transcription. Phenotype results revealed that the HypR regulon confers resistance towards HOCl, rifamipicin and erythromycin stress. Thus, HypS was identified as a novel redox-sensitive repressor that contributes to mycobacterial resistance towards HOCl stress and antibiotics.

In summary, the results of my PhD thesis contributed to a deeper understanding of the impact of redox regulators and antioxidant enzymes towards MSH homeostasis under basal growth conditions and oxidative stress in actinomycetes. I further characterized a novel thiol-based redox regulator that confers resistance to HOCl and antibiotics and could be a future drug target to fight life-threatening tuberculosis infections.

List of Publications

1)Tung QN, Linzner N, Loi VV, Antelmann H. Biosynthesis and functions of bacillithiol in *Firmicutes*. Book chapter no. 21 "Biosynthesis and function of bacillithiol in *Firmicutes*", Book title "Glutathione", Editor Leopold Flohe, CRC Press, Taylor & Francis Group, 2018. **(Review Article)**

2) Linzner N, Loi VV, Fritsch VN, **Tung QN**, Stenzel S, Wirtz M, Hell R, Hamilton C, Tedin K, Fulde M, Antelmann H. *Staphylococcus aureus* uses the bacilliredoxin (BrxAB)/ bacillithiol disulfide reductase (YpdA) redox pathway to defend against oxidative stress under infections. *Front. Microbiol* 10: 1355, 2019. **(Original Article)**

3) Loi VV, Huyen NTT, Busche T, **Tung QN**, Gruhlke CHM, Kalinowski J, Bernhardt J, Slusarenko A, Antelmann H. *Staphylococcus aureus* responds to allicin by global *S*-thioallylation - Role of the Brx/BSH/YpdA pathway and the disulfide reductase MerA to overcome allicin stress. *Free Radic Biol Med* 139: 55-69, 2019. **(Original Article)**

4) Tung QN, Linzner N, Loi VV, Antelmann H. Application of genetically encoded redox biosensors to measure dynamic changes in the glutathione, bacillithiol and mycothiol redox potentials in pathogenic bacteria. *Free Radic Biol Med* 128: 84-96, 2018. **(Review Article)**

5) Tung QN, Loi VV, Busche T, Nerlich A, Mieth M, Milse J, Kalinowski J, Hocke AC, Antelmann H. Stable integration of the Mrx1-roGFP2 biosensor to monitor dynamic changes of the mycothiol redox potential in *Corynebacterium glutamicum*. *Redox Biol* 20: 514-525, 2019. **(Original Article)**

6) Tung QN, Busche T, Loi VV, Kalinowski J, Antelmann H. The redox-sensing MarR-type repressor HypS controls hypochlorite and antimicrobial resistance in *Mycobacterium smegmatis*. Submitted to *Free Radical Biology Medicine* in Nov. 2019. **(Original Article)**

Declaration of personal contribution to the publications

1) Tung QN et al., 2018: Biosynthesis and function of bacillithiol in *Firmicutes*

I contributed to writing of the chapter 20 sub-sections no. 3, 4, 5 about structure, biophysics, biosynthesis, functions of bacillithiol and also section no. 8, 9 about protein *S*-bacillithiolations and its redox regulation by bacilliredoxins. I created draft figures of Fig.1-5 and Fig. 7 for this book chapter.

2) Linzner N et al., 2019: *Staphylococcus aureus* uses the bacilliredoxin (BrxAB)/ bacillithiol disulfide reductase (YpdA) redox pathway to defend against oxidative stress under infections.

I was involved in preparing samples for quantification of LMW thiols and disulfides *in vivo* (Fig. 3). I measured the biochemical activity of YpdA in BSSB reduction and de-bacillithiolation of GapDH-SSB using the BrxA/BSH/YpdA electron pathway *in vitro* (Fig. 9).

3) Loi VV et al., 2019: *Staphylococcus aureus* responds to allicin by global *S*-thioallylation-Role of the Brx/BSH/YpdA pathway and the disulfide reductase MerA to overcome allicin stress.

I contributed by measurements of the biochemical activity of YpdA in the reduction of S-allylmercaptobacillithiol using NADPH coupled electron assay (Fig. 9B). Furthermore, I performed the biochemical assay for inactivation of GapDH of *S. aureus* by *S*-thioallylation under allicin treatment and its reversal by the BrxA/BSH/YpdA pathway *in vitro* (Fig. 10).

4) Tung QN et al., 2018: Application of genetically encoded redox biosensors to measure dynamic changes in the glutathione, bacillithiol and mycothiol redox potentials in pathogenic bacteria.

I contributing to writing of the sections about the LMW thiol mycothiol in actinomycetes (section 1.3) and the Mrx1-roGFP2 biosensor results in mycobacteria (section 2.3) in this review article and drafted figures for LMW thiols (Fig. 1), design of roGFP2 fused biosensors (Fig. 2) and Mrx1-roGFP2 biosensor results summary in mycobacteria (Fig. 7).

5) Tung QN et al., 2019: Stable integration of the Mrx1-roGFP2 biosensor to monitor dynamic changes of the mycothiol redox potential in *Corynebacterium glutamicum*.

I contributed to the concept of the paper, designed the biosensor and performed most experiments for this paper. I measured all kinetics of biosensor oxidation *in vitro* and *in vivo* (Fig. 1-6), performed the phenotype assays (Fig. 7), and live-imaging experiment (Fig. 8). I drafted all figures and wrote the paper together with Haike Antelmann.

6) Tung QN et al., 2019: The redox-sensing MarR-type repressor HypS controls hypochlorite and antimicrobial resistance in *Mycobacterium smegmatis*.

My contribution included the genetic construction of the *hypS* mutant and complemented strains, the gel shift assays, cloning and purification of HypS (Fig. 4). Furthermore, I was involved in the circular dichroism spectroscopy, structural modelling, qRT-PCR results and phenotype assays of mutant strains (Fig. 5, 6, 7). I drafted all figures and wrote the manuscript together with Haike Antelmann.

Introduction and general conclusion

1. Introduction of *Corynebacterium glutamicum* and *Mycobacterium smegmatis* as fast-growing model bacteria for pathogenic actinomycetes

Actinomycetes are gram-positive bacteria with a high GC-content in their genomic DNA (25,178). Actinomycetes are known to produce a variety of secondary metabolites, antibiotics, and other bioactive compounds that have been applied in medicine for treatment of infections (1,2,181). Some members of actinomycetes are pathogens, such as *Mycobacterium tuberculosis* (*Mtb*) and *Corynebacterium diphtheriae* causing severe diseases in humans and animals. The understanding of the mechanisms how these pathogens respond to oxidative stress under infections plays an important role to find new drug targets and to combat drug-resistant strains.

C. glutamicum and *C. diphtheriae* are the best-investigated corynebacteria (18,129). *C. diphtheriae* infects humans through the respiratory tract or skin ulcerations, leading to the basic symptoms, including pharyngitis, fever, swelling of the neck or area surrounding the skin lesion (54,63). Lethality of *C. diphtheriae* is originated from diphtheria toxin that is one of the most potent exotoxins (172). With the development of high-throughput sequencing technologies, the complete genome sequences of *C. diphtheriae* and closely related species have been compared to reveal genomic variations, protein-protein interactions, regulatory mechanisms, and virulence factors. Sequencing of the 2.8 Mb genome of *C. diphtheriae* NCTC13129 revealed 2272 genes resulting in 5293 protein-protein interactions and 98 pathways (67,179). The genome size of *C. glutamicum* ATCC13032 is 3.31 Mb, encoding for 5476 protein-protein interactions and 103 pathways. Only 263 genes of the *C. glutamicum* ATCC13032 genome are not present in the genome of *C. diphtheriae* (76,190). Based on a similar core genome, the industrial important *C. glutamicum* is considered as model bacterium for the pathogen *C. diphtheriae*.

C. glutamicum is a fast growing, biotin-auxotrophic and predominantly aerobic soil bacterium, which was originally isolated in Japan due to its L-glutamate-producing capability (85). *C. glutamicum* is the most important industrial platform bacterium (85,92). About 3.1 million tons of L-glutamate and 2.2 million tons of L-lysine were produced in 2015 during *C. glutamicum* fermentations (13,90). Additionally, strains derived from *C. glutamicum* DelAro are able produce plant polyphenols, including stilbene (pinosylvin, resveratrol, piceatannol) and (2*S*)-flavanones (naringenin, eriodictyol) (77-80). Polyphenols have been shown to exert anti-oxidant, anti-inflammatory and antibiotic effects (110,127).

However, excessive levels polyphenols lead to auto-oxidation and reactive oxygen species (ROS) generation, causing damaging effects (101). The understanding of oxidative stress responses in *C. glutamicum* could lead to improved production capability of bioactive compounds.

Mycobacterium tuberculosis (*Mtb*) is the etiologic agent of life-threatening Tuberculosis disease, causing ~1.7 million human deaths worldwide, and 6.3 million infected patients (Global Tuberculosis Report, WHO 2017) (128). *Mtb* is a slow-growing bacterium that is transmitted through the respiratory tract (87). The treatment of tuberculosis infections are difficult and lengthy which require long-term combination therapies, resulting in multidrug-resistant and extensively drug-resistant strains. Due to its slow growth and intracellular replication inside the phagosome of macrophages, the treatment of *Mtb* infections is even more complicated (43,107,137). *Mtb* divides every 18–24 hours, requiring 3-4 weeks to yield colonies on a Petri dish. The related *Mycobacterium leprae*, which is the causative agents of leprosy, can be only cultivated in the footpad of mice or within the nine-banded armadillo (147). Due to its fast growth, the non-pathogenic *M. smegmatis* often serves as model bacterium for slow-growing pathogenic mycobacteria. *M. smegmatis* mc^2 155 is a laboratory-adapted hyper-transformable strain with an efficient recombination system that maximizes the genetic manipulation in *M. smegmatis* (117). For example, by transformation of an *Mtb* cosmid library into *M. smegmatis*, Rv0577 and Rv0576 were shown to be important virulence factors in *Mtb* (7). Due to high level of sequence identity between *M. smegmatis* and *Mtb*, *M. smegmatis* was used to screen potential antimycobacterial compounds that inactivated the glutamate racemase leading to cell death (138,158). The function of genes that confer resistance to oxidative stress and antibiotics in *Mtb* have been further studied in the model *M. smegmatis* (14,186).

We have employed *M. smegmatis* to study its adaptation towards oxidative stress using redox proteomics approaches and transcriptomics in previous studies (60). In the next chapters, I will summarize the main knowledge about the roles of LMW thiols and thiol-switches under oxidative stress conditions in bacteria with special attention on mycobacteria and corynebacteria as high-GC content actinomycetes.

2. The role of low molecular weight thiols in bacterial redox homeostasis

2.1 Generation of reactive oxygen and chlorine species (ROS, RCS) in bacteria

Low molecular weight (LMW) thiols are important for maintenance of the reduced state of the cytoplasm (14,36,69,98). The redox homeostasis is crucial for bacterial survival and

frequently disrupted by endogenous and exogenous sources of redox-active species. In aerobic bacteria, molecular oxygen (O_2) is the best terminal electron acceptor and reduced by four electrons to water in the respiratory chain (21,55). The one-electron transfer to O_2 leads to generation of reactive oxygen species (ROS), including superoxide radicals ($O_2^{\bullet -}$), hydroxyl radicals (HO•) and hydrogen peroxide (H_2O_2) (55,68,182). $O_2^{\bullet -}$ and H_2O_2 can be also produced by auto-oxidation of flavin co-factors of redox enzymes (89,106,157). Superoxide dismutases (SODs) play an important role in detoxification of $O_2^{\bullet -}$ to generate H_2O_2 (3). About 87% of the total H_2O_2 is generated by incomplete O_2 reduction in the respiratory chain in *Escherichia coli* (50). H_2O_2 leads to the inactivation of proteins and reacts with Fe^{2+} to the highly reactive HO• in the Fenton reaction. HO• is highly toxic and oxidizes all macromolecules of the cell, including nucleic acids, proteins, carbohydrates and lipids (70,73). Lipid peroxidation can further lead to organic hydroperoxides (ROOH) which require specific thiol-dependent peroxiredoxins, such as OhrA for detoxification (55,163).

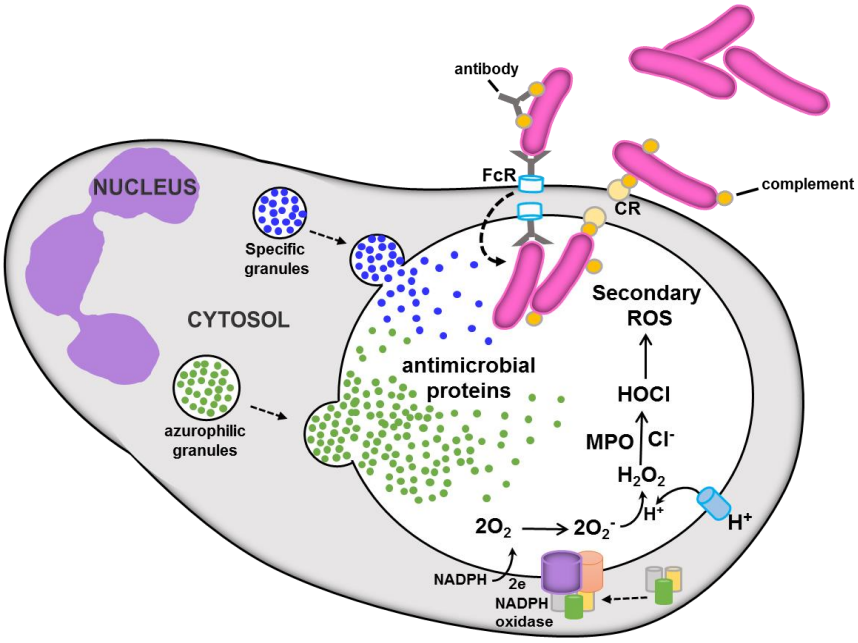

Figure 1. Production of ROS and hypochlorous acid (HOCl) in neutrophils after phagocytosis of pathogenic bacteria. NADPH-dependent oxidase (NOX) generates superoxide anion (O_2^-) that is dismutated to hydrogen peroxide (H_2O_2) by superoxide dismutases (SODs). Granule-localized myeloperoxidase (MPO) catalyzes the reaction of H_2O_2 with Cl^- to form the strong oxidant HOCl to kill bacteria in the phagolysosome. The figure is adapted from reference (88).

In addition, pathogenic bacteria are exposed to the oxidative burst by activated macrophages and neutrophils during infections, such as ROS, RCS as the first line of defense of the innate immune defense (12,95,189). Specifically, O_2^- is generated by the NADPH-dependent oxidase (NOX) through the transfer of electrons from NADPH to O_2 (88). SODs

subsequently dismutate $O_2^{\bullet -}$ to H_2O_2. The myeloperoxidase (MPO) is released from the granules into the phagosome to catalyze the reaction of H_2O_2 with chloride (Cl^-) to form the highly toxic and microbicidal oxidant hypochlorous acid (HOCl) (**Fig. 1**) (3,43,145). MPO generates also other reactive species, such as nitrogen dioxide radicals and tyrosine hydroperoxide (66,86). Since Cl^- is the most abundant in neutrophils, HOCl is the main product of MPO, which kills effectively invading pathogens. HOCl is a strong two-electron oxidant and reacts with high reaction rates with cysteine and methionine, DNA, metal centers and lipids, leading to bacterial killing (12,74,189). In conclusion, bacteria are exposed to various reactive species that are produced during cellular metabolism and in response to external stressors as part of the host immune defense (145,184).

2.2 Post-translational thiol-modifications in response to ROS

It is well-known that excess of ROS causes cell death while physiological levels of ROS function in redox signaling during many physiological and pathological processes (21,145). The primary targets of ROS are the sulfur-containing amino acids cysteine (Cys) and methionine. Cys is the strongest nucleophile and the most rare amino acid in proteins contributing only to 1.9% of all amino acids present in proteins (48,182). Cys residues can undergo thiol-modifications due to the wide range of oxidation states (-2 to +6) of the sulfur atom (182). The reactivity of the Cys thiol group towards ROS depends on its pK_a value (160). Specifically, Cys thiols with neutral pK_a values of 8.4~8.6 are protonated and not redox-sensitive under oxidative stress (132,184). In contrast, Cys thiols with low pK_a are present in the deprotonated thiolate anion form that is redox-sensitive to undergo thiol-oxidation (132). For example, Cys pK_a values of 3.5 and 10 were determined for two active-site Cys residues of the DsbA disulfide oxidoreductase, but only the low pK_a Cys was involved in thiol-oxidation of the substrate (121,132). Thus, the determination of the Cys pK_a is essential to reveal the redox-sensing Cys residues in proteins and their function in redox signaling processes.

Redox-sensitive Cys residues with low pK_a values can undergo different reversible and irreversible post-translational thiol-modifications under oxidative stress. Reversible thiol-disulfide switches are involved in redox signaling processes and protect the thiol group against overoxidation (132). Under oxidative stress, the Cys thiolate anions are oxidized to Cys sulfenic acids (Cys-SOH), which are instable intermediates. Cys-SOH can be further oxidized either to irreversible Cys sulfinic (SO_2H) and sulfonic acids (SO_3H) or to reversible thiol-switches, such as intramolecular or intermolecular protein disulfides or *S*-thiolations with LMW thiols (e.g., *S*-glutathionylations, *S*-bacillithiolations and *S*-mycothiolations)

(**Fig. 2**) (59,98,173). *S*-thiolations function in redox regulation of protein activities and in thiol-protection to prevent the irreversible overoxidation of protein thiols under oxidative stress (98). Thus, *S*-thiolations ensure that essential thiol-containing proteins can be reactivated after recovery from oxidative stress to rescue cellular survival. The reduction of thiol-switches requires LMW thiols, such as glutathione (GSH), bacillithiol (BSH) and mycothiol (MSH) that are present in different bacteria. In addition, enzymatic thiol-disulfide reducing pathways are involved in regeneration of reduced protein thiols to restore protein activities, including the thioredoxin (Trx)/thioredoxin reductase (TrxR) pathway and the glutaredoxin (Grx)/GSH/glutathione reductase (Gor) pathway (98). As part of this PhD thesis, we applied Grx-related bacilliredoxins (Brx), the BSSB reductase (YpdA) and mycoredoxin-1 (Mrx1) in *S. aureus* and *C. glutamicum* which function in reduction mixed disulfides with the LMW thiols BSH and MSH, respectively (94,173).

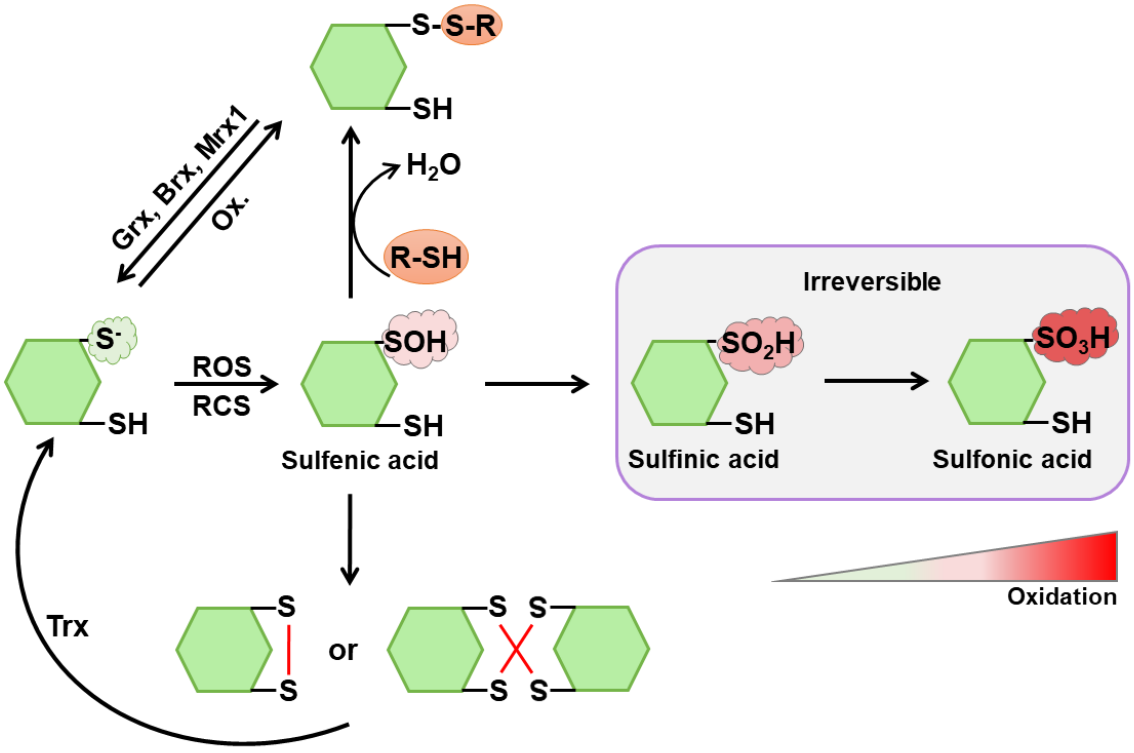

Figure 2. Post-translational thiol-modifications caused by ROS. Oxidation of the Cys thiol group by ROS leads to the Cys sulfenic acid intermediate (-SOH), which can be irreversibly overoxidized to Cys sulfinic (-SO_2H) or sulfonic acids (-SO_3H). In the presence of proximal thiols, Cys-SOH can undergo disulfide formation, including intramolecular or intermolecular protein disulfides, which are reduced by the thioredoxin (Trx)/thioredoxin reductase (TrxR) system. Cys-SOH can also further react to mixed disulfides with low molecular weight thiols (R-SH), termed as protein *S*-thiolations. The reduction of *S*-thiolated proteins is catalyzed by the glutaredoxin (Grx), bacilliredoxin (Brx) or mycoredoxin-1 (Mrx1) pathways. The figure is adapted from references (59,98).

2.3 The role of low molecular weight thiols in Gram-positive bacteria

LMW thiols are small non-protein thiols, which are often produced in millimolar concentrations in prokaryotic and eukaryotic cells (69,98,177). LMW thiols maintain the reduced state of the cytoplasm by detoxification of ROS, RCS, electrophiles, antibiotics and heavy metals (69). GSH is the major LMW thiol in eukaryotes and Gram-negative bacteria which evolved with cyanobacteria as protection mechanism against oxygen toxicity (39,69). However, Gram-positive bacteria do not encode the enzymes for GSH biosynthesis, but instead utilize alternative LMW thiols, such as BSH and MSH (**Fig. 3**). BSH and its derivatives are widespread distributed in the bacterial phyla *Chlorobi, Bacteroidetes, Deinococcus-Thermus, Firmicutes, Acidobacteria, Chlamydiae, Gemmatimonadetes* and *Proteobacteria* (62,98). MSH is the major LMW thiol in actinomycetes and has many functions as thiol cofactor of redox enzymes and in protection against redox stress (98,145,173).

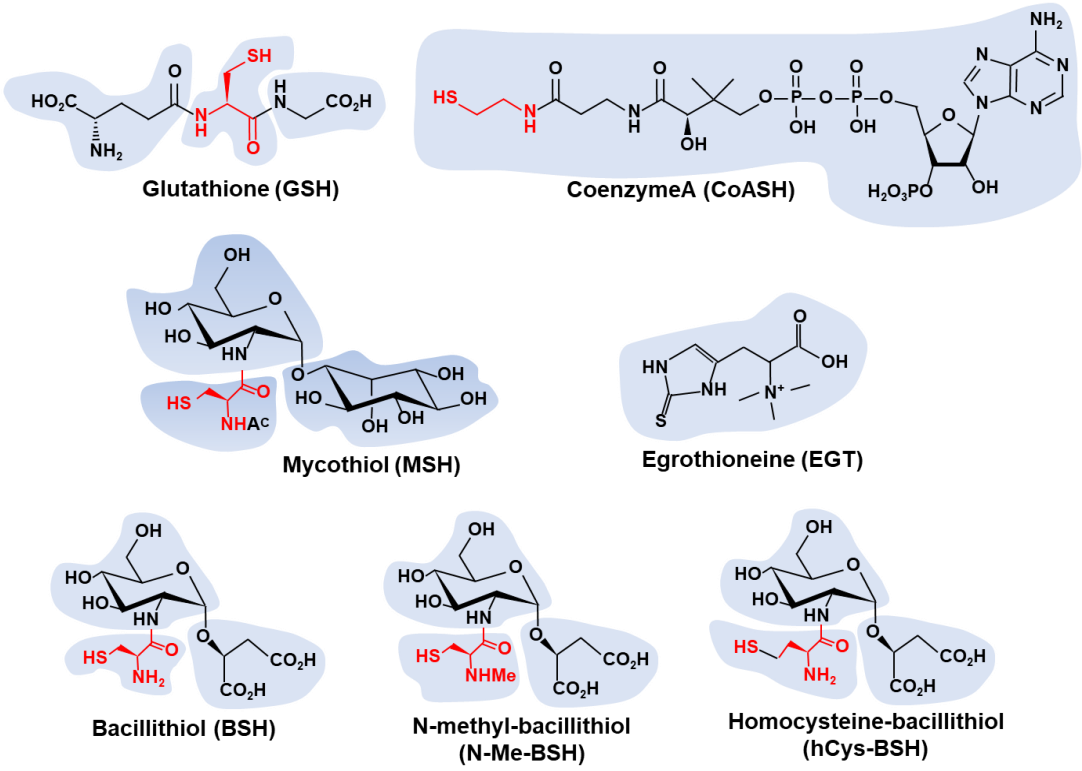

Figure 3. Structure of low molecular weight (LMW) thiols. The major LMW thiol in eukaryotes and Gram-negative bacteria is GSH. MSH and EGT are utilized as alternative LMW thiols in actinomycetes. Members of *Chlorobi, Bacteroidetes, Deinococcus-Thermus, Firmicutes, Acidobacteria, Chlamydiae, Gemmatimonadetes* and *Proteobacteria* produce BSH and its derivatives N-Me-BSH and hCys-BSH. CoASH may function as alternative LMW thiol in *S. aureus, B. subtilis* and *Bacillus anthracis*. The figure is adapted from references (62,69,98).

2.3.1 Biosynthesis, regulation and functions of mycothiol (MSH)

2.3.1.1 Biosynthesis of MSH in actinomycetes

The cysteinyl pseudo-disaccharide MSH is utilized as major LMW thiol in all actinomycetes, including mycobacteria, corynebacteria and streptomycetes (**Fig. 3**) (40,69). MSH biosynthesis is catalyzed by five enzymes using the substrates *myo*-inositol-1-phosphate (Ins-P), UDP-*N*-acetyl glucosamine (UDP-GlcNAc) and Cys **(Fig. 4-5)** (122). In the first step, the glycosyltransferase MshA conjugates Ins-P and UDP-GlcNAc to *N*-acetyl glucosamine *myo*-inositol-1-phosphate (GlcNAc-Ins-P). GlcNAc-Ins-P is dephosphorylated by the MSH phosphatase MshA2, followed by deacetylation by the metal-dependent deacetylase MshB to yield glucosamine inositol [1-O-(2-amino-1-deoxy-a-D-glucopyranosyl)-D-myo-inositol]. In the third step, the Cys ligase MshC conjugates Cys to produce Cys-GlcN-Ins. The final step involved acetylation of the Cys amino group by the MSH acetyltransferase MshD to generate MSH (40,75). MSH is more resistant to metal-catalyzed autoxidation compared to free Cys since the amino and carboxyl groups of Cys are conjugated in MSH (124). The MSH levels vary significantly among actinomycetes. While mycobacteria produce high MSH levels of ~4.6–19 μmol/g raw dry weight (rdw), much lower levels of ~0.3–4 μmol/g rdw were measured in corynebacteria (69,122).

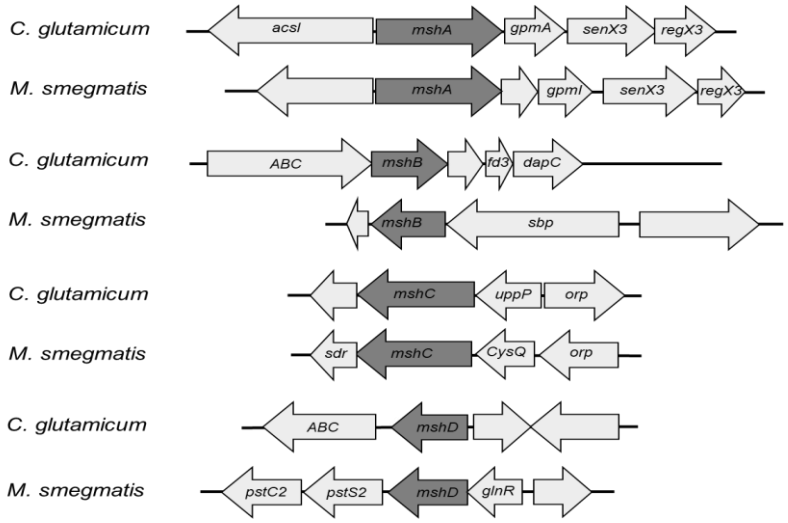

Figure 4. Conservation of gene organization of the *mshA, mshB, mshC, mshD* biosynthesis operons in *C. glutamicum* and *M. smegmatis.*

The MSH biosynthesis genes *mshA, mshB, mshC, mshD* of *C. glutamicum* and *M. smegmatis* are transcribed in four independent operons. However, the gene organization of the *mshA, mshB, mshC, mshD* operons is different in both strains (**Fig. 4**). As demonstrated in *M. smegmatis* and *Mtb*, *mshA* and *mshC* mutants lack MSH, while 1-20 % of wild-type MSH levels were observed in *mshB* and *mshD* mutants (75). The remaining MSH levels in

the *mshB* and *mshD* mutants could be due to substitutions by other unknown enzymes. The lack of MSH leads to an impaired growth in *M. smegmatis* and *Mtb*, but not in *C. glutamicum*. It has been demonstrated that the LMW thiol ergothioneine (EGT) can compensate for absence of MSH in mycobacteria (153,155).

2.3.1.2 Regulation of MSH biosynthesis in actinomycetes

In mycobacteria and corynebacteria, MSH biosynthesis is regulated by the availability of Ins-P, which is an important precursor for the first step of MSH synthesis, but also essential for cell wall biosynthesis (**Fig. 5**) (11). Ins-P can be taken up from the culture medium or synthesized from glucose-6-phosphate (G6P). When Ins-P is limiting, the LacI-type regulator IpsA triggers Ins-P generation by activating the *myo*-inositol-1-phosphate synthase (Ino-1) that catalyzes the production of *myo*-inositol-3-phosphate (I3P) from glucose-6-phosphate. Finally, I3P is dephosphorylated by inositol monophosphatase (IMP) to Ins-P (11). Since IpsA activates *ino-1* expression in the absence of external inositol, deletion of *ipsA* led to an altered cell shape and abolished MSH synthesis (11). Recently, Ino-1 was shown to be involved in the defense against oxidative stress by regulation of MSH levels (26).

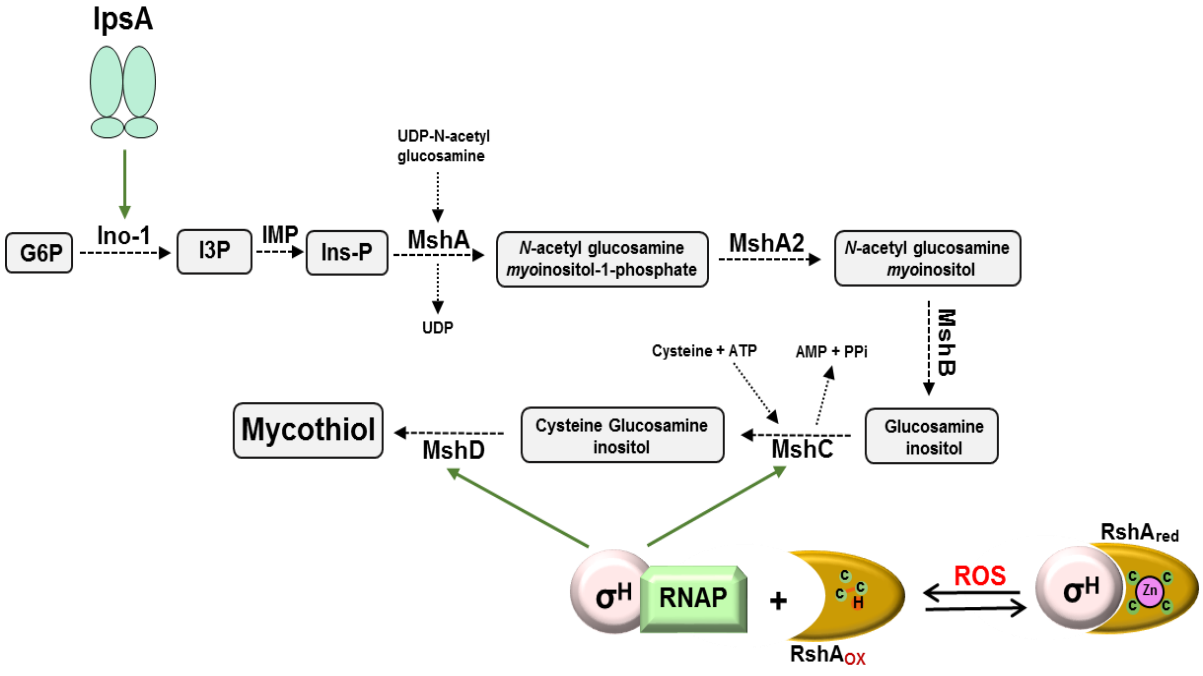

Figure 5. Biosynthesis and regulation of MSH in actinomycetes. The MSH synthesis is catalyzed by five enzymes, including the glycosyltransferase MshA, the phosphatase MshA2, the deacetylase MshB, the ATP-dependent Cys ligase MshC and the acetyltransferase MshD. The genes for MSH biosynthesis enzymes are regulated by the disulfide stress specific sigma factor/anti sigma factor couple SigH/RshA. The transcriptional activator IpsA controls the *myo*-inositol-1-phosphate synthase (Ino-1). The figure is created from references (11,19,69,125,154).

In actinomycetes, the conserved ECF sigma factor SigH controls genes for biosynthesis and recycling of MSH under oxidative and disulfide stress (**Fig. 5**) (19,84). The activity of SigH is regulated by its cognate redox-sensitive ZAS anti sigma factor RshA, which senses ROS and other thiol-reactive compounds (19,30). Under reducing conditions, SigH is sequestered by RshA preventing the interaction of SigH with the RNA polymerase (RNAP) core enzyme (19,30). RshA is oxidized by diamide, NaOCl or H_2O_2 leading to Zn^{2+} release, inactivation of RshA and relief of SigH to initiate transcription of the large SigH disulfide stress regulon (30). The SigH regulon includes genes for the Trx/TrxR reducing system (*trxB, trxB1, trxC*), MSH biosynthesis and recycling (*mshC, mshD, mca, mtr*) and other stress responsive genes (19,118). The Trx/TrxR system and MSH function in reduction of oxidized proteins, including RshA to shut-down the SigH regulon and to restore redox homeostasis (30). Previous study revealed that the *sigH* mutant of *C. glutamicum* is sensitive in growth under H_2O_2 and NaOCl stress (30,168). The results of my PhD thesis revealed using Mrx1-roGFP2 biosensor measurement that the basal E_{MSH} is highly reducing in the *C. glutamicum* wild type (-296 mV) and more oxidized to -286 mV in the *sigH* mutant **(see chapter 5)** (173). In contrast to *C. glutamicum*, SigH of *Mtb* controls genes involved in Cys biosynthesis and sulfate acquisition (100). Since Cys is essential for MSH biosynthesis, the *Mtb sigH* mutant was strongly impaired in survival and pathogenicity during infections (81,103).

2.3.1.3 Functions of MSH as redox cofactor to ensure redox homeostasis

MSH is involved in the detoxification of various redox-active species, xenobiotics, antibiotics, heavy metals and aromatic compounds (69,98). The loss of MSH renders *C. glutamicum* and *M. smegmatis* more sensitive to different redox-active compounds (30,60,75). Under oxidative stress, MSH is oxidized to mycothiol disulfide (MSSM), which is recycled by the NADPH-dependent mycothiol disulfide reductase (Mtr) at the expense of NADPH (**Fig. 6**) (144). In the reductive half-reaction of MSSM reduction, Mtr is reduced by two electrons which are transferred from NADPH to the active site disulfide through the FAD cofactor (125). In the oxidative half-reaction, MSSM is reduced by the two-electron reduced Mtr, leading the formation of enzyme-substrate intermolecular disulfide and release of one MSH molecule (144). This intermolecular disulfide is reduced by a charge-transfer Cys residue to yield oxidized Mtr and to release the second MSH molecule (146) **(Fig. 6)**. In *Mtb*, Mtr is a part of the redox-sensing WhiB3 regulon, which is required for detoxification of ROS and reactive nitrogen species during infections (104,105,146). In *C. glutamicum*, SigH controls *mtr* expression under oxidative stress. The results of the Mrx1-roGFP2

measurements of this study revealed that the *C. glutamicum mtr* mutant had a highly oxidized basal E_{MSH} of -280 mV along all growth phases (173). Moreover, overexpression of Mtr in *C. glutamicum* resulted in increased resistance towards ROS, bactericidal antibiotics and heavy metals due to an increased MSH level which enhances antioxidant activities of MSH-dependent redox enzymes (130,146).

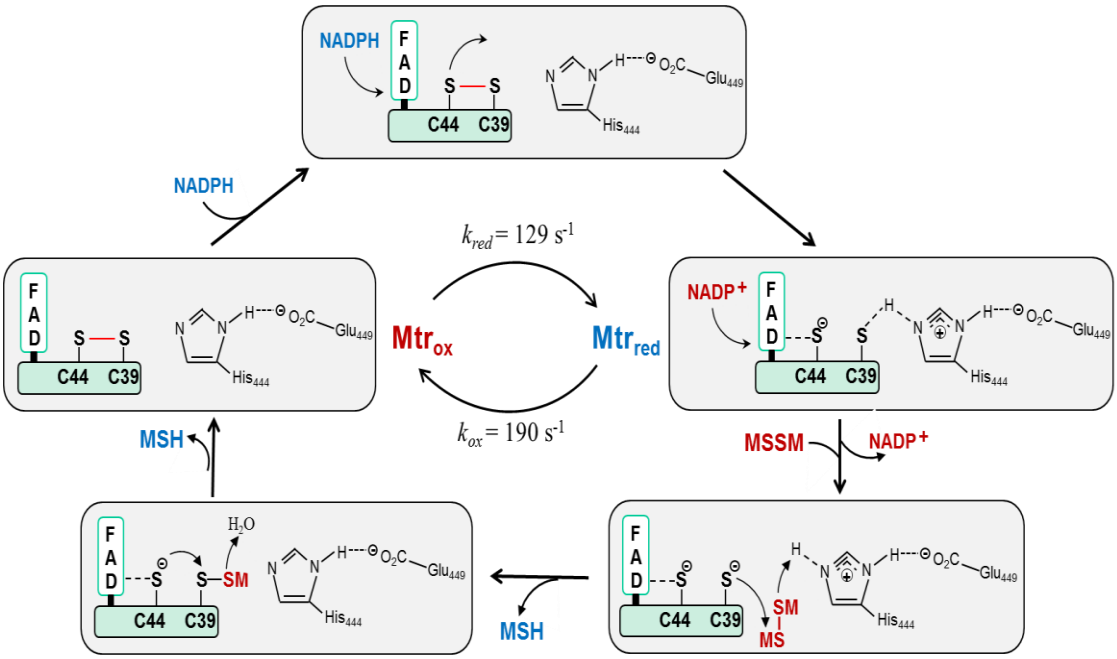

Figure 6. Catalytic mechanism of the mycothiol disulfide reductase Mtr. The oxidized Mtr (Mtr_{ox}) contains a Cys39-Cys44 disulfide bridge, which is reduced by electrons from NADPH via the flavin adenine dinucleotide (FAD) cofactor to generate reduced Mtr (Mtr_{red}). MSSM is attacked by the interchange Cys39, leading to the formation of Cys39-SSM and liberation of first MSH moiety. Subsequently, the Cys39-SSM disulfide bond is attacked by the thiolate of Cys44 yielding Mtr_{ox}. The figure is adapted from references (75,125).

MSH functions as an important thiol cofactor of many redox enzymes that are involved in detoxification of several redox-active compounds, such as arsenate, formaldehyde, RES, maleylpyruvate and methylglyoxal (**Fig. 7**) (69,75,98). The arsenate reductases (CgArsC1/CgArsC2) catalyze arsenate detoxification. First, an As(V)-SM adduct is formed, which is reduced by mycoredoxin-1 (Mrx1), leading to an Mrx1-SSM intermediate and As(III). As(III) is exported out of the cells by two arsenite permeases of the Acr3 family (180). Mrx1-SSM requires MSH for the regeneration of Mrx1, resulting in MSSM formation that is reduced by Mtr (98). For NO detoxification, the MSH-dependent detoxification enzyme MscR displays S-nitrosomycothiol (MSNO) reductase activity to generate MSH sulfonamide (MSO_2H) (125,144). Both MscR and the MSH-dependent formaldehyde dehydrogenase AdhE are involved in the oxidation of formaldehyde to

formate. In *C. glutamicum*, the MSH-dependent maleylpyruvate isomerase converts maleylpyruvate to fumarylpyruvate in the gentisate pathway (42,194).

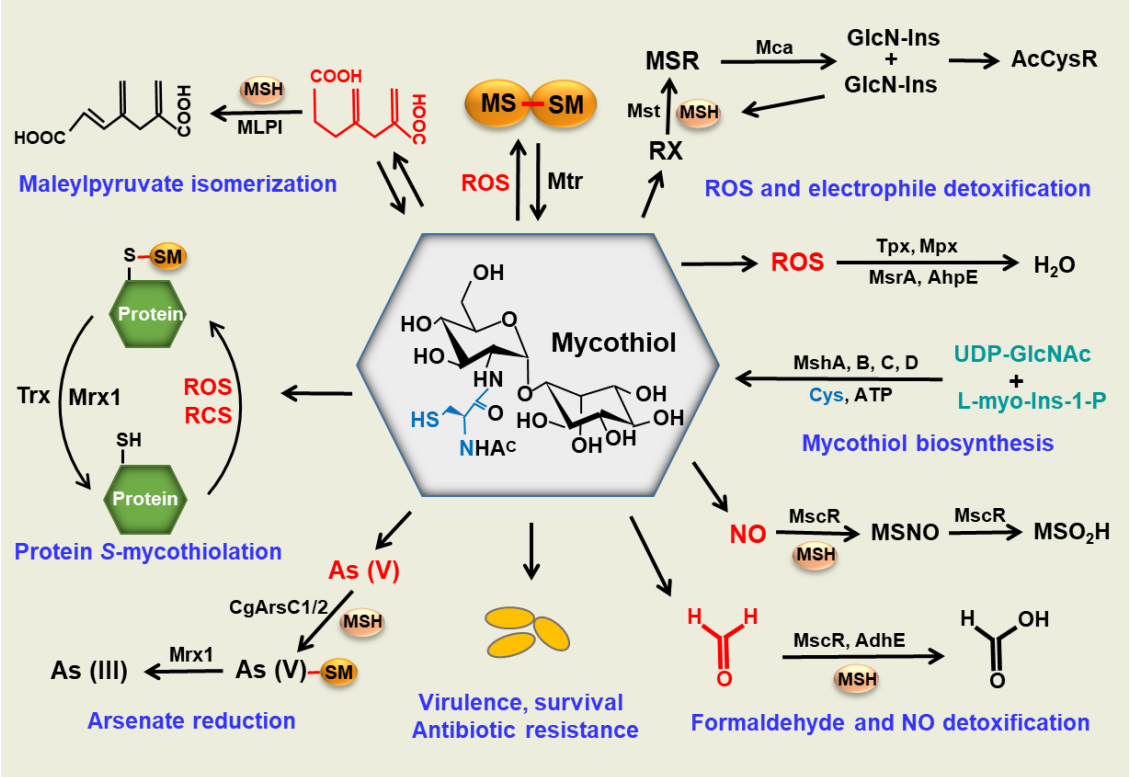

Figure 7. The functions of mycothiol (MSH) in corynebacteria and mycobacteria. Under ROS, MSH is oxidized to mycothiol disulfide (MSSM), which is reduced by the NADPH-dependent mycothiol disulfide reductase (Mtr). MSH *S*-transferases (MST) conjugate MSH to electrophiles (RX) leading to MS-electrophiles (MSR) that are cleaved by the MSH *S*-conjugate amidase (Mca) to mercapturic acids (AcCyS-R). MSH-dependent peroxidases including Mpx, Tpx, MsrA, and AhpE are involved in ROS detoxification. MSH functions as thiol cofactor of the alcohol dehydrogenase MscR and formaldehyde dehydrogenase AdhE in detoxification of NO and formaldehyde. MSH is involved in isomerization of maleylpyruvate to fumarylpyruvate in *C. glutamicum*. Arsenate reductases CgArsC1/CgArsC2 conjugate arsenate As(V) to MSH, generating As(V)-SM which is reduced by mycoredoxin-1 (Mrx1) to As(III). MSH is required for the survival and virulence of mycobacteria under infection and antibiotic treatment. Under NaOCl and H_2O_2 stress, proteins are *S*-mycothiolated and regenerated by the Mrx1/MSH/Mtr and Trx/TrxR pathways. The figure is adapted from references (69,98).

Furthermore, MSH is involved in detoxification of xenobiotics and antibiotics (69). Antibacterial compounds, such as cerulenin and rifamycin, are conjugated with MSH either spontaneously or enzyme-catalyzed by MSH *S*-transferases (MST) (69,125). MSH-*S*-conjugate amidase (Mca) cleaves MSH-*S*-conjugates to mercapturic acid (AcCys-R) and glucosaminylinositol (GlcN-Ins) (75,125). GlcN-Ins is recycled to MSH, and the mercapturic acid derivatives are exported out of the cell (144).

MSH is involved in the evolution of *Mtb* in response to antibiotics. MSH and catalase are important for activation of the first-line anti-TB drug isoniazid (INH) in *Mtb* (69). The enoyl-ACP reductase (InhA) is the target for INH and inhibited by formation of a NAD-INH adduct, which prevents mycolic acid biosynthesis and induces cell lysis (102,173). Sequencing of INH-resistant *Mtb* isolates reveals mutations in both *katG* and *mshA* (72,193). The MSH-dependent nitroreductase Rv2466c also functions in prodrug activation of nitrofurantoin derivatives and thienopyrimidine compounds (4,120,149). Resistant isolates have spontaneous mutations in *Rv2466c* (69,149).

In addition, MSH can function as storage form for cysteine and GlcN-Ins to avoid auto-oxidation of free Cys (69,75,170). To mobilize Cys, MSH is cleaved by the Mca to GlcN-Ins and N-acetyl cysteine (146). The latter can be rapidly deacetylated to regenerate Cys (20,146). Cys can be further converted to pyruvate and alanine by the cysteine desulfhydrase and desulfurase, respectively (20,151,187). Moreover, GlcN-Ins is used as building block for cell envelope synthesis (123).

2.3.1.4 Redox regulation of proteins by *S*-mycothiolation and the Mrx1/MSH/Mtr pathway in actinomycetes

Protein *S*-mycothiolation is a reversible post-translational thiol-modification, which functions in redox-regulation and thiol-protection under oxidative stress (69,146). Under oxidative stress, protein thiols form mixed disulfides with MSH, termed as *S*-mycothiolation (30,98). The reversal of protein *S*-mycothiolations is catalyzed by Mrx1, which is the glutaredoxin homolog of actinomycetes. Mrx1 is part of the Mrx1/MSH/Mtr electron transfer pathway which uses NADPH as electron donor (**Fig. 9**) (69,176). The Mrx1 structure shows a Trx-like fold with a CGYC catalytic active site located at the N-terminus of the first α-helix (69). The active site Cys14 is surface-exposed with a low pK_a value, whereas the resolving Cys17 is buried (176). Mrx1 uses mainly a monothiol mechanism for the reduction of *S*-mycothiolated protein substrates (146). In the monothiol mechanism, the Mrx1 active site Cys14 attacks the *S*-mycothiolated protein, resulting in Mrx1-SSM formation, which is regenerated by MSH, leading to the release of Mrx1 and MSSM (30,69,176) (**Fig. 8A**). For reduction of the *S*-mycothiolated peroxidase AhpE, a dithiol mechanism has been proposed that requires both Cys residues of the CXXC motif of Mrx1 (65) (**Fig. 8B**). The active site Cys14 of Mrx1 forms an intermolecular disulfide with the AhpE substrate, followed by the release of reduced AhpE and oxidized Mrx1 with an intramolecular disulfide (146). Finally, two MSH moieties are required to recycle reduced Mrx1. AhpE has been shown to be

reduced by the monothiol and dithiol mechanisms of Mrx1 (65). The rate constant for *S*-mycothiolation of Mrx1 in the monothiol mechanism is 10-fold lower than for the dithiol mechanism *in vitro* (65).

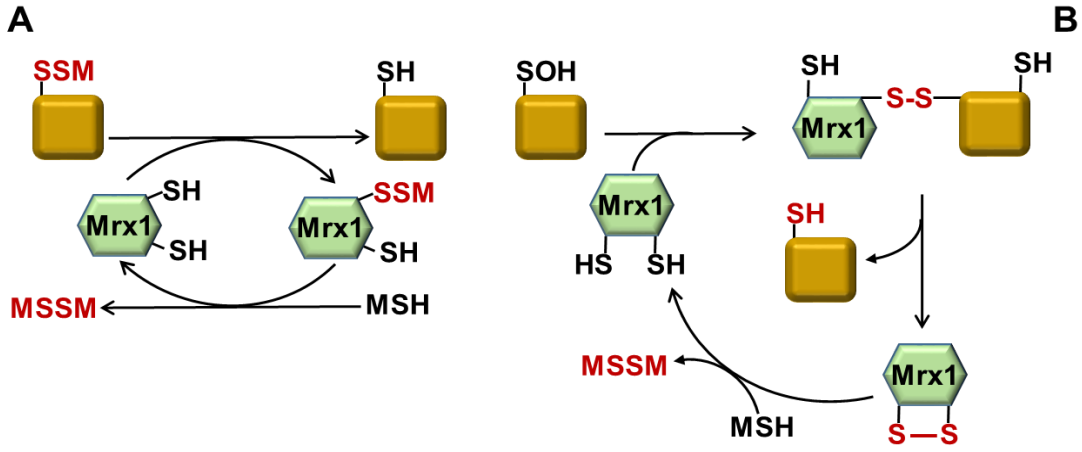

Figure 8. Schematics of the monothiol and dithiol mechanism of Mrx1 for reduction of oxidized protein substrates. **(A)** The reversal of protein *S*-mycothiolations is catalyzed by Mrx1 according to the monothiol mechanism. **(B)** Mrx1 reduces disulfide bonds in proteins by the dithiol mechanism through the formation of a mixed disulfide between the nucleophilic cysteine of Mrx1 and the substrate. Oxidized Mrx1 is recycled to reduced Mrx1 by two MSH molecules. The figure is adapted from references (125,176).

Protein *S*-mycothiolation is a widespread redox modification in actinomycetes and occurred specifically under HOCl stress in corynebacteria and *M. smegmatis* (30,69,162). The identified targets for *S*-mycothiolations are mainly involved in cellular metabolism, protein translation, detoxification and redox-signaling. In *C. glutamicum*, 25 *S*-mycothiolated proteins were identified that function in MSH biosynthesis (Ino1), glycolysis (Fba, Pta, XylB, PckA, GapDH), glycogen and maltodextrin degradation (MalP), serine, cysteine, methionine biosynthesis (SerA, Hom, MetE), nucleotide and thiamine cofactor biosynthesis (GuaB, PurL, NadC, ThiD1, ThiD2), antioxidant functions (Tpx, Mpx, MrsA), methionine sulfoxide reduction (MsrA), heme degradation (HmuO) and protein translation (RpsF, RpsC, RpsM, RplM, TufA, PheT) (**Fig. 9**) (30). Among these targets for *S*-mycothiolations are MetE, GuaB1, GuaB2, Tuf and SerA, which are conserved *S*-thiolated proteins across actinomycetes and firmicutes (31,32).

About 26 and 58 *S*-mycothiolated proteins were identified under NaOCl stress by shotgun proteomics in *C. diphtheriae* and *M. smegmatis*, respectively (30,60,61). The different extends of *S*-mycothiolated proteins in both strains could be due to different MSH contents. *C. diphtheriae* and *C. glutamicum* produce approximately 0.3 and 4 µmol/g raw dry weight (rdw) MSH, respectively, while 6 µmol/g rdw MSH was determined in *M. smegmatis* (61). It might be possible that the LMW thiol EGT compensates for the low level

of MSH as measured in corynebacteria (153). In this work, we have investigated the functions of the mycothiol peroxidase (Mpx) and thiol peroxidase (Tpx) under oxidative stress and their impact on the MSH redox potential in *C. glutamicum*. Both peroxiredoxins are major targets for *S*-mycothiolations in *C. glutamicum*.

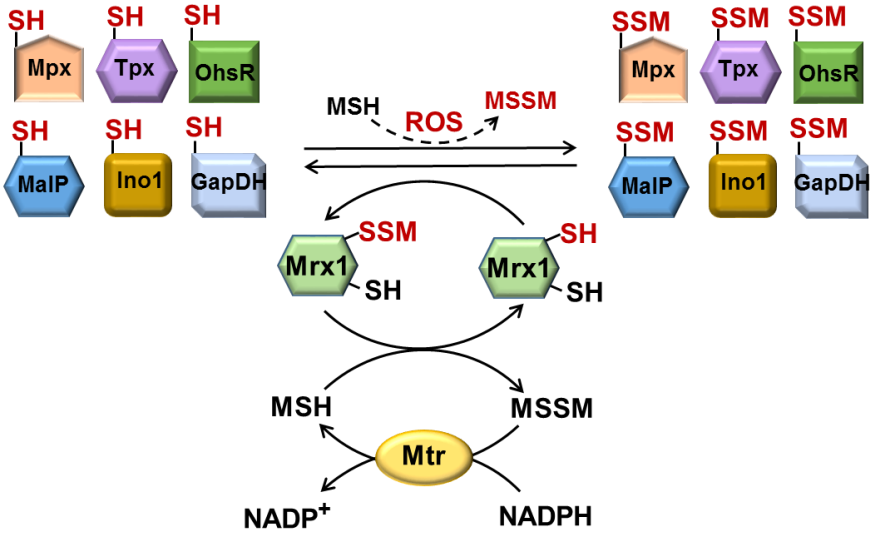

Figure 9. The reduction of protein *S*-mycothiolations by the Mrx1/MSH/Mtr redox pathway in actinomycetes. Under HOCl stress, proteins form mixed disulfides with MSH, termed as *S*-mycothiolations (protein-SSM). *S*-mycothiolated proteins are reduced by Mrx1, leading to Mrx1-SSM formation, which is regenerated by MSH and Mtr at expense of NADPH. The figure is adapted from references (11,26,30,146,162).

Mpx is annotated as glutathione peroxidase and was shown to be involved in the defense against ROS and RCS in *C. glutamicum* (133,183). Mpx catalyzes detoxification of high levels of H_2O_2 and alkyl hydroperoxides *in vitro* (183). Mpx is *S*-mycothiolated under H_2O_2 stress at its peroxidatic Cys36, which inhibits the peroxidase activity (133). Reactivation of Mpx requires reduction by the Mrx1/MSH/Mtr pathway via the monothiol mechanism (30,133). Additionally, *S*-mycothiolated Mpx could be regenerated by the Trx/TrxR pathway. Trx reduces Mpx-SSM, leading to the transfer of MSH moiety to Trx and subsequent Trx intramolecular disulfide formation, which is reduced by TrxR on expense of NADPH (133). However, reduction of Mpx-SSM by the Trx/TrxR pathway was much slower compared to reduction by the Mrx1/MSH/Mtr pathway (133). The Trx/TrxR pathway might compensate when Mrx1 is busy in de-mycothiolation reactions of other proteins under oxidative stress (146). Thus, Mpx shows promiscuity in redox control by the Mrx1 and Trx redox pathways. In our phenotype analyses, we did not detect growth phenotypes of the *mpx* mutant under sub-lethal H_2O_2 stress (173). In addition, the *mpx* mutant did not show differences in the basal E_{MSH} levels along the growth curve in *C. glutamicum* (173). However, the H_2O_2 sensitive phenotype of the *mpx* mutant was previously observed

only with high doses of H_2O_2 in *C. glutamicum* RES167 (133). The expression of *mpx* is controlled by the MarR-type repressor CosR, which is involved in the oxidative stress defense of *C. glutamicum* (161).

Apart from Mpx, the thiol-peroxidase Tpx is regulated by protein *S*-mycothiolations in *C. glutamicum* (30). Tpx was also shown to be required for the survival of *C. glutamicum* under H_2O_2 stress, but the specific function of Tpx depends on the H_2O_2 gradient inside the cell (30,164). Low H_2O_2 levels (< 7.5 mM) result in sulfenylation of the peroxidatic Cys63 with subsequent formation of the Tpx Cys63-SS-Cys97 intramolecular disulfide, which is reduced by the Trx/TrxR system *in vitro* (164). Tpx oxidation inhibits expression of KatA and Mpx under low H_2O_2 levels. Moderate H_2O_2 levels (20 mM) and 0.5 mM MSH lead to *S*-mycothiolation of Tpx, which protects the peroxidatic Cys63 and is reversed by the Mrx1/MSH/Mtr redox pathway *in vitro* (30,164). Increased H_2O_2 levels also lead to induction of the OxyR and CosR regulons resulting in increased expression of KatA and Mpx (161,164). When exposed to an excess of H_2O_2 (25 mM), Cys63 is overoxidized to sulfonic acid, causing Tpx aggregation and formation of the tetrameric form which exhibits chaperone activity to prevent aggregation of oxidatively damaged proteins *in vitro* (164). In conclusion, Tpx functions in H_2O_2 removal as peroxidase and molecular chaperone which depends on the H_2O_2 gradient in the cell causing either reversible or irreversible thiol-modifications in Tpx (164).

Our phenotype results of *tpx* and *mpx* single and double mutants revealed that Tpx and Mpx are dispensible for H_2O_2 detoxification, while the catalase KatA plays the major role since only the *katA* mutant was significantly impaired in H_2O_2 detoxification in *C. glutamicum* **(see chapter 5)** (173). The *katA* mutant showed also a strongly enhanced Mrx1-roGFP2 biosensor oxidation under H_2O_2 stress compared to the wild type, supporting its major contribution to the H_2O_2 resistance of *C. glutamicum*. In contrast, neither increased basal oxidation nor increased H_2O_2 responses were measured for the *mpx* and *tpx* mutants using the Mrx1-roGFP2 biosensor in *C. glutamicum* (173).

2.3.2 Biosynthesis and functions of bacillithiol (BSH) in firmicutes

2.3.2.1 Biosynthesis and functions of BSH in redox homeostasis

BSH is the alpha-anomeric glycoside of L-cysteinyl-D-glucosamine with L-malic acid, which is utilized as LMW thiol in many firmicutes, including *Bacillus* and *Staphylococcus* species **(see chapter 1)** (24,44,69). Moreover, BSH and its derivatives were recently shown to be more widely distributed in the bacterial phyla *Chlorobi*, *Bacteroidetes*, *Deinococcus*-

Thermus, *Firmicutes*, *Acidobacteria*, *Chlamydiae*, *Gemmatimonadetes* and *Proteobacteria* (62,98). BSH is synthesized from the three precursors UDP-*N*-acetylglucosamine, L-malate and Cys. BSH synthesis is catalyzed by the enzymes BshA, BshB1, BshB2 and BshC, although some bacteria have only one BshB enzyme (24,45). In the first step, the glycosyltransferase BshA conjugates malate to GlcNAc to form GlcNAc-Mal, which is deacetylated by BshB1/2. In the third step, the Cys ligase BshC adds Cys to GlcN-Mal generating BSH (44). BSH is involved in the defense against many thiol-reactive compounds, electrophiles, alkylating agents, toxic metals and antibiotics in different firmicutes, such as *B. subtilis* and *S. aureus*, since *bsh* mutants were sensitive to these compounds (24,98). Under oxidative stress, BSH is oxidized to bacillithiol disulfide (BSSB), which is reduced to BSH by the NADPH-dependent flavin disulfide reductase YpdA on expense of NADPH which was biochemically characterized as part of this thesis (**Fig. 10**) (94,111).

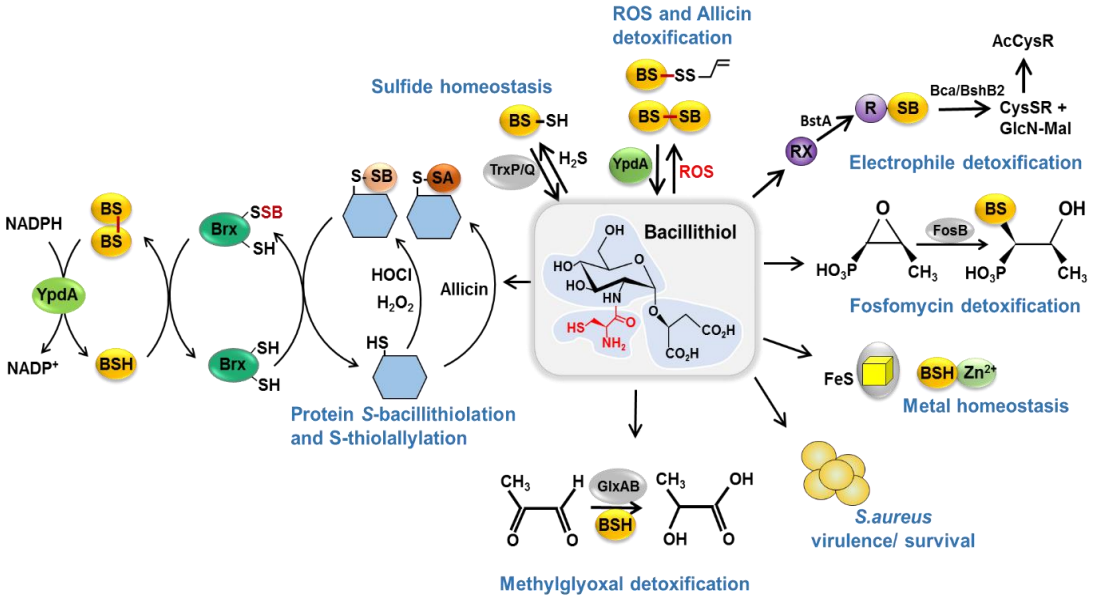

Figure 10. The functions of bacillithiol (BSH) in firmicutes. BSH plays an important role in detoxification of redox-active species, including ROS, RCS, RSS, RES, heavy metals and antibiotics. ROS and allicin trigger the oxidation of BSH generating bacillithiol disulfide (BSSB) and *S*-allylmercaptobacillithiol (BSSA), respectively. The BSH-*S*-transferase (BstA) conjugates electrophiles (RX) to BSH forming BS-electrophiles (BSR). BSR is cleaved by the BSH-S-conjugate amidase (Bca) or BshB2 to generate CysSR and mercapturic acids (AcCySR) that are exported out of the cell. BSH functions as a thiol-cofactor for fosfomycin and methylglycoxal detoxification. BSH is involved in metal homeostasis as Zn^{2+} buffer and in FeS cluster assembly. Moreover, BSH is required for virulence of *S. aureus* under neutrophil and macrophage infections. Allicin, HOCl and H_2O_2 lead to *S*-thiolation of proteins. The reduction of *S*-thiolated proteins is catalyzed by the BrxA/BSH/YpdA pathway. This figure is adapted from references (24,69,98).

BSH is required for detoxification of fosfomycin, reactive electrophiles and methylglyoxal **(Fig. 10)** (23,24,148). The BSH-dependent thiol-*S*-transferase (FosB) conjugates BSH to the C2 position of the epoxide ring of fosfomycin for its detoxification (148). The BSH *S*-transferase BstA was shown to add BSH to toxic electrophiles, including chlorinated hydrocarbons and monobromobimane (126). The resulting BS-electrophiles (BSR) are degraded to GlcNAc-Mal and mercapturic acids (AcCysSR) by the BSH *S*-conjugate amidases Bca or BshB2. AcCysSR is exported by efflux pumps encoded by *yfiS* and *yfiU* (126). Furthermore, BSH was shown to function as cofactor for glyoxalases in methylglyoxal detoxification in *B. subtilis* (23,69). BSH conjugates methylglyoxal to BS-hemithioacetal which is isomerized by the glyoxalase-I (GlxA) to *S*-lactoyl-BSH and further hydrolyzed by glyoxalase-I (GlxB) to lactate that is secreted from the cell (23).

In addition, BSH functions in detoxification of heavy metals and metal homeostasis (24,58,99). Under Zn^{2+} excess, BSH acts as Zn^{2+} buffer to limit Zn^{2+} intoxication. The thiolate, amine and carboxylate groups of BSH have high affinities for metal ions and chelate Zn^{2+} leading to formation of the $(BSH)_2$:Zn^{2+} complex (99). BSH-deficient mutants displayed an impaired accumulation of Zn^{2+} because of increased expression of CadA and CzcD efflux pumps (99). BSH also protects against Zn^{2+} toxicity in cells lacking Zn efflux pumps. In addition, BSH has been shown to be involved in Fe^{2+} and Cu^{2+} homeostasis probably by chelating these metals in *B. subtilis* and *S. aureus* (41,82,150).

BSH was further shown to be required for virulence and macrophage infections in *S. aureus* (68,139). The *S. aureus* USA300 *bshA* mutant and the natural SH1000 *bshC* mutant were more sensitive and impaired in survival inside neutrophils and macrophages in whole blood phagocytosis assays (140,143). However, the contribution of BSH to the protection of *S. aureus* against antimicrobial compounds produced in neutrophils or macrophages is poorly understood.

2.3.2.2 Redox regulation of proteins by *S*-bacillithiolation and the Brx/BSH/YpdA pathway in firmicutes

BSH is involved in post-translational thiol-modifications of proteins, which is termed as protein *S*-bacillithiolation and occurs under HOCl stress (98,173). Protein *S*-bacillithiolations are widespread in different firmicutes. In total, 54 *S*-bacillithiolated proteins were identified using shotgun proteomics under HOCl stress in *B. subtilis*, *Bacillus amyloliquefaciens, Bacillus pumilus, Bacillus megaterium*, *Staphylococcus carnosus* and *S. aureus*, including 8 common and 29 unique *S*-bacillithiolated proteins (31,32). The targets for *S*-bacillithiolations are involved in many cellular pathways, such as the biosynthesis of

amino acids, cofactors and nucleotides, protein translation, detoxification and redox-signaling of ROS. In *S. aureus*, the glycolytic glyceraldehyde-3-phosphate dehydrogenase (GapDH) is the most abundant protein in the Cys-proteome, which is *S*-bacillithiolated under HOCl stress at the conserved active site Cys151 (68). *S*-bacillithiolation leads to inactivation of GapDH which could possibly cause a metabolic reconfiguration from glycolysis to the pentose phosphate pathway, providing NADPH for cellular reducing systems, such as the bacillithiol disulfide reductase (YpdA) and TrxR (135). In this work, we characterized the pathways for de-bacillithiolations as the complete Brx/BSH/YpdA redox pathway (94,97). Previous studies showed that BrxA and BrxB catalyze the reduction of *S*-bacillithiolated MetE and OhrR in *B. subtilis* (45,68,94). The bacilliredoxins BrxA and BrxB also catalyze the reduction of *S*-bacillithiolated GapDH in *S. aureus*, leading to Brx-SSB formation (45). However, the enzyme involved in regeneration of Brx activity has remained elusive for a long time.

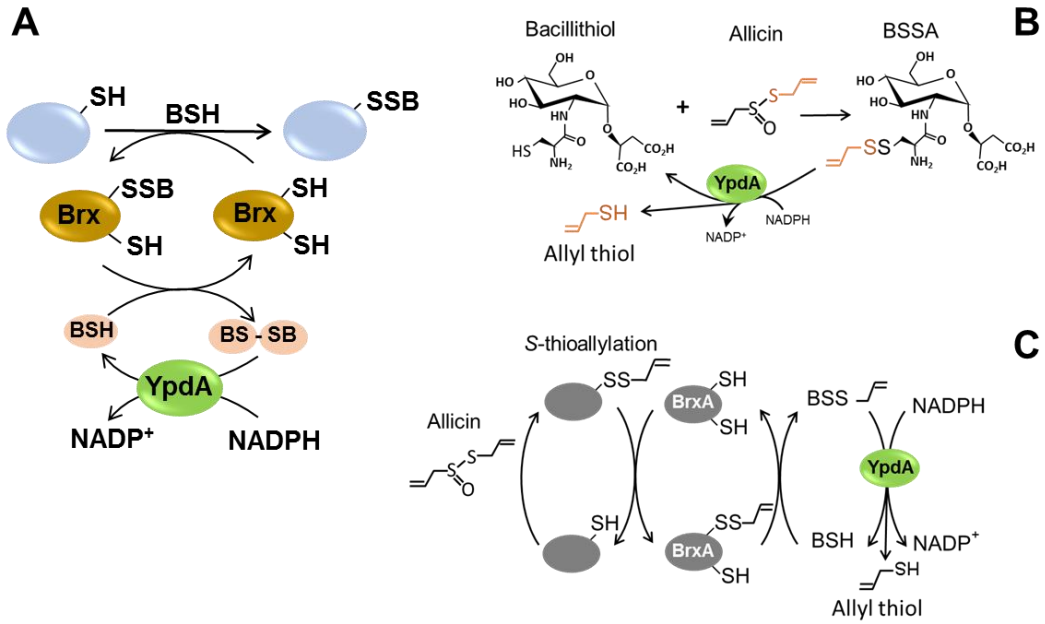

Figure 11. BSH and the Brx/BSH/YpdA pathway function in reversal of *S*-bacillithiolations and *S*-thioallylations. (A) Brx catalyzes the reduction of *S*-bacillithiolated proteins resulting in Brx-SSB formation that is recycled by BSH and YpdA. **(B)** The garlic compound allicin conjugates BSH to *S*-allylmercaptobacillithiol (BSSA), which can be reduced by YpdA to generate BSH and allyl thiol. **(C)** The complete Brx/BSH/YpdA pathway is involved in regeneration of *S*-thioallylated proteins under allicin stress. This figure is adapted from references (94,97).

In this doctoral thesis, I contributed to the biochemical characterization of YpdA as BSSB reductase *in vitro*. YpdA belongs to the flavin disulfide reductase family which uses NADPH as electron donor for reduction of BSSB (111). As revealed by Nico Linzner, the *S. aureus ypdA* mutant showed a strongly enhanced BSSB level and a decreased BSH/BSSB

ratio under control conditions and oxidative stress, indicative for an impaired BSH redox balance (94). Brx-roGFP2 biosensor measurements of Nico Linzner further revealed that the *ypdA* mutant is impaired to regenerate the reduced BSH redox potential (E_{BSH}) under oxidative stress (94). The Tpx-roGFP2 biosensor was applied to reveal an important function of YpdA in detoxification of H_2O_2 and NaOCl (94). Thus, YpdA is essential to regenerate the reduced E_{BSH} during recovery from oxidative stress *in vivo*. I performed NADPH-coupled electron assays with purified YpdA for reduction of different LMW thiol disulfides, such as BSSB, glutathione disulfide (GSSG) and coenzyme A disulfide (94). NADPH consumption of YpdA was only stimulated with BSSB as substrate, but not with any other LMW disulfide. The BSSB reductase activity of YpdA was dependent on the conserved Cys14 active site, which is located in a glycine-rich Rossmann-fold NADPH binding domain ($GGGPC_{14}G$) (94). We further provided evidence that Brx acts in concert with BSH and YpdA in the complete Brx/BSH/YpdA redox cycle for de-bacillithiolation of GapDH-SSB *in vitro* (94) **(Fig. 11A)**. BrxA and BrxB reduce *S*-bacillithiolated GapDH, resulting in Brx-SSB formation. Brx-SSB is reduced by BSH to restore Brx activity, leading to BSSB formation, which is recycled by YpdA on expense of NADPH **(see chapter 2)** (94).

We further studied the role of YpdA and the Brx/BSH/YpdA pathway in protection against allicin stress by regeneration of *S*-thioallylated LMW thiols and protein thiols in *S. aureus* (97). Allicin is a thiol-reactive antimicrobial produced in garlic plants (*Allium sativum*) upon wounding from alliin as precursor (141,167). Allicin was shown to cause a strong thiol-specific oxidative and sulfur stress response and protein damage in the transcriptome of *S. aureus* (97). Allicin leads to depletion of BSH and formation of *S*-thioallylated BSH, termed as *S*-allylmercaptobacillithiol (BSSA) (97). Using biochemical assays I showed that YpdA also uses BSSA as substrate to regenerate BSH **(see chapter 3)** (97). Thus, YpdA can function as BSSA reductase, which depends on the conserved active site Cys14 **(Fig. 11B)** (97). In addition, allicin causes widespread *S*-thioallylation of abundant and redox-sensitive proteins in the proteomes of bacteria, yeast and human cells (9,52,113,115). I could further reveal that the Brx/BSH/YpdA redox pathway catalyzes reduction of *S*-thioallylated GapDH to regenerate its glycolytic activity *in vitro* (97) **(Fig. 11C)**. Taken together, YpdA, BSH and the Brx/BSH/YpdA pathway play important roles in the defense of *S. aureus* against allicin stress to reverse *S*-thioallylations of LMW and protein thiols. Future investigations should reveal the detailed catalytic mechanism of YpdA in BSSB and BSSA reduction.

3. Real-time monitoring of the intrabacterial redox potential with fluorescent protein based redox biosensors

3.1. Dynamic roGFP2-fused redox biosensors for monitoring redox potential changes in eukaryotic and prokaryotic cells

Redox-sensitive roGFP2-based biosensors are meanwhile state-of-the art for the quantification of a thiol-disulfide equilibrium within living cells. Over the last years roGFP2 fused probes have been strongly improved regarding reversibility, quantification and ratiometric properties (108,116,156). The cysteine substitution mutants of the amino acids S147 and Q204 are located on the surface of the ß-barrel in roGFP2 facilitating disulfide bridge formation upon oxidation (38,56) **(Fig. 12A)**. Reduction and oxidation of roGFP2 causes ratiometric changes in the two excitation maxima at 405 and 488 nm, which can be quantified as oxidation degree of the biosensor (156). In reduced roGFP2, the intensity at the 405 nm excitation maximum is low, while intensity at 488 nm excitation maximum is high. Oxidation of roGFP2 leads to increased intensity at the 405 nm maximum and decreased intensity at 488 nm maximum, leading to ratiometric changes in the excitation spectrum **(Fig. 12B)** (108). The 405/488 nm excitation ratio is calculated as oxidation degree of the biosensor which reflects the intracellular GSH redox potential (E_{GSH}) in eukarytotic cells (108,156). Genetically encoded roGFP2 biosensors are widely used to investigate E_{GSH} changes under basal and oxidative stress conditions or in different mutants that are impaired in redox homeostasis. RoGFP2 has a midpoint potential of -280 mV, which enhances the sensitivity of the probe to oxidation (108). Moreover, roGFP2 shows resistance to photoswitching and insensitivity to physiological pH changes, facilitating to study redox potential changes in pathogens under infection conditions inside the acidic phagosome of macrophages (14,108).

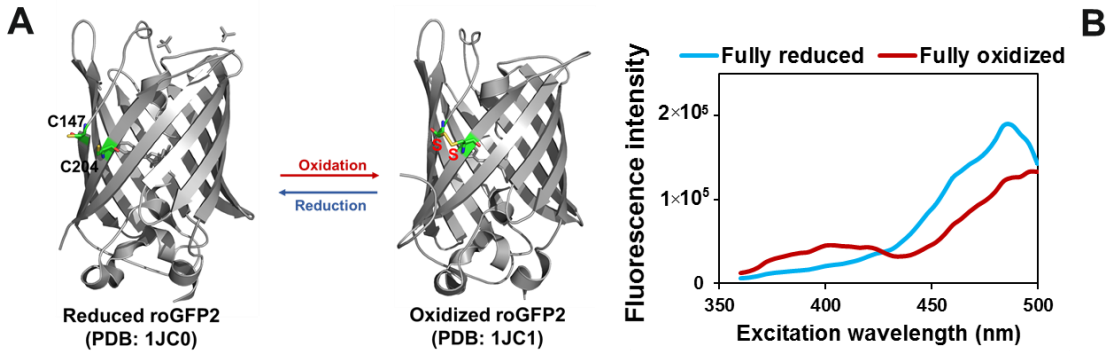

Figure 12. Principle of the ratiometric measurements of roGFP2 biosensor oxidation. (A) Structure of reduced and oxidized roGFP2 and **(B)** ratiometric changes in the excitation maxima at 405 nm and 488 nm upon oxidation. This figure is adapted from references (15,173).

Recently, the roGFP2 probes have been fused to redox enzymes, such as glutaredoxins (Grx) to increase their specificity towards the GSH/GSSG redox pair. Grx1-roGFP2 allows specific equilibration between the 2GSH/GSSG and $roGFP2_{red}$/ $roGFP2_{ox}$ redox couples (108,156). This biosensor is able to monitor nanomolar concentrations of GSSG at high spatio-temporal resolution in living cells and cellular compartments (116,156,173). The steady-state E_{GSH} of cells expressing the Grx-roGFP2 biosensor is similar to that of cells expressing unfused roGFP2, confirming that fused Grx-roGFP2 does not affect the cellular GSH redox potential (108,156). Of note, the Grx1-roGFP2 fused biosensor was shown to be 100,000-fold more sensitive compared to unfused roGFP2 (53).

3.2 Application of the genetically encoded Mrx1-roGFP2 biosensor in mycobacteria

The Mrx1-roGFP2 biosensor has been widely applied as valuable tool to investigate oxidative stress defense mechanisms and the intracellular lifestyle during macrophage infections in the important human pathogen *Mtb* (14,104,114,130,173). The results of Mrx1-roGFP2 measurements in *Mtb* revealed that E_{MSH} inside infected macrophages is heterogeneous with sub-populations showing reduced (-300 mV), oxidized (-240 mV) and basal (-270 mV) levels of E_{MSH} during macrophage infection which depends on different sub-vacuolar macrophage compartments (14,96,173,175) **(Fig. 13)**. In addition, the sub-populations with reduced, oxidized and basal E_{MSH} were different during the time course of infections and also between various multi-drug resistant/ extensively drug-resistant (MDR/XDR) *Mtb* isolates indicating a strongly varying redox balance between *Mtb* isolates. Immune activation further caused an oxidative shift of *Mtb* sub-populations, which resulted from NO stress as part of host innate immune defense (14). The *Mtb* sub-populations were investigated in different vacuolar compartments including early endosomes, autophagosomes and lysosomes. Interestingly, the *Mtb* sub-population located in autophagosome showed almost oxidized E_{MSH}, while those residing in lysosomes were 58% oxidized and the sub-population in early endosomes showed mostly (54%) reduced E_{MSH}. Thus, the biosensor identified the sources of redox heterogeneity as the specific compartments in which *Mtb* resides inside macrophages.

The Mrx1-roGFP2 biosensor was further used to study the impact of ROS-generating anti-TB drugs (e.g., ATD-3169, DAB-10, clofazimine) on the cytoplasmic E_{MSH} of drug-resistant isolates (14,93,174). Low concentrations of ATD-3169 induced redox heterogeneity in MDR/XDR *Mtb* isolates with an irreversible oxidative shift in E_{MSH} (174). This oxidative shift in E_{MSH} might be caused by elevated superoxide generation by the redox-cycling action of the drug. In addition, combination therapies of isoniazid (INH) and inhibitors of

antioxidant responses were found as promising strategy to threat drug resistant *Mtb* isolates (130). Such inhibitors of antioxidant responses were ebselen, vancomycin and phenylarsine oxide that were highly effective in combination with INH to kill drug resistant *Mtb* isolates.

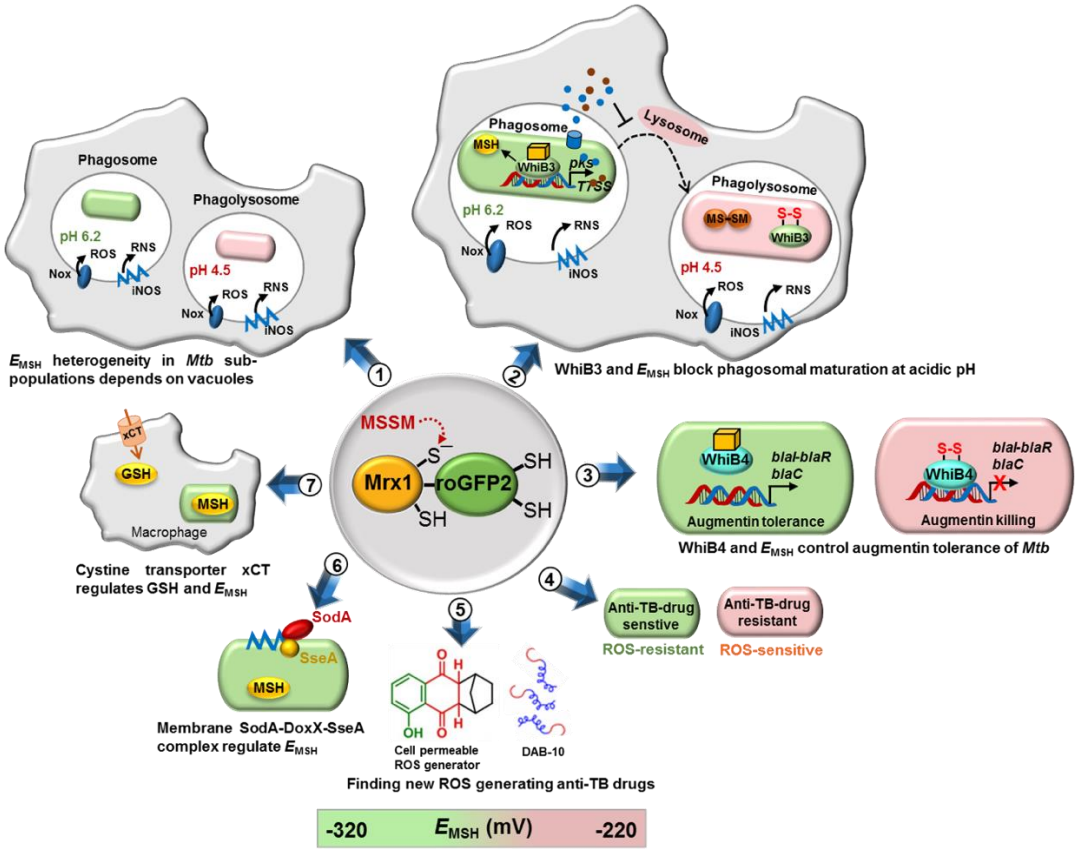

Figure 13. Application of the Mrx1-roGFP2 biosensor for real-time monitoring of the MSH redox potential (E_{MSH}) in *Mtb* to reveal mechanisms of virulence, survival and drug resistance. (1) The oxidative shift of E_{MSH} heterogeneity in *Mtb* sub-populations is caused by specific sub-vacuolar macrophage compartments. **(2)** The WhiB3 sensor and E_{MSH} control type-VII secretion systems and polyketide lipids under acid conditions in the phagosome to inhibit phagosomal maturation. **(3)** The WhiB4 redox sensor and E_{MSH} control expression of ß-lactamase to induce augmentin tolerance in the reduced population and augmentin killing in the oxidized population. **(4)** Isoniazid (INH) resistant *Mtb* isolates have an oxidative E_{MSH} and are highly ROS-sensitive, while INH-sensitive strains are resistant to ROS due to a reduced E_{MSH}. **(5)** Mrx1-roGFP2 biosensor is useful to screen new ROS-generating drugs for E_{MSH} changes as killing mode. **(6)** The membrane-associated oxidoreductase complex (SodA-DoxX-SseA) is involved in radical detoxification and regulates E_{MSH}. **(7)** The cystine-glutamate transporter xCT regulates cystine import into macrophages, resulting in increased host-GSH biosynthesis and reduced E_{MSH} which contributes to TB in a mice infection model. This figure is adapted from references (93,173).

Under infection conditions, *Mtb* utilizes WhiB-like proteins to overcome the oxidative burst of activated macrophages (173). The E_{MSH} was shown to control the activity of the iron-sulfur cluster redox sensor WhiB3 (104). WhiB3 confers acid resistance of *Mtb* which allows survival of *Mtb* inside the acidic phagosome upon immune-stimulation (35,153,165). WhiB3 mediates acid resistance and inhibits phagosomal maturation, which is

linked to changes in E_{MSH} under infections. WhiB3 controls genes for lipid biosynthesis, secretion of the type-VII-secretion effectors and MSH metabolism under acidic stress. The limited decrease in pH upon acidification of the phagosome (pH ~6.2) results in a reductive shift of E_{MSH} sub-populations. WhiB3 and MSH are key regulators for this reductive shift in E_{MSH}. WhiB3 was shown to protect *Mtb* from acid stress by controlling genes that restrict phagosomal maturation to subvert acidification and by down-regulation of the innate immune response. These results revealed a link between phagosome acidification, the reductive shift in E_{MSH} and virulence of Mtb that is controlled by WhiB3 mediating acid resistance and inhibiting phagosomal maturation as mechanism of persistent and chronic *Mtb* infections (104).

Furthermore, the role of E_{MSH} was investigated in the mode of action of the combination therapy with augmentin, consisting of a β-lactam antibiotics (amoxicillin) and a β-lactamase inhibitor (clavulanate) **(Fig. 13)**. Augmentin leads to an oxidative shift in E_{MSH} by causing cell wall stress and ROS generation, which increased its killing effect (114). The FeS-cluster redox sensor WhiB4 was found to act as regulator of β-lactam antibiotics resistance and the oxidative shift in E_{MSH} sub-population under augmentin treatment (114). The oxidized E_{MSH} and oxidation of WhiB4 caused down-regulation of the β-lactamase-encoding *blaC* gene which potentiates ß-lactam drug action to promote the killing of *Mtb*. In contrast, reduction of WhiB4 conferred tolerance to augmentin caused by derepression of the *blaC* gene (114).

Due to the frequent treatment of *Mtb* infections with INH and combination therapies, there is an increasing prevalence of INH and MDR/XDR resistant *Mtb* strains. Thus, the E_{MSH} values were compared for different antibiotic resistant isolates to shed light on the evolution of drug-resistant *Mtb*. Importantly, INH-resistant isolates, MDR/XDR and other drug-resistant clinical *Mtb* isolates displayed an oxidized E_{MSH}, ranging from − 273 mV to − 280 mV **(Fig. 13)** (14,130). The higher ROS-sensitivity of antibiotics resistant isolates was observed using Mrx1-roGFP2 biosensor measurements and survival assays. Thus, the evolution of drug resistance is associated with changes in the basal E_{MSH} and shifted to the oxidized redox state in multiple resistant *Mtb* isolates. It was also shown that antibiotics that produce ROS or block antioxidant responses are in combination with INH more potent to induce oxidative shift in E_{MSH} during infections and should be promising strategies to tackle tuberculosis disease and to combat drug resistant isolates (130).

The Mrx1-roGFP2 biosensor further revealed the function of the novel membrane-associated oxidoreductase complex (MRC), which includes the superoxide dismutase

(SodA), an integral membrane protein (DoxX) and the conserved thiol oxidoreductase (SseA), and was functionally linked to radical detoxification during the oxidative burst **(Fig. 13)** (119,173). Single mutants in each MRC component are similar sensitive to radical stress and showed an oxidized E_{MSH}. Thus, a link between the oxidative stress resistance MRC complex and E_{MSH} in *Mtb* was identified to combat the oxidative burst under infections (119).

For a mice model of tuberculosis, the Mrx1-roGFP2 was applied to reveal a link between E_{MSH} and the xCT transporter required for GSH-uptake into macrophages (173). The GSH pool of macrophages depends on the xCT cystine-glutamate transporter, which is induced during *Mtb* infection. The deletion of xCT resulted in protection against TB and decreased pulmonary pathology in the mice lung. *Mtb* populations showed an oxidized shift of E_{MSH} in the infected mice xCT mutant, which is caused by a decreased GSH pool inside macrophages **(Fig. 13)**. This study reveals a link between macrophage-derived GSH and *Mtb* E_{MSH}. In addition, inhibitors of the xCT transporter were developed as host-directed drugs for TB treatment (22,173).

In summary, the Mrx1-roGFP2 biosensor was applied to study the mechanisms of redox heterogeneity, persistence and survival of *Mtb* under acidic conditions inside macrophage vacuolar compartments, the evolution and changes in E_{MSH} of drug resistant *Mtb* isolates, the regulation and mode of action of combination therapy involving ROS-generating antibiotics as promising future anti-TB drugs. These findings were written in the review published in *Free Radical Biology Medicine* as special biosensor review about applications in bacteria **(see chapter 4)** (173).

3.3. Stable integration of the Mrx1-roGFP2 biosensor to monitor dynamic changes of the mycothiol redox potential in *C. glutamicum*

As one major part of the PhD thesis, I designed a novel genome-encoded Mrx1-roGFP2 biosensor to measure dynamic changes in E_{MSH} in the industrial platform bacterium *C. glutamicum* **(see chapter 5)** (173). Expression of Mrx1-roGFP2 was previously shown to have no effect on cellular metabolism, stress resistance, enabling precise measurement of E_{MSH} changes in *Mtb* (14,156). For construction of the Mrx1-roGFP2 biosensor in *C. glutamicum,* Mrx1 (Cg0964) with the redox-active CxxC motif was fused to roGFP2 (173). Under oxidative stress, increased MSSM levels should react with the Mrx1 active site Cys to *S*-mycothiolated Mrx1, followed by the transfer of the MSH moiety to roGFP2 which rearranges to the roGFP2 disulfide resulting in ratiometric changes of the 400/488 excitation ratios **(Fig. 14)**.

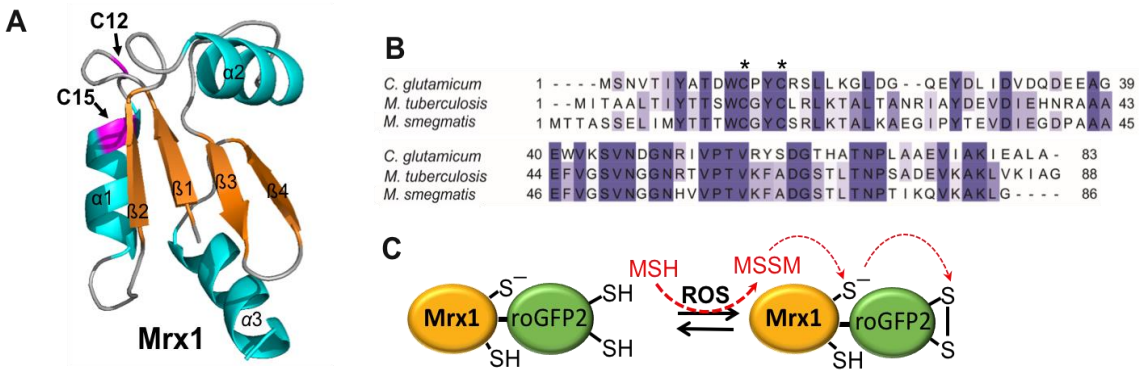

Figure 14. Structure and alignment of Mrx1 homologs, principle and specific response of the Mrx1-roGFP2 biosensor to MSSM. (A) The Mrx1 structure of *C. glutamicum* was modelled using the template of *M. tuberculosis* Rv3198A (PDB code: 2LQO). **(B)** The Mrx1 homologs Cg0964 of *C. glutamicum*, Rv3198A of *M. tuberculosis* and MSMEG_1947 of *M. smegmatis* were aligned with ClustalW2 and presented in Jalview. **(C)** Under ROS stress, MSH is oxidized to MSSM which reacts with Mrx1 to *S*-mycothiolated Mrx1. MSH is transferred from Mrx1 to the roGFP2 moiety leading to *S*-mycothiolated roGFP2 which is rearranged to the roGFP2 disulfide. The roGFP2 disulfide leads to a structural change resulting in ratiometric changes of the 400 and 488 excitation maxima of Mrx1-roGFP2. This figure is from reference (173).

Mrx1-roGFP2 was previously shown to be specifically oxidized by MSSM and oxidants in *Mtb in vitro* (14,173). Thus, we measured the direct response of Mrx1-roGFP2 to oxidants *in vitro*. Our Mrx1-roGFP2 biosensor responds very fast to the oxidants H_2O_2 and NaOCl *in vitro*, when compared to unfused roGFP2 **(see chapter 5)**. These results are in agreement with the Grx1-roGFP2 responses to different oxidants as shown previously (96,116,173). However, expression of plasmid-encoded Mrx1-roGFP2 in *C. glutamicum* resulted only in roGFP2 fluorescence of < 20 % of cells. Thus, we constructed the genome-encoded Mrx1-roGFP2 biosensor, which showed equal fluorescence in the majority of cells (99%) **(Fig. 17)** (173). The results of the genome-integrated Mrx1-roGFP2 biosensor revealed that *C. glutamicum* maintains a highly reducing intrabacterial E_{MSH} throughout the growth curve with basal E_{MSH} levels of ~-296 mV (173). Consistent with the H_2O_2 resistant phenotype, *C. glutamicum* responds only weakly to 40 mM H_2O_2, but is rapidly oxidized by low doses of NaOCl. We further monitored basal E_{MSH} changes and the H_2O_2 response in various mutants which are compromised in redox-signaling of ROS (OxyR, SigH) and in the antioxidant defense (MSH, Mtr, KatA, Mpx, Tpx). While the probe was constitutively oxidized in the *mshC* and *mtr* mutants, a smaller oxidative shift in basal E_{MSH} was observed in the *sigH* mutant **(Fig. 15)**. The catalase KatA was confirmed as major H_2O_2 detoxification enzyme required for fast biosensor re-equilibration upon return to non-stress conditions. In contrast, the peroxiredoxins Mpx and Tpx had only little impact on E_{MSH} and H_2O_2

detoxification **(Fig. 16)**. Further live imaging experiments using confocal laser scanning microscopy revealed the stable biosensor expression and fluorescence at the single cell level **(Fig. 17)** (173).

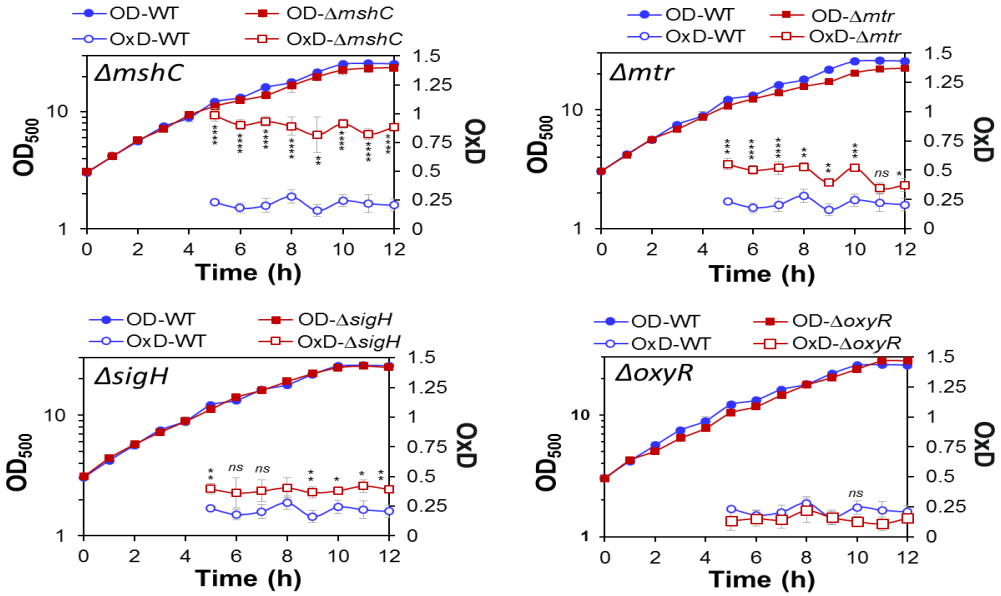

Figure 15. Deletions of *mshC, mtr* and *sigH* affected the basal E_{MSH} during the growth of *C. glutamicum*. The basal level of E_{MSH} was measured using Mrx1-roGFP2 along the growth curve in *C. glutamicum* wild type and in Δ*mshC* **(A)**, Δ*mtr* **(B)**, Δ*sigH* **(C)** and Δ*oxyR* **(D)** mutants. The basal E_{MSH} showed an oxidative shift in the Δ*mshC*, Δ*mtr and* Δ*sigH* mutants, but not in the Δ*oxyR* mutant **(D)**. This figure is from reference (173).

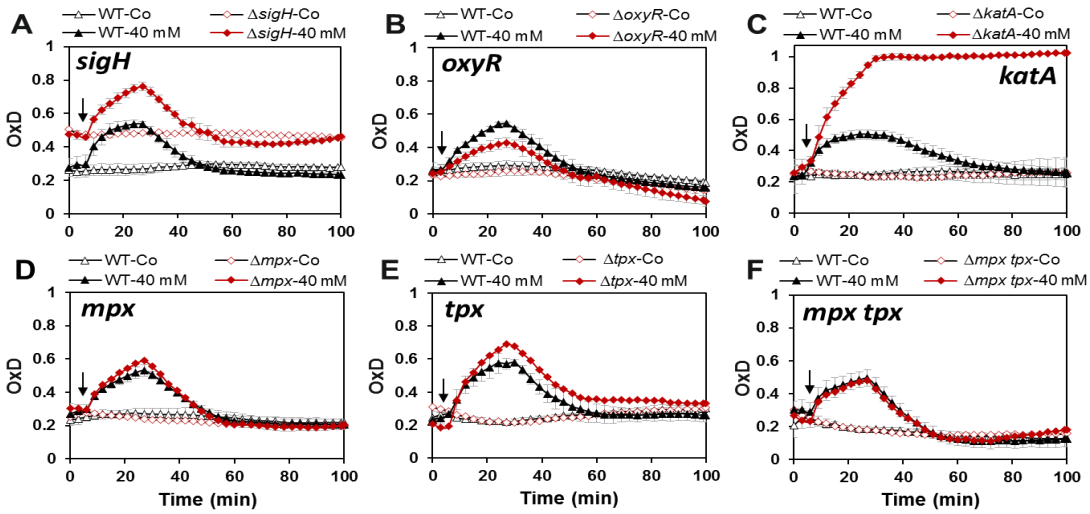

Figure 16. Kinetics of H_2O_2 detoxification in *C. glutamicum* mutants deficient for redox-regulators (OxyR, SigH) or antioxidant enzymes (KatA, Mpx, Tpx). The Mrx1-roGFP2 biosensor response and kinetics of recovery was analyzed under 40 mM H_2O_2 stress in *C. glutamicum* wild type and mutants deficient for the disulfide stress regulatory sigma factor SigH **(A)**, the peroxide-sensitive repressor OxyR **(B)** and the catalases and peroxiredoxins for H_2O_2 detoxification (KatA, Mpx, Tpx) **(C-F)**. This figure is from reference (173).

In conclusion, the stably expressed Mrx1-roGFP2 biosensor was successfully applied to monitor dynamic E_{MSH} changes in *C. glutamicum* during the growth, under oxidative stress and in different mutants revealing the impact of Mtr, SigH, OxyR and KatA for the basal level E_{MSH} and efficient H_2O_2 detoxification under oxidative stress. The Mrx1-roGFP2 can be applied to monitor changes in E_{MSH} during industrial production of amino acids and other bioactive compounds under fermentation conditions in *C. glutamicum*.

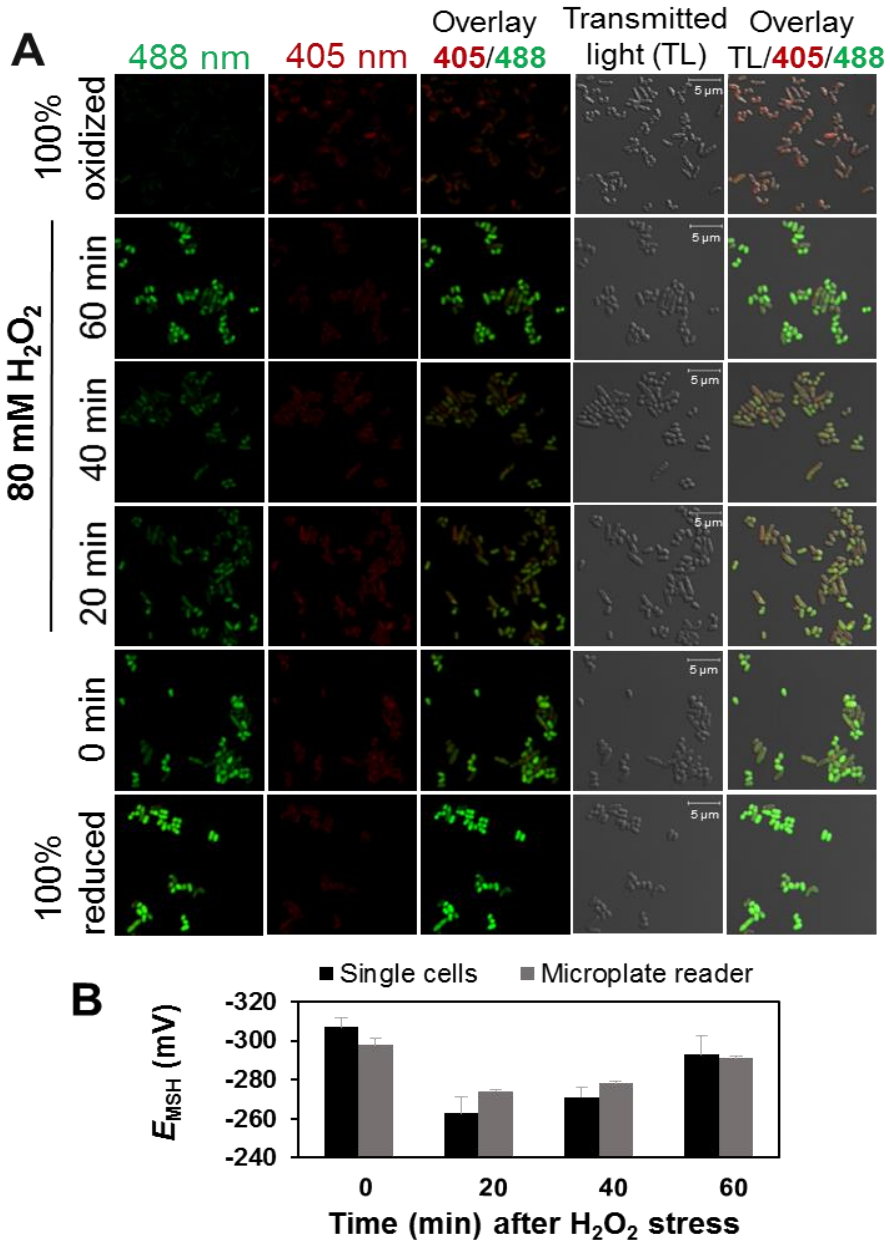

Figure 17. Live-imaging of Mrx1-roGFP2 fluorescence changes in *C. glutamicum* wild type under H_2O_2 stress at the single cell level. (A) *C. glutamicum* wild-type cells expressing Mrx1-roGFP2 were challenged with 80 mM H_2O_2 for 20-60 min, block with 10 mM NEM and visualized by confocal laser scanning microsopy. **(B)** The intracellular E_{MSH} was calculated based on the 405/488 nm excitation ratio of *C. glutamicum* Mrx1-roGFP2 cells after H_2O_2 treatment using confocal imaging and microplate reader measurements. This figure is from reference (173).

4. Thiol based redox-sensor in response to oxidative burst

ROS and RCS affect the cellular redox homeostasis and induce post-translational thiol-modifications in proteins, including protein disulfides that are termed as thiol-redox switches. Bacterial redox-sensing transcription factors often sense ROS and RCS via thiol-modifications, which functions in redox regulation to induce specific ROS or RCS detoxification pathways (34,182). Thiol-modifications of redox-sensing transcription factors often lead to structural and conformational changes of the DNA binding helix-turn-helix motifs, leading to inactivation or activation of the transcriptional regulators to induce transcription of regulons that protect cells against ROS or RCS toxicity (182). Thus far, many different redox-sensing regulators have been discovered as sensors of a wide range of redox-active species (e.g. ROS, RCS, RES) and antibiotics in bacteria, which have been reviewed previously (49,59,95,159). As second part of my thesis, I discovered the novel HOCl-specific redox regulator HypS in mycobacteria, which confers resistance to HOCl stress and antibiotics. In this section, the current state-of-the art of redox-sensing transcriptional regulators for ROS and RCS will be summarized including the results about HypS redox-regulation and functional characterization.

4.1 OxyR as thiol-based peroxide redox sensor of *C. glutamicum*

OxyR is the best-characterized redox-sensing transcription factors which was first discovered in *E. coli* and responds specifically to H_2O_2 stress (10). OxyR belongs to the widely distributed LysR-family of transcription factors, which were characterized as transcriptional activators or repressors (10,28,71,171). In *E. coli*, OxyR functions as tetrameric activator of transcription of a large peroxide regulon (33,191), while the OxyR homolog of *C. glutamicum* was characterized as transcriptional repressor (112,171). The redox-sensing mechanism of OxyR in *E. coli* involves the formation of an intramolecular disulfide between Cys199 and Cys206 in each subunit of the OxyR tetramer (33). OxyR oxidation induces a large conformational change which reorients the DNA binding HTH motifs in each subunit to recruit the RNA polymerase for initiation of transcription of the OxyR regulon (33,109).

The OxyR regulon functions in the defense against H_2O_2 stress, including genes encoding NADH peroxidase (*ahpCF*), catalase (*katG*), glutathione reductase (*gor*), thioredoxin (*trxC*), glutaredoxin (*grxA*). Thus, the OxyR regulon is mainly involved in peroxide detoxification or reduction of protein disulfides to restore redox homeostasis in response to H_2O_2 stress (33,192). The OxyR repressor of *C. glutamicum* and *C. diphtheriae*

controls similar genes, which are associated with H_2O_2 removal and the repair of protein damages **(Fig. 18)** (83,171). In *C. glutamicum*, OxyR represses the transcription of 23 genes, including catalase (*katA*), ferrochelatase (*hemH*), Fe-storage miniferritin (*dpS*) and ferritin (*ftn*), Fe-S-cluster assembly machinery (*sufR*), putative MFS secondary transporter (*proP*) and subunits of cytochrome bd oxidase (*cyd*), which are derepressed in the wild type under H_2O_2 stress and in the *oxyR* mutant (112). The measurements with the Mrx1-roGFP2 biosensor revealed a decreased biosensor response under H_2O_2 stress in the *oxyR* mutant, due to constitutive expression of the catalase KatA which confers a H_2O_2 resistance phenotype (173). In addition, the *katA* mutant was strongly impaired in H_2O_2 detoxification and displayed a very fast and strongly increased biosensor oxidation under H_2O_2 stress (173). These results indicate the major function of the OxyR-controlled catalase KatA in H_2O_2 detoxification in *C. glutamicum* (112,134,173).

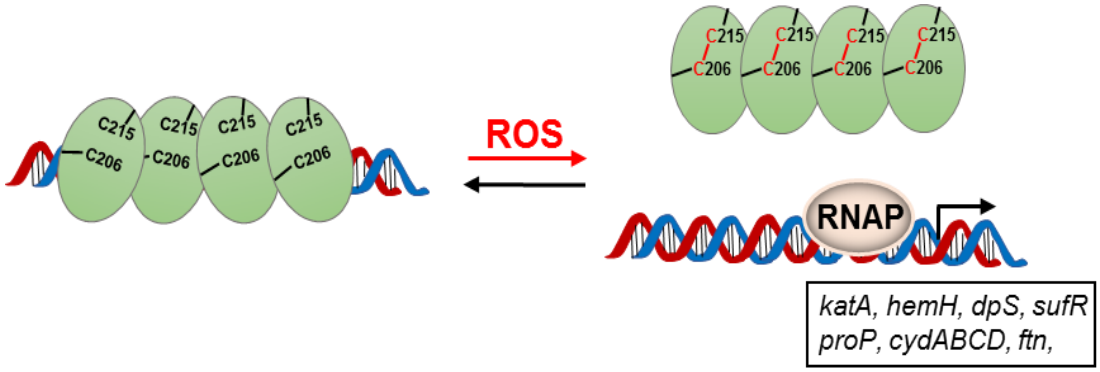

Figure 18. The redox-switch mechanism of the H_2O_2-specific OxyR regulator in *C. glutamicum*. The OxyR repressor senses H_2O_2 stress by formation of an intramolecular disulfide between Cys206 and Cys215 in each subunit of the tetramer, leading to derepression of transcription of the OxyR regulon genes, encoding catalase (*katA*), ferrochelatase (*hemH*), Fe-storage miniferritin (*dpS*), ferritin (*ftn*), Fe-S-cluster assembly machinery (*sufR*), putative MFS secondary transporter (*proP*) and subunits of cytochrome bd oxidase (*cyd*). This figure is adapted from reference (59).

The regulatory mechanism and structural changes of the OxyR repressor of *C. glutamicum* under H_2O_2 stress were recently investigated (134). The *C. glutamicum* OxyR protein has a tetrameric structure which differs from previously published structures of OxyR homologs of other bacteria. The structural and kinetic results revealed that C206, T107, R278, and T136 are located in OxyR active-site pocket and are essential for H_2O_2 binding and reduction. Four N-terminal DNA-binding domains of the OxyR tetramer bind to two distinct operators upstream and downstream of the *katA* transcription start point (134). Oxidation of the active-site Cys206 leads to intramolecular disulfide formation with Cys215, which causes allosteric structural changes at the C-terminal regulatory domain in the dimer

interface. The structural changes in OxyR upon oxidation leads to dissociation of the HTH motifs from the operators to facilitate initiation of transcription by the RNAP (134). The increased expression of KatA leads to ROS detoxification, promoting the growth of *C. glutamicum* during recovery from H_2O_2 stress (134,173).

4.2 The MarR-family of oxidative stress and antibiotic resistance regulators in mycobacteria

The MarR family of multiple antibiotics resistance regulators, as discovered originally for the MarR repressor of *E. coli* (5,6), plays an important role to control drug resistance mechanisms in many human pathogens (49). MarR family proteins are widespread in bacteria and archaea and control a variety of cellular functions, including adaptation to environmental changes, oxidative stress, virulence, metabolism and resistance to phenolic compounds, solvents, disinfections and antibiotics (37,51). In the major pathogen *Mtb*, eight MarR-family homologs have been annotated, including Rv0042c, Rv0880, Rv2011c, Rv1049, Rv2327, Rv0737, Rv2887 and Rv1404 (49). The MarR-type repressor Rv1404 controls acid stress resistance and virulence (57). Rv0678 controls the resistance-nodulation-cell division (RND) transporters MmpS5-MmpL5 (mycobacterial membrane protein small and large) which are involved in lipid and fatty acid export during cell wall biosynthesis (142). Rv0880 is involved in the resistance to the antibiotic bedaquiline (136) and Rv2887 was shown to control the SAM-dependent methyltransferase Rv0560c, which confers resistance to the new anti-mycobacterial imidoazopyridine-based drugs MP-III-71 and pyridobenzimidazole 14 (185,188).

Recently, the structural mechanism of ligand-mediated inhibition of DNA binding activity of Rv2887 was shown in the presence salicylate (SA) and para-aminosalicylic acid (PAS) as anti-mycobacterial drug analogue (46). This provides the basis to design new anti-TB drugs which target MarR-type proteins to combat life-threatening TB-infections.

Structural studies have revealed that MarR-family proteins are homodimers with winged helix-turn-helix (wHTH) motifs in each subunit that bind with their recognition α-helices to palindromic sequences in adjacent major groves of the DNA (37,51). The majority of MarR proteins are transcriptional repressors that negatively control transcription of divergently located genes. The DNA binding activity is often inhibited by small molecules, such as phenolic compounds (e.g. salicylate, benzoate, quinones) or metals, which act as ligands and bind a shared ligand-binding pocket between the wHTH motifs and dimerization domains leading to structural rearrangements of the DNA recognition helices (37,51).

Apart from ligand-binding, some MarR-type regulators have conserved Cys residues, act as redox switches and respond to ROS, RCS or RES by thiol-oxidation or *S*-alkylation (8,59). Structurally well characterized redox-sensitive MarR-type regulators are the MarR/OhrR- and MarR/DUF24-family regulators of *B. subtilis*, *Xanthomonas campestris* and *S. aureus*, which respond to ROS, HOCl and RES via thiol-based mechanisms and control oxidative stress defense mechanisms, quinone detoxification enzymes, virulence and antibiotics resistance (91,95,166). These MarR/OhrR-family proteins have been classified in one-Cys-type and two-Cys-type repressors based on the number of Cys residues and the resulting redox-switch model. Two different redox-switch models of the OhrR-repressors have been mechanistically and structurally characterized in *B. subtilis* and *Xanthomonas campestri* (8,37,51,59,64,91,131,169). The *B. subtilis* $OhrR_{Bs}$ is the prototype of a one-Cys-type repressor, which senses ROOH and NaOCl by thiol-oxidation to Cys-sulfenic acid that reacts further with the low molecular weight thiol bacillithiol to *S*-bacillithiolated OhrR protein (91,166). *S*-bacillithiolation leads to inactivation of OhrR and transcriptional derepression of the *ohrA* peroxiredoxin gene **(Fig. 19)**.

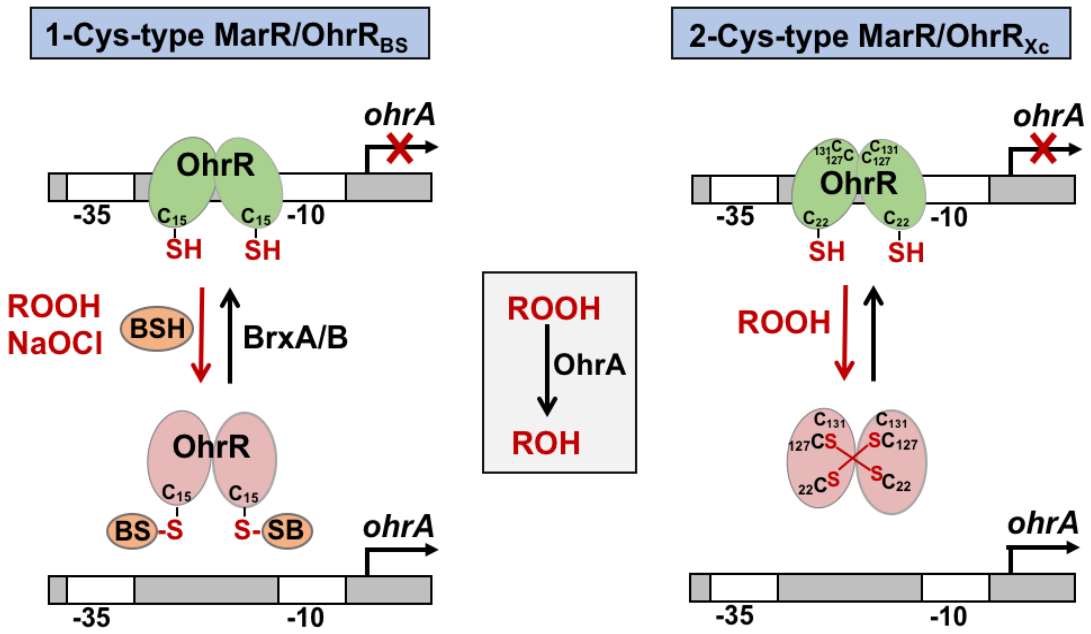

Figure 19. Redox-sensing mechanisms by 1-Cys and 2-Cys-type MarR/OhrR-family repressors. Under organic hydroperoxide (ROOH) stress, the 1-Cys OhrR protein of *B. subtilis* is *S*-bacillithiolated at its Cys15, leading to derepression of *ohrA* that encodes a thiol-dependent peroxiredoxin. The 2-Cys OhrR protein of *X. campestris* is controlled by intersubunit disulfide formation between C22 and C127' of opposing subunits under ROOH stress to regulate *ohrA* expression. This figure is adapted from reference (59).

In contrast, the 2-Cys-type OhrR protein of *X. campestris* was shown to sense OHP via intersubunit disulfide formation between the N-terminal redox-sensing Cys22 and the C-terminal Cys127' of opposing subunits of the OhrR dimer **(Fig. 19)** (64,131,169). This 2-Cys-type oxidation model was confirmed for other two-Cys-type MarR/DUF24-family regulators (HypR, YodB) of *B. subtilis* which are inactivated by intersubunit disulfide formation between N- and C-terminal Cys residues of adjacent subunits (8,59).

In *Mtb*, the redox-sensing MarR/OhrR-type repressor MosR represses transcription of the adjacent *rv1050* gene encoding an uncharacterized oxidoreductase which is involved in the defense against oxidative stress by detoxification of H_2O_2 (17,37). MosR contains four Cys residues (Cys10, Cys12, Cys96, Cys147) and senses H_2O_2 by its redox-sensing Cys12 leading to formation of a Cys10-Cys12 intramolecular disulfide. MosR oxidation occurs under H_2O_2 stress and by INF-γ-activated macrophages leading to structural changes in the DNA binding domain and derepression of *rv1050* oxidoreductase (16).

In the non-pathogenic *M. smegmatis*, OhrR controls expression of the *ohr* peroxiredoxin, which contributes to OHP and INH resistance (47,152). Moreover, the survival of *ohrR* mutant was improved inside macrophages. OhrR senses OHPs also via its conserved Cys13, but the detailed redox-sensing mechanism has yet be explored (47). Since OhrR of *M. smegmatis* belongs to the one-Cys-type OhrR proteins, it is possible that the redox-sensing mechanism of OhrR involves protein *S*-mycothiolation.

Interestingly, the MexR repressor of *Pseudomonas aeruginosa* controls multidrug efflux pumps which are required for the defense against H_2O_2 stress and antibiotics (27,29). Antibiotic-induced ROS production was implicated in the thiol-oxidation sensing mechanism of MexR, which renders *P. aeruginosa* resistant to multiple clinical important antibiotics, such as quinolones, β-lactams, tetracycline, chloramphenicol and novobiocin (27,29). Thus, redox-sensing MarR-type repressors of pathogens often control oxidative stress defense mechanisms and antibiotics resistance to allow adaptation to the host environment. The discovery of new redox-sensing MarR-type regulators that regulate ROS and antimicrobial resistance in *Mtb* opens up new avenues in anti-TB drug research to combat *Mtb* infections. In this PhD I have contributed to this topic by characterization of the novel MarR-type repressor HypS which senses HOCl and controls a multidrug efflux pump HypO that confers HOCl and antibiotics resistance. The results are described in chapter 6 and summarized in the following section.

4.3. HypS as a novel MarR-family redox sensor of hypochlorite stress in *M. smegmatis*

The novel redox-sensing MarR-type repressor HypS (MSMEG_4471) of *M. smegmatis* is widely conserved across different mycobacteria including *Mtb* (Rv2327). In my PhD thesis, I have shown that HypS senses HOCl stress via its conserved Cys58 by intersubunit disulfide formation and regulates expression of the multidrug efflux pump HypO under HOCl stress **(see chapter 6, Fig. 20 and 21)**. Based on the high conservation of the *hypSO* locus and of the regulatory promoter regions, the regulatory model and function of HypS should be similar also in *Mtb*. HypS was previously identified in the global redox proteomics approach OxICAT as highly oxidized exhibiting 42% increased oxidation at its single Cys58 under NaOCl stress (60). DNA binding assays showed that HypS binds specifically to 8-5-8 bp inverted repeat in the promoter regions of the *hypSO* operon, which is conserved across mycobacteria. HypS oxidation under NaOCl stress leads to its inactivation and dissociation of HypS from its promoter DNA. Mutation of Cys58 did not affect the DNA binding activity of HypS, but redox sensing of NaOCl was completely abolished. The role of Cys58 in redox-sensing was further confirmed in growth and survival assays under NaOCl stress, since the *hypSC58S* mutant was unable to complement the NaOCl resistant survival phenotype of the *hypS* mutant.

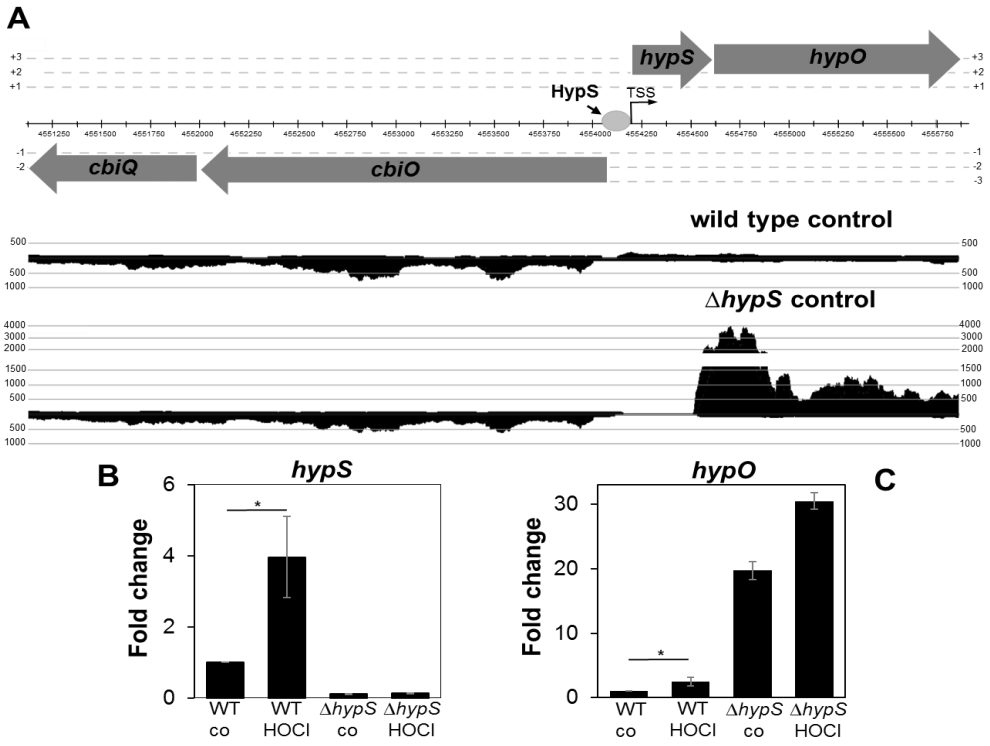

Figure 20. Deletion of *hypS* results in derepression of the *hypSO* operon. (A) The transcriptional landscape of the *hypSO* operon in *M. smegmatis* wild type and the *hypS* mutant confirmed the derepression of the efflux pump-encoding *hypO* in the *hypS* mutant. Transcription of *hypS* **(B)** and *hypO* **(C)** were analyzed using qRT-PCR in the *M. smegmatis* wild type and the *hypS* mutant before (control) and 30 min after exposure to 500 µM NaOCl stress. This figure is from the submitted manuscript (chapter 6).

Using non-reducing SDS-PAGE, we could show that HypS is reversibly oxidized under NaOCl stress to form intersubunit disulfides between Cys58-Cys58' in opposing subunits *in vitro* **(Fig. 21)**. Structural modelling revealed that Cys58 is located in close proximity to Cys58' in the adjacent subunit of the HypS dimer to allow for disulfide formation. HypS oxidation causes its dissociation from the *hypSO* operator *in vitro*, indicating that the DNA binding activity is inhibited in oxidized HypS protein probably due to structural changes in the wHTH motif. However, CD measurements did not reveal major structural changes upon HypS oxidation, suggesting local changes in the wHTH motifs which might lead to loss of DNA binding. Future crystal structure analyses will reveal the conformational changes of HypS upon oxidation.

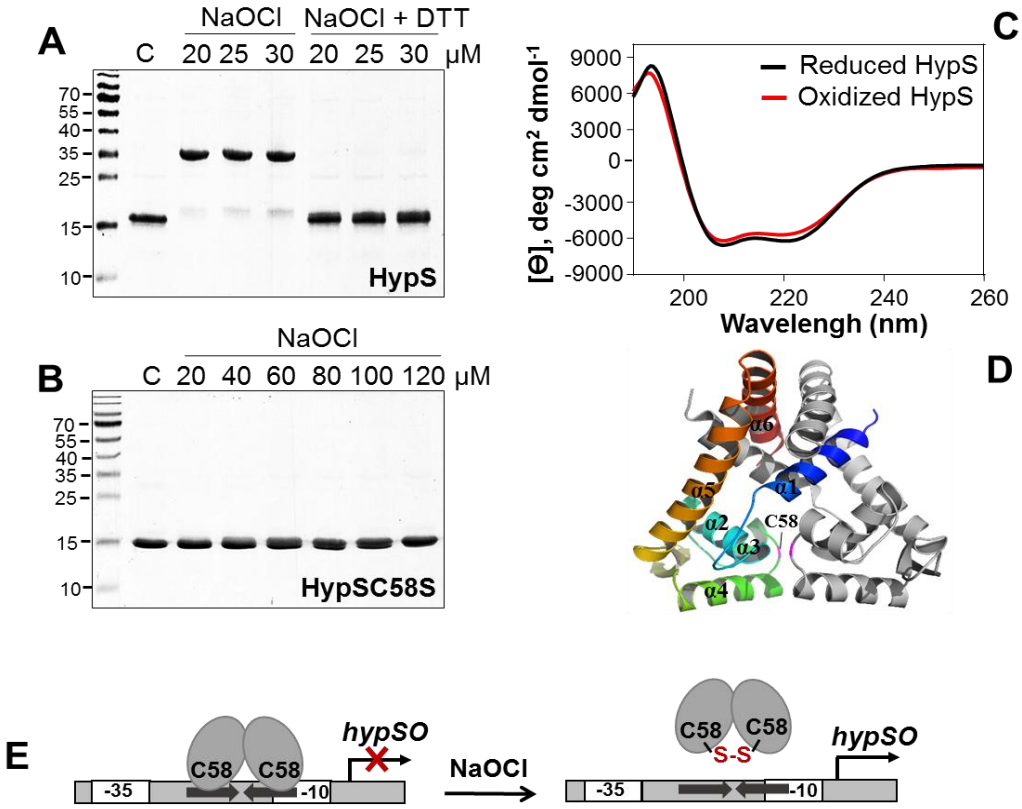

Figure 21. HypS is oxidized to intersubunit disulfides under NaOCl stress. (A) HypS is oxidized by NaOCl to disulphide-linked HypS dimers migrating at the size of 35 kDa, which are reversible with DTT. **(B)** HypSC58S protein is not sensitive to oxidation. **(C)** The CD spectra of reduced and oxidized HypS proteins show a similar strong α-helical content and no major structural changes upon oxidation. **(D)** The structural model of HypS was generated using the template of *M. tuberculosis* H37Rv Rv0880 (PDB code: 4YIF). **(E)** Model for redox-regulation of HypS in *M. smegmatis* in response to NaOCl stress. HypS senses NaOCl stress by Cys58-Cys58' intersubunit disulfide formation, leading to dissociation of HypS from its promoter and derepression of *hypO* transcription, which confers resistance to NaOCl and antibiotics. This figure is from the submitted manuscript (chapter 6).

Inhibition of the repressor activity of HypS due to thiol-oxidation causes derepression of the *hypO*-encoded multidrug efflux pump, which conferred resistance under NaOCl stress and antibiotic exposure, such as rifampicin and erythromycin **(see chapter 6)**. The derepression of the *hypSO* operon in the *hypS* mutant was confirmed by RNA-seq transcriptomics and qRT PCR **(Fig. 20)**. In addition, the deletion of *hypS* resulted in upregulation of 27 genes of the SOS/LexA regulon, indicating a DNA-damage response **(see chapter 6)**. Among the LexA-regulated genes, *MSMEG_0827* encodes another possible drug transporter, which could contribute to the antibiotics resistance phenotype observed in the *hypS* mutant. However, the conserved operator sequence was only detected upstream of the *hypSO* operon, not in any of the up-regulated LexA regulon genes, indicating no direct regulation of *lexA* or LexA-regulon genes by HypS. Thus, the up-regulation of the LexA regulon in the *hypS* mutant requires further investigation.

In conclusion, we have characterized the redox-sensing MarR-type regulator HypS which controls HOCl and antimicrobial resistance through the HypO efflux pump, which is possibly involved in the export of HOCl and the antibiotics, such as rifampicin and erythromycin, in *M. smegmatis.* Of the eight annotated MarR proteins in *Mtb*, fours MarR-type regulators were shown to be implicated in drug resistance, including Rv0678, Rv0880 and Rv2887 (136,142,185,188). Thus, the *Mtb* homologue Rv2327 might be also involved in HOCl and antimicrobial resistance by the control of the HypO homologous efflux pump which remains an interesting subject for future investigations.

5. Conclusion and future perspectives

Bacteria have developed various defense mechanisms for protection against ROS and RCS which are encountered during aerobic respiration, external stressors or infection conditions. LMW thiols, thiol-disulfide oxidoreductases and redox-sensing transcriptional factors are the main factors involved in redox-sensing, detoxification and protein repair to restore the redox and protein homeostasis during recovery from oxidative stress in bacteria. In this doctoral thesis, I have engineered a novel Mrx1-roGFP2 biosensor to monitor dynamic changes in E_{MSH} in different *C. glutamicum* mutants along the growth curve and under oxidative stress. Further applications of this probe should be directed to monitor E_{MSH} changes during industrial fermentation processes or during the switch from anaerobic to aerobic conditions. My results further contributed to the biochemical characterization of YpdA as BSSB and BSSA reductase under ROS and allicin stress in *S. aureus*. Finally, the MarR-family regulator HypS was described as a novel HOCl-sensing redox-switch which contributes to the resistance of *M. smegmatis* towards HOCl and antibiotics. These results shed light on adaptation mechanisms towards oxidative stress in different Gram-positive bacteria, including *C. glutamicum*, *S. aureus, M. smegmatis*. To identify redox-sensitive proteins that are essential for survival under infection conditions can pave the way for developing new drugs to combat life-threatening bacterial infections.

References

1. Abdelmohsen UR, Bayer K, Hentschel U. Diversity, abundance and natural products of marine sponge-associated actinomycetes. *Nat Prod Rep* 31: 381-399, 2014.
2. Abdelmohsen UR, Grkovic T, Balasubramanian S, Kamel MS, Quinn RJ, Hentschel U. Elicitation of secondary metabolism in actinomycetes. *Biotechnol Adv* 33: 798-811, 2015.
3. Abreu IA, Cabelli DE. Superoxide dismutases-a review of the metal-associated mechanistic variations. *Biochim Biophys Acta* 1804: 263-74, 2010.
4. Albesa-Jove D, Chiarelli LR, Makarov V, Pasca MR, Urresti S, Mori G, Salina E, Vocat A, Comino N, Mohorko E, Ryabova S, Pfieiffer B, Lopes Ribeiro AL, Rodrigo-Unzueta A, Tersa M, Zanoni G, Buroni S, Altmann KH, Hartkoorn RC, Glockshuber R, Cole ST, Riccardi G, Guerin ME. Rv2466c mediates the activation of TP053 to kill replicating and non-replicating *Mycobacterium tuberculosis*. *ACS Chem Biol* 9: 1567-75, 2014.
5. Alekshun MN, Levy SB. Alteration of the repressor activity of MarR, the negative regulator of the *Escherichia coli* marRAB locus, by multiple chemicals *in vitro*. *J Bacteriol* 181: 4669-72, 1999.
6. Alekshun MN, Levy SB. The mar regulon: multiple resistance to antibiotics and other toxic chemicals. *Trends Microbiol* 7: 410-3, 1999.
7. Andreu N, Soto CY, Roca I, Martin C, Gibert I. *Mycobacterium smegmatis* displays the *Mycobacterium tuberculosis* virulence-related neutral red character when expressing the Rv0577 gene. *FEMS Microbiol Lett* 231: 283-9, 2004.
8. Antelmann H, Helmann JD. Thiol-based redox switches and gene regulation. *Antioxid Redox Signal* 14: 1049-63, 2011.
9. Arbach M, Santana TM, Moxham H, Tinson R, Anwar A, Groom M, Hamilton CJ. Antimicrobial garlic-derived diallyl polysulfanes: Interactions with biological thiols in *Bacillus subtilis*. *Biochim Biophys Acta Gen Subj* 1863: 1050-1058, 2019.
10. Aslund F, Zheng M, Beckwith J, Storz G. Regulation of the OxyR transcription factor by hydrogen peroxide and the cellular thiol-disulfide status. *Proc Natl Acad Sci U S A* 96: 6161-5, 1999.
11. Baumgart M, Luder K, Grover S, Gatgens C, Besra GS, Frunzke J. IpsA, a novel LacI-type regulator, is required for inositol-derived lipid formation in Corynebacteria and Mycobacteria. *BMC Biol* 11: 122, 2013.
12. Beavers WN, Skaar EP. Neutrophil-generated oxidative stress and protein damage in *Staphylococcus aureus*. *Pathog Dis* 74, 2016.
13. Becker J, Wittmann C. Bio-based production of chemicals, materials and fuels - *Corynebacterium glutamicum* as versatile cell factory. *Curr Opin Biotechnol* 23: 631-40, 2012.
14. Bhaskar A, Chawla M, Mehta M, Parikh P, Chandra P, Bhave D, Kumar D, Carroll KS, Singh A. Reengineering redox sensitive GFP to measure mycothiol redox potential of *Mycobacterium tuberculosis* during infection. *PLoS Pathog* 10: e1003902, 2014.
15. Bilan DS, Belousov VV. New tools for redox biology: From imaging to manipulation. *Free Radic Biol Med* 109: 167-188, 2017.
16. Brugarolas P, Movahedzadeh F, Wang Y, Zhang N, Bartek IL, Gao YN, Voskuil MI, Franzblau SG, He C. The oxidation-sensing regulator (MosR) is a new redox-dependent transcription factor in *Mycobacterium tuberculosis*. *J Biol Chem* 287: 37703-12, 2012.
17. Brugarolas P, Movahedzadeh F, Wang Y, Zhang N, Bartek IL, Gao YN, Voskuil MI, Franzblau SG, He C. The oxidation-sensing regulator (MosR) is a new redox-dependent transcription factor in *Mycobacterium tuberculosis*. *J Biol Chem* 287: 37703-37712, 2012.
18. Burkovski A. Cell envelope of corynebacteria: structure and influence on pathogenicity. *ISRN Microbiol* 2013: 935736-935736, 2013.
19. Busche T, Silar R, Pičmanová M, Pátek M, Kalinowski J. Transcriptional regulation of the operon encoding stress-responsive ECF sigma factor SigH and its anti-sigma factor RshA, and

control of its regulatory network in *Corynebacterium glutamicum*. *BMC genomics* 13: 445-445, 2012.

20. Bzymek KP, Newton GL, Ta P, Fahey RC. Mycothiol import by *Mycobacterium smegmatis* and function as a resource for metabolic precursors and energy production. *J Bacteriol* 189: 6796-805, 2007.
21. Cabiscol E, Tamarit J, Ros J. Oxidative stress in bacteria and protein damage by reactive oxygen species. *Int Microbiol* 3: 3-8, 2000.
22. Cai Y, Yang Q, Liao M, Wang H, Zhang C, Nambi S, Wang W, Zhang M, Wu J, Deng G, Deng Q, Liu H, Zhou B, Jin Q, Feng CG, Sassetti CM, Wang F, Chen X. xCT increases tuberculosis susceptibility by regulating antimicrobial function and inflammation. *Oncotarget* 7: 31001-13, 2016.
23. Chandrangsu P, Dusi R, Hamilton CJ, Helmann JD. Methylglyoxal resistance in *Bacillus subtilis*: contributions of bacillithiol-dependent and independent pathways. *Mol Microbiol* 91: 706-715, 2014.
24. Chandrangsu P, Loi VV, Antelmann H, Helmann JD. The role of bacillithiol in Gram-positive firmicutes. *Antioxid Redox Signal* 28: 445-462, 2018.
25. Chaudhary HS, Yadav J, Shrivastava AR, Singh S, Singh AK, Gopalan N. Antibacterial activity of actinomycetes isolated from different soil samples of Sheopur (A city of central India). *J Adv Pharm Technol Res* 4: 118-123, 2013.
26. Chen C, Chen K, Su T, Zhang B, Li G, Pan J, Si M. Myo-inositol-1-phosphate synthase (Ino-1) functions as a protection mechanism in *Corynebacterium glutamicum* under oxidative stress. *Microbiologyopen*: e721, 2018.
27. Chen H, Hu J, Chen PR, Lan L, Li Z, Hicks LM, Dinner AR, He C. The *Pseudomonas aeruginosa* multidrug efflux regulator MexR uses an oxidation-sensing mechanism. *Proc Natl Acad Sci USA* 105: 13586-91, 2008.
28. Chen H, Xu G, Zhao Y, Tian B, Lu H, Yu X, Xu Z, Ying N, Hu S, Hua Y. A novel OxyR sensor and regulator of hydrogen peroxide stress with one cysteine residue in *Deinococcus radiodurans*. *PloS one* 3: e1602-e1602, 2008.
29. Chen H, Yi C, Zhang J, Zhang W, Ge Z, Yang C-G, He C. Structural insight into the oxidation-sensing mechanism of the antibiotic resistance of regulator MexR. *EMBO Rep* 11: 685-690, 2010.
30. Chi BK, Busche T, Van Laer K, Basell K, Becher D, Clermont L, Seibold GM, Persicke M, Kalinowski J, Messens J, Antelmann H. Protein *S*-mycothiolation functions as redox-switch and thiol protection mechanism in C*orynebacterium glutamicum* under hypochlorite stress. *Antioxid Redox Signal* 20: 589-605, 2014.
31. Chi BK, Gronau K, Mader U, Hessling B, Becher D, Antelmann H. *S*-bacillithiolation protects against hypochlorite stress in *Bacillus subtilis* as revealed by transcriptomics and redox proteomics. *Mol Cell Proteomics* 10: M111.009506, 2011.
32. Chi BK, Roberts AA, Huyen TT, Basell K, Becher D, Albrecht D, Hamilton CJ, Antelmann H. *S*-bacillithiolation protects conserved and essential proteins against hypochlorite stress in firmicutes bacteria. *Antioxid Redox Signal* 18: 1273-95, 2013.
33. Choi H, Kim S, Mukhopadhyay P, Cho S, Woo J, Storz G, Ryu SE. Structural basis of the redox switch in the OxyR transcription factor. *Cell* 105: 103-13, 2001.
34. Chung HS, Wang SB, Venkatraman V, Murray CI, Van Eyk JE. Cysteine oxidative posttranslational modifications: emerging regulation in the cardiovascular system. *Circ Res* 112: 382-92, 2013.
35. Coulson GB, Johnson BK, Zheng H, Colvin CJ, Fillinger RJ, Haiderer ER, Hammer ND, Abramovitch RB. Targeting *Mycobacterium tuberculosis* sensitivity to thiol stress at acidic pH kills the bacterium and potentiates antibiotics. *Cell Chem Biol* 24: 993-1004 e4, 2017.

36. Daugherty A, Powers KM, Standley MS, Kim CS, Purdy GE. *Mycobacterium smegmatis* RoxY is a repressor of oxyS and contributes to resistance to oxidative stress and bactericidal ubiquitin-derived peptides. *J Bacteriol* 193: 6824-6833, 2011.
37. Deochand DK, Grove A. MarR family transcription factors: dynamic variations on a common scaffold. *Crit Rev Biochem Mol Biol* 52: 595-613, 2017.
38. Dooley CT, Dore TM, Hanson GT, Jackson WC, Remington SJ, Tsien RY. Imaging dynamic redox changes in mammalian cells with green fluorescent protein indicators. *J Biol Chem* 279: 22284-93, 2004.
39. Fahey RC. Glutathione analogs in prokaryotes. *Biochim Biophys Acta* 1830: 3182-98, 2013.
40. Fan F, Vetting MW, Frantom PA, Blanchard JS. Structures and mechanisms of the mycothiol biosynthetic enzymes. *Curr Opin Chem Biol* 13: 451-459, 2009.
41. Fang Z, Dos Santos PC. Protective role of bacillithiol in superoxide stress and Fe-S metabolism in *Bacillus subtilis*. *Microbiologyopen* 4: 616-31, 2015.
42. Feng J, Che Y, Milse J, Yin YJ, Liu L, Ruckert C, Shen XH, Qi SW, Kalinowski J, Liu SJ. The gene *ncgl2918* encodes a novel maleylpyruvate isomerase that needs mycothiol as cofactor and links mycothiol biosynthesis and gentisate assimilation in *Corynebacterium glutamicum*. *J Biol Chem* 281: 10778-85, 2006.
43. Flannagan RS, Cosio G, Grinstein S. Antimicrobial mechanisms of phagocytes and bacterial evasion strategies. *Nat Rev Microbiol* 7: 355-66, 2009.
44. Flohe L. *Glutathione*; 2018.
45. Gaballa A, Newton GL, Antelmann H, Parsonage D, Upton H, Rawat M, Claiborne A, Fahey RC, Helmann JD. Biosynthesis and functions of bacillithiol, a major low-molecular-weight thiol in Bacilli. *Proc Natl Acad Sci U S A* 107: 6482-6, 2010.
46. Gao YR, Li DF, Fleming J, Zhou YF, Liu Y, Deng JY, Zhou L, Zhou J, Zhu GF, Zhang XE, Wang DC, Bi LJ. Structural analysis of the regulatory mechanism of MarR protein Rv2887 in *M. tuberculosis*. *Sci Rep* 7: 6471, 2017.
47. Garnica OA, Das K, Dhandayuthapani S. OhrR of *Mycobacterium smegmatis* senses and responds to intracellular organic hydroperoxide stress. *Sci Rep* 7: 3922-3922, 2017.
48. Go YM, Duong DM, Peng J, Jones DP. Protein cysteines map to functional networks according to steady-state level of oxidation. *J Proteomics Bioinform* 4: 196-209, 2011.
49. Gong Z, Li H, Cai Y, Stojkoska A, Xie J. Biology of MarR family transcription factors and implications for targets of antibiotics against tuberculosis. *J Cell Physiol* 234: 19237-19248, 2019.
50. Gonzalez-Flecha B, Demple B. Metabolic sources of hydrogen peroxide in aerobically growing *Escherichia coli*. *J Biol Chem* 270: 13681-7, 1995.
51. Grove A. Regulation of metabolic pathways by MarR family transcription factors. *Comput Struct Biotechnol J* 15: 366-371, 2017.
52. Gruhlke MCH, Antelmann H, Bernhardt J, Kloubert V, Rink L, Slusarenko AJ. The human allicin-proteome: *S*-thioallylation of proteins by the garlic defence substance allicin and its biological effects. *Free Radic Biol Med* 131: 144-153, 2019.
53. Gutscher M, Pauleau AL, Marty L, Brach T, Wabnitz GH, Samstag Y, Meyer AJ, Dick TP. Real-time imaging of the intracellular glutathione redox potential. *Nat Methods* 5: 553-9, 2008.
54. Hadfield TL, McEvoy P, Polotsky Y, Tzinserling VA, Yakovlev AA. The pathology of diphtheria. *J Infect Dis* 181 Suppl 1: S116-20, 2000.
55. Halliwell B, Gutteridge JM. Oxygen toxicity, oxygen radicals, transition metals and disease. *Biochem J* 219: 1-14, 1984.
56. Hanson GT, Aggeler R, Oglesbee D, Cannon M, Capaldi RA, Tsien RY, Remington SJ. Investigating mitochondrial redox potential with redox-sensitive green fluorescent protein indicators. *J Biol Chem* 279: 13044-53, 2004.
57. Healy C, Golby P, MacHugh DE, Gordon SV. The MarR family transcription factor Rv1404 coordinates adaptation of *Mycobacterium tuberculosis* to acid stress via controlled

expression of Rv1405c, a virulence-associated methyltransferase. *Tuberculosis (Edinb)* 97: 154-62, 2016.
58. Helmann JD. Bacillithiol, a new player in bacterial redox homeostasis. *Antioxid Redox Signal* 15: 123-133, 2011.
59. Hillion M, Antelmann H. Thiol-based redox switches in prokaryotes. *Biol Chem* 396: 415-44, 2015.
60. Hillion M, Bernhardt J, Busche T, Rossius M, Maass S, Becher D, Rawat M, Wirtz M, Hell R, Ruckert C, Kalinowski J, Antelmann H. Monitoring global protein thiol-oxidation and protein *S*-mycothiolation in *Mycobacterium smegmatis* under hypochlorite stress. *Sci Rep* 7: 1195, 2017.
61. Hillion M, Imber M, Pedre B, Bernhardt J, Saleh M, Loi VV, Maass S, Becher D, Astolfi Rosado L, Adrian L, Weise C, Hell R, Wirtz M, Messens J, Antelmann H. The glyceraldehyde-3-phosphate dehydrogenase GapDH of *Corynebacterium diphtheriae* is redox-controlled by protein *S*-mycothiolation under oxidative stress. *Sci Rep* 7: 5020, 2017.
62. Hiras J, Sharma SV, Raman V, Tinson RAJ, Arbach M, Rodrigues DF, Norambuena J, Hamilton CJ, Hanson TE. Physiological sudies of chlorobiaceae suggest that bacillithiol derivatives are the most widespread thiols in bacteria. *MBio* 9, 2018.
63. Hirata R, Napoleao F, Monteiro-Leal LH, Andrade AF, Nagao PE, Formiga LC, Fonseca LS, Mattos-Guaraldi AL. Intracellular viability of toxigenic *Corynebacterium diphtheriae* strains in HEp-2 cells. *FEMS Microbiol Lett* 215: 115-9, 2002.
64. Hong M, Fuangthong M, Helmann JD, Brennan RG. Structure of an OhrR-ohrA operator complex reveals the DNA binding mechanism of the MarR family. *Mol Cell* 20: 131-41, 2005.
65. Hugo M, Van Laer K, Reyes AM, Vertommen D, Messens J, Radi R, Trujillo M. Mycothiol/mycoredoxin 1-dependent reduction of the peroxiredoxin AhpE from *Mycobacterium tuberculosis*. *J Biol Chem* 289: 5228-5239, 2014.
66. Hurst JK. What really happens in the neutrophil phagosome? *Free Radic Biol Med* 53: 508-20, 2012.
67. Ikeda M, Nakagawa S. The *Corynebacterium glutamicum* genome: features and impacts on biotechnological processes. *Appl Microbiol Biotechnol* 62: 99-109, 2003.
68. Imber M, Huyen NTT, Pietrzyk-Brzezinska AJ, Loi VV, Hillion M, Bernhardt J, Thärichen L, Kolšek K, Saleh M, Hamilton CJ, Adrian L, Gräter F, Wahl MC, Antelmann H. Protein *S*-bacillithiolation functions in thiol protection and redox regulation of the glyceraldehyde-3-phosphate dehydrogenase Gap in *Staphylococcus aureus* under hypochlorite stress. *Antioxid Redox Signal* 28: 410-430, 2018.
69. Imber M, Pietrzyk-Brzezinska AJ, Antelmann H. Redox regulation by reversible protein *S*-thiolation in Gram-positive bacteria. *Redox Biol* 20: 130-145, 2019.
70. Imlay JA. Pathways of oxidative damage. *Annu Rev Microbiol* 57: 395-418, 2003.
71. Imlay JA. Transcription factors that defend bacteria against reactive oxygen species. *Annu Rev Microbiol* 69: 93-108, 2015.
72. Islam MM, Tan Y, Hameed HMA, Liu Z, Chhotaray C, Liu Y, Lu Z, Cai X, Tang Y, Gao Y, Surineni G, Li X, Tan S, Guo L, Cai X, Yew WW, Liu J, Zhong N, Zhang T. Detection of novel mutations associated with independent resistance and cross-resistance to isoniazid and prothionamide in *Mycobacterium tuberculosis* clinical isolates. *Clin Microbiol Infect*, 2018.
73. Jensen PO, Briales A, Brochmann RP, Wang H, Kragh KN, Kolpen M, Hempel C, Bjarnsholt T, Hoiby N, Ciofu O. Formation of hydroxyl radicals contributes to the bactericidal activity of ciprofloxacin against *Pseudomonas aeruginosa* biofilms. *Pathog Dis* 70: 440-3, 2014.
74. Jo I, Kim D, No T, Hong S, Ahn J, Ryu S, Ha NC. Structural basis for HOCl recognition and regulation mechanisms of HypT, a hypochlorite-specific transcriptional regulator. *Proc Natl Acad Sci U S A* 116: 3740-3745, 2019.
75. Jothivasan VK, Hamilton CJ. Mycothiol: synthesis, biosynthesis and biological functions of the major low molecular weight thiol in actinomycetes. *Nat Prod Rep* 25: 1091-117, 2008.

76. Kalinowski J, Bathe B, Bartels D, Bischoff N, Bott M, Burkovski A, Dusch N, Eggeling L, Eikmanns BJ, Gaigalat L, Goesmann A, Hartmann M, Huthmacher K, Kramer R, Linke B, McHardy AC, Meyer F, Mockel B, Pfefferle W, Puhler A, Rey DA, Ruckert C, Rupp O, Sahm H, Wendisch VF, Wiegrabe I, Tauch A. The complete *Corynebacterium glutamicum* ATCC 13032 genome sequence and its impact on the production of L-aspartate-derived amino acids and vitamins. *J Biotechnol* 104: 5-25, 2003.
77. Kallscheuer N, Vogt M, Bott M, Marienhagen J. Functional expression of plant-derived O-methyltransferase, flavanone 3-hydroxylase, and flavonol synthase in *Corynebacterium glutamicum* for production of pterostilbene, kaempferol, and quercetin. *J Biotechnol* 258: 190-196, 2017.
78. Kallscheuer N, Vogt M, Kappelmann J, Krumbach K, Noack S, Bott M, Marienhagen J. Identification of the phd gene cluster responsible for phenylpropanoid utilization in *Corynebacterium glutamicum*. *Appl Microbiol Biotechnol* 100: 1871-81, 2016.
79. Kallscheuer N, Vogt M, Marienhagen J. A novel synthetic pathway enables microbial production of polyphenols independent from the endogenous aromatic amino acid metabolism. *ACS Synth Biol* 6: 410-415, 2017.
80. Kallscheuer N, Vogt M, Stenzel A, Gatgens J, Bott M, Marienhagen J. Construction of a *Corynebacterium glutamicum* platform strain for the production of stilbenes and (2S)-flavanones. *Metab Eng* 38: 47-55, 2016.
81. Kaushal D, Schroeder BG, Tyagi S, Yoshimatsu T, Scott C, Ko C, Carpenter L, Mehrotra J, Manabe YC, Fleischmann RD, Bishai WR. Reduced immunopathology and mortality despite tissue persistence in a *Mycobacterium tuberculosis* mutant lacking alternative sigma factor, SigH. *Proc Natl Acad Sci U S A* 99: 8330-8335, 2002.
82. Kay KL, Hamilton CJ, Le Brun NE. Mass spectrometry of *B. subtilis* CopZ: Cu(i)-binding and interactions with bacillithiol. *Metallomics* 8: 709-19, 2016.
83. Kim JS, Holmes RK. Characterization of OxyR as a negative transcriptional regulator that represses catalase production in *Corynebacterium diphtheriae*. *PLoS One* 7: e31709, 2012.
84. Kim TH, Kim HJ, Park JS, Kim Y, Kim P, Lee HS. Functional analysis of sigH expression in *Corynebacterium glutamicum*. *Biochem Biophys Res Commun* 331: 1542-7, 2005.
85. Kinoshita S, Udaka S, Shimono M. Studies on the amino acid fermentation Part I. Production of the L-glutamic acid by various microorganisms. *J Gen Appl Microbiol* 3: 193-205, 1957.
86. Klebanoff SJ. Myeloperoxidase: friend and foe. *J Leukoc Biol* 77: 598-625, 2005.
87. Knechel NA. Tuberculosis: pathophysiology, clinical features, and diagnosis. *Crit Care Nurse* 29: 34-43; quiz 44, 2009.
88. Kobayashi SD, Voyich JM, Burlak C, DeLeo FR. Neutrophils in the innate immune response. *Arch Immunol Ther Exp (Warsz)* 53: 505-17, 2005.
89. Korshunov S, Imlay JA. Two sources of endogenous hydrogen peroxide in *Escherichia coli*. *Mol Microbiol* 75: 1389-401, 2010.
90. Lange J, Münch E, Müller J, Busche T, Kalinowski J, Takors R, Blombach B. Deciphering the adaptation of *Corynebacterium glutamicum* in transition from aerobiosis via microaerobiosis to anaerobiosis. *Genes (Basel)* 9: 297, 2018.
91. Lee JW, Soonsanga S, Helmann JD. A complex thiolate switch regulates the *Bacillus subtilis* organic peroxide sensor OhrR. *Proc Natl Acad Sci U S A* 104: 8743-8, 2007.
92. Lee JY, Na YA, Kim E, Lee HS, Kim P. The actinobacterium *Corynebacterium glutamicum*, an industrial workhorse. *J Microbiol Biotechnol* 26: 807-22, 2016.
93. Libardo MDJ, de la Fuente-Nunez C, Anand K, Krishnamoorthy G, Kaiser P, Pringle SC, Dietz C, Pierce S, Smith MB, Barczak A, Kaufmann SHE, Singh A, Angeles-Boza AM. Phagosomal copper-promoted oxidative attack on intracellular *Mycobacterium tuberculosis*. *ACS Infect Dis* 4: 1623-1634, 2018.
94. Linzner N, Loi VV, Fritsch VN, Tung QN, Stenzel S, Wirtz M, Hell R, Hamilton CJ, Tedin K, Fulde M, Antelmann H. *Staphylococcus aureus* uses the bacilliredoxin (BrxAB)/bacillithiol disulfide

reductase (YpdA) redox pathway to defend against oxidative stress under infections. *Front. Microbiol* 10, 2019.

95. Loi VV, Busche T, Tedin K, Bernhardt J, Wollenhaupt J, Huyen NTT, Weise C, Kalinowski J, Wahl MC, Fulde M, Antelmann H. Redox-sensing under hypochlorite stress and infection conditions by the Rrf2-family repressor HypR in *Staphylococcus aureus*. *Antioxid Redox Signal* 29: 615-636, 2018.
96. Loi VV, Harms M, Müller M, Huyen NTT, Hamilton CJ, Hochgräfe F, Pané-Farré J, Antelmann H. Real-time imaging of the bacillithiol redox potential in the human pathogen *Staphylococcus aureus* using a genetically encoded bacilliredoxin-fused redox biosensor. *Antioxidants & redox signaling* 26: 835-848, 2017.
97. Loi VV, Huyen NTT, Busche T, Tung QN, Gruhlke MCH, Kalinowski J, Bernhardt J, Slusarenko AJ, Antelmann H. *Staphylococcus aureus* responds to allicin by global *S*-thioallylation - Role of the Brx/BSH/YpdA pathway and the disulfide reductase MerA to overcome allicin stress. *Free Radic Biol Med* 139: 55-69, 2019.
98. Loi VV, Rossius M, Antelmann H. Redox regulation by reversible protein *S*-thiolation in bacteria. *Front Microbiol* 6: 187-187, 2015.
99. Ma Z, Chandrangsu P, Helmann TC, Romsang A, Gaballa A, Helmann JD. Bacillithiol is a major buffer of the labile zinc pool in *Bacillus subtilis*. *Mol Microbiol* 94: 756-70, 2014.
100. Manganelli R, Voskuil MI, Schoolnik GK, Dubnau E, Gomez M, Smith I. Role of the extracytoplasmic-function sigma factor sigma(H) in *Mycobacterium tuberculosis* global gene expression. *Mol Microbiol* 45: 365-74, 2002.
101. Mao X, Gu C, Chen D, Yu B, He J. Oxidative stress-induced diseases and tea polyphenols. *Oncotarget* 8: 81649-81661, 2017.
102. Marrakchi H, Laneelle G, Quemard A. InhA, a target of the antituberculous drug isoniazid, is involved in a mycobacterial fatty acid elongation system, FAS-II. *Microbiology* 146 (Pt 2): 289-96, 2000.
103. Mehra S, Kaushal D. Functional genomics reveals extended roles of the *Mycobacterium tuberculosis* stress response factor sigmaH. *J Bacteriol* 191: 3965-3980, 2009.
104. Mehta M, Rajmani RS, Singh A. Mycobacterium tuberculosis WhiB3 responds to vacuolar pH-induced changes in mycothiol redox potential to modulate phagosomal maturation and virulence. *J Biol Chem* 291: 2888-903, 2016.
105. Mehta M, Singh A. *Mycobacterium tuberculosis* WhiB3 maintains redox homeostasis and survival in response to reactive oxygen and nitrogen species. *Free Radic Biol Med* 131: 50-58, 2019.
106. Messner KR, Imlay JA. Mechanism of superoxide and hydrogen peroxide formation by fumarate reductase, succinate dehydrogenase, and aspartate oxidase. *J Biol Chem* 277: 42563-71, 2002.
107. Mestre O, Hurtado-Ortiz R, Dos Vultos T, Namouchi A, Cimino M, Pimentel M, Neyrolles O, Gicquel B. High throughput phenotypic selection of *Mycobacterium tuberculosis* mutants with impaired resistance to reactive oxygen species identifies genes important for intracellular growth. *PLoS One* 8: e53486-e53486, 2013.
108. Meyer AJ, Dick TP. Fluorescent protein-based redox probes. *Antioxid Redox Signal* 13: 621-50, 2010.
109. Michan C, Manchado M, Dorado G, Pueyo C. *In vivo* transcription of the *Escherichia coli* oxyR regulon as a function of growth phase and in response to oxidative stress. *J Bacteriol* 181: 2759-64, 1999.
110. Mierziak J, Kostyn K, Kulma A. Flavonoids as important molecules of plant interactions with the environment. *Molecules* 19: 16240-65, 2014.
111. Mikheyeva IV, Thomas JM, Kolar SL, Corvaglia AR, Gaiotaa N, Leo S, Francois P, Liu GY, Rawat M, Cheung AL. YpdA, a putative bacillithiol disulfide reductase, contributes to cellular redox homeostasis and virulence in *Staphylococcus aureus*. *Mol Microbiol* 111: 1039-1056, 2019.

112. Milse J, Petri K, Ruckert C, Kalinowski J. Transcriptional response of *Corynebacterium glutamicum* ATCC 13032 to hydrogen peroxide stress and characterization of the OxyR regulon. *J Biotechnol* 190: 40-54, 2014.
113. Miron T, Listowsky I, Wilchek M. Reaction mechanisms of allicin and allyl-mixed disulfides with proteins and small thiol molecules. *Eur J Med Chem* 45: 1912-8, 2010.
114. Mishra S, Shukla P, Bhaskar A, Anand K, Baloni P, Jha RK, Mohan A, Rajmani RS, Nagaraja V, Chandra N, Singh A. Efficacy of beta-lactam/beta-lactamase inhibitor combination is linked to WhiB4-mediated changes in redox physiology of *Mycobacterium tuberculosis*. *Elife* 6, 2017.
115. Muller A, Eller J, Albrecht F, Prochnow P, Kuhlmann K, Bandow JE, Slusarenko AJ, Leichert LI. Allicin induces thiol stress in bacteria through *S*-allylmercapto modification of protein cysteines. *J Biol Chem* 291: 11477-90, 2016.
116. Muller A, Schneider JF, Degrossoli A, Lupilova N, Dick TP, Leichert LI. Systematic *in vitro* assessment of responses of roGFP2-based probes to physiologically relevant oxidant species. *Free Radic Biol Med* 106: 329-338, 2017.
117. Murphy KC, Papavinasasundaram K, Sassetti CM. Mycobacterial recombineering. *Methods Mol Biol* 1285: 177-99, 2015.
118. Nakunst D, Larisch C, Hüser AT, Tauch A, Pühler A, Kalinowski J. The extracytoplasmic function-type sigma factor SigM of *Corynebacterium glutamicum* ATCC 13032 is involved in transcription of disulfide stress-related genes. *J Bacteriol* 189: 4696-4707, 2007.
119. Nambi S, Long JE, Mishra BB, Baker R, Murphy KC, Olive AJ, Nguyen HP, Shaffer SA, Sassetti CM. The oxidative stress network of *Mycobacterium tuberculosis* reveals coordination between radical detoxification systems. *Cell Host Microbe* 17: 829-37, 2015.
120. Negri A, Javidnia P, Mu R, Zhang X, Vendome J, Gold B, Roberts J, Barman D, Ioerger T, Sacchettini JC, Jiang X, Burns-Huang K, Warrier T, Ling Y, Warren JD, Oren DA, Beuming T, Wang H, Wu J, Li H, Rhee KY, Nathan CF, Liu G, Somersan-Karakaya S. Identification of a mycothiol-dependent nitroreductase from *Mycobacterium tuberculosis*. *ACS Infect Dis* 4: 771-787, 2018.
121. Nelson JW, Creighton TE. Reactivity and ionization of the active site cysteine residues of DsbA, a protein required for disulfide bond formation *in vivo*. *Biochemistry* 33: 5974-83, 1994.
122. Newton GL, Arnold K, Price MS, Sherrill C, Delcardayre SB, Aharonowitz Y, Cohen G, Davies J, Fahey RC, Davis C. Distribution of thiols in microorganisms: mycothiol is a major thiol in most actinomycetes. *J Bacteriol* 178: 1990-1995, 1996.
123. Newton GL, Av-Gay Y, Fahey RC. A novel mycothiol-dependent detoxification pathway in mycobacteria involving mycothiol *S*-conjugate amidase. *Biochemistry* 39: 10739-46, 2000.
124. Newton GL, Bewley CA, Dwyer TJ, Horn R, Aharonowitz Y, Cohen G, Davies J, Faulkner DJ, Fahey RC. The structure of U17 isolated from *Streptomyces clavuligerus* and its properties as an antioxidant thiol. *Eur J Biochem* 230: 821-5, 1995.
125. Newton GL, Buchmeier N, Fahey RC. Biosynthesis and functions of mycothiol, the unique protective thiol of Actinobacteria. *Microbiol Mol Biol Rev* 72: 471-94, 2008.
126. Newton GL, Leung SS, Wakabayashi JI, Rawat M, Fahey RC. The DinB superfamily includes novel mycothiol, bacillithiol, and glutathione *S*-transferases. *Biochemistry* 50: 10751-60, 2011.
127. Nijveldt RJ, van Nood E, van Hoorn DE, Boelens PG, van Norren K, van Leeuwen PA. Flavonoids: a review of probable mechanisms of action and potential applications. *Am J Clin Nutr* 74: 418-25, 2001.
128. Ogbo FA, Ogeleka P, Okoro A, Olusanya BO, Olusanya J, Ifegwu IK, Awosemo AO, Eastwood J, Page A. Tuberculosis disease burden and attributable risk factors in Nigeria, 1990-2016. *Trop Med Health* 46: 34-34, 2018.

129. Ott L, McKenzie A, Baltazar MT, Britting S, Bischof A, Burkovski A, Hoskisson PA. Evaluation of invertebrate infection models for pathogenic corynebacteria. *FEMS Immunol Med Microbiol* 65: 413-21, 2012.
130. Padiadpu J, Baloni P, Anand K, Munshi M, Thakur C, Mohan A, Singh A, Chandra N. Identifying and tackling emergent vulnerability in drug-resistant mycobacteria. *ACS Infect Dis* 2: 592-607, 2016.
131. Panmanee W, Vattanaviboon P, Poole LB, Mongkolsuk S. Novel organic hydroperoxide-sensing and responding mechanisms for OhrR, a major bacterial sensor and regulator of organic hydroperoxide stress. *J Bacteriol* 188: 1389-95, 2006.
132. Paulsen CE, Carroll KS. Cysteine-mediated redox signaling: chemistry, biology, and tools for discovery. *Chem Rev* 113: 4633-79, 2013.
133. Pedre B, Van Molle I, Villadangos AF, Wahni K, Vertommen D, Turell L, Erdogan H, Mateos LM, Messens J. The *Corynebacterium glutamicum* mycothiol peroxidase is a reactive oxygen species-scavenging enzyme that shows promiscuity in thiol redox control. *Mol Microbiol* 96: 1176-91, 2015.
134. Pedre B, Young D, Charlier D, Mourenza A, Rosado LA, Marcos-Pascual L, Wahni K, Martens E, A GdlR, Belousov VV, Mateos LM, Messens J. Structural snapshots of OxyR reveal the peroxidatic mechanism of H_2O_2 sensing. *Proc Natl Acad Sci U S A* 115: E11623-e11632, 2018.
135. Peralta D, Bronowska AK, Morgan B, Doka E, Van Laer K, Nagy P, Grater F, Dick TP. A proton relay enhances H_2O_2 sensitivity of GAPDH to facilitate metabolic adaptation. *Nat Chem Biol* 11: 156-63, 2015.
136. Peterson EJR, Ma S, Sherman DR, Baliga NS. Network analysis identifies Rv0324 and Rv0880 as regulators of bedaquiline tolerance in *Mycobacterium tuberculosis*. *Nat Microbiol* 1: 16078-16078, 2016.
137. Philips JA. Mycobacterial manipulation of vacuolar sorting. *Cell Microbiol* 10: 2408-15, 2008.
138. Poen S, Nakatani Y, Opel-Reading HK, Lasse M, Dobson RC, Krause KL. Exploring the structure of glutamate racemase from *Mycobacterium tuberculosis* as a template for anti-mycobacterial drug discovery. *Biochem J* 473: 1267-80, 2016.
139. Posada AC, Kolar SL, Dusi RG, Francois P, Roberts AA, Hamilton CJ, Liu GY, Cheung A. Importance of bacillithiol in the oxidative stress response of *Staphylococcus aureus*. *Infect Immun* 82: 316-32, 2014.
140. Pother DC, Gierok P, Harms M, Mostertz J, Hochgrafe F, Antelmann H, Hamilton CJ, Borovok I, Lalk M, Aharonowitz Y, Hecker M. Distribution and infection-related functions of bacillithiol in *Staphylococcus aureus*. *Int J Med Microbiol* 303: 114-23, 2013.
141. Rabinkov A, Zhu XZ, Grafi G, Galili G, Mirelman D. Alliin lyase (Alliinase) from garlic (*Allium sativum*). Biochemical characterization and cDNA cloning. *Appl Biochem Biotechnol* 48: 149-71, 1994.
142. Radhakrishnan A, Kumar N, Wright CC, Chou TH, Tringides ML, Bolla JR, Lei HT, Rajashankar KR, Su CC, Purdy GE, Yu EW. Crystal structure of the transcriptional regulator Rv0678 of *Mycobacterium tuberculosis*. *J Biol Chem* 289: 16526-40, 2014.
143. Rajkarnikar A, Strankman A, Duran S, Vargas D, Roberts AA, Barretto K, Upton H, Hamilton CJ, Rawat M. Analysis of mutants disrupted in bacillithiol metabolism in *Staphylococcus aureus*. *Biochem Biophys Res Commun* 436: 128-33, 2013.
144. Rawat M, Av-Gay Y. Mycothiol-dependent proteins in actinomycetes. *FEMS Microbiol Rev* 31: 278-92, 2007.
145. Reniere ML. Reduce, induce, thrive: bacterial redox sensing during pathogenesis. *J Bacteriol* 200, 2018.
146. Reyes AM, Pedre B, De Armas MI, Tossounian MA, Radi R, Messens J, Trujillo M. Chemistry and redox biology of mycothiol. *Antioxid Redox Signal* 28: 487-504, 2018.
147. Reyrat JM, Kahn D. *Mycobacterium smegmatis*: an absurd model for tuberculosis? *Trends Microbiol* 9: 472-4, 2001.

148. Roberts AA, Sharma SV, Strankman AW, Duran SR, Rawat M, Hamilton CJ. Mechanistic studies of FosB: a divalent-metal-dependent bacillithiol-*S*-transferase that mediates fosfomycin resistance in *Staphylococcus aureus*. *Biochem J* 451: 69-79, 2013.
149. Rosado LA, Wahni K, Degiacomi G, Pedre B, Young D, de la Rubia AG, Boldrin F, Martens E, Marcos-Pascual L, Sancho-Vaello E, Albesa-Jove D, Provvedi R, Martin C, Makarov V, Versees W, Verniest G, Guerin ME, Mateos LM, Manganelli R, Messens J. The antibacterial prodrug activator Rv2466c is a mycothiol-dependent reductase in the oxidative stress response of *Mycobacterium tuberculosis*. *J Biol Chem* 292: 13097-13110, 2017.
150. Rosario-Cruz Z, Chahal HK, Mike LA, Skaar EP, Boyd JM. Bacillithiol has a role in Fe-S cluster biogenesis in *Staphylococcus aureus*. *Mol Microbiol* 98: 218-42, 2015.
151. Rybniker J, Pojer F, Marienhagen J, Kolly GS, Chen JM, van Gumpel E, Hartmann P, Cole ST. The cysteine desulfurase IscS of *Mycobacterium tuberculosis* is involved in iron-sulfur cluster biogenesis and oxidative stress defence. *Biochem J* 459: 467-78, 2014.
152. Saikolappan S, Das K, Dhandayuthapani S. Inactivation of the organic hydroperoxide stress resistance regulator OhrR enhances resistance to oxidative stress and isoniazid in *Mycobacterium smegmatis*. *Journal of bacteriology* 197: 51-62, 2015.
153. Saini V, Cumming BM, Guidry L, Lamprecht DA, Adamson JH, Reddy VP, Chinta KC, Mazorodze JH, Glasgow JN, Richard-Greenblatt M, Gomez-Velasco A, Bach H, Av-Gay Y, Eoh H, Rhee K, Steyn AJC. Ergothioneine maintains redox and bioenergetic homeostasis essential for drug susceptibility and virulence of *Mycobacterium tuberculosis*. *Cell Rep* 14: 572-585, 2016.
154. Sao Emani C, Williams MJ, Van Helden PD, Taylor MJC, Carolis C, Wiid IJ, Baker B. Generation and characterization of thiol-deficient *Mycobacterium tuberculosis* mutants. *Sci Data* 5: 180184, 2018.
155. Sao Emani C, Williams MJ, Wiid IJ, Baker B. The functional interplay of low molecular weight thiols in *Mycobacterium tuberculosis*. *J Biomed Sci* 25: 55, 2018.
156. Schwarzlander M, Dick TP, Meyer AJ, Morgan B. Dissecting redox biology using fluorescent protein sensors. *Antioxid Redox Signal* 24: 680-712, 2016.
157. Seaver LC, Imlay JA. Are respiratory enzymes the primary sources of intracellular hydrogen peroxide? *J Biol Chem* 279: 48742-50, 2004.
158. Sengupta S, Nagaraja V. Inhibition of DNA gyrase activity by *Mycobacterium smegmatis* MurI. *FEMS Microbiol Lett* 279: 40-7, 2008.
159. Sevilla E, Bes MT, Gonzalez A, Peleato ML, Fillat MF. Redox-based transcriptional regulation in prokaryotes: Revisiting model mechanisms. *Antioxid Redox Signal* 30: 1651-1696, 2019.
160. Shaked Z, Szajewski RP, Whitesides GM. Rates of thiol-disulfide interchange reactions involving proteins and kinetic measurements of thiol pKa values. *Biochemistry* 19: 4156-66, 1980.
161. Si M, Chen C, Su T, Che C, Yao S, Liang G, Li G, Yang G. CosR is an oxidative stress sensing a MarR-type transcriptional repressor in *Corynebacterium glutamicum*. *Biochem J* 475: 3979-3995, 2018.
162. Si M, Su T, Chen C, Liu J, Gong Z, Che C, Li G, Yang G. OhsR acts as an organic peroxide-sensing transcriptional activator using an *S*-mycothiolation mechanism in *Corynebacterium glutamicum*. *Microb Cell Fact* 17: 200-200, 2018.
163. Si M, Wang J, Xiao X, Guan J, Zhang Y, Ding W, Chaudhry MT, Wang Y, Shen X. Ohr protects *Corynebacterium glutamicum* against organic hydroperoxide induced oxidative stress. *PLoS One* 10: e0131634, 2015.
164. Si M, Wang T, Pan J, Lin J, Chen C, Wei Y, Lu Z, Wei G, Shen X. Graded response of the multifunctional 2-Cysteine peroxiredoxin, CgPrx, to increasing levels of hydrogen peroxide in *Corynebacterium glutamicum*. *Antioxid Redox Signal* 26: 1-14, 2017.
165. Singh A, Guidry L, Narasimhulu KV, Mai D, Trombley J, Redding KE, Giles GI, Lancaster JR, Jr., Steyn AJ. *Mycobacterium tuberculosis* WhiB3 responds to O2 and nitric oxide via its [4Fe-4S]

cluster and is essential for nutrient starvation survival. *Proc Natl Acad Sci U S A* 104: 11562-7, 2007.

166. Soonsanga S, Lee JW, Helmann JD. Conversion of *Bacillus subtilis* OhrR from a 1-Cys to a 2-Cys peroxide sensor. *J Bacteriol* 190: 5738-45, 2008.
167. Stoll A, Seebeck E. [The specificity of the alliinase from *Allium sativum*]. *C R Hebd Seances Acad Sci* 232: 1441-2, 1951.
168. Su T, Si M, Zhao Y, Liu Y, Yao S, Che C, Chen C. A thioredoxin-dependent peroxiredoxin Q from *Corynebacterium glutamicum* plays an important role in defense against oxidative stress. *PLoS One* 13: e0192674-e0192674, 2018.
169. Sukchawalit R, Loprasert S, Atichartpongkul S, Mongkolsuk S. Complex regulation of the organic hydroperoxide resistance gene (ohr) from *Xanthomonas* involves OhrR, a novel organic peroxide-inducible negative regulator, and posttranscriptional modifications. *J Bacteriol* 183: 4405-12, 2001.
170. Sundquist AR, Fahey RC. The function of gamma-glutamylcysteine and bis-gamma-glutamylcystine reductase in *Halobacterium halobium*. *J Biol Chem* 264: 719-25, 1989.
171. Teramoto H, Inui M, Yukawa H. OxyR acts as a transcriptional repressor of hydrogen peroxide-inducible antioxidant genes in *Corynebacterium glutamicum* R. *FEBS J* 280: 3298-312, 2013.
172. Timms VJ, Nguyen T, Crighton T, Yuen M, Sintchenko V. Genome-wide comparison of *Corynebacterium diphtheriae* isolates from Australia identifies differences in the Pan-genomes between respiratory and cutaneous strains. *BMC Genomics* 19: 869, 2018.
173. Tung QN, Loi VV, Busche T, Nerlich A, Mieth M, Milse J, Kalinowski J, Hocke AC, Antelmann H. Stable integration of the Mrx1-roGFP2 biosensor to monitor dynamic changes of the mycothiol redox potential in *Corynebacterium glutamicum*. *Redox Biol* 20: 514-525, 2018.
174. Tyagi P, Dharmaraja AT, Bhaskar A, Chakrapani H, Singh A. *Mycobacterium tuberculosis* has diminished capacity to counteract redox stress induced by elevated levels of endogenous superoxide. *Free Radic Biol Med* 84: 344-354, 2015.
175. van der Heijden J, Bosman ES, Reynolds LA, Finlay BB. Direct measurement of oxidative and nitrosative stress dynamics in *Salmonella* inside macrophages. *Proc Natl Acad Sci U S A* 112: 560-565, 2015.
176. Van Laer K, Buts L, Foloppe N, Vertommen D, Van Belle K, Wahni K, Roos G, Nilsson L, Mateos LM, Rawat M, van Nuland NA, Messens J. Mycoredoxin-1 is one of the missing links in the oxidative stress defence mechanism of Mycobacteria. *Mol Microbiol* 86: 787-804, 2012.
177. Van Laer K, Hamilton CJ, Messens J. Low-molecular-weight thiols in thiol-disulfide exchange. *Antioxid Redox Signal* 18: 1642-53, 2013.
178. Ventura M, Canchaya C, Tauch A, Chandra G, Fitzgerald GF, Chater KF, van Sinderen D. Genomics of Actinobacteria: tracing the evolutionary history of an ancient phylum. *Microbiol Mol Biol Rev* 71: 495-548, 2007.
179. Viana MVC, Figueiredo H, Ramos R, Guimarães LC, Pereira FL, Dorella FA, Selim SAK, Salaheldean M, Silva A, Wattam AR, Azevedo V. Comparative genomic analysis between *Corynebacterium pseudotuberculosis* strains isolated from buffalo. *PLoS ONE* 12: e0176347, 2017.
180. Villadangos AF, Van Belle K, Wahni K, Dufe VT, Freitas S, Nur H, De Galan S, Gil JA, Collet JF, Mateos LM, Messens J. *Corynebacterium glutamicum* survives arsenic stress with arsenate reductases coupled to two distinct redox mechanisms. *Mol Microbiol* 82: 998-1014, 2011.
181. Vining LC. Secondary metabolism, inventive evolution and biochemical diversity — a review. *Gene* 115: 135-140, 1992.
182. Wall SB, Oh JY, Diers AR, Landar A. Oxidative modification of proteins: an emerging mechanism of cell signaling. *Front Physiol* 3: 369, 2012.

183. Wang T, Gao F, Kang Y, Zhao C, Su T, Li M, Si M, Shen X. Mycothiol peroxidase Mpx protects *Corynebacterium glutamicum* against acid stress by scavenging ROS. *Biotechnol Lett* 38: 1221-8, 2016.
184. Wani R, Nagata A, Murray BW. Protein redox chemistry: post-translational cysteine modifications that regulate signal transduction and drug pharmacology. *Front Pharmacol* 5: 224-224, 2014.
185. Warrier T, Kapilashrami K, Argyrou A, Ioerger TR, Little D, Murphy KC, Nandakumar M, Park S, Gold B, Mi J, Zhang T, Meiler E, Rees M, Somersan-Karakaya S, Porras-De Francisco E, Martinez-Hoyos M, Burns-Huang K, Roberts J, Ling Y, Rhee KY, Mendoza-Losana A, Luo M, Nathan CF. N-methylation of a bactericidal compound as a resistance mechanism in *Mycobacterium tuberculosis*. *Proc Natl Acad Sci U S A* 113: E4523-30, 2016.
186. Wei J, Dahl JL, Moulder JW, Roberts EA, O'Gaora P, Young DB, Friedman RL. Identification of a *Mycobacterium tuberculosis* gene that enhances mycobacterial survival in macrophages. *J Bacteriol* 182: 377-84, 2000.
187. Wheeler PR, Coldham NG, Keating L, Gordon SV, Wooff EE, Parish T, Hewinson RG. Functional demonstration of reverse transsulfuration in the *Mycobacterium tuberculosis* complex reveals that methionine is the preferred sulfur source for pathogenic Mycobacteria. *J Biol Chem* 280: 8069-78, 2005.
188. Winglee K, Lun S, Pieroni M, Kozikowski A, Bishai W. Mutation of Rv2887, a marR-like gene, confers *Mycobacterium tuberculosis* resistance to an imidazopyridine-based agent. *Antimicrob Agents Chemother* 59: 6873-81, 2015.
189. Winterbourn CC, Kettle AJ, Hampton MB. Reactive oxygen species and neutrophil function. *Annu Rev Biochem* 85: 765-92, 2016.
190. Yukawa H, Omumasaba CA, Nonaka H, Kos P, Okai N, Suzuki N, Suda M, Tsuge Y, Watanabe J, Ikeda Y, Vertes AA, Inui M. Comparative analysis of the *Corynebacterium glutamicum* group and complete genome sequence of strain R. *Microbiology* 153: 1042-58, 2007.
191. Zheng M, Aslund F, Storz G. Activation of the OxyR transcription factor by reversible disulfide bond formation. *Science* 279: 1718-21, 1998.
192. Zheng M, Wang X, Templeton LJ, Smulski DR, LaRossa RA, Storz G. DNA microarray-mediated transcriptional profiling of the *Escherichia coli* response to hydrogen peroxide. *J Bacteriol* 183: 4562-70, 2001.
193. Zhou A, Nawaz M, Duan Y, Moore JE, Millar BC, Xu J, Yao Y. Molecular characterization of isoniazid-resistant *Mycobacterium tuberculosis* isolates from Xi'an, China. *Microb Drug Resist* 17: 275-81, 2011.
194. Zhou NY, Fuenmayor SL, Williams PA. *nag* genes of *Ralstonia* (formerly *Pseudomonas*) sp. strain U2 encoding enzymes for gentisate catabolism. *J Bacteriol* 183: 700-8, 2001.

Chapter 1

Biosynthesis and functions of bacillithiol in *Firmicutes*

Quach Ngoc Tung[1], Nico Linzner[1], Vu Van Loi[1], Haike Antelmann[1#]

[1]*Freie Universität Berlin, Institute for Biology-Microbiology, D-14195 Berlin, Germany*

Published in: Book chapter No. 20, Book title "Glutathione", CRC Press, Taylor & Francis Group (2018)
https://doi.org/10.1201/9781351261760

[#]**Corresponding author:** haike.antelmann@fu-berlin.de

Personal contribution:

I contributed to writing of the chapter 20 sub-sections no. 3, 4, 5 about structure, biophysics, biosynthesis, functions of bacillithiol and also section no. 8, 9 about protein *S*-bacillithiolations and its redox regulation by bacilliredoxins. I created draft figures of Fig.1-5 and Fig. 7 for this book chapter.

Chapter 2

Staphylococcus aureus uses the bacilliredoxin (BrxAB)/ bacillithiol disulfide reductase (YpdA) redox pathway to defend against oxidative stress under infections

Nico Linzner[1], Vu Van Loi[1], Verena Nadin Fritsch[1], Quach Ngoc Tung[1], Saskia Stenzel[1], Markus Wirtz[2], Rüdiger Hell[2], Chris Hamilton[3], Karsten Tedin[4], Marcus Fulde[4] and Haike Antelmann[1#]

[1]*Freie Universität Berlin, Institute for Biology-Microbiology, D-14195 Berlin, Germany*
[2]*Plant Molecular Biology, Centre for Organismal Studies Heidelberg, University of Heidelberg, Heidelberg, Germany*
[3]*School of Pharmacy, University of East Anglia, Norwich Research Park, Norwich, NR4 7TJ, UK*
[4]*Freie Universität Berlin, Institute of Microbiology and Epizootics, Centre for Infection Medicine, D-14163 Berlin, Germany*

Published in: Frontiers in Microbiology 10: 1355. (2019)
https://doi.org/10.3389/fmicb.2019.01355

[#]**Corresponding author:** haike.antelmann@fu-berlin.de

Personal contribution:

I was involved in preparing samples for quantification of LMW thiols and disulfides *in vivo* (Fig. 3). I measured the activity of YpdA in BSSB reduction and de-bacillithiolation of GapDH-SSB using the BrxA/BSH/YpdA electron pathway *in vitro* (Fig. 9).

frontiers in Microbiology

ORIGINAL RESEARCH
published: 18 June 2019
doi: 10.3389/fmicb.2019.01355

Staphylococcus aureus Uses the Bacilliredoxin (BrxAB)/Bacillithiol Disulfide Reductase (YpdA) Redox Pathway to Defend Against Oxidative Stress Under Infections

*Nico Linzner[1], Vu Van Loi[1], Verena Nadin Fritsch[1], Quach Ngoc Tung[1], Saskia Stenzel[1], Markus Wirtz[2], Rüdiger Hell[2], Chris J. Hamilton[3], Karsten Tedin[4], Marcus Fulde[4] and Haike Antelmann[1]**

[1] Institute for Biology – Microbiology, Freie Universität Berlin, Berlin, Germany, [2] Plant Molecular Biology, Centre for Organismal Studies Heidelberg, Heidelberg University, Heidelberg, Germany, [3] School of Pharmacy, University of East Anglia, Norwich, United Kingdom, [4] Institute of Microbiology and Epizootics, Centre for Infection Medicine, Freie Universität Berlin, Berlin, Germany

OPEN ACCESS

Edited by:
Boris Macek,
University of Tübingen, Germany

Reviewed by:
Alberto A. Iglesias,
National University of the Littoral, Argentina
Ivan Mijakovic,
Chalmers University of Technology, Sweden
Bruno Manta,
New England Biolabs, United States

***Correspondence:**
Haike Antelmann
haike.antelmann@fu-berlin.de

Specialty section:
This article was submitted to Microbial Physiology and Metabolism, a section of the journal Frontiers in Microbiology

Received: 03 February 2019
Accepted: 31 May 2019
Published: 18 June 2019

Citation:
Linzner N, Loi VV, Fritsch VN, Tung QN, Stenzel S, Wirtz M, Hell R, Hamilton CJ, Tedin K, Fulde M and Antelmann H (2019) Staphylococcus aureus Uses the Bacilliredoxin (BrxAB)/Bacillithiol Disulfide Reductase (YpdA) Redox Pathway to Defend Against Oxidative Stress Under Infections. Front. Microbiol. 10:1355. doi: 10.3389/fmicb.2019.01355

Staphylococcus aureus is a major human pathogen and has to cope with reactive oxygen and chlorine species (ROS, RCS) during infections. The low molecular weight thiol bacillithiol (BSH) is an important defense mechanism of *S. aureus* for detoxification of ROS and HOCl stress to maintain the reduced state of the cytoplasm. Under HOCl stress, BSH forms mixed disulfides with proteins, termed as *S*-bacillithiolations, which are reduced by bacilliredoxins (BrxA and BrxB). The NADPH-dependent flavin disulfide reductase YpdA is phylogenetically associated with the BSH synthesis and BrxA/B enzymes and was recently suggested to function as BSSB reductase (Mikheyeva et al., 2019). Here, we investigated the role of the complete bacilliredoxin BrxAB/BSH/YpdA pathway in *S. aureus* COL under oxidative stress and macrophage infection conditions *in vivo* and in biochemical assays *in vitro*. Using HPLC thiol metabolomics, a strongly enhanced BSSB level and a decreased BSH/BSSB ratio were measured in the *S. aureus* COL Δ*ypdA* deletion mutant under control and NaOCl stress. Monitoring the oxidation degree (OxD) of the Brx-roGFP2 biosensor revealed that YpdA is required for regeneration of the reduced BSH redox potential (E_{BSH}) upon recovery from oxidative stress. In addition, the Δ*ypdA* mutant was impaired in H_2O_2 detoxification as measured with the novel H_2O_2-specific Tpx-roGFP2 biosensor. Phenotype analyses further showed that BrxA and YpdA are required for survival under NaOCl and H_2O_2 stress *in vitro* and inside murine J-774A.1 macrophages in infection assays *in vivo*. Finally, NADPH-coupled electron transfer assays provide evidence for the function of YpdA in BSSB reduction, which depends on the conserved Cys14 residue. YpdA acts together with BrxA and BSH in de-bacillithiolation of *S*-bacillithiolated GapDH. In conclusion, our results point to a major role of the BrxA/BSH/YpdA pathway in BSH redox homeostasis in *S. aureus* during recovery from oxidative stress and under infections.

Keywords: *Staphylococcus aureus*, oxidative stress, bacillithiol, bacilliredoxin, bacillithiol disulfide reductase, YpdA, roGFP2

INTRODUCTION

Staphylococcus aureus is an important human pathogen, which can cause many diseases, ranging from local soft-tissue and wound infections to life-threatening systemic and chronic infections, such as endocarditis, septicaemia, bacteraemia, pneumonia or osteomyelitis (Archer, 1998; Lowy, 1998; Boucher and Corey, 2008). Due to the prevalence of methicillin-resistant *S. aureus* isolates, which are often resistant to multiple antibiotics, treatment options are limited to combat *S. aureus* infections (Livermore, 2000). Therefore, the "European Center of Disease Prevention and Control" has classified *S. aureus* as one out of six ESKAPE pathogens which are the leading causes of nosocomial infections worldwide (Pendleton et al., 2013). During infections, activated macrophages and neutrophils produce reactive oxygen and chlorine species (ROS, RCS) in large quantities, including H_2O_2 and HOCl with the aim to kill invading pathogens (Winterbourn and Kettle, 2013; Hillion and Antelmann, 2015; Beavers and Skaar, 2016; Winterbourn et al., 2016).

Low molecular weight thiols play important roles in the defense against ROS and HOCl in bacterial pathogens and are required for survival, host colonization, and pathogenicity (Loi et al., 2015; Tung et al., 2018). Gram-negative bacteria produce GSH as major LMW thiol, which is absent in most Gram-positive bacteria (Fahey, 2013). Instead, many firmicutes utilize BSH as alternative LMW thiol (**Figure 1A**), which is essential for virulence of *S. aureus* in macrophage infection assays (Newton et al., 2012; Pöther et al., 2013; Posada et al., 2014; Chandrangsu et al., 2018). A recent study identified a BSH derivative with an *N*-methylated cysteine as *N*-methyl-BSH in anaerobic phototrophic *Chlorobiaceae*, suggesting that BSH derivatives are more widely distributed and not restricted to Gram-positive firmicutes (Hiras et al., 2018). In *S. aureus* and *Bacillus subtilis*, BSH was characterized as cofactor of thiol-*S*-transferases (e.g., FosB), glyoxalases, peroxidases, and other redox enzymes that are involved in detoxification of ROS, HOCl, methylglyoxal, toxins, and antibiotics (Chandrangsu et al., 2018). In addition, BSH participates in post-translational thiol-modifications under HOCl stress by formation of BSH mixed protein disulfides, termed as protein *S*-bacillithiolations (Chi et al., 2011, 2013; Imber et al., 2018a,c).

Protein *S*-bacillithiolation functions in thiol-protection and redox regulation of redox-sensing regulators, metabolic enzymes and antioxidant enzymes (Chi et al., 2011, 2013; Loi et al., 2015; Imber et al., 2018a,b,c). In *S. aureus*, the glycolytic glyceraldehyde-3-phosphate dehydrogenase (GapDH) and the aldehyde dehydrogenase AldA were identified as most abundant *S*-bacillithiolated proteins that are inactivated under HOCl stress (Imber et al., 2018a,b). In *B. subtilis*, the methionine synthase MetE and the OhrR repressor are *S*-bacillithiolated under HOCl stress leading to methionine auxotrophy and derepression of the OhrR-controlled *ohrA* peroxiredoxin gene, respectively (Fuangthong et al., 2001; Lee et al., 2007; Chi et al., 2011).

Reduction of *S*-bacillithiolated OhrR, MetE, and GapDH proteins is catalyzed by the bacilliredoxins (BrxA/B) in *B. subtilis* and *S. aureus in vitro* (Gaballa et al., 2014; Chandrangsu et al., 2018). BrxA (YphP) and BrxB (YqiW) are paralogous thioredoxin-fold proteins of the UPF0403 family with an unusual CGC active site that are conserved in BSH-producing firmicutes (**Supplementary Figure S1**). Upon de-bacillithiolation, the BSH moiety is transferred to the Brx active site, resulting in BrxA-SSB formation (**Figure 1B**). However, the Brx associated thiol-disulfide reductase involved in regeneration of Brx activity is not known. In GSH-producing bacteria, Grx catalyze the reduction of *S*-glutathionylated proteins, which requires GSH for regeneration of Grx, resulting in GSSG formation (Lillig et al., 2008; Allen and Mieyal, 2012). The regeneration of GSH is catalyzed by the flavoenzyme Gor, which belongs to the pyridine nucleotide disulfide reductases and recycles GSSG on expense of NADPH (Argyrou and Blanchard, 2004; Deponte, 2013).

Phylogenomic profiling of protein interaction networks using EMBL STRING search has suggested the flavoenzyme YpdA (SACOL1520) as putative NADPH-dependent BSSB reductase (**Supplementary Figure S1**), since YpdA co-occurs together with BrxA/B and the BSH biosynthesis enzymes (BshA/B/C) only in BSH-producing bacteria, such as *B. subtilis* and *S. aureus* (**Supplementary Figure S2**; Gaballa et al., 2010). While our work was in progress, a recent study provides first evidence for the function of YpdA as putative BSSB reductase in *S. aureus in vivo* since an increased BSSB level and a decreased BSH/BSSB ratio was measured in the Δ*ypdA* mutant under control and H_2O_2 stress conditions (Mikheyeva et al., 2019). YpdA overproduction was shown to increase the BSH level and contributes to

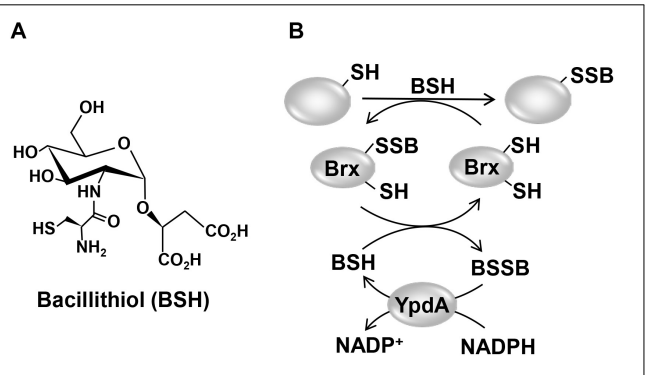

FIGURE 1 | Structure of the LMW thiol bacillithiol (BSH) **(A)** and mechanism of the bacilliredoxin (Brx)/BSH/YpdA de-bacillithiolation pathway **(B)**. **(A)** Bacillithiol is composed of glucosamine, malate, and cysteine. **(B)** Under HOCl stress, BSH leads to *S*-bacillithiolation of proteins which are reduced by bacilliredoxins (BrxA/B), resulting in the transfer of BSH to the Brx active site (Brx-SSB). BSH functions in Brx-SSB reduction to restore Brx activity, leading to BSSB formation. The BSSB reductase YpdA (SACOL1520) regenerates BSH on expense of NADPH.

Abbreviations: BSH, bacillithiol; BSSB, bacillithiol disulfide; BrxA/B, bacilliredoxin A (YphP)/bacilliredoxin B (YqiW); CFUs, colony forming units; DTT, dithiothreitol; E_{BSH}, bacillithiol redox potential; GapDH, glyceraldehyde 3-phosphate dehydrogenase; GSH, glutathione; GSSG, glutathione disulfide; Gor, glutathione disulfide reductase; Grx, glutaredoxins; HOCl, hypochlorous acid; LMW, low molecular weight; Mtr, mycothiol disulfide reductase; NaOCl, sodium hypochlorite; OD_{500}, optical density at 500 nm; rdw, raw dry weight; RCS, reactive chlorine species; ROS, reactive oxygen species; YpdA, bacillithiol disulfide reductase.

oxidative stress resistance, fitness, and virulence of *S. aureus* (Mikheyeva et al., 2019). However, biochemical evidence for the function of YpdA as BSSB reductase and the association of YpdA to the BrxA/B enzymes have not been demonstrated in *B. subtilis* or *S. aureus*.

In this work, we aimed to investigate the role of the complete BrxAB/BSH/YpdA pathway in *S. aureus in vivo* and *in vitro*. We used phenotype and biochemical analyses, HPLC metabolomics and redox biosensor measurements to study the physiological role of the Brx/BSH/YpdA redox pathway in *S. aureus* under oxidative stress and macrophage infection assays. Our data point to important roles of both BrxA and YpdA in the oxidative stress defense for regeneration of reduced E_{BSH} and de-bacillithiolation upon recovery from oxidative stress. Biochemical assays further provide evidence for the function of YpdA as BSSB reductase *in vitro*, which acts in the BrxA/BSH/YpdA electron pathway in de-bacillithiolation of GapDH-SSB.

MATERIALS AND METHODS

Bacterial Strains, Growth, and Survival Assays

Bacterial strains, plasmids and primers used in this study are listed in **Supplementary Tables S1, S2, S3**. For cloning and genetic manipulation, *Escherichia coli* was cultivated in LB medium. For stress experiments, *S. aureus* COL wild type and mutant strains were cultivated in LB, RPMI, or Belitsky minimal medium and exposed to the different compounds during the exponential growth as described previously (Loi et al., 2017, 2018b). NaOCl, methylglyoxal, diamide, methylhydroquinone, DTT, cumene hydroperoxide (80% w/v), H_2O_2 (35% w/v), and monobromobimane were purchased from Sigma Aldrich.

Cloning, Expression, and Purification of His-Tagged Brx-roGFP2, Tpx-roGFP2, GapDH, BrxA, YpdA, and YpdAC14A Proteins in *E. coli*

Construction of plasmids pET11b-*brx-roGFP2* for expression of the Brx-roGFP2 biosensor was described previously (Loi et al., 2017). The pET11b-derived plasmids for overexpression of the His-tagged GapDH and BrxA (SACOL1321) proteins were generated previously (Imber et al., 2018a). The plasmid pET11b-*brx-roGFP2* was used as a template for construction of the Tpx-roGFP2 biosensor to replace *brx* by the *tpx* gene of *S. aureus*. The *tpx* gene (*SACOL1762*) was PCR-amplified from chromosomal DNA of *S. aureus* COL using primers pET-tpx-for-NheI and pET-tpx-rev-SpeI (**Supplementary Table S3**), digested with *Nhe*I and *Bam*HI and cloned into plasmid pET11b-*brx-roGFP2* to generate pET11b-*tpx-roGFP2*. To construct plasmids pET11b-*ypdA* or pET11b-*ypdAC14A*, the *ypdA* gene (*SACOL1520*) was PCR-amplified from chromosomal DNA of *S. aureus* COL with pET-ypdA-for-NdeI or pET-ypdAC14A-for-NdeI as forward primers and pET-ypdA-rev-BamHI as reverse primer (**Supplementary Table S3**), digested with *Nde*I and *Bam*HI and inserted into plasmid pET11b (Novagen). For expression of His-tagged proteins (GapDH, BrxA, YpdA, YpdAC14A, Tpx-roGFP2), *E. coli* BL21(DE3) *plys*S carrying plasmids pET11b-*gap,* pET11b-*brxA,* pET11b-*ypdA*, pET11b-*ypdAC14A* and pET11b-*tpx-roGFP2* was cultivated in 1 l LB medium until an OD_{600} of 0.8 followed by addition of 1 mM IPTG (isopropyl-β-D-thiogalactopyranoside) for 16 h at 25°C. His_6-tagged GapDH, BrxA, YpdA, YpdAC14A, and Tpx-roGFP2 proteins were purified using His Trap™ HP Ni-NTA columns (5 ml; GE Healthcare, Chalfont St Giles, United Kingdom) and the ÄKTA purifier liquid chromatography system (GE Healthcare) as described (Loi et al., 2018b).

Construction of *S. aureus* COL Δ*ypdA,* Δ*brxAB* and Δ*brxAB*Δ*ypdA* Clean Deletion Mutants and Complemented Mutant Strains

Staphylococcus aureus COL Δ*ypdA* (*SACOL1520*), Δ*brxA* (*SACOL1464*), and Δ*brxB* (*SACOL1558*) single deletion mutants as well as the Δ*brxAB* double and Δ*brxAB*Δ*ypdA* triple mutants were constructed using pMAD as described (Arnaud et al., 2004; Loi et al., 2018b). Briefly, the 500 bp up- and downstream regions of *ypdA*, *brxA,* and *brxB* were amplified using gene-specific primers (**Supplementary Table S3**), fused by overlap extension PCR and ligated into the *Bgl*II and *Sal*I sites of plasmid pMAD. The pMAD constructs were electroporated into *S. aureus* RN4220 and further transduced into *S. aureus* COL using phage 81 (Rosenblum and Tyrone, 1964). The clean marker-less deletions of *ypdA*, *brxA,* or *brxB* were selected after plasmid excision as described (Loi et al., 2018b). All mutants were clean deletions of internal gene regions with no genetic changes in the up- and downstream encoding genes. The deletions of the internal gene regions were verified by PCR and DNA sequencing. The Δ*brxAB* and Δ*brxAB*Δ*ypdA* double and triple mutants were obtained by transduction and excision of pMAD-Δ*brxB* into the Δ*brxA* mutant, leading to the Δ*brxAB* deletion and of plasmid pMAD-Δ*ypdA* into the Δ*brxAB* mutant, resulting in the Δ*brxAB*Δ*ypdA* knockout. For construction of *ypdA, brxA,* and *brxB* complemented strains, the xylose-inducible ectopic *E. coli/S. aureus* shuttle vector pRB473 was applied (Brückner et al., 1993). Primers pRB-ypdA, pRB-brxA, and pRB-brxB (**Supplementary Table S3**) were used for amplification of the genes, which were cloned into pRB473 after digestion with *Bam*HI and *Kpn*I to generate plasmids pRB473-*ypdA*, pRB473-*brxA,* and pRB473-*brxB,* respectively. The pRB473 constructs were confirmed by PCR and DNA sequencing and transduced into the Δ*ypdA* and Δ*brxAB* deletion mutants as described (Loi et al., 2017).

Construction of Tpx-roGFP2 and Brx-roGFP2 Biosensor Fusions in *S. aureus* COL

The *tpx-roGFP2* fusion was amplified from plasmid pET11b-*tpx-roGFP2* with primers pRB-tpx-roGFP2-for-BamHI and pRB-tpx-roGFP2-rev-SacI and digested with *Bam*HI and *Sac*I (**Supplementary Table S3**). The PCR product was cloned into

pRB473 generating plasmid pRB473-*tpx-roGFP2*, which was confirmed by DNA sequencing. The biosensor plasmids pRB473-*tpx-roGFP2* and pRB473-*brx-roGFP2* were electroporated into *S. aureus* RN4220 and further transferred to the *S. aureus* COL Δ*ypdA*, Δ*brxAB* and Δ*brxAB*Δ*ypdA* mutants by phage transduction as described (Loi et al., 2017).

Northern Blot Experiments

Northern blot analyses were performed using RNA isolated from *S. aureus* COL before and 15 min after exposure to 0.5 mM methylglyoxal, 0.75 mM formaldehyde, 1 mM NaOCl, 10 mM H_2O_2, 2 mM diamide, and 45 μM methylhydroquinone as described (Wetzstein et al., 1992). Hybridizations were conducted using digoxigenin-labeled antisense RNA probes for *ypdA, brxA,* and *brxB* that were synthesized *in vitro* using T7 RNA polymerase and primers ypdA-NB-for/rev, brxA-NB-for/rev, or brxB-NB-for/rev (**Supplementary Table S3**) as in previous studies (Tam le et al., 2006).

HPLC Thiol Metabolomics for Quantification of LMW Thiols and Disulfides

For preparation of thiol metabolomics samples, *S. aureus* COL WT, Δ*ypdA* and Δ*brxAB* mutants as well as the *ypdA* complemented strains were grown in RPMI medium to an OD_{500} of 0.9 and exposed to 2 mM NaOCl stress for 30 min. The intracellular amounts of reduced and oxidized LMW thiols and disulfides (BSH, BSSB, cysteine and cystine) were extracted from the *S. aureus* cells, labeled with monobromobimane and measured by HPLC thiol metabolomics as described (Chi et al., 2013).

Western Blot Analysis

Staphylococcus aureus strains were grown in LB until an OD_{540} of 2, transferred to Belitsky minimal medium and treated with 100 μM NaOCl for 60 and 90 min. Cytoplasmic proteins were prepared and subjected to non-reducing BSH-specific Western blot analysis using the polyclonal rabbit anti-BSH antiserum as described previously (Chi et al., 2013). The de-bacillithiolation reactions with purified GapDH-SSB and the BrxA/BSH/YpdA/NADPH pathway were also subjected to non-reducing BSH-specific Western blots.

Brx-roGFP2 and Tpx-roGFP2 Biosensor Measurements

Staphylococcus aureus COL, Δ*ypdA* and Δ*brxAB* mutant strains expressing the Brx-roGFP2 and Tpx-roGFP2 biosensor plasmids were grown in LB and used for measurements of the biosensor oxidation degree (OxD) along the growth curves and after injection of the oxidants H_2O_2 and NaOCl as described previously (Loi et al., 2017). The fully reduced and oxidized control samples of Tpx-roGFP2 expression strains were treated with 15 mM DTT and 20 mM cumene hydroperoxide, respectively. The Brx-roGFP2 and Tpx-roGFP2 biosensor fluorescence emission was measured at 510 nm after excitation at 405 and 488 nm using the CLARIOstar microplate reader (BMG Labtech). The OxD of the Brx-roGFP2 and Tpx-roGFP2 biosensors was determined for each sample and normalized to fully reduced and oxidized controls as described (Loi et al., 2017) according to the Eq. (1):

$$O{\times}D = \frac{I405_{sample} \times I488_{red} - I405_{red} \times I488_{sample}}{I405_{sample} \times I488_{red} - I405_{sample} \times I488_{ox} + I405_{ox} \times I488_{sample} - I405_{red} \times I488_{sample}} \quad (1)$$

The values of $I405_{sample}$ and $I488_{sample}$ are the observed fluorescence excitation intensities at 405 and 488 nm, respectively. The values of $I405_{red}$, $I488_{red}$, $I405_{ox}$, and $I488_{ox}$ represent the fluorescence intensities of fully reduced and oxidized controls, respectively.

Based on the OxD values and the previously determined $E^{o'}_{roGFP2} = -280$ mV (Dooley et al., 2004), the BSH redox potential (E_{BSH}) can be calculated using to the Nernst equation (2):

$$E_{BSH} = E_{roGFP2} = E^{o'}_{roGFP2} - \left(\frac{RT}{2F}\right) \times \ln\left(\frac{1 - OxD}{OxD}\right) \quad (2)$$

Biochemical Assays for NADPH-Dependent BSSB Reduction by YpdA and De-Bacillithiolation of GapDH-SSB Using the BrxA/BSH/YpdA Electron Pathway *in vitro*

Before the activity assays, the purified BrxA, YpdA, and YpdAC14A proteins were prereduced with 10 mM DTT followed by DTT removal with Micro Biospin 6 columns (Biorad). For the biochemical activity assays of the specific BSSB reductase activity, 12.5 μM of purified YpdA and YpdAC14A proteins were incubated with 40 μM BSSB, 40 μM GSSG, or 40 μM coenzyme A disulfide and 500 μM NADPH in 20 mM Tris, 1.25 mM EDTA, pH 8.0. NADPH consumption of YpdA and YpdAC14A was measured immediately after the start of the reaction as absorbance change at 340 nm using the Clariostar microplate reader. The NADPH-dependent BrxA/BSH/YpdA electron pathway was reconstituted *in vitro* for de-bacillithiolation of GapDH-SSB. About 60 μM of purified GapDH was *S*-bacillithiolated with 600 μM BSH in the presence of 6 mM H_2O_2 for 5 min. Excess of BSH and H_2O_2 were removed with Micro Biospin 6 columns, which were equilibrated with 20 mM Tris, 1.25 mM EDTA, pH 8.0. Before starting the de-bacillithiolation assay using the BrxA/BSH/YpdA electron pathway, 2.5 μM GapDH-SSB was incubated with 12.5 μM BrxA, 40 μM BSH, and 500 μM NADPH in 20 mM Tris, 1.25 mM EDTA, pH 8.0 at room temperature for 30 min. Next, 12.5 μM YpdA or YpdAC14A proteins were added to the reaction mix at 30°C for 8 min and NADPH consumption was measured at 340 mm. The biochemical activity assays were performed in four replicate experiments.

Infection Assays With Murine Macrophage Cell Line J-774A.1

The murine cell line J774A.1 was cultivated in Iscove's modified Dulbecco MEM medium (Biochrom) with 10% heat inactivated

fetal bovine serum (FBS) and used for *S. aureus* infection assays as described (Loi et al., 2018b). Macrophages were infected with *S. aureus* cells at a multiplicity of infection (MOI) of 1:25. One hour after infection, the cell culture medium was replaced and 150 μg/ml gentamycin was added for 1 h to kill extracellular bacteria and to stop the uptake of *S. aureus*. The *S. aureus* cells were harvested at 2, 4, and 24 h post infection. To determine the percentage of surviving *S. aureus* cells, infected macrophages were lysed with 0.1% Triton X-100 and the supernatant of internalized bacteria was plated on brain heart infusion (BHI) agar plates. The CFUs were counted after incubation for 24–36 h at 37°C (Loi et al., 2018b).

Statistical Analyses

Statistical analysis of growth and survival assays was performed using the Student's unpaired two-tailed *t*-test by the graph prism software. The statistics of the J-774.1 macrophage infection assays was calculated using the one-way ANOVA and Tukey's multiple comparisons *post hoc* test by the graph prism software. The results of the statistical tests are included in the figure legends.

RESULTS

Transcription of *ypdA*, *brxA,* and *brxB* Is Induced Under Disulfide Stress by Diamide and NaOCl in *S. aureus* COL

The bacilliredoxins BrxA (SACOL1464) and BrxB (SACOL1558) of *S. aureus* share an unusual CGC active site and are highly conserved in BSH-producing firmicutes (**Supplementary Figure S1**; Gaballa et al., 2014). The pyridine nucleotide disulfide oxidoreductase YpdA (SACOL1520) belongs to the FAD/NAD(P)-binding domain superfamily (IPR036188) and was annotated as putative BSSB reductase due to its phylogenetic co-occurence with the BSH biosynthesis enzymes and BrxA/B in BSH-producing firmicutes (**Supplementary Figure S2**; Gaballa et al., 2010). We used Northern blot analysis to investigate whether transcription of *brxA*, *brxB,* and *ypdA* is co-regulated and up-regulated under thiol-specific stress conditions, such as 0.5 mM methylglyoxal, 0.75 mM formaldehyde, 1 mM NaOCl, 10 mM H_2O_2, 2 mM diamide and 45 μM methylhydroquinone (**Figure 2**). The *brxA* gene is co-transcribed with *SACOL1465-66-67* in a 2 kb operon and *brxB* is located in the 1.6 kb *SACOL1557-brxB-SACOL1559* operon. The genes co-transcribed together with *brxA* and *brxB* encode proteins of unknown functions. The Northern blot results revealed significant basal transcription of the *brxA, brxB,* and *ypdA* genes and operons in the control, and strong induction under disulfide stress provoked by NaOCl and diamide. Of note, the *brxB* operon was stronger induced under disulfide stress compared to the *brxA* operon (**Figure 2**). No up-regulation of the *brxA, brxB,* and *ypdA* specific mRNAs was detected upon H_2O_2, aldehyde and quinone stress. The co-regulation of BrxA/B and YpdA under disulfide stress suggests that they act in the same pathway to regenerate

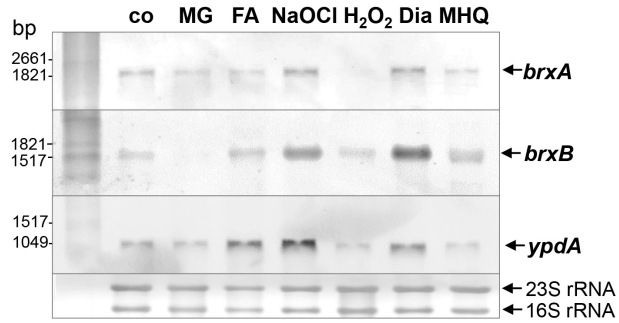

FIGURE 2 | Transcription of *brxA*, *brxB,* and *ypdA* is induced by disulfide stress in *S. aureus*. Northern blot analysis was used to analyze transcription of *brxA*, *brxB,* and *ypdA* in *S. aureus* COL wild type before (co) and 15 min after exposure to 0.5 mM methylglyoxal (MG), 0.75 mM formaldehyde (FA), 1 mM NaOCl, 10 mM H_2O_2, 2 mM diamide (Dia), and 45 μM methylhydroquinone (MHQ) stress at an OD_{500} of 0.5. The arrows point toward the transcript sizes of the *brxA*, *brxB,* and *ypdA* specific genes and operons. The methylene blue-stained bands of the 16S and 23S rRNAs are shown as RNA loading control at the bottom.

S-bacillithiolated proteins under NaOCl stress upon recovery from oxidative stress.

The BSSB Level Is Significantly Increased and the BSH/BSSB Ratio Is Decreased in the *S. aureus* Δ*ypdA* Mutant

To investigate the physiological role of BrxA/B and YpdA under oxidative stress and in BSH redox homeostasis, we constructed Δ*brxAB* and Δ*ypdA* deletion mutants. Using HPLC thiol metabolomics, the intracellular levels of BSH and BSSB were determined in the Δ*brxAB* and Δ*ypdA* mutants under control and NaOCl stress after monobromobimane derivatisation of LMW thiols and disulfides. In the *S. aureus* COL wild type, a BSH level of 1.6–1.9 μmol/g rdw was determined, which was not significantly different in the Δ*ypdA* and Δ*brxAB* mutants (**Figure 3A**). Exposure of *S. aureus* to 2 mM NaOCl stress caused a five to sixfold decreased intracellular BSH level in the wild type, Δ*ypdA* and Δ*brxAB* mutants (**Figure 3A**). The level of BSSB was similar in control and NaOCl-treated cells of the wild type and Δ*brxAB* mutant (∼0.05 μmol/g rdw) (**Figure 3B**). Most interestingly, the Δ*ypdA* mutant showed a significantly twofold increased BSSB level under control and NaOCl stress compared to the wild type (**Figure 3B**), confirming previous data (Mikheyeva et al., 2019). Thus, the BSH/BSSB ratio is ∼2–3-fold decreased in the Δ*ypdA* mutant under control and NaOCl relative to the parent (**Figure 3C**). The increased BSSB levels and the decreased BSH/BSSB redox ratio in the Δ*ypdA* mutant could be restored to wild type levels in the *ypdA* complemented strain. In addition, a significantly 1.5-fold increased cysteine level was measured in the Δ*ypdA* mutant under NaOCl stress, but no changes in the level of cystine (**Supplementary Figures S3A–C**). The cysteine levels could be also restored to wild type level in the *ypdA* complemented

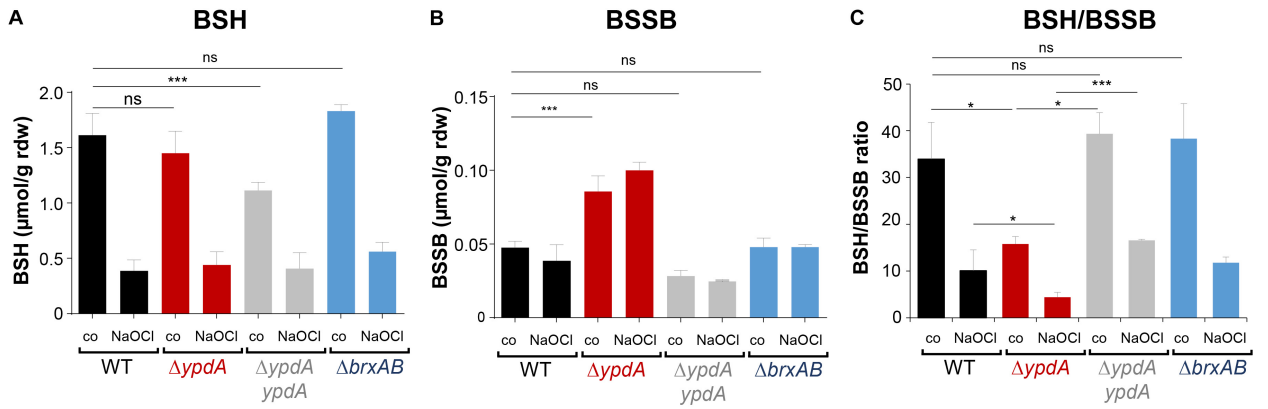

FIGURE 3 | The BSSB level is strongly increased and the BSH/BSSB redox ratio is decreased in the *S. aureus* COL Δ*ypdA* mutant under control and NaOCl stress. The levels of BSH **(A)**, BSSB **(B)** and the BSH/BSSB redox ratio **(C)** were determined in *S. aureus* COL wild type (WT), the Δ*ypdA* and Δ*brxAB* mutants as well as in the *ypdA* complemented strain before (co) and 30 min after treatment with 2 mM NaOCl stress. LMW thiols and disulfides were labeled with monobromobimane and measured using HPLC-thiol-metabolomics. Mean values and standard deviations (SD) of four biological replicates are shown. $^{ns}p > 0.05$; $^{*}p \leq 0.01$, and $^{***}p \leq 0.001$.

strain. These results indicate that YpdA is important to maintain the reduced level of BSH under control and NaOCl stress, supporting previous results (Mikheyeva et al., 2019), while the bacilliredoxins BrxA/B are dispensible for the cellular BSH/BSSB redox balance during the growth and under oxidative stress in *S. aureus*.

The *S. aureus* Δ*ypdA* Mutant Is Impaired to Regenerate the Reduced BSH Redox Potential and to Detoxify H_2O_2 Under Oxidative Stress

Next, we applied the Brx-roGFP2 biosensor to monitor the changes of its OxD in *S. aureus* COL wild type, the Δ*ypdA* and Δ*brxAB* mutants during the growth and under oxidative stress (Loi et al., 2017). Using the Nernst equation the OxD values were used to calculate the changes in the BSH redox potential (E_{BSH}) in wild type and mutant strains (see section "Materials and Methods" for details). Measurements of the Brx-roGFP2 OxD in LB medium along the growth did not reveal notable differences in the basal level of E_{BSH} between wild type, Δ*ypdA* and Δ*brxAB* mutant strains (**Supplementary Figures S4A,B, S5A,B** and **Supplementary Table S4**). The basal level of E_{BSH} varied from −282 to −295 mV in the wild type and from −286 to −299 mV in the Δ*ypdA* and Δ*brxAB* mutants in different growth phases (**Supplementary Figures S5A,B** and **Supplementary Table S4**). Thus, we monitored the biosensor OxD and calculated the E_{BSH} changes in Δ*ypdA* and Δ*brxAB* mutants after exposure to sub-lethal doses of 100 µM NaOCl and 100 mM H_2O_2 to identify functions for BrxAB or YpdA under oxidative stress. The Brx-roGFP2 biosensor was strongly oxidized under NaOCl and H_2O_2 stress in the wild type, the Δ*ypdA* and Δ*brxAB* mutants (**Figures 4A–D**). The calculated E_{BSH} increased upon NaOCl stress from −286 to −254 mV in the wild type, from −285 to −247 mV in the Δ*ypdA* mutant and from −288 to −259 mV in the Δ*brxAB* mutant (**Supplementary Figures S5C,D** and **Supplementary Table S5**). This indicates a stronger increase of E_{BSH} by NaOCl stress in the Δ*ypdA* mutant compared to the wild type. Regeneration of the reduced basal level E_{BSH} occurred already after 2 h reaching values of −269 mV in the wild type and −274 mV in the Δ*brxAB* mutant (**Figure 4B**, **Supplementary Figure S5D**, and **Supplementary Table S5**). However, the Δ*ypdA* mutant was significantly impaired to recover the reduced state and E_{BSH} values remained high with −252 mV after 2 h of NaOCl stress (**Figure 4A**, **Supplementary Figure S5C**, and **Supplementary Table S5**). Of note, the defect of the Δ*ypdA* mutant to restore the reduced state of E_{BSH} was reproducible with both oxidants, H_2O_2 and NaOCl (**Figures 4A,C**, **Supplementary Figures S5C,E**, and **Supplementary Table S6**). While recovery of reduced E_{BSH} after H_2O_2 stress was fast in the wild type and Δ*brxAB* mutant reaching E_{BSH} values of −280 and −283 mV already after 60 min, the Δ*ypdA* mutant was still oxidized after 2 h with high E_{BSH} values of −264 mV (**Supplementary Figures S5E,F** and **Supplementary Table S6**). These Brx-roGFP2 measurements document the important role of YpdA to reduce BSSB and to regenerate the reduced E_{BSH} during the recovery phase of cells from oxidative stress.

We further hypothesized that the Δ*ypdA* mutant is defective in H_2O_2 detoxification due to its increased BSSB levels. To analyse the kinetics of H_2O_2 detoxification in the Δ*ypdA* mutant, we constructed a genetically encoded H_2O_2-specific Tpx-roGFP2 biosensor. First, we verified that Tpx-roGFP2 showed the same ratiometric changes of the excitation spectrum in the fully reduced and oxidized state *in vitro* and *in vivo* as previously measured for Brx-roGFP2 (**Supplementary Figures S6A,B**). Tpx-roGFP2 was shown to respond strongly to low levels of 0.5–1 µM H_2O_2 *in vitro* and was fully oxidized with 100 mM H_2O_2 inside *S. aureus* COL wild type cells indicating the utility of the probe to measure H_2O_2 detoxification kinetics in *S. aureus* (**Supplementary Figures S6C,D**). Measurements of Tpx-roGFP2 oxidation along the growth in LB medium

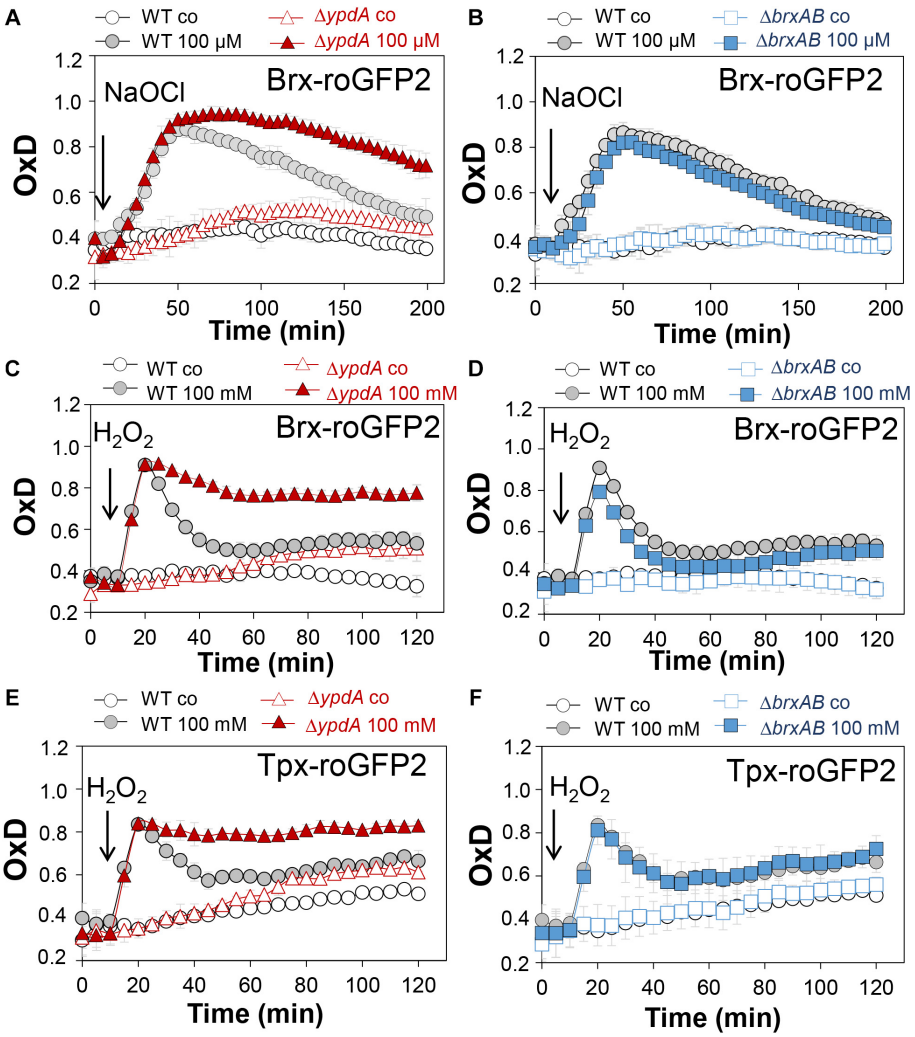

FIGURE 4 | Brx-roGFP2 and Tpx-roGFP2 biosensors measurements of the OxD indicate that the *S. aureus* Δ*ypdA* mutant is impaired to regenerate the reduced state of E_{BSH} and to detoxify H_2O_2 during recovery from oxidative stress. **(A–D)** Response of the Brx-roGFP2 biosensor to 100 µM NaOCl and 100 mM H_2O_2 stress in *S. aureus* COL WT, the Δ*ypdA* **(A,C)** and Δ*brxAB* **(B,D)** mutants. **(E,F)** Response of the Tpx-roGFP2 biosensor under 100 mM H_2O_2 stress in the *S. aureus* COL WT, the Δ*ypdA* and Δ*brxAB* mutants. The Brx-roGFP2 biosensor responses are shown as OxD values and the corresponding E_{BSH} changes were calculated using the Nernst equation and presented in **Supplementary Figure S5** and **Supplementary Tables S5, S6**. Mean values and SD of three biological replicates are shown.

revealed a similar high OxD of ∼0.5–0.6 in the wild type, Δ*brxAB* and Δ*ypdA* mutant strains (**Supplementary Figures S4C,D**). The absence of BrxA/B or YpdA did not affect the biosensor OxD under non-stress conditions, which further provides evidence for roles under oxidative stress. Thus, we monitored the H_2O_2 response of Tpx-roGFP2 and the kinetics of H_2O_2 detoxification in the Δ*ypdA* and Δ*brxAB* mutants. Interestingly, Tpx-roGFP2 showed a similar response to 100 mM H_2O_2 in all strains, but the Δ*ypdA* mutant was significantly impaired in H_2O_2 detoxification compared to the wild type (**Figures 4E,F**). These results clearly confirmed that the Δ*ypdA* mutant is defective to recover from oxidative stress due to its higher BSSB level resulting in an oxidized E_{BSH} as revealed using Brx-roGFP2 and thiol-metabolomics studies.

S-Bacillithiolation of GapDH Is Not Affected in Δ*ypdA* and Δ*brxAB* Mutants or in *ypdA*, *brxA*, and *brxB* Complemented Strains

In *S. aureus*, the glyceraldehyde-3 phosphate dehydrogenase GapDH was previously identified as most abundant *S*-bacillithiolated protein under NaOCl stress that is visible as major band in BSH-specific non-reducing Western blots (Imber et al., 2018a). Since GapDH activity could be recovered with purified BrxA *in vitro* previously (Imber et al., 2018a), we analyzed the pattern of GapDH *S*-bacillithiolation in the Δ*brxAB* and Δ*ypdA* mutants as well as in *ypdA*, *brxA* and *brxB* complemented strains *in vivo*. However, the amount of *S*-bacillithiolated GapDH was similar after

100 μM NaOCl stress between wild type, Δ*brxAB* and Δ*ypdA* mutants and complemented strains (**Figures 5A,B**). This indicates that the absence of the BrxAB/YpdA pathway does not affect the level of *S*-bacillithiolation of GapDH under NaOCl stress.

The Bacilliredoxins BrxA/B and the Putative BSSB Reductase YpdA Are Important for Growth and Survival Under Oxidative Stress and Macrophage Infections

Next, we analyzed the physiological role of the BrxA/B/YpdA pathway for growth and survival of *S. aureus* under H_2O_2 and NaOCl stress. The growth of the Δ*ypdA* and Δ*brxAB* mutants in RPMI medium without stress exposure was comparable to the wild type (**Figures 6A,C**). Interestingly, both Δ*brxAB* and Δ*ypdA* mutants displayed a small, but statistically significant growth delay after exposure to sub-lethal amounts of 1.5 mM NaOCl compared to the wild type, while no growth delay was observed with sub-lethal 10 mM H_2O_2 (**Figures 6A,C**, **7A,B**). This might indicate that BrxAB and YpdA function in the same pathway as already suggested by phylogenomic profiling using STRING search (**Supplementary Figure S2**). Determination of viable counts revealed significantly ∼2-fold decreased survival rates of both Δ*brxAB* and Δ*ypdA* mutants after exposure to lethal doses of 3.5 mM NaOCl and 40 mM H_2O_2 relative to the wild type (**Figures 6F,G**, **7C,D**). These oxidant sensitive growth and survival phenotypes of the Δ*brxAB* and Δ*ypdA* mutants could be restored back to wild type levels by complementation with *brxA* and *ypdA,* respectively (**Figures 6B,D,F,G**, **7C,D**). However, complementation of the Δ*brxAB* mutant with *brxB* did not restore the growth and viability of the wild type under NaOCl stress (**Figures 6E,G**), although xylose-inducible *brxB* expression of plasmid pRB473-*brxB* could be verified in Northern blots (**Supplementary Figure S7**). Moreover, the Δ*brxAB*Δ*ypdA* triple mutant displayed the same sensitivity as the Δ*brxAB* mutant to 40 mM H_2O_2 and 3 mM NaOCl indicating that BrxA and YpdA function in the same pathway for reduction of *S*-bacillithiolated proteins (**Figures 7D** and **Supplementary Figure S8C**).

To investigate the function of the BrxA/B/YpdA pathway under infection-relevant conditions, we measured the intracellular survival of the Δ*brxAB* and Δ*ypdA* mutants in phagocytosis assays inside murine macrophages of the cell line J-774A.1, as previously (Loi et al., 2018b). The viable counts (CFUs) of internalized *S. aureus* cells were determined at 2, 4, and 24 h post infection of the macrophages. The number of surviving cells decreased to 21.3% at 24 h post infection for the *S. aureus* COL wild type, but more strongly to 11.4 and 10.2% for the Δ*ypdA* and Δ*brxAB* mutants (**Figures 8A,C**). Thus, the number of viable counts was significantly ∼2-fold lower for both Δ*brxAB* and Δ*ypdA* mutants at 24 h post infection compared to the wild type. These sensitive phenotypes of the Δ*ypdA* and Δ*brxAB* mutants under macrophage infections could be restored to 80% of wild type levels after complementation with plasmid-encoded *ypdA* or *brxA*, respectively (**Figures 8B,D**). However, complementation with *brxB* did not restore the survival defect of the Δ*brxAB* mutant, pointing again to the major role of BrxA in this pathway.

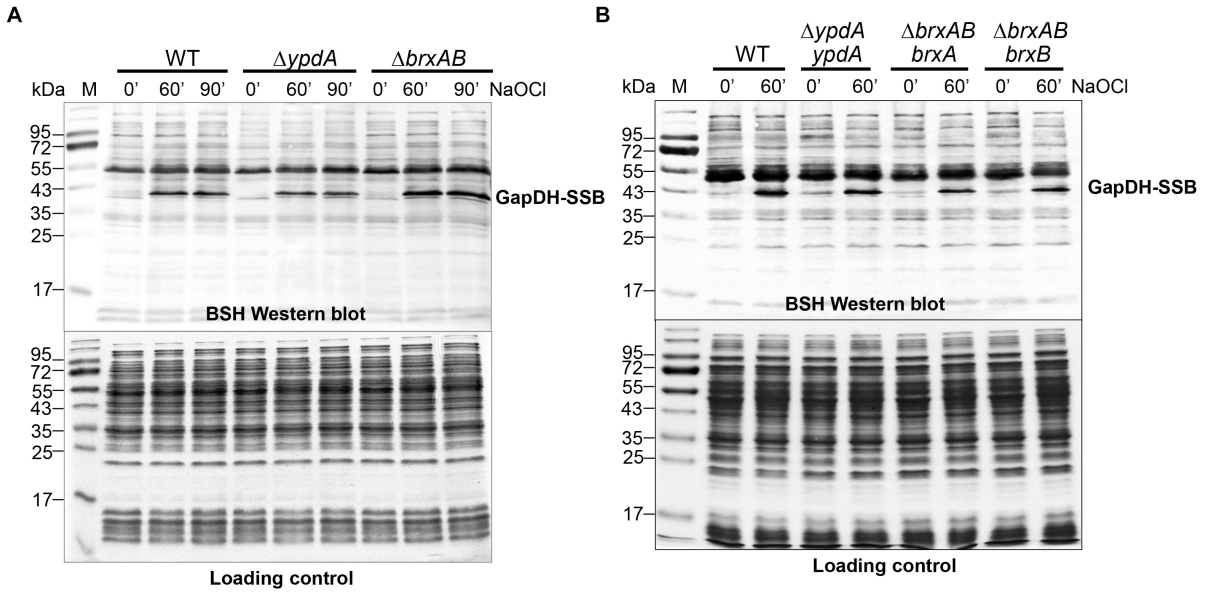

FIGURE 5 | Protein *S*-bacillithiolation of GapDH is not affected in the Δ*ypdA* and Δ*brxAB* mutants **(A)** or in the *ypdA*, *brxA,* and *brxB* complemented strains **(B)** as revealed by non-reducing BSH Western blots. The prominent GapDH-SSB band is visible in the cell extracts of NaOCl-treated *S. aureus* cells using non-reducing BSH Western blots. Other bands visible under control and stress conditions are proteins cross-reactive with the polyclonal rabbit anti-BSH antibodies. The amount of GapDH-SSB is similar in the WT, Δ*ypdA* and Δ*brxAB* mutants **(A)** as well as in the *ypdA*, *brxA,* and *brxB* complemented strains **(B)**. The SDS PAGE loading control is shown at the bottom for comparison.

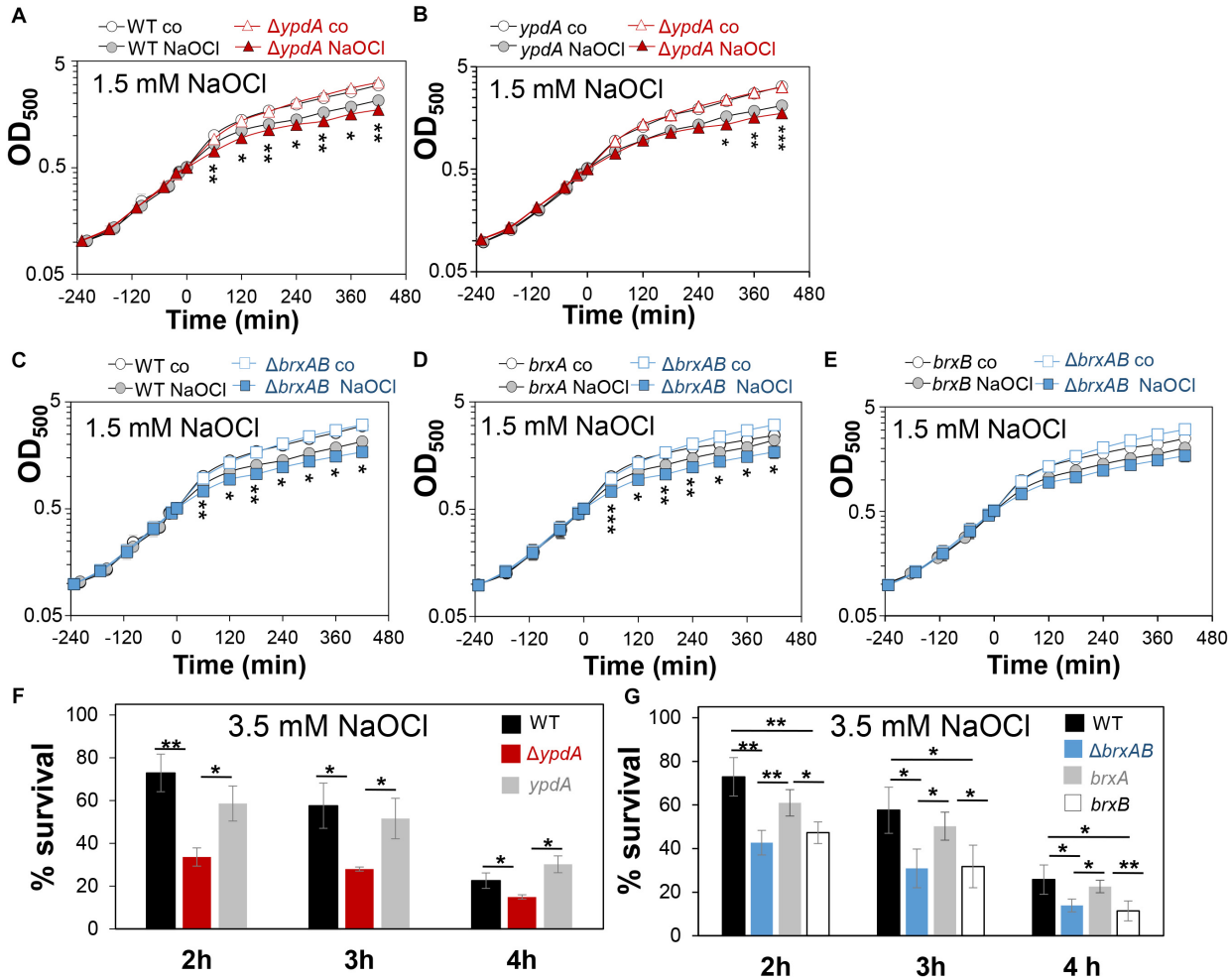

FIGURE 6 | The *S. aureus* Δ*ypdA* and Δ*brxAB* mutants are more sensitive under NaOCl stress. **(A–E)** Growth curves of *S. aureus* COL WT, Δ*ypdA* and Δ*brxAB* mutants as well as *ypdA*, *brxA,* and *brxB* complemented strains in RPMI medium after exposure to 1.5 mM NaOCl stress at an OD_{500} of 0.5. **(F,G)** Survival rates were determined as CFUs for *S. aureus* COL WT, Δ*ypdA* and Δ*brxAB* mutants as well as *ypdA*, *brxA,* and *brxB* complemented strains at 2, 3, and 4 h after treatment with 3.5 mM NaOCl. Survival of the untreated control was set to 100%. Mean values and SD of 3–4 biological replicates are presented. The statistics was calculated using a Student's unpaired two-tailed *t*-test by the graph prism software. Symbols are: $^{ns}p > 0.05$, $^{*}p \leq 0.05$, and $^{**}p \leq 0.01$.

Taken together, our results revealed that the bacilliredoxin BrxA and the putative BSSB reductase YpdA are required for improved survival of *S. aureus* inside macrophages to resist the oxidative burst. Our data suggest that BrxA and YpdA act together in the BrxA/BSH/YpdA pathway to regenerate *S*-bacillithiolated proteins and to restore the BSH redox potential upon recovery from oxidative stress during infections.

The Flavin Disulfide Reductase YpdA Functions in BSSB Reduction and De-Bacillithiolation of GapDH-SSB in the BrxA/BSH/YpdA Electron Transfer Assay *in vitro*

Next, we aimed to analyze the catalytic activity of purified YpdA in a NADPH-coupled assay with BSSB as substrate *in vitro,* since biochemical evidence for the function of YpdA as BSSB reductase activity *in vitro* is still missing (Mikheyeva et al., 2019). The His-tagged YpdA protein was purified as yellow colored enzyme and the UV-visible spectrum revealed the presence of the FAD co-factor indicated by the two absorbance peaks at 375 and 450 nm (**Supplementary Figure S9**). Incubation of YpdA protein with BSSB resulted in significant and fast consumption of NADPH as measured by a rapid absorbance decrease at 340 nm (**Figure 9A**). Only little NADPH consumption was measured with YpdA alone in the absence of the BSSB substrate supporting previous finding that YpdA consumes NADPH alone (Mikheyeva et al., 2019). However, in our assays, BSSB significantly enhanced NADPH consumption by YpdA compared to the control reaction without BSSB. No increased NADPH consumption was measured with coenzyme A disulphide ($CoAS_2$) or GSSG as substrate indicating the specificity of YpdA for BSSB (**Figure 9A**). In addition, we investigated the role of the conserved Cys14 of YpdA for the BSSB reductase activity in the NADPH-coupled assay.

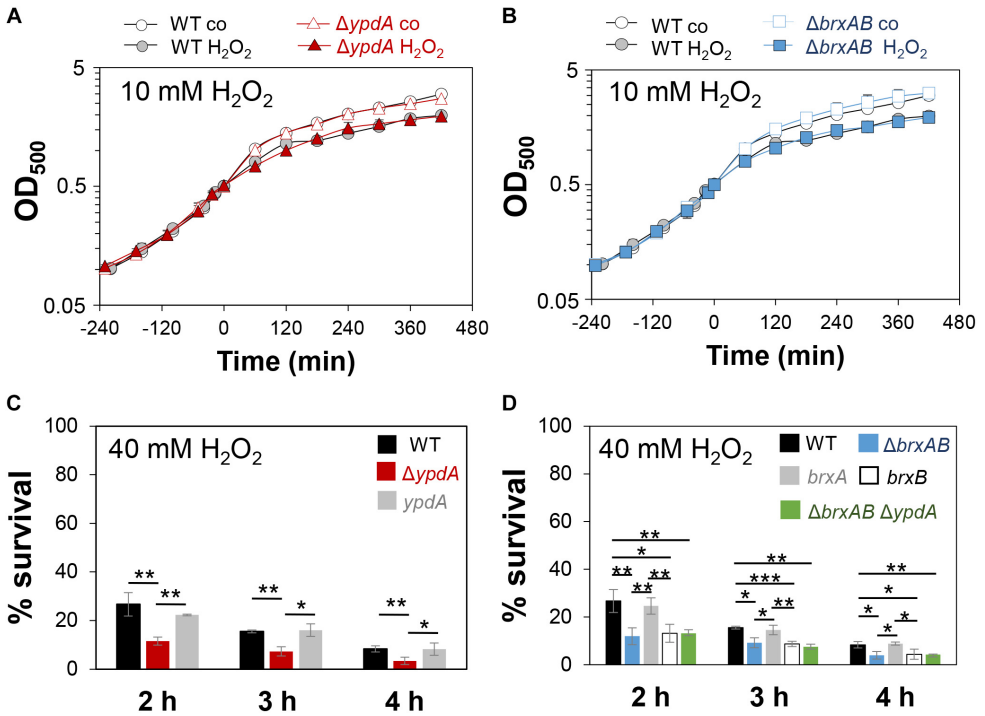

FIGURE 7 | The *S. aureus* Δ*ypdA* and Δ*brxAB* mutants show increased sensitivities to H_2O_2 stress. **(A,B)** Growth curves of *S. aureus* COL WT, the Δ*ypdA* and Δ*brxAB* mutants in RPMI after exposure to 10 mM H_2O_2 stress at an OD_{500} of 0.5. **(C,D)** Survival rates were determined as CFUs for *S. aureus* COL WT, Δ*ypdA*, Δ*brxAB* and Δ*brxAB*Δ*ypdA* mutants as well as *ypdA*, *brxA*, *brxB* complemented strains at 2, 3, and 4 h after treatment with 40 mM H_2O_2. Survival of the untreated control was set to 100%. Mean values and SD of 3–5 biological replicates are presented. The statistics was calculated using a Student's unpaired two-tailed *t*-test by the graph prism software. Symbols are: $^{ns}p > 0.05$, $^{*}p \leq 0.05$, and $^{**}p \leq 0.01$.

NADPH-consumption of YpdAC14A upon BSSB reduction was much slower and similar to the control reaction of YpdA and YpdAC14A without BSSB (**Figure 9B**).

Our *in vivo* data support that YpdA and BrxA act together in the BrxA/BSH/YpdA de-bacillithiolation pathway. Thus, we analyzed NADPH-consumption by the BrxA/BSH/YpdA electron pathway in de-bacillithiolation of GapDH-SSB *in vitro*. The de-bacillithiolation assays revealed fast NADPH consumption in the complete BrxA/BSH/YpdA coupled assays (**Figure 9C**). NADPH consumption by YpdA was slower in the absence of BrxA and might be caused by residual BSSB in the BSH samples. The control reaction of GapDH-SSB with BrxA did not consume NADPH and only little NADPH consumption was measured with BrxA, BSH and the YpdAC14A mutant protein in de-bacillithiolation of GapDH-SSB (**Figure 9D**).

In addition, BSH-specific non-reducing Western blots were used to investigate if BrxA and the complete BrxA/BSH/YpdA pathway catalyze de-bacillithiolation of GapDH-SSB (**Figure 9E**). The BSH-blots showed that BrxA is sufficient for de-bacillithiolation of GapDH-SSB, since all reactions of GapDH-SSB with BrxA lead to complete de-bacillithiolation with and without YpdA or YpdAC14A plus NADPH. However, the reactions of GapDH-SSB with YpdA/NADPH alone did not lead to reduction of GapDH-SSB, indicating the main role of BrxA in de-bacillithiolation while YpdA functions in regeneration of BSH in the BrxA/BSH/YpdA/NADPH redox cycle.

In conclusion, our biochemical assays revealed that YpdA functions as BSSB reductase in an NADPH coupled assay. Cys14 of YpdA is important for the BSSB reductase activity *in vitro*. Thus, YpdA facilitates together with BrxA the reduction of *S*-bacillithiolated GapDH in the BrxA/BSH/YpdA redox pathway upon recovery from oxidative stress.

DISCUSSION

The putative disulfide reductase YpdA was previously shown to be phylogenetically associated with the BSH biosynthesis enzymes and bacilliredoxins (**Supplementary Figure S2**), providing evidence for a functional Brx/BSH/YpdA pathway in BSH-producing bacteria (Gaballa et al., 2010). Recent work confirmed the importance of YpdA for the BSH/BSSB redox balance and survival under oxidative stress and neutrophil infections in *S. aureus in vivo* (Mikheyeva et al., 2019). Here, we have studied the role of the bacilliredoxins BrxA/B and the BSSB reductase YpdA in the defense of *S. aureus* against oxidative stress *in vivo* and their biochemical function in the de-bacillithiolation pathway *in vitro*. Transcription of *brxA*, *brxB* and *ypdA* is strongly upregulated under disulfide stress, provoked by diamide and NaOCl. About two to fourfold increased transcription of *ypdA*, *brxA*, and *brxB* was previously found under H_2O_2, diamide and NaOCl stress, by the antimicrobial surface coating

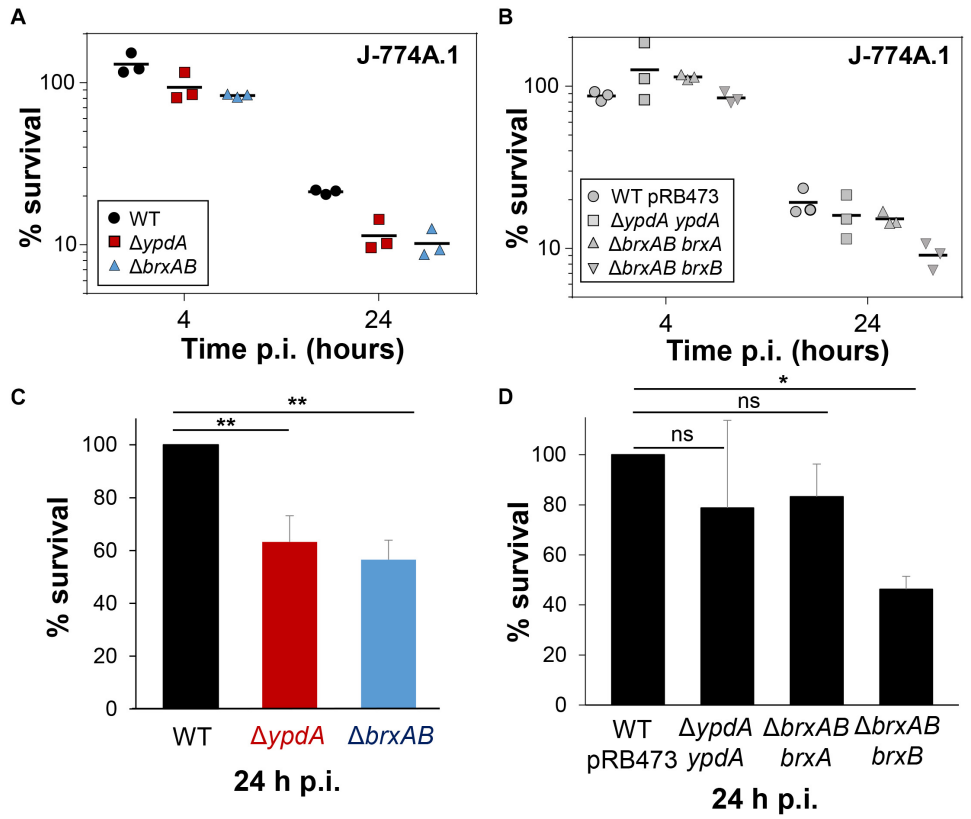

FIGURE 8 | YpdA and BrxA/B promote the intracellular survival of *S. aureus* inside murine macrophages during infections. **(A,B)** The survival of *S. aureus* WT, Δ*ypdA* and Δ*brxAB* mutants and complemented strains was analyzed 2, 4 and 24 h post infection (p.i.) of the murine macrophage cell line J-774A.1 by CFU counting. The percentages in survival of the Δ*ypdA* and Δ*brxAB* mutants and complemented strains were calculated after 4 and 24 h in relation to the 2 h time point, which was set to 100%. **(C,D)** The average percentage in survival was calculated for Δ*ypdA* and Δ*brxAB* mutants **(C)** and complemented strain **(D)** in relation to the WT and WT with empty plasmid pRB473, which were set to 100%. Error bars represent the SEM and the statistics were calculated using one-way ANOVA and Tukey's multiple comparisons *post hoc* test using the graph prism software ($p = 0.0050$ for WT/Δ*ypdA*, $p = 0.0022$ for WT/Δ*brxAB* and $p = 0.026$ for WT pRB473/Δ*brxAB brxB*). Symbols: $^{ns}p > 0.05$; $^{*}p \leq 0.05$, and $^{**}p \leq 0.01$.

composed of Ag^{+} and Ru^{+} (AGXX®) and after exposure to azurophilic granule proteins in *S. aureus* (Palazzolo-Ballance et al., 2008; Posada et al., 2014; Mäder et al., 2016; Loi et al., 2018a,b; Mikheyeva et al., 2019). The elevated transcription of *brxA, brxB,* and *ypdA* under disulfide stress correlated with the up-regulation of the *bshA*, *bshB,* and *bshC* genes for BSH biosynthesis in *S. aureus* and *B. subtilis* (Chi et al., 2011; Nicolas et al., 2012; Loi et al., 2018a,b). The *bshA, bshB,* and *bshC* genes and operons are under control of the disulfide stress-specific Spx regulator in *B. subtilis,* which controls a large regulon for thiol-redox homeostasis (Gaballa et al., 2013). Thus, genes for BSH biosynthesis and the BrxA/B/YpdA pathway might be also regulated by Spx in *S. aureus*.

The co-regulation of BrxA/B and YpdA under disulfide stress points to their function in the same pathway in *S. aureus*. HOCl, diamide and AGXX® were shown to cause a strong disulfide stress response in the transcriptome and protein *S*-bacillithiolation in the proteome of *S. aureus* (Imber et al., 2018a; Loi et al., 2018a,b). Thus, the BrxA/B and YpdA redox enzymes are up-regulated under conditions of protein *S*-bacillithiolations, connecting their functions to the de-bacillithiolation pathway. We could show here that NaOCl stress leads to five to sixfold depletion of the cellular pool of reduced BSH in the *S. aureus* COL wild type, which was not accompanied by an enhanced BSSB level. In the previous study, 20 mM H_2O_2 resulted in twofold reduction of BSH and threefold increase of BSSB in the *S. aureus* wild type (Mikheyeva et al., 2019). Most probably, the increased BSSB level under NaOCl stress was used for protein *S*-bacillithiolation in our study (Imber et al., 2018a), while sub-lethal 20 mM H_2O_2 might not lead to an increase in *S*-bacillithiolation in the previous study (Mikheyeva et al., 2019).

The BSH/BSSB redox ratio of *S. aureus* wild type cells was determined as ∼35:1 under control conditions and decreased threefold to 10:1 under NaOCl. Of note, this basal BSH/BSSB ratio in *S. aureus* COL wild type was higher compared to the basal BSH/BSSB ratio of ∼17:1 as determined previously in the *bshC* repaired SH1000 strain (Mikheyeva et al., 2019). In *E. coli*, the GSH/GSSG redox ratio was determined in the range between 30:1 and 100:1 (Hwang et al., 1995; Van Laer et al., 2013), which is similar as measured for the basal BSH/BSSB ratio in *S. aureus* COL. The differences in the BSH/BSSB ratios might be related to different *S. aureus* strain

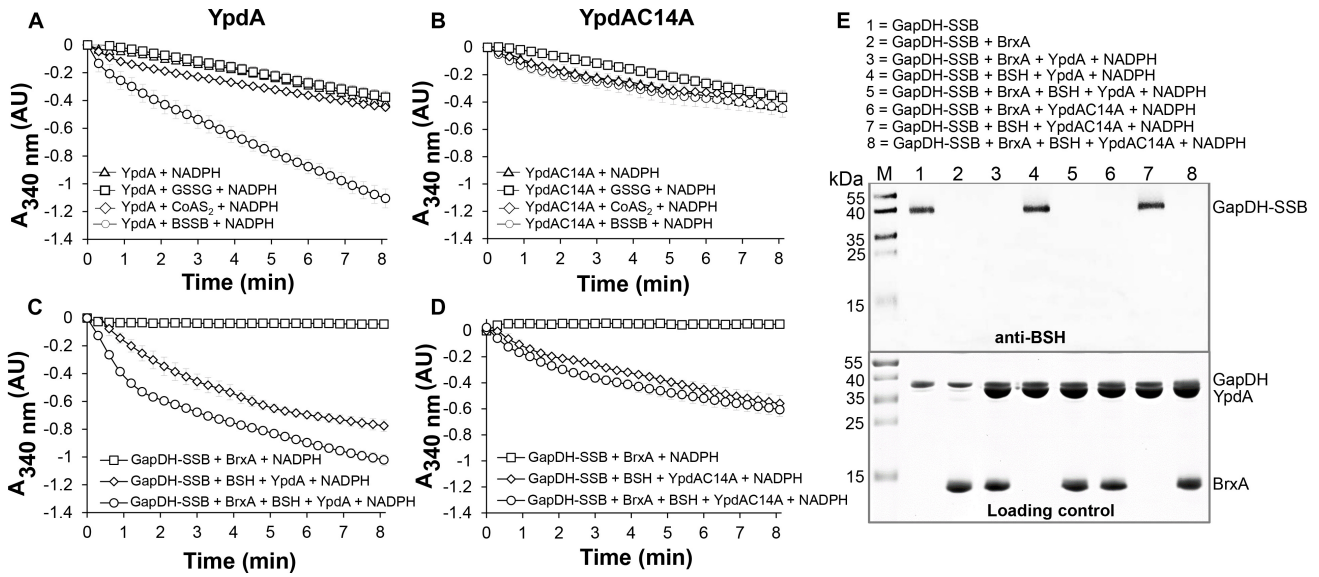

FIGURE 9 | YpdA functions as BSSB reductase in the NADPH-coupled BrxA/BSH/YpdA electron pathway for de-bacillithiolation of GapDH-SSB *in vitro*. **(A)** Purified YpdA is able to reduce BSSB back to BSH with electrons from NADPH as measured by the absorbance change at 340 nm. Only little NADPH consumption was measured with YpdA alone in the absence of BSSB, with coenzymeA disulfide (CoAS2) or glutathione disulfide (GSSG) **(A)** and in the YpdAC14A mutant **(B)** indicating the function of the conserved Cys14 as active site of YpdA for BSSB reduction. **(C)** NADPH consumption of YpdA was measured in the coupled BrxA/BSH/YpdA de-bacillithiolation assay for reduction of GapDH-SSB. While fast NADPH consumption was measured upon de-bacillithiolation of GapDH-SSB with purified YpdA **(C)**, the reaction was much slower with the YpdAC14A mutant **(D)**. The coupled assays were conducted with 2.5 μM Gap-SSB, 12.5 μM BrxA, 40 μM BSH, 500 μM NADPH in 20 mM Tris, 1.25 mM EDTA, pH 8.0. After 30-min incubation, 12.5 μM YpdA or YpdAC14A proteins were added to the reaction mix and NADPH consumption was monitored at 340 nm as a function of time. Mean values and SEM of four independent experiments are shown. **(E)** The de-bacillithiolation of GapDH-SSB is catalyzed by BrxA or the complete BrxA/BSH/YpdA pathway, but not by YpdA alone as shown by non-reducing BSH-specific Western blots. The loading controls are shown below as Coomassie-stained SDS-PAGE with the same de-bacillithiolation reactions of GapDH-SSB as in the BSH-blot.

backgrounds or growth conditions. Nevertheless, NaOCl and H_2O_2 decreased the BSH/BSSB ratio in our and the previous study (Mikheyeva et al., 2019). In the *S. aureus* Δ*brxAB* mutant, we also measured a threefold decrease of the BSH/BSSB ratio from control conditions (38:1) to NaOCl (12:1). However, the Δ*ypdA* mutant showed a twofold enhanced BSSB level in control and NaOCl-treated cells, leading to a significantly decreased BSH/BSSB ratio under control (17:1) and NaOCl stress (5:1). These results support previous results of the *bshC* repaired SH1000, showing a decreased BSH/BSSB ratio under control (6:1) to H_2O_2 stress (2:1) (Mikheyeva et al., 2019), although both ratios were again much lower as in our study. Taken together, our data indicate that BrxAB are dispensable for the BSH redox homeostasis, while YpdA is essential for BSSB reduction to maintain the reduced pool of BSH and a high BSH/BSSB ratio in *S. aureus*.

Brx-roGFP2 biosensor measurements provide further support that YpdA is the candidate BSSB reductase. The Δ*ypdA* mutant was significantly impaired to restore reduced E_{BSH} during recovery from NaOCl and H_2O_2 stress as calculated using the Nernst equation based on the OxD values of the Brx-roGFP2 biosensor measurements (**Supplementary Tables S5, S6**). Moreover, application of the Tpx-roGFP2 biosensor revealed a delay in H_2O_2 detoxification in Δ*ypdA* mutant cells during the recovery phase. These results clearly support the important role of YpdA as BSSB reductase particularly under oxidative stress to recover reduced E_{BSH} required for detoxification of ROS.

These *in vivo* data were further corroborated by biochemical activity assays of YpdA for BSSB reduction in a NADPH-coupled assay. While little NADPH consumption was measured in the presence of YpdA alone, BSSB significantly enhanced NADPH consumption, supporting the crucial role of YpdA as BSSB reductase *in vitro*. Further electron transfer assays revealed that YpdA functions together with BrxA and BSH in reduction of GapDH-SSB *in vitro*. Previous de-bacillithiolation assays have revealed regeneration of GapDH activity by BrxA *in vitro* (Imber et al., 2018a). Here, we confirmed that BrxA activity is sufficient for complete de-bacillithiolation of GapDH-SSB *in vitro*, while YpdA alone had no effect on the GapDH-SSB reduction. Thus, BrxA catalyzes reduction of *S*-bacillithiolated proteins and YpdA is involved in BSH regeneration in the complete BrxA/BSH/YpdA redox cycle.

The BSSB reductase activity of YpdA was shown to be dependent on the conserved Cys14, which is located in the glycine-rich Rossmann-fold NAD(P)H binding domain ($GGGPC_{14}G$) (Bragg et al., 1997; Mikheyeva et al., 2019). Cys14 might be *S*-bacillithiolated by BSSB and reduced by electron transfer from NADPH via the FAD co-factor. Cys14 was previously identified as oxidized under NaOCl stress in the *S. aureus* redox proteome using the OxICAT method, further supporting its role as active site Cys and its *S*-bacillithiolation

during the BrxA/BSH/YpdA catalytic cycle (Imber et al., 2018a). The catalytic mechanism of BSSB reduction via Cys14 of YpdA is an interesting subject of future studies.

Previous phenotype results of the Δ*ypdA* mutant revealed that YpdA is important for survival of *S. aureus* in infection assays with human neutrophils (Mikheyeva et al., 2019). Our phenotype analyses further showed protective functions of the complete BrxA/BSH/YpdA redox pathway for growth and survival of *S. aureus* under oxidative stress *in vitro* and in macrophage infections *in vivo*. The Δ*ypdA* and Δ*brxAB* mutants were significantly impaired in growth and survival after exposure to sub-lethal and lethal doses of NaOCl and displayed survival defects under lethal H_2O_2. Moreover, the H_2O_2 and NaOCl-sensitivity and the defect to recover reduced E_{BSH} in the Δ*brxAB*Δ*ypdA* triple mutant was comparable with that of the Δ*ypdA* mutant (**Figure 7D** and **Supplementary Figure S8**). These results clearly indicate that BrxA/B and YpdA function in the same de-bacillithiolation pathway, which is an important defense mechanism of *S. aureus* against oxidative stress.

Based on previous bacilliredoxin activity assays *in vitro*, both BrxA and BrxB should use a monothiol mechanism to reduce *S*-bacillithiolated client proteins, such as OhrR, GapDH and MetE in *B. subtilis* and *S. aureus* (Gaballa et al., 2014; Imber et al., 2018a). Most di-thiol Grx of *E. coli* (Grx1, Grx2, and Grx3) use the monothiol mechanism for de-glutathionylation of proteins (Lillig et al., 2008; Allen and Mieyal, 2012; Loi et al., 2015). In the monothiol mechanism, the nucleophilic thiolate of the Brx CGC motif attacks the *S*-bacillithiolated protein, resulting in reduction of the protein substrate and Brx-SSB formation. Brx-SSB is then recycled by BSH, leading to increased BSSB formation. YpdA reduces BSSB back to BSH with electrons from NADPH (**Figure 1B**). The oxidation-sensitive phenotypes of Δ*ypdA* and Δ*brxAB* mutants could be complemented by plasmid-encoded *ypdA* and *brxA*, but not *brxB*, respectively. These results provide evidence for the function of the BrxA/BSH/YpdA de-bacillithiolation pathway using the monothiol-Brx mechanism in *S. aureus*.

Similar phenotypes were found for mutants lacking related redox enzymes of the GSH and mycothiol pathways in other bacteria. In *E. coli*, strains lacking the Gor and Grx are more sensitive under diamide and cumene hydroperoxide stress (Alonso-Moraga et al., 1987; Vlamis-Gardikas et al., 2002; Lillig et al., 2008). In *Mycobacterium smegmatis*, the mycoredoxin-1 mutant displayed an oxidative stress-sensitive phenotype (Van Laer et al., 2012). In *Corynebacterium glutamicum*, deficiency of the Mtr resulted in an oxidized mycothiol redox potential (Tung et al., 2019), and Mtr overexpression contributed to improved oxidative stress resistance (Si et al., 2016). Taken together, our results revealed that not only BSH, but also BrxA and YpdA are required for virulence and promote survival in infection assays inside murine macrophages.

In several human pathogens, such as *Streptococcus pneumoniae, Listeria monocytogenes, Salmonella Typhimurium*, and *Pseudomonas aeruginosa*, LMW thiols or the Gor are required for virulence, colonization and to resist host-derived oxidative or nitrosative stress (Potter et al., 2012; Song et al., 2013; Reniere et al., 2015; Tung et al., 2018; Wongsaroj et al., 2018). *S. aureus* BSH deficient mutants showed decreased survival in murine macrophages and in human whole blood infections (Pöther et al., 2013; Posada et al., 2014). The virulence mechanisms might be related to a lack of BSH regeneration and decreased recovery of inactivated *S*-bacillithiolated proteins inside macrophages. Future studies should elucidate the targets for *S*-bacillithiolations that are reduced by the BrxA/BSH/YpdA pathway inside macrophages, increasing survival, metabolism or persistence under infections.

In summary, our results showed the importance of the BrxA/BSH/YpdA redox pathway to resist oxidative stress and macrophage infection in *S. aureus*. Through measurements of the BSH/BSSB redox ratio and E_{BSH}, we provide evidence that the NADPH-dependent disulfide reductase YpdA regenerates BSH and restores reduced E_{BSH} upon recovery from oxidative stress in *S. aureus*. Finally, biochemical evidence for YpdA as BSSB reductase and for the role of BrxA/BSH/YpdA pathway in de-bacillithiolation was provided *in vitro*. The detailed biochemical mechanism of YpdA and the cross-talk of the Trx and Brx systems in de-bacillithiolation under oxidative stress and infections are subject of our future studies.

AUTHOR CONTRIBUTIONS

HA and NL designed the experiments of this study. NL, VVL, VNF, QNT and SS constructed the mutants, performed the experiments and analyzed the data of this manuscript. MW and RH performed the HPLC thiol metabolomics analyses and analyzed the data. KT and MF contributed with the infection assays to this work. CH synthesized BSH and BSSB for the biochemical assays of the manuscript. NL and HA wrote the manuscript. All authors contributed with corrections of the manuscript.

FUNDING

In this work, HA was supported by an ERC Consolidator Grant (GA 615585) MYCOTHIOLOME and grants from the Deutsche Forschungsgemeinschaft (AN746/4-1 and AN746/4-2) within the SPP1710, by the SFB973 project C08N, and by the SFB/TR84 project B06. We further thank funding by the SPP1710 grants HE1848/16-1 and WI3560/2-1 to RH and MW.

ACKNOWLEDGMENTS

We acknowledge support by the Open Access Publication Initiative of Freie Universität Berlin.

SUPPLEMENTARY MATERIAL

The Supplementary Material for this article can be found online at: https://www.frontiersin.org/articles/10.3389/fmicb.2019.01355/full#supplementary-material

REFERENCES

Allen, E. M., and Mieyal, J. J. (2012). Protein-thiol oxidation and cell death: regulatory role of glutaredoxins. *Antioxid. Redox Signal.* 17, 1748–1763. doi: 10.1089/ars.2012.4644

Alonso-Moraga, A., Bocanegra, A., Torres, J. M., Lopez-Barea, J., and Pueyo, C. (1987). Glutathione status and sensitivity to GSH-reacting compounds of *Escherichia coli* strains deficient in glutathione metabolism and/or catalase activity. *Mol. Cell Biochem.* 73, 61–68.

Archer, G. L. (1998). *Staphylococcus aureus*: a well-armed pathogen. *Clin. Infect. Dis.* 26, 1179–1181. doi: 10.1086/520289

Argyrou, A., and Blanchard, J. S. (2004). Flavoprotein disulfide reductases: advances in chemistry and function. *Progr. Nucleic Acid Res. Mol. Biol.* 78, 89–142. doi: 10.1016/s0079-6603(04)78003-4

Arnaud, M., Chastanet, A., and Débarbouillé, M. (2004). New vector for efficient allelic replacement in naturally nontransformable, low-GC-content, gram-positive bacteria. *Appl. Environ. Microbiol.* 70, 6887–6891. doi: 10.1128/aem.70.11.6887-6891.2004

Beavers, W. N., and Skaar, E. P. (2016). Neutrophil-generated oxidative stress and protein damage in *Staphylococcus aureus*. *Pathog. Dis.* 74:ftw060. doi: 10.1093/femspd/ftw060

Boucher, H. W., and Corey, G. R. (2008). Epidemiology of methicillin-resistant *Staphylococcus aureus*. *Clin. Infect Dis.* 46(Suppl. 5), S344–S349. doi: 10.1086/533590

Bragg, P. D., Glavas, N. A., and Hou, C. (1997). Mutation of conserved residues in the NADP(H)-binding domain of the proton translocating pyridine nucleotide transhydrogenase of *Escherichia coli*. *Arch. Biochem. Biophys.* 338, 57–66. doi: 10.1006/abbi.1996.9797

Brückner, R., Wagner, E., and Götz, F. (1993). Characterization of a sucrase gene from *Staphylococcus xylosus*. *J. Bacteriol.* 175, 851–857. doi: 10.1128/jb.175.3.851-857.1993

Chandrangsu, P., Loi, V. V., Antelmann, H., and Helmann, J. D. (2018). The role of bacillithiol in Gram-positive *Firmicutes*. *Antioxid. Redox Signal.* 28, 445–462. doi: 10.1089/ars.2017.7057

Chi, B. K., Gronau, K., Mäder, U., Hessling, B., Becher, D., and Antelmann, H. (2011). *S*-bacillithiolation protects against hypochlorite stress in *Bacillus subtilis* as revealed by transcriptomics and redox proteomics. *Mol. Cell Proteo.* 10:M111009506. doi: 10.1074/mcp.M111.009506

Chi, B. K., Roberts, A. A., Huyen, T. T., Bäsell, K., Becher, D., Albrecht, D., et al. (2013). *S*-bacillithiolation protects conserved and essential proteins against hypochlorite stress in *Firmicutes* bacteria. *Antioxid. Redox Signal.* 18, 1273–1295. doi: 10.1089/ars.2012.4686

Deponte, M. (2013). Glutathione catalysis and the reaction mechanisms of glutathione-dependent enzymes. *Biochim. Biophys. Acta* 1830, 3217–3266. doi: 10.1016/j.bbagen.2012.09.018

Dooley, C. T., Dore, T. M., Hanson, G. T., Jackson, W. C., Remington, S. J., and Tsien, R. Y. (2004). Imaging dynamic redox changes in mammalian cells with green fluorescent protein indicators. *J. Biol. Chem.* 279, 22284–22293. doi: 10.1074/jbc.m312847200

Fahey, R. C. (2013). Glutathione analogs in prokaryotes. *Biochim. Biophys. Acta* 1830, 3182–3198. doi: 10.1016/j.bbagen.2012.10.006

Fuangthong, M., Atichartpongkul, S., Mongkolsuk, S., and Helmann, J. D. (2001). OhrR is a repressor of *ohrA*, a key organic hydroperoxide resistance determinant in *Bacillus subtilis*. *J. Bacteriol.* 183, 4134–4141. doi: 10.1128/jb.183.14.4134-4141.2001

Gaballa, A., Antelmann, H., Hamilton, C. J., and Helmann, J. D. (2013). Regulation of *Bacillus subtilis* bacillithiol biosynthesis operons by Spx. *Microbiology* 159, 2025–2035. doi: 10.1099/mic.0.070482-0

Gaballa, A., Chi, B. K., Roberts, A. A., Becher, D., Hamilton, C. J., Antelmann, H., et al. (2014). Redox regulation in *Bacillus subtilis*: The bacilliredoxins BrxA(YphP) and BrxB(YqiW) function in de-bacillithiolation of S-bacillithiolated OhrR and MetE. *Antioxid. Redox Signal.* 21, 357–367. doi: 10.1089/ars.2013.5327

Gaballa, A., Newton, G. L., Antelmann, H., Parsonage, D., Upton, H., Rawat, M., et al. (2010). Biosynthesis and functions of bacillithiol, a major low-molecular-weight thiol in Bacilli. *Proc. Natl. Acad. Sci. U.S.A.* 107, 6482–6486. doi: 10.1073/pnas.1000928107

Hillion, M., and Antelmann, H. (2015). Thiol-based redox switches in prokaryotes. *Biol. Chem.* 396, 415–444. doi: 10.1515/hsz-2015-0102

Hiras, J., Sharma, S. V., Raman, V., Tinson, R. A. J., Arbach, M., Rodrigues, D. F., et al. (2018). Physiological studies of *Chlorobiaceae* suggest that bacillithiol derivatives are the most widespread thiols in bacteria. *MBio* 9:e01603-18. doi: 10.1128/mBio.01603-18

Hwang, C., Lodish, H. F., and Sinskey, A. J. (1995). Measurement of glutathione redox state in cytosol and secretory pathway of cultured cells. *Methods Enzymol.* 251, 212–221. doi: 10.1016/0076-6879(95)51123-7

Imber, M., Huyen, N. T. T., Pietrzyk-Brzezinska, A. J., Loi, V. V., Hillion, M., Bernhardt, J., et al. (2018a). Protein *S*-bacillithiolation functions in thiol protection and redox regulation of the glyceraldehyde-3-phosphate dehydrogenase Gap in *Staphylococcus aureus* under hypochlorite stress. *Antioxid. Redox Signal.* 28, 410–430. doi: 10.1089/ars.2016.6897

Imber, M., Loi, V. V., Reznikov, S., Fritsch, V. N., Pietrzyk-Brzezinska, A. J., Prehn, J., et al. (2018b). The aldehyde dehydrogenase AldA contributes to the hypochlorite defense and is redox-controlled by protein *S*-bacillithiolation in *Staphylococcus aureus*. *Redox. Biol.* 15, 557–568. doi: 10.1016/j.redox.2018.02.001

Imber, M., Pietrzyk-Brzezinska, A. J., and Antelmann, H. (2018c). Redox regulation by reversible protein *S*-thiolation in Gram-positive bacteria. *Redox. Biol.* 20, 130–145. doi: 10.1016/j.redox.2018.08.017

Lee, J. W., Soonsanga, S., and Helmann, J. D. (2007). A complex thiolate switch regulates the *Bacillus subtilis* organic peroxide sensor OhrR. *Proc. Natl. Acad. Sci. U.S.A.* 104, 8743–8748. doi: 10.1073/pnas.0702081104

Lillig, C. H., Berndt, C., and Holmgren, A. (2008). Glutaredoxin systems. *Biochim. Biophys. Acta* 1780, 1304–1317. doi: 10.1016/j.bbagen.2008.06.003

Livermore, D. M. (2000). Antibiotic resistance in staphylococci. *Int. J. Antimicrob. Agents* 16(Suppl. 1), S3–S10.

Loi, V. V., Busche, T., Preuss, T., Kalinowski, J., Bernhardt, J., and Antelmann, H. (2018a). The AGXX antimicrobial coating causes a thiol-specific oxidative stress response and protein S-bacillithiolation in *Staphylococcus aureus*. *Front. Microbiol.* 9:3037. doi: 10.3389/fmicb.2018.03037

Loi, V. V., Busche, T., Tedin, K., Bernhardt, J., Wollenhaupt, J., Huyen, N. T. T., et al. (2018b). Redox-sensing under hypochlorite stress and infection conditions by the Rrf2-family repressor HypR in *Staphylococcus aureus*. *Antioxid. Redox Signal.* 29, 615–636. doi: 10.1089/ars.2017.7354

Loi, V. V., Harms, M., Müller, M., Huyen, N. T. T., Hamilton, C. J., Hochgräfe, F., et al. (2017). Real-time imaging of the bacillithiol redox potential in the human pathogen *Staphylococcus aureus* using a genetically encoded bacilliredoxin-fused redox biosensor. *Antioxid. Redox Signal.* 26, 835–848. doi: 10.1089/ars.2016.6733

Loi, V. V., Rossius, M., and Antelmann, H. (2015). Redox regulation by reversible protein *S*-thiolation in bacteria. *Front. Microbiol.* 6:187. doi: 10.3389/fmicb.2015.00187

Lowy, F. D. (1998). *Staphylococcus aureus* infections. *N. Engl. J. Med.* 339, 520–532.

Mäder, U., Nicolas, P., Depke, M., Pane-Farre, J., Debarbouille, M., Van Der Kooi-Pol, M. M., et al. (2016). *Staphylococcus aureus* transcriptome architecture: from laboratory to infection-mimicking conditions. *PLoS Genet.* 12:e1005962. doi: 10.1371/journal.pgen.1005962

Mikheyeva, I. V., Thomas, J. M., Kolar, S. L., Corvaglia, A. R., Gaiotaa, N., Leo, S., et al. (2019). YpdA, a putative bacillithiol disulfide reductase, contributes to cellular redox homeostasis and virulence in *Staphylococcus aureus*. *Mol. Microbiol.* 111, 1039–1056. doi: 10.1111/mmi.14207

Newton, G. L., Fahey, R. C., and Rawat, M. (2012). Detoxification of toxins by bacillithiol in *Staphylococcus aureus*. *Microbiology* 158, 1117–1126. doi: 10.1099/mic.0.055715-0

Nicolas, P., Mäder, U., Dervyn, E., Rochat, T., Leduc, A., Pigeonneau, N., et al. (2012). Condition-dependent transcriptome reveals high-level regulatory architecture in *Bacillus subtilis*. *Science* 335, 1103–1106. doi: 10.1126/science.1206848

Palazzolo-Ballance, A. M., Reniere, M. L., Braughton, K. R., Sturdevant, D. E., Otto, M., Kreiswirth, B. N., et al. (2008). Neutrophil microbicides induce a pathogen survival response in community-associated methicillin-resistant *Staphylococcus aureus*. *J. Immunol.* 180, 500–509. doi: 10.4049/jimmunol.180.1.500

Pendleton, J. N., Gorman, S. P., and Gilmore, B. F. (2013). Clinical relevance of the ESKAPE pathogens. *Expert Rev. Anti. Infect. Ther.* 11, 297–308. doi: 10.1586/eri.13.12

Posada, A. C., Kolar, S. L., Dusi, R. G., Francois, P., Roberts, A. A., Hamilton, C. J., et al. (2014). Importance of bacillithiol in the oxidative stress response of *Staphylococcus aureus*. *Infect. Immun.* 82, 316–332. doi: 10.1128/IAI.01074-13

Pöther, D. C., Gierok, P., Harms, M., Mostertz, J., Hochgräfe, F., Antelmann, H., et al. (2013). Distribution and infection-related functions of bacillithiol in *Staphylococcus aureus*. *Int. J. Med. Microbiol.* 303, 114–123. doi: 10.1016/j.ijmm.2013.01.003

Potter, A. J., Trappetti, C., and Paton, J. C. (2012). *Streptococcus pneumoniae* uses glutathione to defend against oxidative stress and metal ion toxicity. *J. Bacteriol.* 194, 6248–6254. doi: 10.1128/JB.01393-12

Reniere, M. L., Whiteley, A. T., Hamilton, K. L., John, S. M., Lauer, P., Brennan, R. G., et al. (2015). Glutathione activates virulence gene expression of an intracellular pathogen. *Nature* 517, 170–173. doi: 10.1038/nature14029

Rosenblum, E. D., and Tyrone, S. (1964). Serology, density, and morphology of staphylococcal phages. *J. Bacteriol.* 88, 1737–1742.

Si, M., Zhao, C., Zhang, B., Wei, D., Chen, K., Yang, X., et al. (2016). Overexpression of mycothiol disulfide reductase enhances *Corynebacterium glutamicum* robustness by modulating cellular redox homeostasis and antioxidant proteins under oxidative stress. *Sci. Rep.* 6:29491. doi: 10.1038/srep29491

Song, M., Husain, M., Jones-Carson, J., Liu, L., Henard, C. A., and Vazquez-Torres, A. (2013). Low-molecular-weight thiol-dependent antioxidant and antinitrosative defences in *Salmonella* pathogenesis. *Mol. Microbiol.* 87, 609–622. doi: 10.1111/mmi.12119

Tam le, T., Eymann, C., Albrecht, D., Sietmann, R., Schauer, F., Hecker, M., et al. (2006). Differential gene expression in response to phenol and catechol reveals different metabolic activities for the degradation of aromatic compounds in *Bacillus subtilis*. *Environ. Microbiol.* 8, 1408–1427. doi: 10.1111/j.1462-2920.2006.01034.x

Tung, Q. N., Linzner, N., Loi, V. V., and Antelmann, H. (2018). Application of genetically encoded redox biosensors to measure dynamic changes in the glutathione, bacillithiol and mycothiol redox potentials in pathogenic bacteria. *Free Radic. Biol. Med.* 128, 84–96. doi: 10.1016/j.freeradbiomed.2018.02.018

Tung, Q. N., Loi, V. V., Busche, T., Nerlich, A., Mieth, M., Milse, J., et al. (2019). Stable integration of the Mrx1-roGFP2 biosensor to monitor dynamic changes of the mycothiol redox potential in *Corynebacterium glutamicum*. *Redox. Biol.* 20, 514–525. doi: 10.1016/j.redox.2018.11.012

Van Laer, K., Buts, L., Foloppe, N., Vertommen, D., Van Belle, K., Wahni, K., et al. (2012). Mycoredoxin-1 is one of the missing links in the oxidative stress defence mechanism of Mycobacteria. *Mol. Microbiol.* 86, 787–804. doi: 10.1111/mmi.12030

Van Laer, K., Hamilton, C. J., and Messens, J. (2013). Low-molecular-weight thiols in thiol-disulfide exchange. *Antioxid. Redox Signal.* 18, 1642–1653. doi: 10.1089/ars.2012.4964

Vlamis-Gardikas, A., Potamitou, A., Zarivach, R., Hochman, A., and Holmgren, A. (2002). Characterization of *Escherichia coli* null mutants for glutaredoxin 2. *J. Biol. Chem.* 277, 10861–10868.

Wetzstein, M., Völker, U., Dedio, J., Löbau, S., Zuber, U., Schiesswohl, M., et al. (1992). Cloning, sequencing, and molecular analysis of the *dnaK* locus from *Bacillus subtilis*. *J. Bacteriol.* 174, 3300–3310. doi: 10.1128/jb.174.10.3300-3310.1992

Winterbourn, C. C., and Kettle, A. J. (2013). Redox reactions and microbial killing in the neutrophil phagosome. *Antioxid. Redox Signal.* 18, 642–660. doi: 10.1089/ars.2012.4827

Winterbourn, C. C., Kettle, A. J., and Hampton, M. B. (2016). Reactive oxygen species and neutrophil function. *Annu. Rev. Biochem.* 85, 765–792. doi: 10.1146/annurev-biochem-060815-014442

Wongsaroj, L., Saninjuk, K., Romsang, A., Duang-Nkern, J., Trinachartvanit, W., Vattanaviboon, P., et al. (2018). *Pseudomonas aeruginosa* glutathione biosynthesis genes play multiple roles in stress protection, bacterial virulence and biofilm formation. *PLoS One* 13:e0205815. doi: 10.1371/journal.pone.0205815

Conflict of Interest Statement: The authors declare that the research was conducted in the absence of any commercial or financial relationships that could be construed as a potential conflict of interest.

Chapter 3

Staphylococcus aureus responds to allicin by global *S*-thioallylation – Role of the Brx/BSH/YpdA pathway and the disulfide reductase MerA to overcome allicin stress

Vu Van Loi[1], Nguyen Thi Thu Huyen[1□], Tobias Busche[1,2], Quach Ngoc Tung[1], Martin Clemens Horst Gruhlke[3], Jörn Kalinowski[2], Jörg Bernhardt[1,4], Alan Slusarenko[3] and Haike Antelmann[1#]

[1]*Freie Universität Berlin, Institute for Biology-Microbiology, D-14195 Berlin, Germany*
[2]*Center for Biotechnology, Bielefeld University, D-33594 Bielefeld, Germany*
[3]*Department of Plant Physiology, RWTH Aachen University, D-52056 Aachen, Germany*
[4]*Institute for Microbiology, University of Greifswald, D-17489 Greifswald, Germany*
[□]*Current address: Ho Chi Minh University of Food Industry, Faculty of Biotechnology, Ho Chi Minh City, Vietnam*

Published in: Free Radical Biology and Medicine 139: 55-69. (2019)
https://doi.org/10.1016/j.freeradbiomed.2019.05.018

[#]**Corresponding author:** haike.antelmann@fu-berlin.de

Personal contribution:

I contributed by measurements of the biochemical activity of YpdA in the reduction of S-allylmercaptobacillithiol using NADPH coupled electron assay (Fig. 9B). Furthermore, I performed the biochemical assay for inactivation of GapDH of *S. aureus* by *S*-thioallylation under allicin treatment and its reversal by the BrxA/BSH/YpdA pathway *in vitro* (Fig. 10).

Chapter 4

Application of genetically encoded redox biosensors to measure dynamic changes in the glutathione, bacillithiol and mycothiol redox potentials in pathogenic bacteria

Quach Ngoc Tung[1], Nico Linzner[1], Vu Van Loi[1], Haike Antelmann[1#]

[1]*Freie Universität Berlin, Institute for Biology-Microbiology, D-14195 Berlin, Germany*

Published in: Free Radical Biology and Medicine 128: 84-96. (2018)
https://doi.org/10.1016/j.freeradbiomed.2018.02.018

[#]**Corresponding author:** haike.antelmann@fu-berlin.de

Personal contribution:

I contributing to writing of the sections about the LMW thiol mycothiol in actinomycetes (section 1.3) and the Mrx1-roGFP2 biosensor results in mycobacteria (section 2.3) in this review article and drafted figures for LMW thiols (Fig. 1), design of roGFP2 fused biosensors (Fig. 2) and Mrx1-roGFP2 biosensor results summary in mycobacteria (Fig. 7).

Chapter 5

Stable integration of the Mrx1-roGFP2 biosensor to monitor dynamic changes of the mycothiol redox potential in *Corynebacterium glutamicum*

Quach Ngoc Tung[1], Vu Van Loi[1], Tobias Busche[1,2], Andreas Nerlich[3], Maren Mieth[3], Johanna Milse[2], Jörn Kalinowski[2], Andreas C. Hocke[3] and Haike Antelmann[1#]

[1]*Institute for Biology-Microbiology, Freie Universität Berlin, D-14195 Berlin, Germany*
[2]*Center for Biotechnology (CeBiTec), Universitätsstraße 25, D-33615 Bielefeld, Germany*
[3]*Department of Internal Medicine/Infectious Diseases and Respiratory Medicine, Charité -Universitätsmedizin Berlin, D-10117 Berlin, Germany*

Published in: Redox Biology 20: 514-525. (2019)
https://doi.org/10.1016/j.redox.2018.11.012

[#]**Corresponding author:** haike.antelmann@fu-berlin.de

Personal contribution:

I contributed to the concept of the paper, designed the biosensor and performed most experiments for this paper. I measured all kinetics of biosensor oxidation *in vitro* and *in vivo* (Fig. 1-6), performed the phenotype assays (Fig. 7), and live-imaging experiment (Fig. 8). I drafted all figures and wrote the paper together with Haike Antelmann.

Redox Biology 20 (2019) 514–525

Contents lists available at ScienceDirect

Redox Biology

journal homepage: www.elsevier.com/locate/redox

Research Paper

Stable integration of the Mrx1-roGFP2 biosensor to monitor dynamic changes of the mycothiol redox potential in *Corynebacterium glutamicum*

Quach Ngoc Tung[a], Vu Van Loi[a], Tobias Busche[a,b], Andreas Nerlich[c], Maren Mieth[c], Johanna Milse[b], Jörn Kalinowski[b], Andreas C. Hocke[c], Haike Antelmann[a,*]

[a] Freie Universität Berlin, Institute for Biology-Microbiology, D-14195 Berlin, Germany
[b] Center for Biotechnology (CeBiTec), Universitätsstraße 25, D-33615 Bielefeld, Germany
[c] Department of Internal Medicine/Infectious Diseases and Respiratory Medicine, Charité -Universitätsmedizin Berlin, D-10117 Berlin, Germany

ARTICLE INFO

Key words:
Corynebacterium glutamicum
Mycothiol
Mycothiol redox potential
Mrx1-roGFP2

ABSTRACT

Mycothiol (MSH) functions as major low molecular weight (LMW) thiol in the industrially important *Corynebacterium glutamicum*. In this study, we genomically integrated an Mrx1-roGFP2 biosensor in *C. glutamicum* to measure dynamic changes of the MSH redox potential (E_{MSH}) during the growth and under oxidative stress. *C. glutamicum* maintains a highly reducing intrabacterial E_{MSH} throughout the growth curve with basal E_{MSH} levels of ~ − 296 mV. Consistent with its H_2O_2 resistant phenotype, *C. glutamicum* responds only weakly to 40 mM H_2O_2, but is rapidly oxidized by low doses of NaOCl. We further monitored basal E_{MSH} changes and the H_2O_2 response in various mutants which are compromised in redox-signaling of ROS (OxyR, SigH) and in the antioxidant defense (MSH, Mtr, KatA, Mpx, Tpx). While the probe was constitutively oxidized in the *mshC* and *mtr* mutants, a smaller oxidative shift in basal E_{MSH} was observed in the *sigH* mutant. The catalase KatA was confirmed as major H_2O_2 detoxification enzyme required for fast biosensor re-equilibration upon return to non-stress conditions. In contrast, the peroxiredoxins Mpx and Tpx had only little impact on E_{MSH} and H_2O_2 detoxification. Further live imaging experiments using confocal laser scanning microscopy revealed the stable biosensor expression and fluorescence at the single cell level. In conclusion, the stably expressed Mrx1-roGFP2 biosensor was successfully applied to monitor dynamic E_{MSH} changes in *C. glutamicum* during the growth, under oxidative stress and in different mutants revealing the impact of Mtr and SigH for the basal level E_{MSH} and the role of OxyR and KatA for efficient H_2O_2 detoxification under oxidative stress.

1. Introduction

The Gram-positive soil bacterium *Corynebacterium glutamicum* is the most important industrial platform bacterium that produces millions of tons of L-glutamate and L-lysine every year as well as other value-added products [1–4]. In addition, *C. glutamicum* serves as model bacterium for the related pathogens *Corynebacterium diphtheriae and Corynebacterium jeikeium* [5]. In its natural soil habitat and during industrial production, *C. glutamicum* is exposed to reactive oxygen species (ROS), such as hydrogen peroxide (H_2O_2) which is generated as consequence of the aerobic lifestyle [6–8]. The low molecular weight (LMW) thiol mycothiol (MSH) functions as glutathione surrogate in detoxification of ROS and other thiol-reactive compounds in all actinomycetes, including *C. glutamicum* and mycobacteria to maintain the reduced state of the cytoplasm [9–11]. Thus, MSH-deficient mutants are sensitive to various thiol-reactive compounds, although the secreted histidine-derivative ergothioneine (EGT) also functions as alternative LMW thiol [12–16].

Abbreviations: Brx, bacilliredoxin; Brx-roGFP2, bacilliredoxin-fused roGFP2 biosensor; BSH, bacillithiol; BSSB, bacillithiol disulfide; CBB, Coomassie Brilliant Blue; CLSM, confocal laser scanning microscopy; CHP, cumene hydroperoxide; DTT, dithiothreitol; ECF, extracytoplasmic function; EGT, ergothioneine; E_{MSH}, mycothiol redox potential; Grx1-roGFP2, glutaredoxin-fused roGFP2 biosensor; GSH, glutathione; GSSG, glutathione disulfide; H_2O_2, hydrogen peroxide; HOCl, hypochloric acid; IPTG, isopropyl-β-D-thiogalactopyranoside; KatA, catalase; LB, Luria Bertani; LMW thiol, low molecular weight thiol; Mrx1, mycoredoxin-1; Mrx1-roGFP2, mycoredoxin-1-fused roGFP2 biosensor; MSH, mycothiol; MSSM, mycothiol disulfide; Mpx, mycothiol peroxidase; Mtr, mycothiol disulfide reductase; NaOCl, sodium hypochlorite; NEM, N-ethylmaleimide; OD_{500}, optical density at 500 nm; OxD, oxidation degree; PAGE, polyacrylamide gel electrophoresis; PCR, polymerase chain reaction; RCS, reactive chlorine species; roGFP2, redox-sensitive green fluorescent protein; ROS, reactive oxygen species; SDS, sodium dodecyl sulfate; SEM, standard error of the mean; SigH, RNA polymerase sigma-H factor; TL, transmitted light; Tpx, thiol peroxidase; Trx, thioredoxin; TrxR, thioredoxin reductase

* Correspondence to: Institute of Biology-Microbiology, Freie Universität Berlin, Königin-Luise-Strasse 12-16, D-14195 Berlin, Germany.
E-mail address: haike.antelmann@fu-berlin.de (H. Antelmann).

https://doi.org/10.1016/j.redox.2018.11.012
Received 5 September 2018; Received in revised form 8 November 2018; Accepted 15 November 2018
Available online 17 November 2018

MSH is a thiol-cofactor for many redox enzymes and is oxidized to mycothiol disulfide (MSSM) under oxidative stress. The NADPH-dependent mycothiol disulfide reductase (Mtr) catalyzes the reduction of MSSM back to MSH to maintain the highly reducing MSH redox potential (E_{MSH}) [17,18]. Overexpression of Mtr has been shown to increase the fitness, stress tolerance and MSH/MSSM ratio during exposure to ROS, antibiotics and alkylating agents in *C. glutamicum* [19]. Under hypochloric acid (HOCl) stress, MSH functions in protein *S*-mycothiolations as discovered in *C. glutamicum, C. diphtheriae* and *Mycobacterium smegmatis* [15,16,20]. In *C. glutamicum,* 25 *S*-mycothiolated proteins were identified under HOCl stress that include the peroxiredoxins (Tpx, Mpx, AhpE) and methionine sulfoxide reductases (MsrA, MsrB) as antioxidant enzymes that were inhibited by *S*-mycothiolation [16,21–26]. The regeneration of their antioxidant activities required the mycoredoxin-1 (Mrx1)/MSH/Mtr redox pathway, but could be also coupled to the thioredoxin/ thioredoxin reductase (Trx/TrxR) pathway which both operate in de-mycothiolation [9,10,27]. Detailed biochemical studies on the redox-regulation of antioxidant and metabolic enzymes (Tpx, Mpx, MsrA, GapDH) showed that both, the Mrx1 and Trx pathways function in de-mycothiolation at different kinetics. Mrx1 was much faster in regeneration of GapDH and Mpx activities during recovery from oxidative stress compared to the Trx pathway [20,21,23–26].

The enzymes for MSH biosynthesis and the Trx/TrxR systems are under control of the alternative extracytoplasmic function (ECF) sigma factor SigH which is sequestered by its cognate redox-sensitive anti sigma factor RshA in non-stressed cells [28–30]. RshA is oxidized under disulfide stress leading to structural changes and relief of SigH to initiate transcription of the large SigH disulfide stress regulon [16,31–33]. In addition, the LysR-type transcriptional repressor OxyR plays a major role in the peroxide response in *C. glutamicum* which controls genes encoding antioxidant enzymes for H_2O_2 detoxification and iron homeostasis, such as the catalase (*katA*), two miniferritins (*dps, ftnA*), the Suf machinery and ferrochelatase (*hemH*) [30,34]. Thus, SigH and OxyR can be regarded as main regulatory systems for the defense under disulfide and oxidative stress to maintain the redox balance in actinomycetes.

The standard thiol-redox potential of MSH was previously determined with biophysical methods as $E^{0'}$(MSSM/MSH) of − 230 mV which is close to that of glutathione (GSH) [35]. However, Mrx1 was also recently fused to redox-sensitive green fluorescent protein (roGFP2) to construct a genetically encoded Mrx1-roGFP2 redox biosensor for dynamic measurement of E_{MSH} changes inside mycobacterial cells. E_{MSH} values of ~-300 mV were calculated using the Mrx1-roGFP2 biosensor in mycobacteria that were much lower compared to values obtained with biophysical methods [35,36]. This Mrx1-roGFP2 biosensor was successfully applied for dynamic E_{MSH} measurements in the pathogen *Mycobacterium tuberculosis* (*Mtb*). Using Mrx1-roGFP2, E_{MSH} changes were studied in drug-resistant *Mtb* isolates, during intracellular replication and persistence in the acidic phagosomes of macrophages [36–38]. Mrx1-roGFP2 was also applied as tool in drug research to screen for ROS-generating anti-tuberculosis drugs or to reveal the mode of action of combination therapies based on E_{MSH} changes [36,39–41]. The *Mtb* population exhibited redox heterogeneity of E_{MSH} during infection inside macrophages which was dependent on sub-vacuolar compartments and the cytoplasmic acidification controlled by WhiB3 [36,38]. Thus, application of the Mrx1-roGFP2 biosensor provided novel insights into redox changes of *Mtb*. However, Mrx1-roGFP2 has not been applied in the industrial platform bacterium *C. glutamicum*.

In this work, we designed a genetically encoded Mrx1-roGFP2 biosensor that was genomically integrated and expressed in *C. glutamicum*. The biosensor was successfully applied to measure dynamic E_{MSH} changes during the growth, under oxidative stress and in various mutant backgrounds to study the impact of antioxidant systems (MSH, KatA, Mpx, Tpx) and their major regulators (OxyR, SigH) under basal and oxidative stress conditions. Our results revealed a highly reducing basal E_{MSH} of ~-296 mV that is maintained throughout the growth of *C. glutamicum*. H_2O_2 stress had only little effect on E_{MSH} changes in the wild type due to its H_2O_2 resistance, which was dependent on the catalase KatA supporting its major role for H_2O_2 detoxification. Confocal imaging further confirmed equal Mrx1-roGFP2 fluorescence in all cells indicating that the biosensor strain is well suited for industrial application to quantify E_{MSH} changes in *C. glutamicum* at the single cell level.

2. Materials and methods

2.1. Bacterial strains and growth conditions

Bacterial strains, plasmids and primers are listed in Tables S1 and S2. For cloning and genetic manipulation, *Escherichia coli* was cultivated in Luria Bertani (LB) medium at 37 °C. The *C. glutamicum* ATCC13032 wild type as well as the Δ*mshC,* Δ*mtr,* Δ*oxyR,* Δ*sigH*, Δ*katA,* Δ*mpx,* Δ*tpx* and Δ*mpx tpx* mutant strains were used in this study for expression of the Mrx1-roGFP2 biosensor which are described in Table S1. All *C. glutamicum* strains were cultivated in heart infusion medium (HI; Difco) at 30 °C overnight under vigorous agitation. The overnight culture was inoculated in CGC minimal medium supplemented with 1% glucose to an optical density at 500 nm (OD_{500}) of 3.0 and grown until OD_{500} of 8.0 for stress exposure as described [16]. *C. glutamicum* mutants were cultivated in the presence of the antibiotics nalidixic acid (50 μg/ml) and kanamycin (25 μg/ml).

2.2. Construction, expression and purification of His-tagged Mrx1-roGFP2 protein in E. coli

The *mrx1* gene (*cg0964*) was amplified from chromosomal DNA of *C. glutamicum* ATCC13032 by PCR using the primer pair Cgmrx1-roGFP2-*Nde*I-FOR and pQE60-Cgmrx1-roGFP2-*Spe*I-REV. The PCR product was digested with *Nde*I and *Spe*I and cloned into plasmid pET11b-*brx-roGFP2* [42] to exchange the *brx* sequence by *mrx1* with generation of plasmid pET11b-*mrx1-roGFP2* **(**Table S1**)**. The correct sequence was confirmed by PCR and DNA sequencing.

The *E. coli* BL21 (DE3) *plysS* expression strain containing the plasmid pET11b-*mrx1-roGFP2* was grown in 1 l LB medium until OD_{600} of 0.6 at 37 °C, followed by induction with 1 mM IPTG (isopropyl-β-D-thiogalactopyranoside) for 16 h at 25 °C. Recombinant His_6-tagged Mrx1-roGFP2 protein was purified using His Trap™ HP Ni-NTA columns (5 ml; GE Healthcare, Chalfont St Giles, UK) and the ÄKTA purifier liquid chromatography system (GE Healthcare) according to the instructions of the manufacturer (USB). The purified protein was dialyzed against 10 mM Tris-HCl (pH 8.0), 100 mM NaCl and 30% glycerol and stored at − 80 °C. Purity of the protein was analyzed after sodium dodecyl sulfate-polyacrylamide gel electrophoresis (SDS-PAGE) and Coomassie brilliant blue (CBB) staining.

2.3. Construction of katA, mtr, mpx and tpx deletion mutants in C. glutamicum

The vector pK18*mobsacB* was used to create marker-free deletions in *C. glutamicum* (1). The gene-SOEing method of Horton (2) was used to construct pK18*mobsacB* derivatives to perform allelic exchange of the *katA* and *mtr* genes in the chromosome of *C. glutamicum* ATCC13032 using the primers listed in Table S2. The constructs include the *katA* and *mtr* genes with flanking regions and internal deletions (Δ*katA* [1555 bp] and Δ*mtr* [1382 bp]). The pK18*mobsacB* derivatives were sub-cloned in *E. coli* JM109 (Table S1) and transformed into *C. glutamicum* ATCC13032. The pK18*mobsacB*::Δ*tpx* plasmid containing the *tpx* flanking regions was constructed previously (3) and transformed into the *C. glutamicum* Δ*mpx* mutant (3). The gene replacement in the chromosome of *C. glutamicum* ATCC13032 resulted in Δ*katA* and Δ*mtr* single deletion mutants and the gene replacement of *tpx* in the

chromosome of *C. glutamicum* Δ*mpx* resulted in the *C. glutamicum* Δ*mpx tpx* double deletion mutant. The deletions were confirmed by PCR using the primers in Table S2.

2.4. Construction of C. glutamicum Mrx1-roGFP2 biosensor strains

For construction of the genomically integrated Mrx1-roGFP2 biosensor, a 237 bp fragment of *mrx1* (*cg0964*) was fused to *roGFP2* containing a 30-amino acid linker $(GGSGG)_6$ under control of the strong P_{tuf} promoter of the *C. glutamicum tuf* gene encoding the translation elongation factor EF-Tu. The P_{tuf}-Mrx1-roGFP2 fusion was codon-optimized, synthesized with flanking *Mun*I and *Xho*I restriction sites and sub-cloned into PUC-SP by Bio Basic resulting in PUC-SP::P_{tuf}-*mrx1-roGFP2*. For genomic integration of the biosensor into the *cg1121-cg1122* intergenic region of *C. glutamicum* (Table S1), the vector pK18*mobsacB-cg1121-cg1122* was used [43], kindly provided by Julia Frunzke, Forschungszentrum Jülich. The vector was PCR amplified with primers pk18_MunI and pk18_XhoI to swap the restrictions sites. After digestion of the pk18*mobsacB-cg1121-cg1122* PCR product and the PUC-SP::P_{tuf}-*mrx1-roGFP2* plasmid with *Mun*I and *Xho*I, both digestion products were ligated to obtain pK18*mobsacB-cg1121-cg1121*-P_{tuf}-*mrx1-roGFP2*. The resulting plasmid was sequenced with biosensor_seq_primer_1 and biosensor_seq_primer_2. Transfer of the plasmid into *C. glutamicum* strains (Table S1) was performed by electroporation and screening for double homologous recombination events using the conditional lethal effect of the *sacB* gene as described [16,43]. Correct integration of P_{tuf}-*mrx1-roGFP2* into the *cg1121-cg1122* intergenic region was verified by colony PCR using 2 primer pairs (pk18_INT_Cg_Test_rev, pk18_INT_Cg_Test_fwd and FUB_7_seq_wo_linker_fwd; FUB_8_seq_wo_linker_rev) (Table S2).

The Mrx1-roGFP2 biosensor was further cloned into the *E. coli-C. glutamicum* shuttle vector pEKEx2 for ectopic expression of Mrx1-roGFP2 under the IPTG-inducible *tac* promoter. The *mrx1-roGFP2* fusion was amplified from plasmid pET11b-*mrx1-roGFP2* using primer pair pEKEx2-Cgmrx1-*Bam*HI-For and pEKEx2-roGFP2-*Kpn*I-Rev (Table S2). The PCR product and plasmid pEKEx2 were digested with *BamH*I and *Kpn*I, followed by ligation to generate plasmid pEKEx2-*mrx1-roGFP2*. The resulting plasmid was cloned in *E. coli*, sequenced and electroporated into *C. glutamicum*. Induction of the *C. glutamicum* strain expressing pEKEx2-encoded Mrx1-roGFP2 was performed with 1 mM IPTG.

2.5. Characterization of recombinant Mrx1-roGFP2 biosensor in vitro

The purified Mrx1-roGFP2 protein was reduced with 10 mM dithiothreitol (DTT) for 20 min, desalted with Micro-Bio spin columns (Bio-Rad), and diluted to a final concentration of 1 μM in 100 mM potassium phosphate buffer, pH 7.0. The oxidation degree (OxD) of the biosensor was determined by calibration to fully reduced and oxidized probes which were generated by treatment of the probes with 10 mM DTT and 5 mM diamide for 5 min, respectively [42]. The thiol disulfides and oxidants were injected into the microplate wells (BD Falcon 353219) 60 s after the start of measurements. Emission was measured at 510 nm after excitation at 400 and 488 nm using the CLARIOstar microplate reader (BMG Labtech) with the Control software version 5.20 R5. Gain setting was adjusted for each excitation maximum. The data were analyzed using the MARS software version 3.10 and exported to Excel. Each *in vitro* measurement was performed in triplicate.

2.6. Measurements of Mrx1-roGFP2 biosensor oxidation in C. glutamicum in vivo

C. glutamicum wild type and mutant strains expressing stably integrated Mrx1-roGFP2 were grown overnight in HI medium and inoculated into CGC medium with 1% glucose to a starting OD_{500} of 3.0. For stress experiments, the strains were cultivated for 8 h until they have reached an OD_{500} of 14–16. Cells were harvested by centrifugation, washed twice with CGC minimal medium, adjusted to an OD_{500} of 40 in CGC medium and transferred to the microplate reader. Aliquots were treated for 15 min with 10 mM DTT and 20 mM cumene hydroperoxide (CHP) for fully reduced and oxidized controls, respectively. Injection of the oxidants was performed 5 min after the start of microplate reader measurements.

For the OxD measurements along the growth curves, cells were harvested by centrifugation at different time points and washed in 100 mM potassium phosphate buffer, pH 7.0. Aliquots were treated with 20 mM CHP and 10 mM DTT for fully reduced and oxidized controls, respectively. Samples and controls were incubated with 10 mM N-ethylmaleimide (NEM) to block free thiols and transferred to microplate wells. The Mrx1-roGFP2 biosensor fluorescence emission was measured at 510 nm after excitation at 400 and 488 nm using the CLARIOstar microplate reader (BMG Labtech). The OxD of biosensor was calculated for each sample and normalized to fully reduced and oxidized controls as described previously [42,44] based to the following Eq. (1).

$$\mathrm{OxD} = \frac{I400_{\mathrm{sample}} \times I488_{\mathrm{red}} - I400_{\mathrm{red}} \times I488_{\mathrm{sample}}}{I400_{\mathrm{sample}} \times I488_{\mathrm{red}} - I400_{\mathrm{sample}} \times I488_{\mathrm{ox}} + I400_{\mathrm{ox}} \times I488_{\mathrm{sample}} - I400_{\mathrm{red}} \times I488_{\mathrm{sample}}} \quad (1)$$

The values of $I400_{\mathrm{sample}}$ and $I488_{\mathrm{sample}}$ are the observed fluorescence excitation intensities at 400 and 488 nm, respectively. The values of $I400_{\mathrm{red}}$, $I488_{\mathrm{red}}$, $I400_{\mathrm{ox}}$ and $I488_{\mathrm{ox}}$ represent the fluorescence intensities of fully reduced and oxidized controls, respectively.

Based on the OxD and $E^{o'}_{\mathrm{roGFP2}} = -280$ mV [45], the MSH redox potential was calculated according to the Nernst Eq. (2) as follows:

$$E_{\mathrm{MSH}} = E_{\mathrm{roGFP2}} = E^{o'}_{\mathrm{roGFP2}} - \left(\frac{\mathrm{RT}}{2\mathrm{F}}\right) * \mathrm{In}\left(\frac{1 - \mathrm{OxD}}{\mathrm{OxD}}\right) \quad (2)$$

2.7. Confocal laser scanning microscopy of Mrx1-roGFP2 biosensor strains

C. glutamicum wild type expressing Mrx1-roGFP2 was grown in HI medium for 48 h, exposed to 80 mM H_2O_2 for different times and washed in potassium phosphate buffer, pH 7.0. Cells were blocked with 10 mM NEM, and imaged using a LSM 780 confocal laser-scanning microscope with a 63 × /1.4 NA Plan-Apochromat oil objective controlled by the Zen 2012 software (Carl-Zeiss, Jena, Germany). Fluorescence excitation was performed at 405 and 488 nm with laser power adjustment to 15% and 25%, respectively. For both excitation wavelengths, emission was collected between 491 and 580 nm. Fully reduced and oxidized controls were prepared with 10 mM DTT and 10 mM diamide, respectively. Images were analyzed by the Zen 2 software and Fiji/ImageJ [42,46]. Fluorescent intensities were measured after excitation at 405 and 488 nm and the images false-colored in red and green, respectively. Auto-fluorescence was recorded and subtracted. Quantification of the OxD and E_{MSH} values was performed based on the 405/488 nm excitation ratio of mean fluorescence intensities as described [42,46].

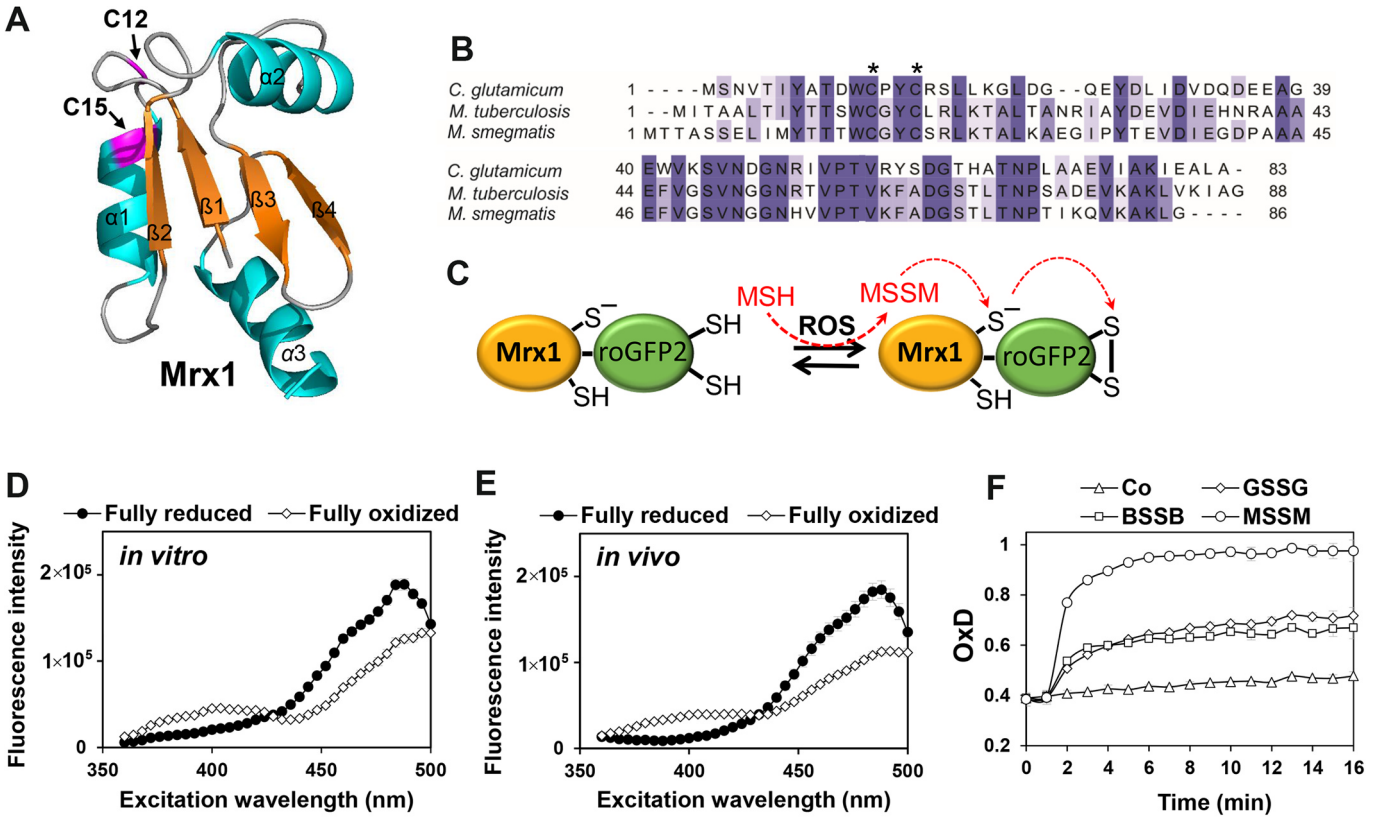

Fig. 1. Structure and alignment of Mrx1 homologs, principle and specific response of the Mrx1-roGFP2 biosensor to MSSM. (A) The Mrx1 structure of *C. glutamicum* was modelled using SWISS-MODEL (https://swissmodel.expasy.org/) and visualized with PyMol using the template of *M. tuberculosis* Rv3198A (PDB code: 2LQO). The Cys12 active site and Cys15 resolving site of the CXXC motif of Mrx1 are labelled with arrows. **(B)** The Mrx1 homologs Cg0964 of *C. glutamicum*, Rv3198A of *M. tuberculosis* and MSMEG_1947 of *M. smegmatis* were aligned with ClustalW2 and presented in Jalview. Intensity of the blue color gradient is based on 50% identity. Conserved Cys residues are marked with asterisks. **(C)** The principle of the Mrx1-roGFP2 biosensor oxidation is shown. Under ROS stress, MSH is oxidized to MSSM which reacts with Mrx1 to *S*-mycothiolated Mrx1. MSH is transferred from Mrx1 to the roGFP2 moiety leading to *S*-mycothiolated roGFP2 which is rearranged to the roGFP2 disulfide. The roGFP2 disulfide leads to a structural change resulting in ratiometric changes of the 400 and 488 excitation maxima of Mrx1-roGFP2. **(D, E)** The ratiometric response of the Mrx1-roGFP2 biosensor in the reduced and oxidized state *in vitro* **(D)** and after expression in *C. glutamicum in vivo* **(E)**. For fully reduced and oxidized Mrx1-roGFP2, 10 mM DTT and 5 mM diamide were used *in vitro* as well as 10 mM DTT and 20 mM CHP *in vivo* (n = 5). The fluorescence excitation spectra were monitored using the microplate reader. **(F)** The purified Mrx1-roGFP2 biosensor (1 μM) responds most strongly to 100 μM of MSSM, but only weakly to BSSB and GSSG *in vitro* (n = 3). The thiol disulfides were injected into the microplate wells 60 s after the start of the measurements of the Mrx1-roGFP2 biosensor response. The control (Co) indicates the measurement of the Mrx1-roGFP2 biosensor response without thiol-disulfides. The OxD was calculated based on the 400/488 nm excitation ratio with emission measured at 510 nm. Mean values and standard error of the mean (SEM) are shown in all graphs.

3. Results

3.1. The Mrx1-roGFP2 biosensor of C. glutamicum responds most specifically to MSSM in vitro

Previous studies have revealed a specific response of the Mrx1-roGFP2 biosensor to MSSM *in vitro*, which was based on a fusion of mycobacterial Mrx1 to roGFP2 [36]. Here we aimed to engineer a related Mrx1-roGFP2 biosensor for the MSH-producing industrially important bacterium *C. glutamicum*. Mrx1 (Cg0964) of *C. glutamicum* exhibits a similar redox-active CxxC motif and shares 46.8% and 42.1% sequence identity with Mrx1 homologs of *M. tuberculosis* H37Rv (Rv3198A) and *M. smegmatis* mc^{2}155 (MSMEG_1947), respectively (Fig. 1**AB**) [27]. The principle of the Mrx1-roGFP2 biosensor to measure intrabacterial E_{MSH} changes was shown previously [14,36]. MSSM reacts with Mrx1 to form *S*-mycothiolated Mrx1, followed by the transfer of the MSH moiety to roGFP2 which rearranges to the roGFP2 disulfide resulting in ratiometric changes of the 400/488 excitation ratio [14,36] (Fig. 1C).

Mrx1 of *C. glutamicum* was fused to roGFP2 and first purified as His-tagged Mrx1-roGFP2 protein to verify the specific Mrx1-roGFP2 biosensor response to MSSM *in vitro*. In addition, Mrx1-roGFP2 was integrated into the genome of *C. glutamicum* wild type in the intergenic region between *cg1121-cg1122* and placed under control of the strong P_{tuf} promoter using the pK18*mobsacB-int* plasmid as constructed previously [43]. First, the Mrx1-roGFP2 biosensor response of the purified biosensor and of the stably integrated Mrx1-roGFP2 fusion were compared under fully reduced (DTT) and fully oxidized (diamide) conditions. The Mrx1-roGFP2 biosensor fluorescence excitation spectra were similar under *in vitro* and *in vivo* conditions exhibiting the same excitation maxima at 400 and 488 nm for fully reduced and oxidized probes (Fig. 1**DE**). Thus, the Mrx1-roGFP2 probe is well suited to monitor dynamic E_{MSH} changes during the growth and under oxidative stress in *C. glutamicum*. In addition, it was verified that purified Mrx1-roGFP2 reacts very fast and most strongly to low levels of 100 μM MSSM, although weaker responses were also observed with bacillithiol disulfide (BSSB) and glutathione disulfide (GSSG) which are, however, not physiologically relevant for *C. glutamium* (Fig. 1**F**).

Furthermore, we assessed the direct response of Mrx1-roGFP2 and unfused roGFP2 to the oxidants H_2O_2 and NaOCl to compare the sensitivities of the probes for direct oxidation (Fig. 2). This was important since a previous study showed a high sensitivity of fused Grx-roGFP2 and roGFP2-Orp1 to 10-fold molar excess of 2 μM NaOCl [47]. In our *in vitro* experiments, the Mrx1-roGFP2 and roGFP2 probes did not respond

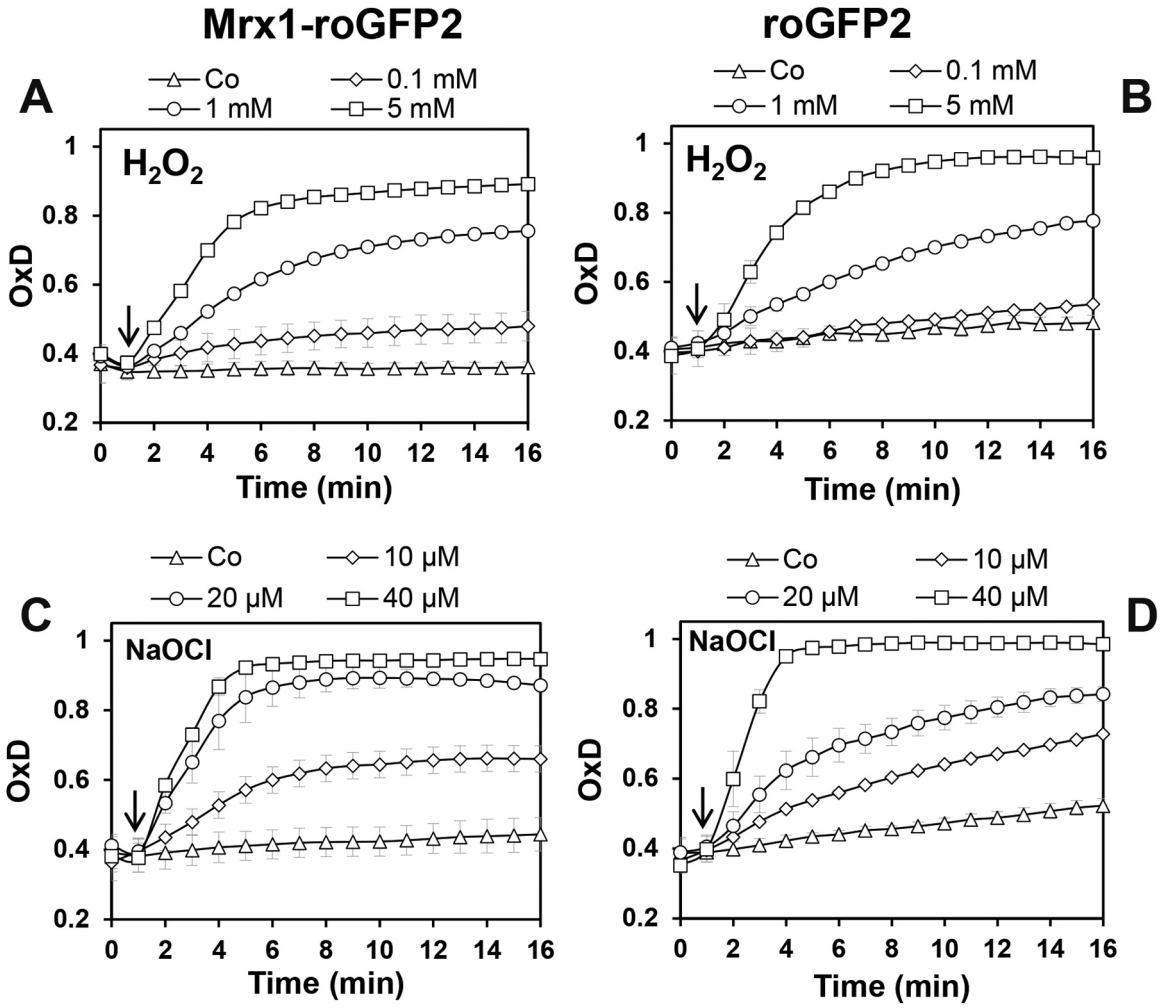

Fig. 2. The response of the purified Mrx1-roGFP2 and roGFP2 biosensors to H_2O_2 and NaOCl *in vitro*. Purified Mrx1-roGFP2 and roGFP2 probes (1 µM) were treated with increasing concentrations of 0.1–5 mM H_2O_2 **(A, B)** and 10–40 µM NaOCl **(C, D)**, respectively. The oxidants were injected into the microplate wells 60 s after the start of the measurements of the Mrx1-roGFP2 biosensor response as indicated by arrows. The control (Co) indicates the measurement of the Mrx1-roGFP2 and roGFP2 response without oxidants. The OxD was calculated based on the 400/488 nm excitation ratios with emission at 510 nm and related to the fully oxidized (5 mM diamide) and reduced controls (10 mM DTT). Mean values of 5 independent experiments are shown and error bars represent the SEM.

to 100 µM H_2O_2 as in previous studies. Only 1–5 mM H_2O_2 lead to a direct oxidation of both probes with a faster response of the Mrx1-roGFP2 fusion. Both probes were rapidly oxidized by 10–40 µM NaOCl *in vitro*, and again Mrx1-roGFP2 was more sensitive to thiol-oxidation by NaOCl compared to unfused roGFP2 (Fig. 2). The rapid oxidation of roGFP2 and fused roGFP2 biosensors to low levels of HOCl is in agreement with previous studies [47] and was also observed using the Brx-roGFP2 biosensor in *S. aureus* [42]. The higher sensitivity of fused roGFP2 biosensors (Brx-roGFP2, Mrx1-roGFP2) to NaOCl indicates that the redox active Cys residues of Brx or Mrx1 are more susceptible for thiol-oxidation compared to the thiols of roGFP2. In conclusion, our Mrx1-roGFP2 probe is highly specific to low levels of MSSM. The response of Mrx1-roGFP2 to higher levels of 1 mM H_2O_2 *in vitro* are not expected to occur inside *C. glutamicum* cells due to its known H_2O_2 resistance mediated by the highly efficient catalase.

3.2. The intracellular redox balance was affected in mutants with defects of MSH, Mtr and SigH

Next, we applied the genomically expressed Mrx1-roGFP2 biosensor to monitor the perturbations of basal level E_{MSH} along the growth curve in various *C. glutamicum* mutant backgrounds, which had deletions of major antioxidant systems (MSH, Mtr, KatA, Tpx, Mpx) and redox-sensing regulators (OxyR, SigH) (Figs. 3 and 4). The oxidation degree was calculated in *C. glutamicum* wild type and mutants during the 5–12 h time points representing the log phase and transition to stationary phase in defined CGC medium. The biosensor oxidation of each *C. glutamicum* sample was normalized between 0 and 1 based on the fully reduced (DTT) and oxidized (CHP) controls. It is interesting to note, that *C. glutamicum* wild type cells maintained a highly reducing and stable E_{MSH} of ~-296 mV with little fluctuations during the log and stationary phase (Table S3). Thus, this basal level E_{MSH} of *C. glutamicum* is very similar to that measured in *M.* smegmatis previously (E_{MSH} of ~−300) [36].

In agreement with previous studies of bacillithiol (BSH)- and GSH-deficient mutants, the absence of MSH resulted in constitutive oxidation of the Mrx1-roGFP2 biosensor in the *mshC* mutant (Fig. 3**A**). This indicates an impaired redox state in the *mshC* mutant and the importance of MSH as major LMW thiol to maintain the redox balance in *C. glutamicum* (Fig. 3**A**). We hypothesize that increased levels of ROS may lead to constitutive biosensor oxidation in the MSH-deficient mutant since the *mshC* mutant had a H_2O_2-sensitive phenotype in previous studies [48]. The high MSH/MSSM redox balance is maintained by the NADPH-dependent mycothiol disulfide reductase Mtr which reduces MSSM back to MSH [9]. The importance of Mtr to maintain a reduced E_{MSH} was also supported by our biosensor measurements which

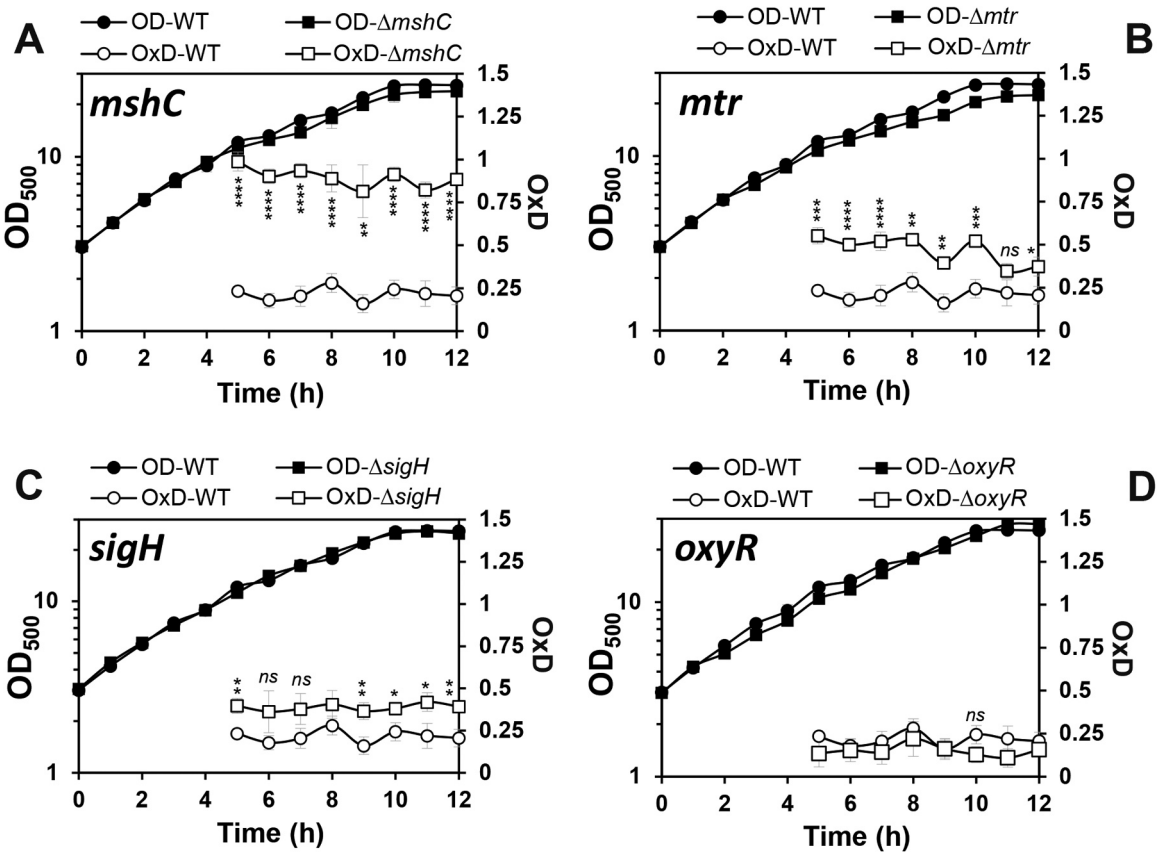

Fig. 3. Deletions of *mshC, mtr* and *sigH* affected the basal E_{MSH} during the growth of *C. glutamicum*. The basal level of E_{MSH} was measured using Mrx1-roGFP2 along the growth curve in *C. glutamicum* wild type and in Δ*mshC* **(A)**, Δ*mtr* **(B)**, Δ*sigH* **(C)** and Δ*oxyR* **(D)** mutants. The basal E_{MSH} showed an oxidative shift in the Δ*mshC,* Δ*mtr and* Δ*sigH* mutants, but not in the Δ*oxyR* mutant **(D)**. OxD was calculated based on the 400/488 nm excitation ratios with emission at 510 nm and related to the fully oxidized and reduced controls. Mean values and SEM of four independent experiments are shown and *p*-values were calculated by the Student's unpaired two-tailed *t*-test by the graph prism software ($^{ns}p > 0.05$; *p < 0.05; **p < 0.01; ***p < 0.001; and ****p < 0.0001).

revealed an oxidative shift in E_{MSH} to −280.2 mV in the *mtr* mutant during all growth phases (Fig. 3**B,** Table S3).

The alternative ECF sigma factor SigH controls a large disulfide stress regulon mainly involved in the redox homeostasis, including genes for thioredoxins and thioredoxin reductases (TrxAB), mycoredoxin-1 (Mrx1) and genes for MSH biosynthesis and recycling (MshA, Mca, Mtr) [9,28,29,32]. The *C. glutamicum sigH* mutant showed an increased sensitivity to ROS and NaOCl stress [16,28,29]. Mrx1-roGFP2 biosensor measurements confirmed a slightly more oxidized E_{MSH} of − 286 mV in the *sigH* mutant supporting the regulatory role of SigH for the redox balance (Fig. 3**C,** Table S3). However, the oxidative E_{MSH} shift was lower in the *sigH* mutant compared to the *mtr* mutant. In conclusion, our Mrx1-roGFP2 biosensor results document the important role of MSH, Mtr and SigH to maintain the redox homeostasis in *C. glutamicum* during the growth.

In addition to MSH, *C. glutamicum* encodes many antioxidant enzymes that are involved in H_2O_2 detoxification and confer strong resistance of *C. glutamicum* to millimolar levels of H_2O_2. The H_2O_2 scavenging systems in *C. glutamicum* are the major vegetative catalase (KatA) and the peroxiredoxins (Tpx, Mpx). The catalase is highly efficient for detoxification at high H_2O_2 levels while Tpx and Mpx are more involved in reduction of physiological low levels of H_2O_2 generated during the aerobic growth [49]. In *C. glutamicum*, expression of *katA* is induced by H_2O_2 and controlled by the redox-sensing OxyR repressor which is inactivated under H_2O_2 stress [34]. Thus, the *oxyR* mutant exhibits increased H_2O_2 resistance due to constitutive derepression of *katA* [34]. Here, we were interested in the contribution of OxyR, and the antioxidant enzymes KatA, Tpx and Mpx to maintain the reduced basal level E_{MSH} in *C. glutamicum*. In all mutants with deletions of *oxyR*, *katA*, *tpx* and *mpx*, the basal level of E_{MSH} was still highly reducing and comparable to the wild type during different growth phases (Fig. 3**D,** Fig. 4**A–D,** Table S3). Thus, we can conclude that the major antioxidant enzymes for H_2O_2 detoxification (KatA, Mpx and Tpx) do not contribute to the reduced basal E_{MSH} level in *C. glutamicum* during aerobic growth. These results further point to the main roles of these H_2O_2 scavenging systems under conditions of oxidative stress to recover the reduced state of E_{MSH} which was investigated in the next section.

3.3. Mrx1-roGFP2 biosensor responses in C. glutamicum under oxidative stress in vivo

Next, we were interested to determine the kinetics of Mrx1-roGFP2 biosensor oxidation in *C. glutamicum* under H_2O_2 and NaOCl stress and the recovery of reduced E_{MSH}. *C. glutamicum* can survive even 100 mM H_2O_2 without killing effect which depends on the very efficient catalase KatA [34]. In accordance with the H_2O_2 resistant phenotype, the Mrx1-roGFP2 biosensor did not respond to 10 mM H_2O_2 in *C. glutamicum* wild type cells and was only weakly oxidized by 40 mM H_2O_2 (Fig. 5**A**). *C. glutamicum* cells were able to recover the reduced E_{MSH} within 40–60 min after H_2O_2 treatment. Importantly, even 100 mM H_2O_2 did not further enhance the biosensor oxidation degree, indicating highly efficient antioxidant systems (data not shown).

In contrast, *C. glutamicum* was more sensitive to sub-lethal doses of NaOCl stress and showed a moderate biosensor oxidation by 0.5–1 mM NaOCl, while 1.5 mM NaOCl resulted in the fully oxidation of the probe. Moreover, cells were unable to regenerate the reduced basal level of E_{MSH} within 80 min after NaOCl exposure, which could be only restored with 10 mM DTT **(**Fig. 5**B).**

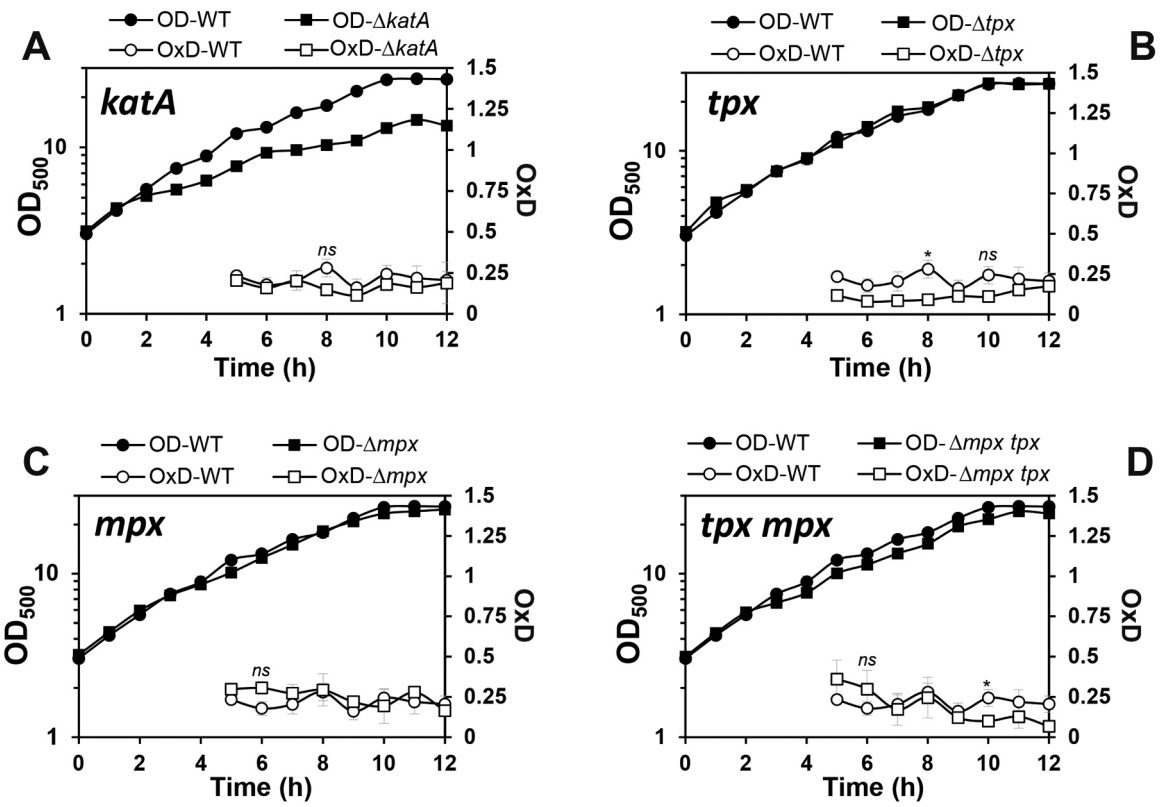

Fig. 4. The absence of the antioxidant enzymes KatA, Tpx and Mpx has no influence on the basal level E_{MSH} during the growth of *C. glutamicum*. The basal level of E_{MSH} was measured using the Mrx1-roGFP2 along the growth curve in *C. glutamicum* wild type and Δ*katA* **(A)**, Δ*tpx* **(B)**, Δ*mpx* **(C)** and Δ*tpx mpx* **(D)** mutants, but was not affected compared to the wild type. OxD was calculated based on the 400/488 nm excitation ratios with emission at 510 nm and related to the fully oxidized and reduced controls. Mean values and SEM of four independent experiments are shown and *p*-values were calculated by the Student's unpaired two-tailed *t*-test by the graph prism software ($^{ns}p > 0.05$; $^{*}p < 0.05$; $^{**}p < 0.01$; $^{***}p < 0.001$; and $^{****}p < 0.0001$).

Since H_2O_2 is the more physiological oxidant in *C. glutamicum*, we studied the biosensor response under 40 mM H_2O_2 stress in the various mutants deficient for MSH and Mtr, antioxidant enzymes (KatA, Mpx, Tpx) and redox regulators (SigH, OxyR). The *sigH* mutant showed an increased basal level of E_{MSH} of ~-286 mV as noted earlier (Fig. 3**C**), but a similar oxidation increase with 40 mM H_2O_2 and recovery of the reduced state after 40 min compared to the wild type (Fig. 6**A**). The similar kinetics of biosensor oxidation and regeneration in wild type and

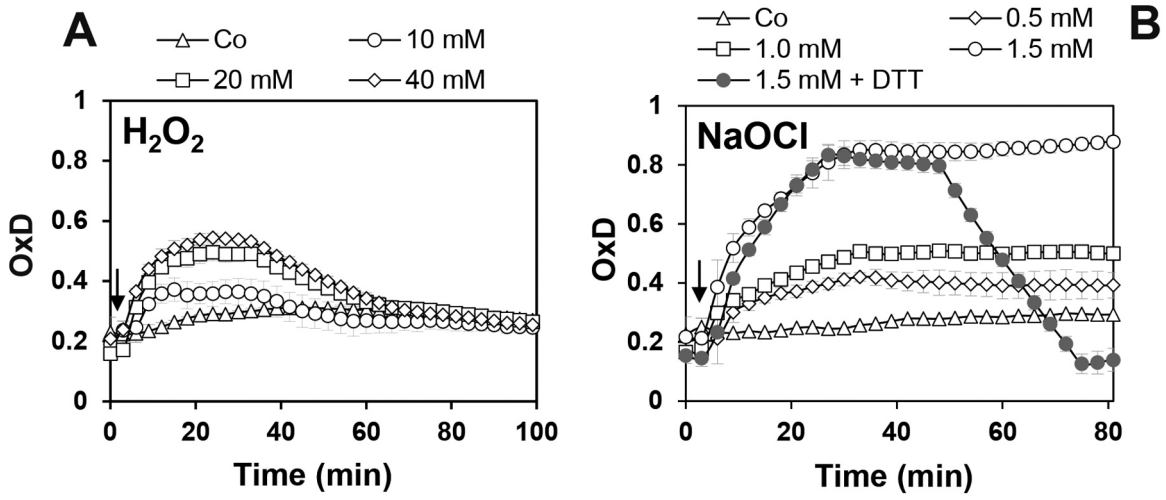

Fig. 5. The Mrx1-roGFP2 biosensor responds weakly to H_2O_2 and strongly to NaOCl in *C. glutamicum* wild type cells. The Mrx1-roGFP2 biosensor was weakly oxidized by 10–40 mM H_2O_2 in *C. glutamicum* wild type ($p = 0.0002$ at 20 mM H_2O_2; $p < 0.0001$ at 40 mM H_2O_2) **(A)**, but rapidly and fully by low doses of 0.5–1.5 mM NaOCl ($p = 0.007$ at 0.5 mM NaOCl; $p = 0.0004$ at 1.0 mM NaOCl; $p < 0.0001$ at 1.5 mM NaOCl) **(B).** While cells could recover the reduced state after 50 min of H_2O_2 exposure **(A)**, regeneration of Mrx1-roGFP2 was not possible in NaOCl-stressed cells **(B)**. To analyze the reversibility of Mrx1-roGFP2 oxidation in NaOCl-treated cells, 10 mM DTT was added 45 min after NaOCl exposure resulting in recovery of reduced E_{MSH} **(B).** Mean values and SEM of three independent experiments are shown in all graphs and *p*-values are calculated by a Student's unpaired two-tailed *t*-test by the graph prism software. The addition of oxidants to *C. glutamicum* cells was performed 5 min after the start of the measurements and is indicated by arrows. The control (Co) denotes the response of the Mrx1-roGFP2 probe inside *C. glutamicum* wild type cells in the absence of oxidants.

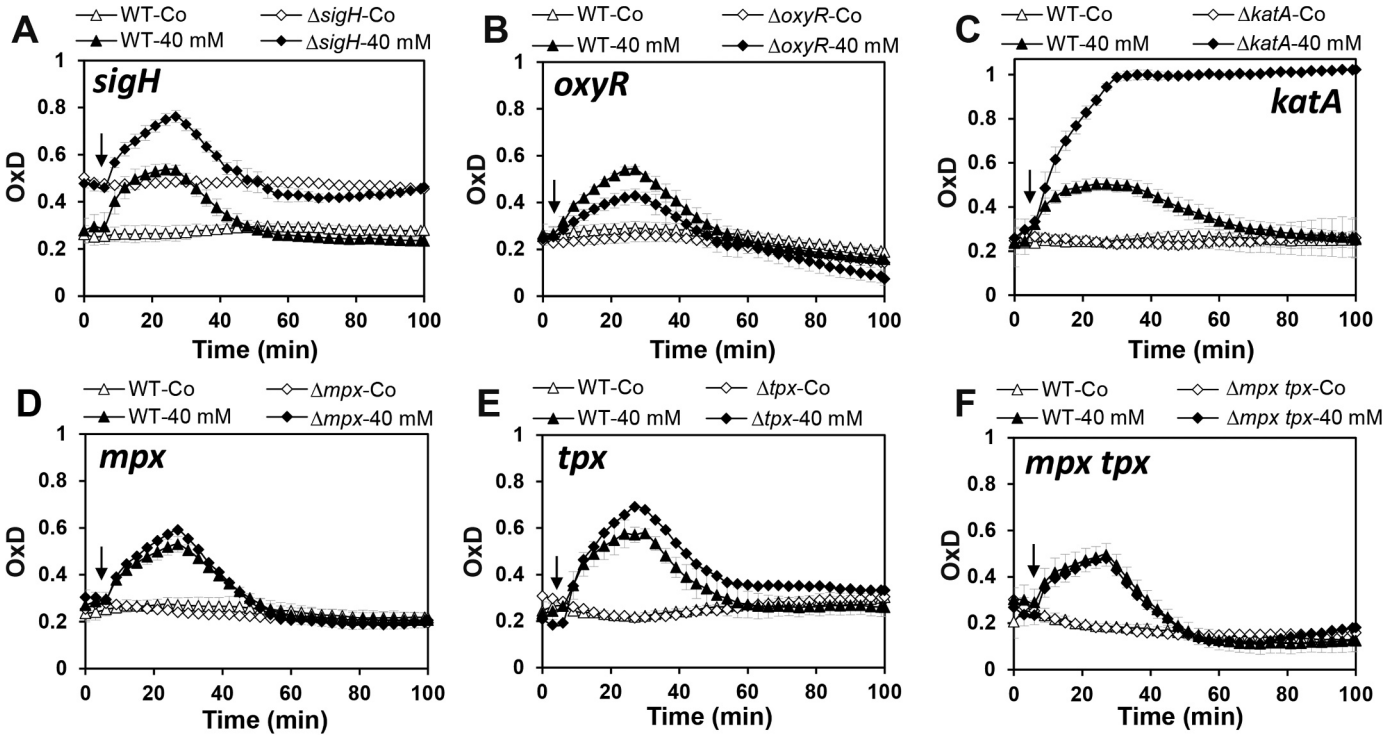

Fig. 6. Kinetics of H_2O_2 detoxification in *C. glutamicum* mutants deficient for redox-regulators (OxyR, SigH) or antioxidant enzymes (KatA, Mpx, Tpx). The Mrx1-roGFP2 biosensor response and kinetics of recovery was analyzed under 40 mM H_2O_2 stress in *C. glutamicum* wild type and mutants deficient for the disulfide stress regulatory sigma factor SigH **(A)**, the peroxide-sensitive repressor OxyR **(B)** and the catalases and peroxiredoxins for H_2O_2 detoxification (KatA, Mpx, Tpx) **(C-F)**. The *sigH* mutant showed a higher E_{MSH} basal level of E_{MSH}, but the response and recovery under H_2O_2 stress was similar to the wild type **(A)**. The constitutive derepression of *katA* in the *oxyR* mutant resulted in a lower Mrx1-roGFP2 biosensor response under H_2O_2 stress ($p = 0.006$ WT versus *oxyR* H_2O_2) **(B)**. The catalase KatA is essential for H_2O_2 detoxification as revealed by the strong oxidation increase of the *katA* mutant and the lack of regeneration of reduced E_{MSH} ($p < 0.0001$ WT versus *katA* H_2O_2) **(C)**. The Mrx1-roGFP2 biosensor response of the *tpx* mutant was only slightly increased under H_2O_2 stress ($p = 0.0017$ WT versus *tpx* H_2O_2) **(E)**, but not in *mpx* and *mpx tpx* mutants ($p = 0.7981$ or $p = 0.9489$ WT versus *tpx* or *mpx tpx* H_2O_2) **(D, F)**. Mean values and SEM of three independent experiments are shown in all graphs and *p*-values are obtained by a Student's unpaired two-tailed *t*-test by the graph prism software. The addition of oxidants to *C. glutamicum* wild type and mutant cells was performed 5 min after the start of the measurements and is indicated by arrows. The control (Co) shows the response of the Mrx1-roGFP2 probe inside *C. glutamicum* wild type and mutant cells without H_2O_2 treatment.

sigH mutant cells may indicate that MSH is not directly involved in H_2O_2 detoxification. In contrast, the *oxyR* mutant showed a lower H_2O_2 response than the wild type, but required the same time of 40 min for recovery of the reduced state of E_{MSH} (Fig. 6**B**). The derepression of *katA* in the *oxyR* mutant is most likely responsible for the lower biosensor oxidation under H_2O_2 stress [34,50]. This hypothesis was supported by the very fast response of *katA* mutant cells to 40 mM H_2O_2 stress, resulting in fully oxidation of the biosensor due to the lack of H_2O_2 detoxification in the absence of KatA (Fig. 6**C**). Exposure of *katA* mutant cells to 40 mM H_2O_2 might cause enhanced oxidation of MSH to MSSM leading to full biosensor oxidation with no recovery of the reduced state. In contrast, kinetic biosensor measurements under H_2O_2 stress revealed only slightly increased oxidation in the *tpx* mutant while the *mpx* mutant showed the same oxidation increase like the wild type (Fig. 6**DE**). However, the H_2O_2 response of the *mpx tpx* mutant was similar compared to the wild type, indicating that Tpx and Mpx do not contribute significantly to H_2O_2 detoxification during exposure to high levels of 40 mM H_2O_2 stress, while KatA plays the major role (Fig. 6**F**). The small oxidation increase in the *tpx* mutant might indicate additional roles of Tpx for detoxification of low levels of H_2O_2 as found in previous studies [51]. Altogether, our studies on the kinetics of the Mrx1-roGFP2 biosensor response under H_2O_2 stress support that KatA plays the most important role in H_2O_2 detoxification in *C. glutamicum*.

To correlate increased biosensor responses under H_2O_2 stress to peroxide sensitive phenotypes, we compared the growth of the wild type and mutants after exposure to 80 mM H_2O_2 (Fig. 7). Exposure of the wild type to 80 mM H_2O_2 did not significantly affect the growth rate indicating the high level of H_2O_2 resistance in *C. glutamicum*. Of all mutants, only the *katA* mutant was significantly impaired in growth under non-stress conditions and lysed after exposure to 80 mM H_2O_2 (Fig. 7**C**). In contrast, deletions of *sigH, oxyR, tpx* and *mpx* did not significantly affect the growth under control and H_2O_2 stress conditions (Fig. 7**AB, DE**). However, we observed a slightly decreased growth rate of the *mpx tpx* mutant in response to 80 mM H_2O_2 stress supporting the residual contribution of thiol-dependent peroxiredoxins in the peroxide stress response (Fig. 7**F**). Overall, the growth curves are in agreement with the biosensor measurements indicating the major role of KatA for detoxification of high levels of H_2O_2 and the recovery of cells from oxidative stress.

3.4. Single cell measurements of E_{MSH} changes under H_2O_2 stress using confocal imaging

To verify the biosensor response under H_2O_2 stress in *C. glutamicum* at the single cell level, we quantified the 405/488 nm fluorescence excitation ratio in *C. glutamicum* cells expressing stably integrated Mrx1-roGFP2 using confocal laser scanning microscopy (CLSM) **(**Fig. 8**A)**. For control, we used fully reduced and oxidized *C. glutamicum* cells treated with DTT and diamide, respectively. In the confocal microscope, most cells exhibited similar fluorescence intensities at the 405 and 488 nm excitation maxima, respectively, indicating that the Mrx1-roGFP2 biosensor was equally expressed in 99% of cells. Fully reduced and untreated *C. glutamicum* control cells exhibited a bright fluorescence intensity at the 488 nm excitation maximum which was false-

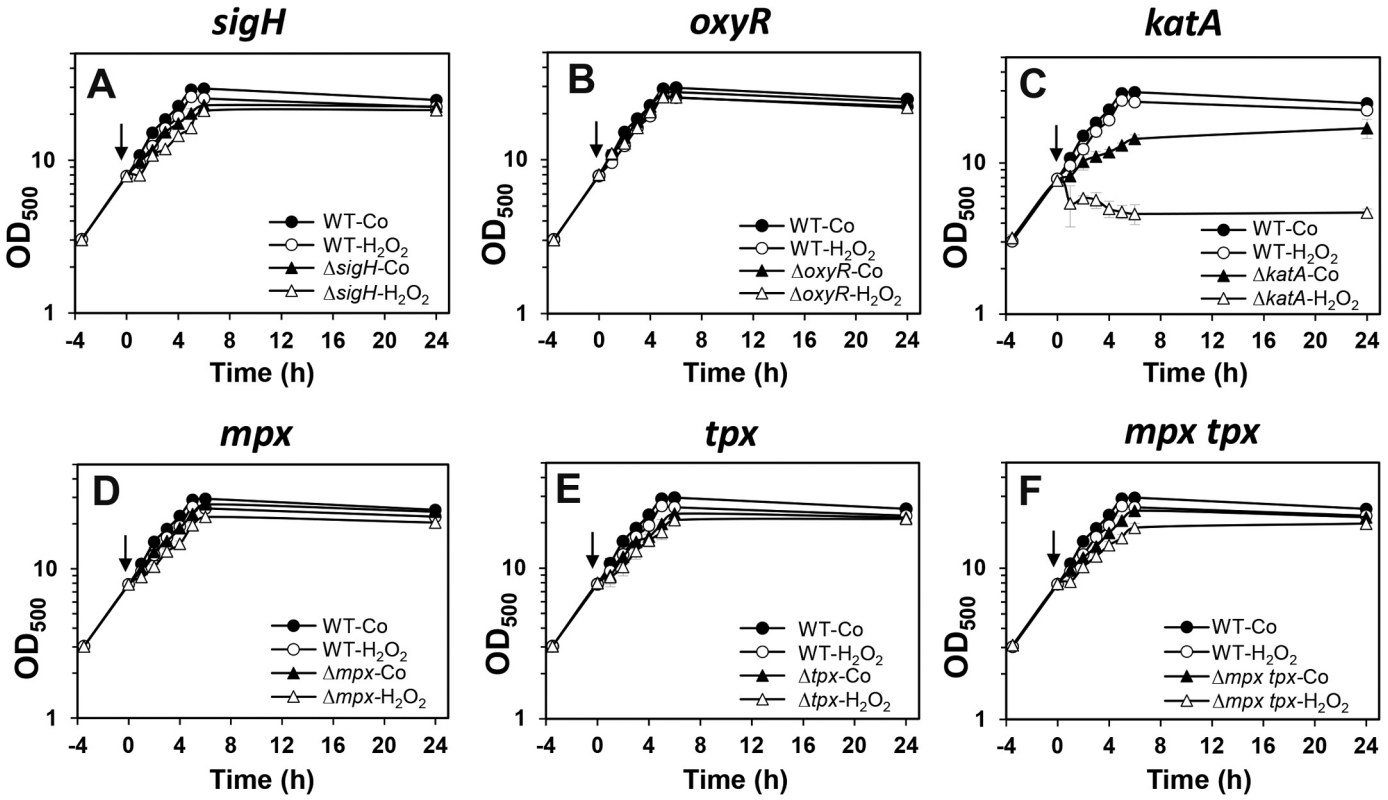

Fig. 7. H_2O_2 sensitivity of *C. glutamicum* mutants deficient for redox-regulators (OxyR, SigH) or antioxidant enzymes (KatA, Mpx, Tpx). The growth of various mutants with deletions of redox-sensitive regulators and antioxidant systems was compared after exposure to 80 mM H_2O_2, including Δ*sigH* **(A)**, Δ*oxyR* **(B)**, Δ*katA* **(C)**, Δ*mpx* **(D)**, Δ*tpx* **(E)**, Δ*mpx tpx* mutants **(F)**. Only the absence of KatA resulted in a strong H_2O_2 sensitive phenotype, while all other mutants were not affected by 80 mM H_2O_2 similar as the wild type. Mean values and SEM of three independent experiments are shown in all graphs. The time points of H_2O_2 exposure during the growth curves are set to '0' and denoted with arrows. The control (Co) shows the growth curve of the *C. glutamicum* wild type and mutant strains without H_2O_2 stress exposure.

colored in green, while the 405 nm excitation maximum was low and false-colored in red (Fig. 8**A**). In agreement with the microplate reader results, the basal E_{MSH} was highly reducing and calculated as −307 mV for the single cell population (Fig. 8**B,** Table S4). Treatment of cells with 80 mM H_2O_2 for 20 min resulted in a decreased fluorescence intensity at the 488 nm excitation maximum and a slightly increased signal at the 405 nm excitation maximum, causing an oxidative shift of E_{MSH}. Specifically, the E_{MSH} of control cells was increased to −263 mV after 20 min H_2O_2 treatment. The recovery phase could be also monitored at the single cell level after 40 and 60 min of H_2O_2 stress, as revealed by the regeneration of reduced E_{MSH} of −271 mV and −293 mV, respectively (Fig. 8**B,** Table S4). The oxidative E_{MSH} shift after H_2O_2 treatment and the recovery of reduced E_{MSH} were comparable between the microplate reader measurements and confocal imaging (Fig. 8**B**). This confirms the reliability of biosensor measurements at both single cell level and for a greater cell population using the microplate reader.

4. Discussion

Here, we have successfully designed the first genome-integrated Mrx1-roGFP2 biosensor that was applied in the industrial platform bacterium *C. glutamicum* which is of high biotechnological importance. During aerobic respiration and under industrial production processes, *C. glutamicum* is frequently exposed to ROS, such as H_2O_2. Thus, *C. glutamicum* is equipped with several antioxidant systems, including MSH and the enzymatic ROS-scavengers KatA, Mpx and Tpx. Moreover, Mpx and Tpx are dependent on the MSH cofactor required for recycling during recovery from oxidative stress [16,21,22]. The kinetics of H_2O_2 detoxification has been studied for catalases and peroxiredoxins in many different bacteria. However, the roles of many H_2O_2 detoxification enzymes are unknown and many seem to be redundant and not essential [49]. There is also a knowledge gap to which extent the H_2O_2 detoxification enzymes contribute to the reduced redox balance under aerobic growth conditions and under oxidative stress.

Thus, we applied this stably integrated Mrx1-roGFP2 biosensor to measure dynamic E_{MSH} changes to study the impact of antioxidant systems (MSH, KatA, Mpx, Tpx) and their major regulators (OxyR, SigH) under basal conditions and ROS exposure. The basal E_{MSH} was highly reducing with ~-296 mV during the exponential growth and stationary phase in *C. glutamicum* wild type, but maintained reduced also in the *katA*, *mpx* and *tpx* mutants. In contrast, the probe was strongly oxidized in *mshC* and *mtr* mutants indicating the major role of MSH for the overall redox homeostasis under aerobic growth conditions. While the enzymatic ROS scavengers KatA, Mpx and Tpx did not contribute to the reduced basal level of E_{MSH} during the growth, the catalase KatA was essential for efficient H_2O_2 detoxification and the recovery of the reduced E_{MSH} under H_2O_2 stress. In contrast, both MSH-dependent peroxiredoxins Tpx and Mpx did not play a significant role in the H_2O_2 defense and recovery from stress, which was evident in the *tpx mpx* double mutant. These results were supported by growth phenotype analyses, revealing the strongest H_2O_2-sensitive growth phenotype for the *katA* mutant, while the growth of the *mpx tpx* double mutant was only slightly affected under H_2O_2 stress. These biosensor and phenotype results clearly support the major role of the catalase KatA for H_2O_2 detoxification.

Since expression of *katA* is controlled by the OxyR repressor, we observed even a lower H_2O_2 response of the *oxyR* mutant, due to the constitutive derepression of *katA* as determined previously [34]. In contrast, the *sigH* mutant showed an enhanced basal E_{MSH} during

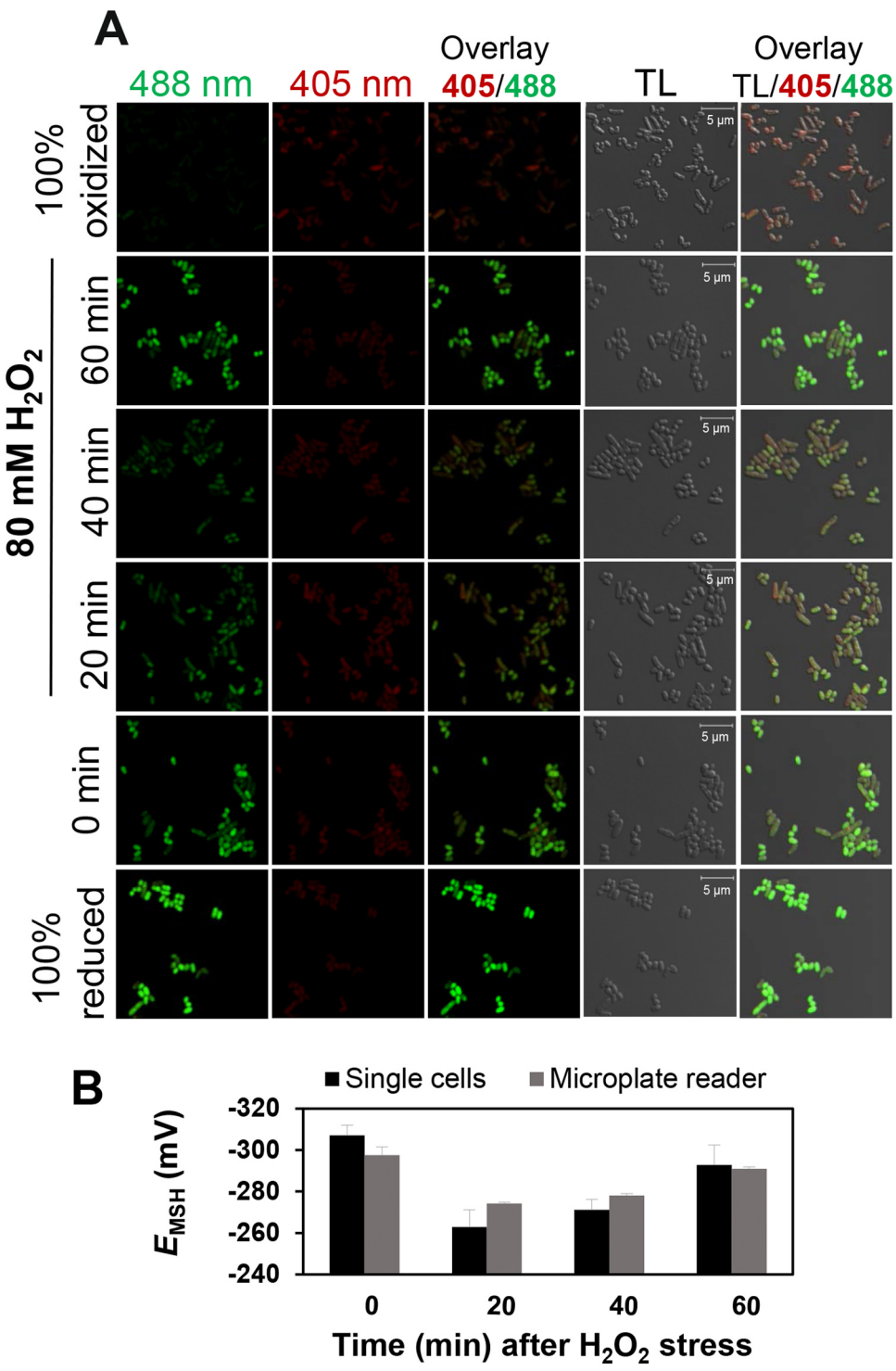

Fig. 8. Live-imaging of Mrx1-roGFP2 fluorescence changes in *C. glutamicum* wild type under H_2O_2 stress at the single cell level. **(A)** *C. glutamicum* wild type cells expressing Mrx1-roGFP2 were challenged with 80 mM H_2O_2 for 20–60 min, blocked with 10 mM NEM and visualized by confocal laser scanning microscopy (CLSM). The time point '0' indicates the untreated *C. glutamicum* wild type sample. Fully reduced and oxidized control samples were obtained after treatment of cells with 10 mM DTT and 10 mM diamide, respectively. Fluorescence intensities at the 405 and 488 nm excitation maxima are false-colored in red and green, respectively. Emission was measured between 491 and 580 nm. The oxidation degree is shown as overlay images of the transmitted light (TL)/405/488 channels. Images were analyzed by Zen software and Fiji/ImageJ at separate channels. **(B)** The intracellular E_{MSH} was calculated based on the 405/488 nm excitation ratio of *C. glutamicum* Mrx1-roGFP2 cells after H_2O_2 treatment using confocal imaging and microplate reader measurements. Mean values and SEM of three independent experiments are shown. Bars, 5 µm.

aerobic growth, since SigH controls enzymes for MSH biosynthesis and recycling (MshA, Mca, Mtr) which contribute to reduced E_{MSH} [29,32]. However, the *sigH* mutant was not impaired in its H_2O_2 response of Mrx1-roGFP2, since H_2O_2 detoxification is the role of KatA. Thus, we have identified unique roles of SigH and Mtr to control the basal E_{MSH} level, while OxyR and KatA play the major role in the recovery of reduced E_{MSH} under oxidative stress.

In previous work, the kinetics for H_2O_2 detoxification by catalases and peroxiredoxins was been measured using the unfused roGFP2 biosensor in the Gram-negative bacterium *Salmonella* Typhimurium [52]. The deletion of catalases affected the detoxification efficiency of H_2O_2 strongly, while mutations in peroxidases (*ahpCF*, *tsaA*) had only a minor effect on the H_2O_2 detoxifying power. These results are consistent with our data and previous results in *E. coli*, which showed that catalases are the main H_2O_2 scavenging enzymes at higher H_2O_2 concentrations, while peroxidases are more efficient at lower H_2O_2 doses [53]. The reason for the lower efficiency of H_2O_2 detoxification by peroxidases might be due to low NAD(P)H levels under oxidative stress that are not sufficient for recycling of oxidized peroxidases under high H_2O_2 levels [53]. Overall, these data are in agreement with our Mrx1-roGFP2 measurements in the *katA, tpx* and *mpx* mutants in *C. glutamicum*.

However, *C. glutamicum* differs from *E. coli* by its strong level of H_2O_2 resistance since *C. glutamicum* is able to grow with 100 mM H_2O_2 and the biosensor did not respond to 10 mM H_2O_2. In contrast, 1–5 mM H_2O_2 resulted in a maximal roGFP2 biosensor response with different detoxification kinetics in *E. coli* [52]. Since the high H_2O_2 resistance and detoxification power was attributed to the catalases, it will be interesting to analyze the differences between activities and structures of the catalases of *C. glutamicum* and *E. coli*. Of note, due to its remarkable high catalase activity, KatA of *C. glutamicum* is even commercially applied at Merck (CAS Number 9001-05-2). However, the structural features of KatA that are responsible for its high catalase activity are unknown.

While our biosensor results confirmed the strong H_2O_2 detoxification power of the catalase KatA [51], the roles of the peroxiredoxins Mpx and Tpx for H_2O_2 detoxification are less clear in *C. glutamicum*. Both Tpx and Mpx were previously identified as *S*-mycothiolated proteins in the proteome of NaOCl-exposed *C. glutamicum* cells [16]. *S*-mycothiolation inhibited Tpx and Mpx activities during H_2O_2 detoxification *in vitro*, which could be restored by the Trx and Mrx1 pathways [16,21,22]. Moreover, Tpx displayed a gradual response to increasing H_2O_2 levels and was active as Trx-dependent peroxiredoxin to detoxify low doses H_2O_2 while high levels H_2O_2 resulted in overoxidation of Tpx [51]. Overoxidation of Tpx caused oligomerization to activate the chaperone function of Tpx. Since *mpx* and *katA* are both induced under H_2O_2 stress, they were suggested to compensate for the inactivation of Tpx for detoxification of high doses of H_2O_2. Previous analyses showed that the *katA* and *mpx* mutants are more sensitive to 100–150 mM H_2O_2 [21,22]. In our analyses, the *mpx* mutant was not more sensitive to 80 mM H_2O_2 and displayed the same H_2O_2 response like the wild type, while the *katA* mutant showed a strong H_2O_2 sensitivity and responded strongly to H_2O_2 in the biosensor measurements. Thus, our biosensor and phenotype results clearly support the major role of KatA in detoxification of high doses H_2O_2 *in vivo*.

Finally, we confirmed using confocal imaging further that the genomically expressed Mrx1-roGFP2 biosensor shows equal fluorescence in the majority of cells indicating that the biosensor strain is suited for industrial application to quantify E_{MSH} changes in *C. glutamicum* at the single cell level or under production processes. Previous Mrx1-roGFP2 biosensor applications involved plasmid-based systems which can result in different fluorescence intensities within the cellular population due to different copy numbers. Moreover, plasmids can be lost under long term experiments when the selection pressure is decreased due to degradation or inactivation of the antibiotics.

We also compared the fluorescence intensities of the plasmid-based expression of Mrx1-roGFP2 using the IPTG-inducible pEKEx2 plasmid with the stably integrated Mrx1-roGFP2 strain in this work (Fig. S1). Using confocal imaging, the plasmid-based Mrx1-roGFP2 biosensor strain showed only roGFP2 fluorescence in < 20% of cells, while the genomically expressed biosensor was equally expressed and fluorescent in 99% of cells. The integration of the Mrx1-roGFP2 biosensor was performed into the *cg1121–1122* intergenic region and the biosensor was expressed from the strong P_{tuf} promoter using the pK18*mobsacB* construct designed previously for an Lrp-biosensor to measure L-valine production [54]. Previous live cell imaging using microfluidic chips revealed that only 1% of cells with the Lrp-biosensor were non-fluorescent due to cell lysis or dormancy [54]. Thus, expression of roGFP2 fusions from strong constitutive promoters should circumvent the problem of low roGFP2 fluorescence intensity after genomic integration. The advantage and utility of a stably integrated Grx1-roGFP2 biosensor has been also recently demonstrated in the malaria parasite *Plasmodium falciparum* which can circumvent low transfection frequency of plasmid-based roGFP2 fusions [55]. Moreover, quantifications using the microplate reader are more reliable, less time-consuming and reproducible with strains expressing genomic biosensors compared to measurements using confocal microscopy [55]. Thus, stably integrated redox biosensors should be the method of the choice for future applications of roGFP2 fusions to monitor redox changes in a greater cellular population.

In conclusion, in this study we designed a novel Mrx1-roGFP2 biosensor to monitor dynamic E_{MSH} changes in *C. glutamicum* during the growth, under oxidative stress and in mutants with defects in redox-signaling and H_2O_2 detoxification. This probe revealed the impact of Mtr and SigH to maintain highly reducing E_{MSH} throughout the growth and the main role of KatA and OxyR for efficient H_2O_2 detoxification and the regeneration of the redox balance. This probe is now available for application in engineered production strains to monitor the impact of industrial production of amino acids on the cellular redox state. In addition, the effect of genome-wide mutations on E_{MSH} changes can be followed in *C. glutamicum* in real-time during the growth, under oxidative stress and at the single cell level.

Acknowledgements

The authors wish to thank Julia Frunzke (Forschungszentrum Jülich, Germany) for providing the plasmid pK18*mobsacB-cg1121-cg1122*. This work was supported by an European Research Council (ERC) Consolidator grant (GA 615585) MYCOTHIOLOME and grants from the Deutsche Forschungsgemeinschaft, Germany (AN746/4-1 and AN746/4-2) within the SPP1710 on “Thiol-based Redox switches”, by the Research Training Group GRK1947 (project C01) and by the SFB973 (project C08) to H.A. This work is further supported by the DFG TR84 (project B06) to A.C.H. and H.A.

Author disclosure statement

No competing financial interests exist.

Appendix A. Supplementary material

Supplementary data associated with this article can be found in the online version at doi:10.1016/j.redox.2018.11.012.

References

[1] S.A. Heider, V.F. Wendisch, Engineering microbial cell factories: metabolic engineering of *Corynebacterium glutamicum* with a focus on non-natural products, Biotechnol. J. 10 (8) (2015) 1170–1184.
[2] V.F. Wendisch, J.M.P. Jorge, F. Perez-Garcia, E. Sgobba, Updates on industrial production of amino acids using *Corynebacterium glutamicum*, World J. Microbiol. Biotechnol. 32 (6) (2016) 105.
[3] J. Yang, S. Yang, Comparative analysis of *Corynebacterium glutamicum* genomes: a new perspective for the industrial production of amino acids, BMC Genom. 18 (Suppl. 1) (2017) S940.
[4] J. Becker, G. Giesselmann, S.L. Hoffmann, C. Wittmann, *Corynebacterium glutamicum* for sustainable bioproduction: from metabolic physiology to systems metabolic engineering, Adv. Biochem. Eng. Biotechnol. 162 (2018) 217–263.
[5] J. Frunzke, M. Bramkamp, J.E. Schweitzer, M. Bott, Population heterogeneity in *Corynebacterium glutamicum* ATCC 13032 caused by prophage CGP3, J. Bacteriol. 190 (14) (2008) 5111–5119.
[6] J.A. Imlay, Transcription factors that defend bacteria against reactive oxygen species, Annu. Rev. Microbiol. 69 (2015) 93–108.
[7] J.A. Imlay, Cellular defenses against superoxide and hydrogen peroxide, Annu. Rev. Biochem. 77 (2008) 755–776.
[8] J.A. Imlay, The molecular mechanisms and physiological consequences of oxidative stress: lessons from a model bacterium, Nat. Rev. Microbiol. 11 (7) (2013) 443–454.
[9] V.V. Loi, M. Rossius, H. Antelmann, Redox regulation by reversible protein *S*-thiolation in bacteria, Front. Microbiol. 6 (2015) 187.
[10] A.M. Reyes, B. Pedre, M.I. De Armas, M.A. Tossounian, R. Radi, J. Messens, M. Trujillo, Chemistry and redox biology of mycothiol, Antioxid. Redox Signal 28 (6) (2018) 487–504.
[11] G.L. Newton, N. Buchmeier, R.C. Fahey, Biosynthesis and functions of mycothiol, the unique protective thiol of Actinobacteria, Microbiol. Mol. Biol. Rev. 72 (3) (2008) 471–494.
[12] C. Sao Emani, M.J. Williams, I.J. Wiid, N.F. Hiten, A.J. Viljoen, R.D. Pietersen, P.D. van Helden, B. Baker, Ergothioneine is a secreted antioxidant in *Mycobacterium smegmatis*, Antimicrob. Agents Chemother. 57 (7) (2013) 3202–3207.
[13] P. Ta, N. Buchmeier, G.L. Newton, M. Rawat, R.C. Fahey, Organic hydroperoxide

resistance protein and ergothioneine compensate for loss of mycothiol in *Mycobacterium smegmatis* mutants, J. Bacteriol. 193 (8) (2011) 1981–1990.
[14] Q.N. Tung, N. Linzner, V.V. Loi, H. Antelmann, Application of genetically encoded redox biosensors to measure dynamic changes in the glutathione, bacillithiol and mycothiol redox potentials in pathogenic bacteria, Free Radic. Biol. Med. 128 (2018) 84–96.
[15] M. Hillion, J. Bernhardt, T. Busche, M. Rossius, S. Maass, D. Becher, M. Rawat, M. Wirtz, R. Hell, C. Rückert, J. Kalinowski, H. Antelmann, Monitoring global protein thiol-oxidation and protein *S*-mycothiolation in *Mycobacterium smegmatis* under hypochlorite stress, Sci. Rep. 7 (1) (2017) 1195.
[16] B.K. Chi, T. Busche, K. Van Laer, K. Bäsell, D. Becher, L. Clermont, G.M. Seibold, M. Persicke, J. Kalinowski, J. Messens, H. Antelmann, Protein *S*-mycothiolation functions as redox-switch and thiol protection mechanism in *Corynebacterium glutamicum* under hypochlorite stress, Antioxid. Redox Signal 20 (4) (2014) 589–605.
[17] V.K. Jothivasan, C.J. Hamilton, Mycothiol: synthesis, biosynthesis and biological functions of the major low molecular weight thiol in actinomycetes, Nat. Prod. Rep. 25 (6) (2008) 1091–1117.
[18] A. Kumar, W. Nartey, J. Shin, M.S.S. Manimekalai, G. Gruber, Structural and mechanistic insights into mycothiol disulphide reductase and the mycoredoxin-1-alkylhydroperoxide reductase E assembly of *Mycobacterium tuberculosis*, Biochim. Biophys. Acta 1861 (9) (2017) 2354–2366.
[19] M. Si, C. Zhao, B. Zhang, D. Wei, K. Chen, X. Yang, H. Xiao, X. Shen, Overexpression of mycothiol disulfide reductase enhances *Corynebacterium glutamicum* robustness by modulating cellular redox homeostasis and antioxidant proteins under oxidative stress, Sci. Rep. 6 (2016) 29491.
[20] M. Hillion, M. Imber, B. Pedre, J. Bernhardt, M. Saleh, V.V. Loi, S. Maass, D. Becher, L. Astolfi Rosado, L. Adrian, C. Weise, R. Hell, M. Wirtz, J. Messens, H. Antelmann, The glyceraldehyde-3-phosphate dehydrogenase GapDH of *Corynebacterium diphtheriae* is redox-controlled by protein *S*-mycothiolation under oxidative stress, Sci. Rep. 7 (1) (2017) 5020.
[21] B. Pedre, I. Van Molle, A.F. Villadangos, K. Wahni, D. Vertommen, L. Turell, H. Erdogan, L.M. Mateos, J. Messens, The *Corynebacterium glutamicum* mycothiol peroxidase is a reactive oxygen species-scavenging enzyme that shows promiscuity in thiol redox control, Mol. Microbiol. 96 (6) (2015) 1176–1191.
[22] M. Si, Y. Xu, T. Wang, M. Long, W. Ding, C. Chen, X. Guan, Y. Liu, Y. Wang, X. Shen, S.J. Liu, Functional characterization of a mycothiol peroxidase in *Corynebacterium glutamicum* that uses both mycoredoxin and thioredoxin reducing systems in the response to oxidative stress, Biochem. J. 469 (1) (2015) 45–57.
[23] M.A. Tossounian, B. Pedre, K. Wahni, H. Erdogan, D. Vertommen, I. Van Molle, J. Messens, *Corynebacterium diphtheriae* methionine sulfoxide reductase A exploits a unique mycothiol redox relay mechanism, J. Biol. Chem. 290 (18) (2015) 11365–11375.
[24] M. Hugo, K. Van Laer, A.M. Reyes, D. Vertommen, J. Messens, R. Radi, M. Trujillo, Mycothiol/mycoredoxin 1-dependent reduction of the peroxiredoxin AhpE from *Mycobacterium tuberculosis*, J. Biol. Chem. 289 (8) (2014) 5228–5239.
[25] M. Si, Y. Feng, K. Chen, Y. Kang, C. Chen, Y. Wang, X. Shen, Functional comparison of methionine sulphoxide reductase A and B in *Corynebacterium glutamicum*, J. Gen. Appl. Microbiol. 63 (5) (2017) 280–286.
[26] M. Si, L. Zhang, M.T. Chaudhry, W. Ding, Y. Xu, C. Chen, A. Akbar, X. Shen, S.J. Liu, *Corynebacterium glutamicum* methionine sulfoxide reductase A uses both mycoredoxin and thioredoxin for regeneration and oxidative stress resistance, Appl. Environ. Microbiol. 81 (8) (2015) 2781–2796.
[27] K. Van Laer, L. Buts, N. Foloppe, D. Vertommen, K. Van Belle, K. Wahni, G. Roos, L. Nilsson, L.M. Mateos, M. Rawat, N.A. van Nuland, J. Messens, Mycoredoxin-1 is one of the missing links in the oxidative stress defence mechanism of Mycobacteria, Mol. Microbiol. 86 (4) (2012) 787–804.
[28] T.H. Kim, H.J. Kim, J.S. Park, Y. Kim, P. Kim, H.S. Lee, Functional analysis of sigH expression in *Corynebacterium glutamicum*, Biochem. Biophys. Res. Commun. 331 (4) (2005) 1542–1547.
[29] S. Ehira, H. Teramoto, M. Inui, H. Yukawa, Regulation of *Corynebacterium glutamicum* heat shock response by the extracytoplasmic-function sigma factor SigH and transcriptional regulators HspR and HrcA, J. Bacteriol. 191 (9) (2009) 2964–2972.
[30] M. Hillion, H. Antelmann, Thiol-based redox switches in prokaryotes, Biol. Chem. 396 (5) (2015) 415–444.
[31] J.B. Bae, J.H. Park, M.Y. Hahn, M.S. Kim, J.H. Roe, Redox-dependent changes in RsrA, an anti-sigma factor in *Streptomyces coelicolor*: zinc release and disulfide bond formation, J. Mol. Biol. 335 (2) (2004) 425–435.
[32] T. Busche, R. Silar, M. Picmanova, M. Patek, J. Kalinowski, Transcriptional regulation of the operon encoding stress-responsive ECF sigma factor SigH and its anti-sigma factor RshA, and control of its regulatory network in *Corynebacterium glutamicum*, BMC Genom. 13 (1) (2012) 445.
[33] J.G. Kang, M.S. Paget, Y.J. Seok, M.Y. Hahn, J.B. Bae, J.S. Hahn, C. Kleanthous, M.J. Büttner, J.H. Roe, RsrA, an anti-sigma factor regulated by redox change, EMBO J. 18 (15) (1999) 4292–4298.
[34] J. Milse, K. Petri, C. Rückert, J. Kalinowski, Transcriptional response of *Corynebacterium glutamicum* ATCC 13032 to hydrogen peroxide stress and characterization of the OxyR regulon, J. Biotechnol. 190 (2014) 40–54.
[35] S.V. Sharma, K. Van Laer, J. Messens, C.J. Hamilton, Thiol redox and pKa properties of mycothiol, the predominant low-molecular-weight thiol cofactor in the Actinomycetes, Chembiochem 17 (18) (2016) 1689–1692.
[36] A. Bhaskar, M. Chawla, M. Mehta, P. Parikh, P. Chandra, D. Bhave, D. Kumar, K.S. Carroll, A. Singh, Reengineering redox sensitive GFP to measure mycothiol redox potential of *Mycobacterium tuberculosis* during infection, PLoS Pathog. 10 (1) (2014) e1003902.
[37] A.J. Meyer, T.P. Dick, Fluorescent protein-based redox probes, Antioxid. Redox Signal 13 (5) (2010) 621–650.
[38] M. Mehta, R.S. Rajmani, A. Singh, *Mycobacterium tuberculosis* WhiB3 responds to vacuolar pH-induced changes in mycothiol redox potential to modulate phagosomal maturation and virulence, J. Biol. Chem. 291 (6) (2016) 2888–2903.
[39] S. Mishra, P. Shukla, A. Bhaskar, K. Anand, P. Baloni, R.K. Jha, A. Mohan, R.S. Rajmani, V. Nagaraja, N. Chandra, A. Singh, Efficacy of beta-lactam/beta-lactamase inhibitor combination is linked to WhiB4-mediated changes in redox physiology of *Mycobacterium tuberculosis*, Elife 6 (2017) e25624.
[40] J. Padiadpu, P. Baloni, K. Anand, M. Munshi, C. Thakur, A. Mohan, A. Singh, N. Chandra, Identifying and tackling emergent vulnerability in drug-resistant mycobacteria, ACS Infect. Dis. 2 (9) (2016) 592–607.
[41] P. Tyagi, A.T. Dharmaraja, A. Bhaskar, H. Chakrapani, A. Singh, *Mycobacterium tuberculosis* has diminished capacity to counteract redox stress induced by elevated levels of endogenous superoxide, Free Radic. Biol. Med. 84 (2015) 344–354.
[42] V.V. Loi, M. Harms, M. Müller, N.T.T. Huyen, C.J. Hamilton, F. Hochgräfe, J. Pane-Farre, H. Antelmann, Real-time imaging of the bacillithiol redox potential in the human pathogen *Staphylococcus aureus* using a genetically encoded bacilliredoxin-fused redox biosensor, Antioxid. Redox Signal 26 (15) (2017) 835–848.
[43] A.M. Nanda, A. Heyer, C. Kramer, A. Grünberger, D. Kohlheyer, J. Frunzke, Analysis of SOS-induced spontaneous prophage induction in *Corynebacterium glutamicum* at the single-cell level, J. Bacteriol. 196 (1) (2014) 180–188.
[44] B. Morgan, M.C. Sobotta, T.P. Dick,, Measuring, E(GSH) and H2O2 with roGFP2-based redox probes, Free Radic. Biol. Med. 51 (11) (2011) 1943–1951.
[45] C.T. Dooley, T.M. Dore, G.T. Hanson, W.C. Jackson, S.J. Remington, R.Y. Tsien, Imaging dynamic redox changes in mammalian cells with green fluorescent protein indicators, J. Biol. Chem. 279 (21) (2004) 22284–22293.
[46] M. Schwarzländer, M.D. Fricker, C. Müller, L. Marty, T. Brach, J. Novak, L.J. Sweetlove, R. Hell, A.J. Meyer, Confocal imaging of glutathione redox potential in living plant cells, J. Microsc. 231 (2) (2008) 299–316.
[47] A. Müller, J.F. Schneider, A. Degrossoli, N. Lupilova, T.P. Dick, L.I. Leichert, Systematic *in vitro* assessment of responses of roGFP2-based probes to physiologically relevant oxidant species, Free Radic. Biol. Med. 106 (2017) 329–338.
[48] Y.B. Liu, M.X. Long, Y.J. Yin, M.R. Si, L. Zhang, Z.Q. Lu, Y. Wang, X.H. Shen, Physiological roles of mycothiol in detoxification and tolerance to multiple poisonous chemicals in *Corynebacterium glutamicum*, Arch. Microbiol. 195 (6) (2013) 419–429.
[49] S. Mishra, J. Imlay, Why do bacteria use so many enzymes to scavenge hydrogen peroxide? Arch. Biochem. Biophys. 525 (2) (2012) 145–160.
[50] H. Teramoto, M. Inui, H. Yukawa, OxyR acts as a transcriptional repressor of hydrogen peroxide-inducible antioxidant genes in *Corynebacterium glutamicum* R, FEBS J. 280 (14) (2013) 3298–3312.
[51] M. Si, T. Wang, J. Pan, J. Lin, C. Chen, Y. Wei, Z. Lu, G. Wei, X. Shen, Graded response of the multifunctional 2-Cysteine peroxiredoxin, CgPrx, to increasing levels of hydrogen peroxide in *Corynebacterium glutamicum*, Antioxid. Redox Signal 26 (1) (2017) 1–14.
[52] J. van der Heijden, S.L. Vogt, L.A. Reynolds, J. Pena-Diaz, A. Tupin, L. Aussel, B.B. Finlay, Exploring the redox balance inside gram-negative bacteria with redox-sensitive GFP, Free Radic. Biol. Med. 91 (2016) 34–44.
[53] L.C. Seaver, J.A. Imlay, Alkyl hydroperoxide reductase is the primary scavenger of endogenous hydrogen peroxide in, *Escherichia coli*, J. Bacteriol. 183 (24) (2001) 7173–7181.
[54] N. Mustafi, A. Grunberger, R. Mahr, S. Helfrich, K. Noh, B. Blombach, D. Kohlheyer, J. Frunzke, Application of a genetically encoded biosensor for live cell imaging of L-valine production in pyruvate dehydrogenase complex-deficient *Corynebacterium glutamicum* strains, PLoS One 9 (1) (2014) e85731.
[55] A.K. Schuh, M. Rahbari, K. Heimsch, F. Mohring, S. Gabryszewski, S. Weder, K. Buchholz, S. Rahlfs, D.A. Fidock, K. Becker, Stable integration and comparison of hGrx1-roGFP2 and sfroGFP2 redox probes in the malaria parasite *Plasmodium falciparum*, ACS Infect. Dis. 4 (11) (2018) 1602–1612.

Chapter 6

The redox-sensing MarR-type repressor HypS controls hypochlorite and antimicrobial resistance in *Mycobacterium smegmatis*

Quach Ngoc Tung[1], Tobias Busche[2], Vu Van Loi[1], Jörn Kalinowski[2] and Haike Antelmann[1#]

[1]Freie Universität Berlin, Institute for Biology-Microbiology, D-14195 Berlin, Germany
[2]Center for Biotechnology, Bielefeld University, D-33594 Bielefeld, Germany

Submitted to: Free Radical Biology and Medicine in Nov. 2019

[#]**Corresponding author:** haike.antelmann@fu-berlin.de

Personal contribution:

My contribution included the genetic construction of the *hypS* mutant and complemented strains, the gel shift assays, cloning and purification of HypS (Fig. 4). Furthermore, I was involved in the circular dichroism spectroscopy, structural modelling, qRT PCR results and phenotype assays of mutant strains (Fig. 5, 6, 7). I drafted all figures and wrote the manuscript together with Haike Antelmann.

The redox-sensing MarR-type repressor HypS controls hypochlorite and antimicrobial resistance in *Mycobacterium smegmatis*

Quach Ngoc Tung[1], Tobias Busche[2], Vu Van Loi[1], Jörn Kalinowski[2] and Haike Antelmann[1]*

Departments & Institutions:

[1]*Institute for Biology-Microbiology, Freie Universität Berlin, D-14195 Berlin, Germany*

[2]*Center for Biotechnology (CeBiTec), Universitätsstraße 25, 33615 Bielefeld, Germany*

Running title: Control of HOCl resistance by HypS in *M. smegmatis*

***Corresponding author:**

Haike Antelmann, Institute for Biology-Microbiology, Freie Universität Berlin,

Königin-Luise-Strasse 12-16, D-14195 Berlin, Germany,

Tel: +49-(0)30-838-51221, Fax: +49-(0)30-838-451221

E-mail: haike.antelmann@fu-berlin.de

Key words: MarR-type regulator/ hypochlorite/ redox-sensing/ *Mycobacterium smegmatis*

ABSTRACT

MarR family transcription factors often control antioxidant enzymes, multidrug efflux pumps or virulence factors in bacterial pathogens and confer resistance towards oxidative stress and antibiotics. In this study, we have characterized the function and redox-regulatory mechanism of the MarR-type regulator HypS in *Mycobacterium smegmatis*. RNA-seq transcriptomics and qRT-PCR analyses of the *hypS* mutant revealed that *hypS* is autoregulated and represses transcription of the co-transcribed *hypO* gene which encodes a multidrug efflux pump. DNA binding activity of HypS to the 8-5-8 bp inverted repeat sequence upstream of the *hypSO* operon was inhibited under NaOCl stress. However, the HypSC58S mutant protein was not impaired in DNA-binding under NaOCl stress *in vitro*, indicating an important role of Cys58 in redox sensing of NaOCl stress. HypS was shown to be inactivated by Cys58-Cys58' intersubunit disulfide formation under HOCl stress, resulting in derepression of *hypO* transcription. Phenotype results revealed that the HypS regulon confers resistance towards HOCl, rifampicin and erythromycin stress. In conclusion, HypS was identified as a novel redox-sensitive repressor that contributes to mycobacterial resistance towards HOCl stress and antibiotics.

INTRODUCTION

Mycobacterium tuberculosis (Mtb), the etiologic agent of live-threatening tuberculosis disease (TB), remains a major health problem with 1.5 million human deaths in 2019 [1]. Due to its intracellular replication and slow-growing lifestyle, treatment of *Mtb* infections are difficult and lengthy which often require drug combination therapies. Extensive use of antibiotics results in multiple, extensively and totally drug resistant isolates (MDR, XDR, TDR) as well as latent or persistent *Mtb* infections, which are ineffective to antibiotic treatment [2-5]. There is an urgent need to discover new drugs or antibiotics targets and to understand the underlying resistance mechanisms to combat the emerging problem of drug resistance in TB infections.

The MarR family of multiple antibiotics resistance regulators, as discovered originally for the MarR repressor of *E. coli* [6, 7], plays an important role to control drug resistance mechanisms in many human pathogens [8]. MarR family proteins are widespread in bacteria and archaea and control a variety of cellular functions, including adaptation to environmental changes, oxidative stress, virulence, metabolism and resistance to phenolic compounds, solvents, disinfections and antibiotics [9, 10]. In *Mtb*, eight MarR-family homologs have been annotated, including Rv0042c, Rv0880, Rv2011c, Rv1049, Rv2327, Rv0737, Rv2887 and Rv1404 [8]. The MarR-type repressor Rv1404 has been shown to regulate acid stress resistance and virulence [11]. Rv0678 controls the resistance-nodulation-cell division (RND) transporters MmpS5-MmpL5 (mycobacterial membrane protein small and large) which are involved in lipid and fatty acid export during cell wall biosynthesis [12]. Rv0880 is involved in the resistance to the antibiotic bedaquiline [13] and Rv2887 was shown to control the SAM-dependent methyltransferase Rv0560c, which confers resistance to the new anti-mycobacterial imidoazopyridine-based drugs MP-III-71 and pyridobenzimidazole 14 [14, 15]. Recently, the structural mechanism of ligand-mediated inhibition of DNA binding activity of Rv2887 was shown in the presence salicylate (SA) and para-aminosalicylic acid (PAS) as anti-mycobacterial drug analogue [16]. This provides the basis to design new anti-TB drugs which target MarR-type proteins to combat life-threatening TB-infections.

Structural studies have revealed that MarR-family proteins are homodimers with winged helix-turn-helix (wHTH) motifs in each subunit that bind with their recognition α-helices to palindromic sequences in adjacent major groves of the DNA [9, 10]. The majority of MarR proteins are transcriptional repressors that negatively control transcription of divergently located genes. The DNA binding activity is often inhibited by small molecules, such as phenolic compounds (e.g. salicylate, benzoate, quinones) or metals, which act as ligands and bind a shared ligand-binding pocket between the wHTH motifs and dimerization domains leading to structural rearrangements of the DNA recognition helices [9, 10].

Apart from ligand-binding, some MarR-type regulators have conserved Cys residues, act as redox switches and respond to reactive oxygen, chlorine or electrophile species (ROS, RCS, RES) by thiol-oxidation or *S*-alkylation [17, 18]. Structurally well characterized redox-sensitive MarR-type regulators are the MarR/OhrR- and MarR/DUF24-family regulators of *Bacillus subtilis*, *Xanthomonas campestris* and *Staphylococcus aureus*, which respond to ROS, HOCl and RES via thiol-based mechanisms and control oxidative stress defense mechanisms, quinone detoxification enzymes, virulence and antibiotics resistance [17-23]. In *Mtb,* the redox-sensing MarR/OhrR-type repressor MosR represses transcription of the adjacent *rv1050* gene encoding an uncharacterized oxidoreductase which is involved in the defense against oxidative stress [9, 24]. Interestingly, the MexR repressor of *Pseudomonas aeruginosa* controls multidrug efflux pumps which are required for the defense against H_2O_2 stress and antibiotics [25, 26]. Antibiotic-induced ROS production was implicated in the thiol-oxidation sensing mechanism of MexR, which renders *P. aeruginosa* resistant to multiple clinical important antibiotics, such as quinolones, β-lactams, tetracycline, chloramphenicol and novobiocin [25, 26]. Thus, redox-sensing MarR-type repressors of pathogens often control oxidative stress defense mechanisms and antibiotics resistance to allow adaptation to the host environment. The discovery of new redox-sensing MarR-type regulators that regulate ROS and antimicrobial resistance in *Mtb* opens up new avenues in anti-TB drug research to combat *Mtb* infections.

We used *Mycobacterium smegmatis* as model to identify a new redox-sensing MarR-type repressor MSMEG_4471, which has a close homolog in *Mtb* (Rv2327) and confers resistance to the strong oxidant HOCl and antibiotics. MSMEG_4471 was previously identified using the redox proteomics approach (OxICAT) as highly oxidized (42%) at its single Cys58 residue under HOCl stress and hence was renamed as HypS [27]. In this work, we have characterized the function and redox-sensing mechanism of HypS under HOCl stress in *M. smegmatis*. Transcriptional studies revealed that HypS negatively controls its own expression and that of the co-transcribed *MSMEG_4472* (*hypO*) gene that codes for a multidrug efflux pump of the major facilitator superfamily (MFS). Our results showed that Cys58 of HypS is important for redox-sensing of HOCl stress. The thiol-based sensing mechanism involves HypS oxidation to intermolecular disulfides under HOCl stress leading to repressor inactivation. Phenotype analyses further revealed that the HypS-regulated efflux pump HypO confers HOCl and antimicrobial resistance. Thus, HypS is important to ensure mycobacterial survival under ROS and antibiotics stress and could be a valuable future drug target to design new anti-TB drugs.

MATERIALS AND METHODS

Bacterial strains, growth and survival assays. Bacterial strains, plasmids and primers are listed in **Tables S1 and S2**. For cloning and genetic manipulation, *E. coli* was cultivated at 37°C in Luria Bertani (LB) medium. *M. smegmatis* mc^2155 wild type and *hypS* mutant strains were grown as overnight culture in LB supplemented with 0.05% Tween80 at 37°C under vigorous agitation. The overnight culture was transferred to Hartmans-de Bont minimal medium as described [28] and adjusted to an optical density at 500 nm (OD_{500}) of 0.02-0.04. *M. smegmatis* was cultivated until an OD_{500} of 0.4 and treated with oxidants and antibiotics, including 100 µM NaOCl, 14 µM erythromycin, 12 µM rifampicin to monitor growth and survival phenotypes [27, 29]. For survival assays, 10 µl of serial dilutions were spotted onto LB agar plates with 0.05% Tween80 for 72 hours. Antibiotics were used for selection as follows:

ampicillin (100 µg/ml), kanamycin (50 µg/ml), hygromycin (200 µg/ml), zeocin (25 µg/ml) for *E. coli,* and hygromycin (50 µg/ml), zeocin (10 µg/ml) for *M. smegmatis*.

Cloning, expression and purification of His_6-tagged HypS and HypSC58S mutant proteins in *E. coli.* *MSMEG_4471* (renamed *hypS*) was amplified from chromosomal DNA of *M. smegmatis* mc^2155 by PCR using primers MSMEG_4471_fw and MSEMG_4471_rev **(Table S2)**. The PCR product was digested with *Nhe*I and *Sac*I and ligated into expression vector pET28aTEV that was cut by the same enzymes to generate plasmid pET28aTEV-*hypS*. The resulting plasmid was confirmed by PCR and DNA sequencing.

For construction of the expression plasmid encoding the HypSC58S protein, primers MSMEG_4471_fw_Csy_Ser and MSMEG_4471_rev_Csy_Ser were used to amplify plasmid pET28aTEV-*hypS* **(Table S2)**. The PCR product was digested with *Dpn*I, which cleaves methylated DNA to remove the parental plasmid, and transformed into *E. coli* DH5α competent cells [30]. Plasmid pET28aTEV-*hypSC58S* was verified by PCR and DNA sequencing.

The *E. coli* BL21 (DE3) p*lysS* expression strains with plasmids pET28aTEV-*hypS* or pET28aTEV-*hypSC58S* were grown in 1 l LB to an OD_{600} of 0.6 at 37°C, followed by induction with 1 mM IPTG (isopropyl-β-D-thiogalactopyranoside) for 4 hours at 37°C. Recombinant His_6-tagged HypS and HypSC58S proteins were purified using His Trap™ HP Ni-NTA columns (5 ml; GE Healthcare, Chalfont St Giles, UK) and the ÄKTA purifier liquid chromatography system (GE Healthcare) according to the instructions of the manufacturer (USB). The proteins were extensively dialyzed against 10 mM Tris-HCl (pH 8.0), 100 mM NaCl and 30% glycerol and stored at -80°C. Purity of the proteins was analyzed after sodium dodecyl sulfate polyacrylamide gel electrophoresis (SDS-PAGE) and Coomassie brilliant-blue staining.

Construction of the *hypS* deletion mutant, *hypS* and *hypSC58S* complemented strains. The *hypS* deletion mutant was constructed using a specialized mycobacterial recombination system based on phage Che9c-encoded proteins [31]. 500 bp up- and downstream regions of *hypS* were amplified from the genome of *M. smegmatis* mc^2155 wild type using primers listed

in **Table S2**. The up- and downstream PCR products were ligated as left and right flanking regions, respectively, together with the hygromycin cassette of plasmid pJSC284. The construct was digested with *Xba*I and *Xho*I to obtain the linear allelic exchange substrate that was electroporated into *M. smegmatis* mc^{2}155-pJV53 [32]. Hygromycin-resistant colonies were isolated and streaked out several times to select for the loss of pJV53. The *hypS* deletion mutant was confirmed by PCR.

The complemented *hypS* and *hypSC58S* strains were constructed using the pSGV53 plasmid as described previously [32]. The *hypS* gene was amplified from the genome of *M. smegmatis* mc^{2}155 using primers Pmpt64**-**hypS-NdeI-F and pSGV53-hypS-Bam-R. The *hypSC58S* allele was generated using in two first-round PCRs using primers Pmpt64**-**hypS-NdeI-F, pSGV53-hypSC58R and pSGV53-hypSC58F, pSGV53-hypS-Bam-R. The two PCR products were hybridized and subsequently fused together in the second-round PCR using primers Pmpt64**-**hypS-NdeI-F and pSGV53-hypS-Bam-R **(Table S2)**. The *hypS* and *hypSC58S* constructs were digested with *Nde*I and *Bam*HI and inserted into plasmid pSGV53 digested with the same enzymes to generate plasmids pSGV53-*hypS* and pSGV53-*hypSC58S*. The plasmids were electroporated into the *hypS* mutant to construct the *hypS* and *hypSC58S* complemented strains.

RNA-seq transcriptome analysis and bioinformatics. *M. smegmatis* mc^{2}155 wild type and *hypS* mutant strains were grown to an OD_{500} of 0.4 in 3 biological replicates and harvested before (control) and 30 min after exposure to 500 µM NaOCl stress. Cells were disrupted in lysis buffer containing 3 mM EDTA and 200 mM NaCl with a Precellys Evolution ribolyzer (Bertin technologies). RNA isolation was performed using the acid phenol extraction protocol as described [33]. The RNA quality was checked by Trinean Xpose (Gentbrugge, Belgium) and the Agilent RNA Nano 6000 kit using an Agilent 2100 Bioanalyzer (Agilent Technologies, Boblingen, Germany). Library preparation, next generation cDNA sequencing and read assembly were carried out as described previously [34]. Differential gene expression analysis of 3 biological replicates was performed using DESeq2 [35] with ReadXplorer v2.2 [33] as

described [34] using an adjusted p-value cut-off of P ≤ 0.01 and a signal intensity ratio (M-value) cut-off of ≥ 1.0 or ≤ -1.0. The RNA-seq raw data are available in the Array Express database https://www.ebi.ac.uk/arrayexpress/ under the accession number E-MTAB-8534.

Electrophoretic mobility shift assay (EMSA). The 262 bp DNA promoter fragment covering the region from -177 to +85 relative to the transcriptional start site (TSS) was amplified using PCR with primers prom_4471_up and prom_4471_down **(Table S2)**. For the DNA-binding assays with the shorter DNA fragment, a 40 bp *hypS* promoter fragment was amplified using primers HypS_4471_hypS_fwd and HypS_4471_hypS_rev according to the previously published protocol [36]. As negative control, the 154 bp upstream region of *MSMEG_5346* encoding a c-di-AMP receptor regulator (DarR), was amplified using primers DarR-competitive-F, DarR-competitive-R **(Table S2)** [37]. To identify the inverted repeat as specific DNA binding sequence, T and G at the right half of the repeat were each replaced by G and T using PCR mutagenesis. Briefly, two PCRs were performed using primers HypS-4471-8-5-8-F, HypS-M-R and HypS-M-F, HypS-4471-8-5-8-R and subsequently fused together to generate the mutated 150 bp promoter probe (IR-M). For DNA binding reactions, 0.75 ng of the promoter fragments were incubated with DTT-reduced or NaOCl-oxidized HypS or HypSC58S proteins for 30 min at room temperature in EMSA binding buffer [34]. EMSAs were performed using 4% native PAGE as described [34].

Quantitative real-time PCR (qRT-PCR) analysis. RNA was isolated from 2 biological and 2 technical replicates from the *M. smegmatis* mc^2155 wild type and the *hypS* mutant under control conditions and 30 min after exposure to 500 µM NaOCl as described [27, 34]. The relative abundance of mRNA levels of *hypS* and *hypO* were analyzed using qRT-PCR analysis as described previously [38].

Circular dichroism (**CD) spectroscopy.** CD spectra of reduced and NaOCl-oxidized HypS were obtained using a Jasco J-810 spectropolarimeter with a HAAKE WKL recirculating chiller

(D-76227, Karlsruhe). The reduced and oxidized proteins were measured at 10 µM in 20 mM potassium phosphate buffer (pH 7.5). The quartz cuvettes (2 mm path length, Suprasil Hellma) were set at a constant temperature of 25°C with a Jasco PTC-423S Peltier-type thermocouple [34]. Secondary structure elements were calculated using the program DichroWeb (http://dichroweb.cryst.bbk.ac.uk).

RESULTS

The MarR-type repressor MSMEG_4471 (HypS) was identified as NaOCl-sensitive thiol switch in the redox protome of *Mycobacterium smegmatis*. We have previously used the redox proteomics approach OxICAT to quantify the redox state of 1098 Cys residues in *M. smegmatis* [27]. In total, 381 Cys residues (33.6%) showed >10% increased oxidations under NaOCl stress, including 40 *S*-mycothiolated proteins. Among those NaOCl-sensitive proteins were redox-sensitive transcriptional regulators, including the RseA and RshA anti-sigma factors and the Zur and NrdR repressors. These redox regulators were inactivated by oxidation as revealed by the increased transcription of the SigH, SigE, Zur and NrdR regulons in the RNA-seq transcriptome. The uncharacterized MarR-type regulator MSMEG_4471 (HypS) was among the most strongly oxidized proteins under NaOCl stress with 12% basal oxidation and 54% oxidation under NaOCl stress at its single Cys58 [27] **(Fig. 1)**.

Based on the genome location, *hypS* is co-transcribed with its downstream target gene, *MSMEG_4472* (renamed *hypO*), encoding a multidrug efflux pump of the major facilitator superfamily (MFS) of secondary PMF-dependent transporters [39-41]. In addition, the MSMEG_4469-70 (*cbiOQ*) operon is divergently transcribed upstream of the *hypSO* operon. The *cbiOQ* operon is predicted to encode a cobalt ABC transport system. Both *hypSO* and *cbiOQ* operon are highly conserved and co-occur in the genomes of other mycobacteria **(Fig. S1A)**. In addition, HypS shares the conserved Cys58 and an overall sequence identity of 68.5% with orthologs of *M. tuberculosis* H37Rv (Rv2327), *M. bovis* AF2122/97 (Mb2354) and *M. marinum* (MMAR_3627) **(Fig. S1B)**. Based on the increased oxidation of HypS at Cys58

under NaOCl stress, we were interested to study the role and redox-sensing mechanism of HypS under NaOCl stress and antibiotics in more detail in *M. smegmatis*.

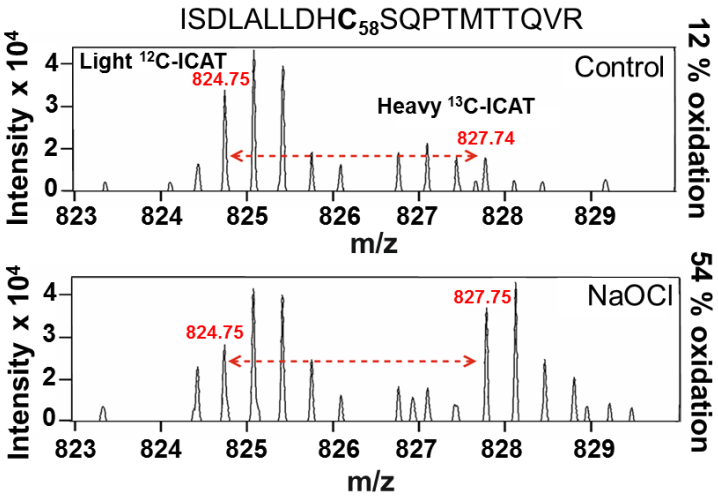

Figure 1. HypS is strongly oxidized at its redox-sensing Cys58 under NaOCl stress. Previous OxICAT analysis indicated a 42% oxidation increase at the Cys58 peptide under NaOCl stress [27]. For OxICAT, cytoplasmic proteins were harvested before (control) and 30 min after NaOCl stress and reduced Cys residues labelled by light ^{12}C-ICAT [27]. All disulfides were reduced by Tris (2-carboxyethyl) phosphine (TCEP) and labelled by heavy ^{13}C-ICAT reagent. The oxidation state of Cys58 was determined as 12 % and 54 % under control and NaOCl stress conditions, respectively.

RNA-seq transcriptomics identifies HypS as repressor of the *hypSO* operon. To study the function of HypS in *M. smegmatis*, a *hypS* deletion mutant was constructed using the mycobacterial recombination system based on phage Che9c-encoded proteins to replace *hypS* by the hygromycin resistance cassette [31]. RNA was isolated from the wild type (WT) and the *hypS* mutant under control and NaOCl stress and subjected to RNA-seq transcriptome analysis to quantify the changes in gene expression using DeSeq2 [35]. For significant expression changes, the log2 fold change (M-value) cut off of ±1.00 was chosen (95% confidence, $p \leq 0.01$) representing a minimal change of 2-fold. In total, 347 genes were significant differentially transcribed based on the M-value threshold of 2-fold in the *hypS* mutant as compared to the wild type under control conditions **(Fig. 2, Table S3-S5)**. These included 223 up-regulated and 124 down-regulated genes in the *hypS* deletion mutant. Among the most strongly up-regulated transcripts in the *hypS* mutant was the *hypS* co-transcribed *hypO gene,* encoding the multi drug efflux pump (log2 fold change of 5.1). This indicates that HypS represses transcription of *hypO* under non-stress conditions. Apart from *hypO*, some

remaining reads mapped also to the truncated *hypS* transcript of 71 nucleotides as shown in the ReadExplorer view **(Fig. 2)** explaining the 2-fold induction in the *hypS* mutant. The expression of *hypS* and *hypO* is also induced under NaOCl stress in the transcriptome of the wild type (log2 fold changes of 1.9). The RNA-seq results were verified by qRT-PCR showing 4.0-fold and 2.8-fold upregulation of *hypS* and *hypO* in the wild type under NaOCl stress and 20-fold constitutive derepression of *hypO* in the *hypS* mutant control **(Fig. 3AB)**. Together our data support that HypS acts as repressor of the *hypSO* operon under control conditions and is inactivated under NaOCl stress, leading to derepression of transcription of the *hypSO* operon.

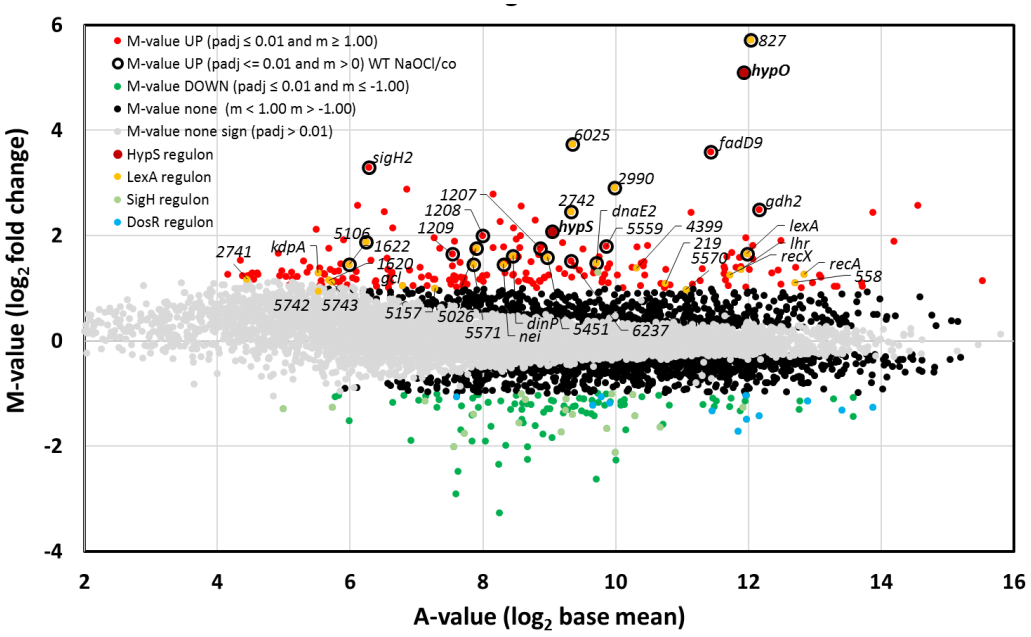

Figure 2. RNA-Seq transcriptomics of the *M. smegmatis hypS* mutant versus the wild type under control conditions. For RNA-seq transcriptome profiling, *M. smegmatis* wild type and the *hypS* mutant were grown in 3 biological replicates and harvested during the exponential growth at an OD_{500} of 0.4. The gene expression profile of the *hypS* mutant compared to wild type is shown as ratio/intensity scatter plot (M/A-plot) which is based on the differential gene expression analysis using DeSeq2 [35]. Colored dots indicate significantly induced (red) or repressed (green) transcripts (M-value ≥ 1.00 or ≤ -1.00; adjusted P-value ≤ 0.01). Dots surrounded with black thick lines represent transcripts significantly induced in the wild type under NaOCl stress. Black symbols are genes transcribed below the M-value cut off of 1.00 > M > -1.00 (P ≤ 0.01). Grey symbols denote transcripts with no fold-changes in the *hypS* mutant (P > 0.01). LexA regulon genes (yellow) are up-regulated in the *hypS* mutant. Genes of the SigH regulon (light green) and DosR regulon (light blue) are down-regulated in the *hypS* mutant. The corresponding RNA-Seq expression data are presented in **Tables S3-S4**.

In addition, the majority of 27 LexA regulon genes were highly up-regulated in the *hypS* mutant control. Among these, MSMEG_0827 encodes for a major facility superfamily transporter and was most strongly induced (log2 fold change of 5.7) in the *hypS* mutant

(Tables S3-S5, Fig. 2). Using the MEME suite, we identified the *M. tuberculosis* LexA binding site (published in the collecTF database) in the promoter region of 22 LexA regulon genes that are upregulated in *hypS* mutant [42, 43] **(Table S8)**. The LexA regulon indicates an SOS and DNA damage response controlling DNA repair enzymes, such as endonucleases, DNA repair polymerases and helicases. Interestingly, the LexA regulon was also strongly induced under NaOCl stress in the wild type transcriptome **(Table S4)** (log2 fold changes up to 6.4). Whether the induction of the SOS response in the *hypS* mutant is a direct or indirect regulatory effect of *hypS* deletion remains to be elucidated. In addition, other genes for transcriptional regulators are up-regulated in the *hypS* mutant, such as sigma factors SigH2 (MSMEG_0573), MSMEG_1970 and MSMEG_0219) as well as regulators of the AraC family (MSMEG_5563), SmoR (MSMEG_5575), LuxR family (MSMEG_0331, MSMEG_5651, MSMEG_0330), DeoR family (MSMEG_3606 and MSMEG_3264) and LacI family (MSMEG_3599) **(Table S3-S4)**.

In the *hypS* mutant, 124 genes are significantly down-regulated (M-value ≥ 1.00 or ≤ -1.00; adjusted P-value ≤ 0.01), which include 23 genes regulated by the disulphide stress specific ECF sigma factors SigH and SigE (**Tables S3,S4,S6**). The SigH and SigE regulons are most strongly up-regulated by 500 µM NaOCl in the wild type with log2 fold changes between 4-7 as described previously [27] (**Table S5-S6**). Among those SigH/SigE regulons genes, several genes for hypothetical proteins (MSMEG_3004, MSMEG_5558, MSMEG_4141, MSMEG_0757, MSMEG_6498) are 2-3-fold up-regulated in the *hypS* mutant. Four genes encoding oxidoreductases/dehydrogenases (MSMEG_1114, MSMEG_6859, MSMEG_3137, MSMEG_6753) display log2 fold changes of 4.6-6.3 in the wild type under NaOCl stress and are 2-3 fold induced in the *hypS* mutant, which could be involved in the oxidative stress response. The down-regulation of the SigH regulon in the *hypS* mutant could be caused by the increased resistance towards NaOCl stress due to up-regulation of the HypO efflux pump.

Apart from the SigH regulon, 14 genes of the DosR dormancy regulon, also known as DevR regulon, are 2-3-fold down-regulated in the *hypS* mutant **(Table S7)**. All down-regulated DosR regulon genes in the *hypS* mutant are strongly induced in the wild type under NaOCl

stress, such as *devR2* (MSMEG_5244), genes encoding universal stress proteins (MSMEG_5245, MSMEG_3945 and MSMEG_3950) and hypothetical proteins (MSMEG_3935, MSMEG_3942, MSMEG_3943 and MSMEG_3949). The down-regulation of many stress-related genes may be related again to the higher oxidative stress resistance of the *hypS* mutant.

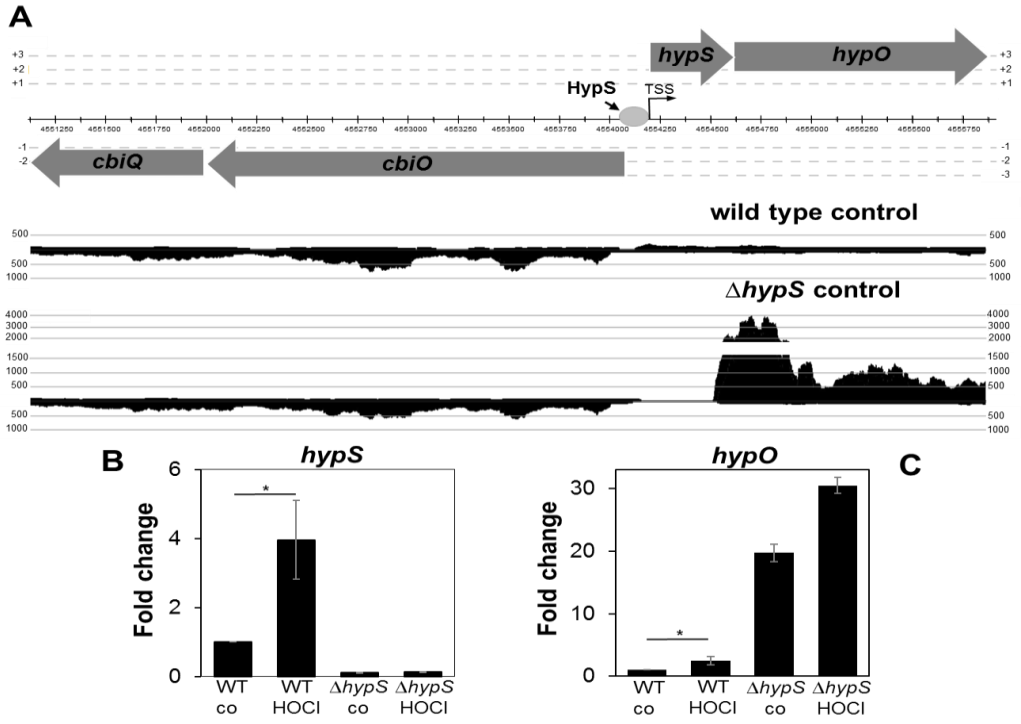

Figure 3. Deletion of *hypS* results in derepression of the *hypSO* operon. (A) The transcriptional landscape of the *hypSO* operon in *M. smegmatis* wild type and the *hypS* mutant is displayed with Read-Explorer [33], which confirmed the derepression of the efflux pump-encoding *hypO* in the *hypS* mutant. The mapped reads of the gene expression profile of the *hypSO* operon and the divergently transcribed *cbiOQ* operon were shown for three merged biological replicates. **(B, C)** Transcription of *hypS* **(B)** and *hypO* **(C)** was analyzed using qRT-PCR in the *M. smegmatis* wild type and the *hypS* mutant before (control) and 30 min after exposure to 500 µM NaOCl stress**.** The transcript levels were normalized to the mRNA level of the wild type under control conditions which were set to 1. Error bars represent the standard deviation of mean (SEM) of 2-3 biological replicates and the statistics was calculated using a Student's unpaired two-tailed t-test by the GraphPad Prism software (p = 0.0412 for *hypS*-fold change; p = 0.0487 for *hypO*-fold change). Symbols: $^{ns}p > 0.05$; *p ≤ 0.05

HypS recognizes a palindromic motif and specifically binds to its promoter *in vitro.* The RNA-seq and qRT-PCR results revealed that HypS functions as redox-sensing repressor and negatively regulates expression of the *hypSO* operon. The single Cys58 of HypS should be the redox-sensing Cys that is oxidized under NaOCl stress, leading to the dissociation of HypS

from its promoter region and derepression of *hypSO* operon transcription. As MarR-type repressor, the HypS dimer should bind directly to an inverted repeat overlapping with the *hypSO* promoter region.

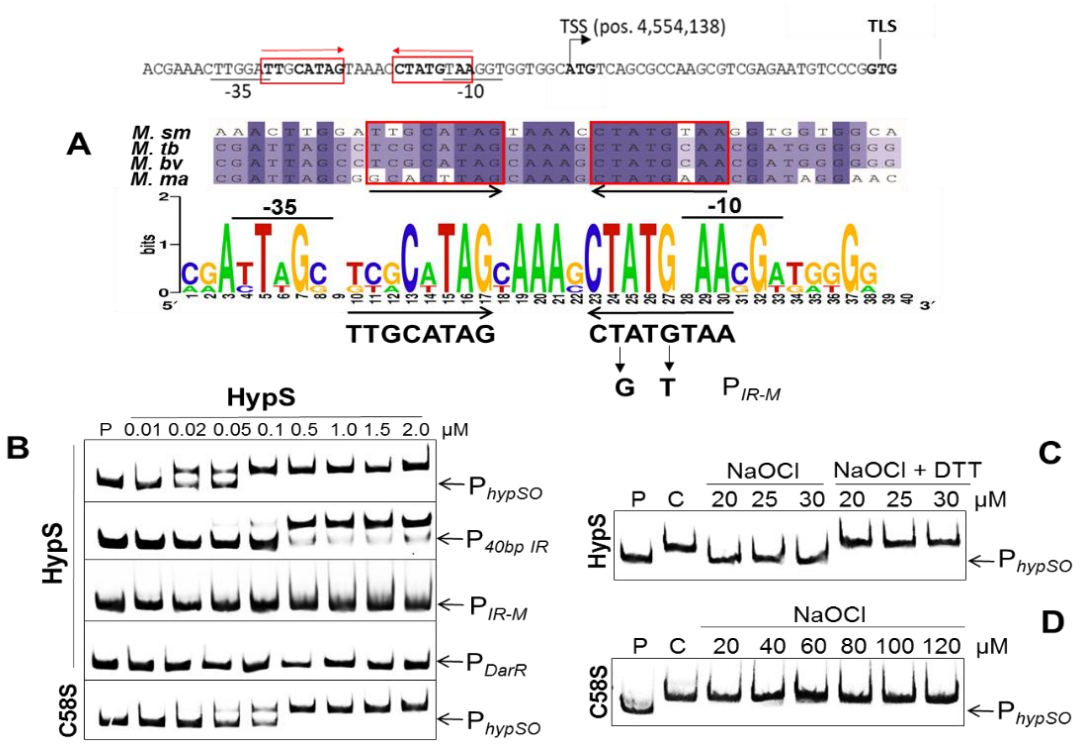

Figure 4. DNA binding activity of HypS to an upstream inverted repeat is inhibited under NaOCl stress *in vitro*. (A) Mapping of the 5' end (TSS) and the SigA-dependent promoter upstream of the *hypSO* operon was performed using 5' RNA-seq. An 8-5-8 bp inverted repeat was identified as HypS operator overlapping with the -10 and -35 promoter regions upstream of the *hypSO* operon. The upstream promoter regions of the *hypSO* homologues of different mycobacteria share the conserved operator as aligned using ClustalW2. The consensus sequence of the inverted repeat was generated by WebLogo. **(B)** EMSAs were conducted with increasing amounts of HypS and HypSC58S proteins to analyse the specific DNA binding activity of HypS to its upstream promoter region *in vitro*. The DNA probes include a 262 bp promoter fragment (-177 to +85), a 40 bp HypS operator fragment, the unspecific *darR* promoter probe and a 150 bp HypS operator probe with two base substitutions. **(C)** The DNA binding activity of HypS could be inhibited with NaOCl and restored with 10 mM DTT. **(D)** However, DNA binding activity of HypSC58S mutant protein was not abolished under NaOCl stress, indicating that Cys58 is required redox-sensing of NaOCl. ''P'' indicates the free probe, ''C'' is the HypS-DNA complex.

Based on 5' RNA-seq data, we used the MEME software to identify the putative promoter sequence and a conserved inverted repeat in the upstream region of the *hypSO* operon **(Fig. 4A)**. The transcriptional start site (TSS) of *hypS* was mapped at position 4,554,138 which is preceded by typical SigA dependent promoter TTGGAT-N_{17}-TAAGGT matching the SigA promoter consensus TTGACA-N_{18}-TANNNT [44]. The 8-5-8 bp inverted

repeat sequence TTGCATAG-N_4-CTATGTAA with one mismatch was detected in the *hypSO* upstream region as possible HypS binding site that overlapped with the -35 and -10 promoter regions **(Fig. 4A)**. We searched for the conservation of the putative HypS operator sequence upstream of homologous *hypSO* operons in the genomes of other mycobacteria. Multiple sequence alignment revealed a high conservation of the 8-5-8 bp inverted repeat sequence in the *hypSO* upstream promoter regions across various mycobacteria **(Fig. 4A)**.

Next, we used electrophoretic mobility shift assays (EMSA) to examine the binding of HypS to the 262 bp *hypSO* upstream promoter region ranging from −177 to +85 relative to the TSS *in vitro*. The DNA binding assays revealed that HypS binds with high affinity at a Kd of 0.07 µM to the *hypSO* promoter region **(Fig. 4B)**. To verify that HypS binds specifically to the predicted 8-5-8 bp operator sequence, EMSAs were performed using a shorter 40 bp DNA probe that just covered the -10 and -35 promoter region including the IR. HypS was able to bind with slightly decreased affinity to the short 40 bp IR probe. However, HypS was unable to bind to the DNA probe with mutated IR sequences (IR-M) in which the bases T and G of the right half of the repeats were exchanged by G and T **(Fig. 4B)**. In addition, no band-shift was observed in the HypS DNA binding reaction with the non-specific *darA* promoter DNA containing a 14 bp DarR binding motif (ATACT-N_5-AGTAT) [37]. These results indicate that HypS binds specifically to the 8-5-8 bp operator sequence in the *hypSO* upstream promoter region.

Since Cys58 of HypS was identified as NaOCl-sensitive using OxICAT, we analyzed the effect of the C58S mutation on DNA-binding and redox-sensing of HypS. HypSC58S protein showed ~2.2-fold decreased DNA binding affinity compared to HypS under reducing conditions, indicating that Cys58 is not essential for DNA binding activity of HypS **(Fig. 4B)**. However, treatment of HypS with 20-30 µM NaOCl resulted in loss of DNA binding activity and dissociation of HypS from the operator DNA **(Fig. 4C)**. The DNA binding activity of NaOCl-treated HypS could be restored with DTT, indicating that HypS is inactivated by reversible thiol-oxidation under NaOCl stress. Additionally, DNA binding of the HypSC58S mutant protein to promoter probe was not inhibited after NaOCl exposure **(Fig. 4D)**. These results support that

HypS senses HOCl stress via the redox-sensing Cys58 by a reversible thiol-switch mechanism leading to HypS inactivation and dissociation from the *hypSO* promoter DNA.

HypS senses NaOCl stress by intersubunit disulfide formation. To investigate the redox-sensing mechanism of HypS under NaOCl stress, we used non-reducing SDS-PAGE to study whether HypS forms intermolecular disulfides upon NaOCl oxidation. Treatment of HypS with 20-30 µM NaOCl resulted in the formation of HypS disulfide linked dimers at the size of 35 kDa, which could be reversed with DTT **(Fig. 5A)**. Since Cys58 is the only Cys residue present in the HypS protein sequence, NaOCl leads to inactivation of HypS by formation of Cys58-Cys58' intersubunit disulfides, crosslinking both subunit of the HypS dimer. As control, no disulfide linked dimer formation was observed for the HypSC58S mutant protein under NaOCl stress in the non-reducing SDS-PAGE **(Fig. 5B)**. These results suggest that Cys58 is positioned in close vicinity in both subunits in the structure of the HypS dimer, allowing intersubunit disulfide formation upon oxidation.

To confirm this notion, the structure of HypS was modelled based on available crystal structures of related MarR-type regulators that are present in the PDB database. HypS shares 29% sequence identity to the MarR-type regulator Rv0880 of *M. tuberculosis*, which served as template to model the HypS structure with SWISS-MODEL (https://swissmodel.expasy.org) **(Fig. 5D)**. In the structural model of the HypS dimer, each subunit consists of six α-helices and two β-sheets, arranged in the order α1-α2-α3-α4-β1-β2-α5-α6, similar as in other MarR-type regulators **(Fig. 5D, Fig. S2)**. While the α1, α5 and α6 helices are involved in dimerization, the α2, α3, α4 helices and the β1, β2 sheets form the DNA binding wHTH motif [9, 10]. In the predicted HypS structure, Cys58 is located in the loop that connects the α3 and α4 helices in each monomer **(Fig. 5D)**. Thus, both Cys58 and Cys58' residues of adjacent subunits could be positioned in close vicinity, which might enable intersubunit disulfide formation without major conformation changes.

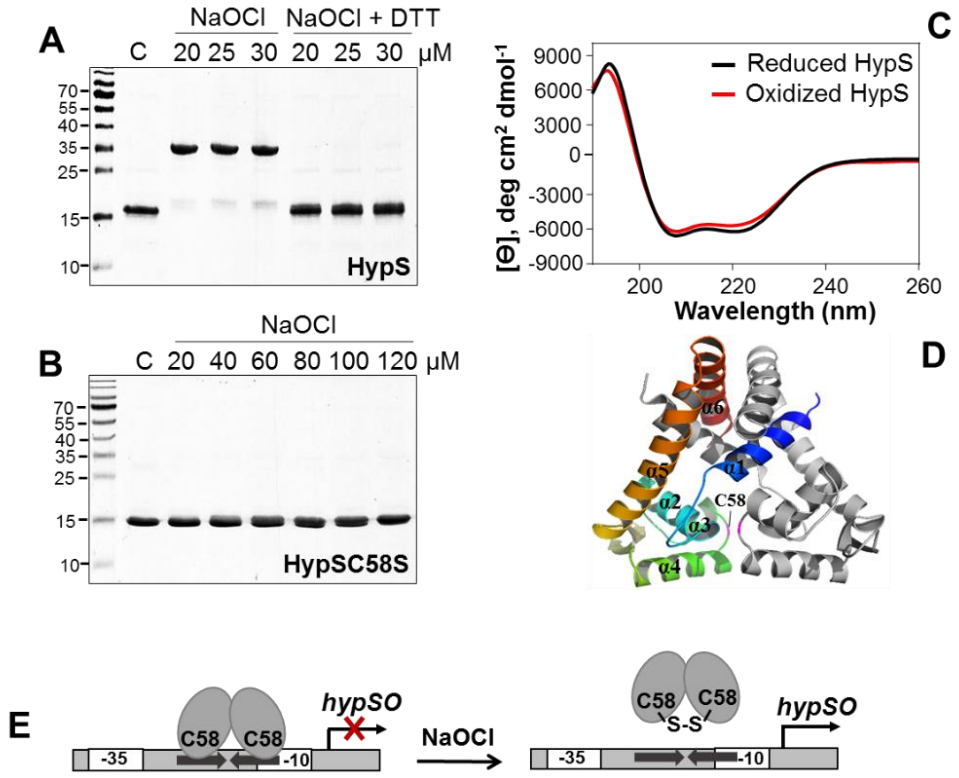

Figure 5. HypS is oxidized to intersubunit disulfides under NaOCl stress. (A, B) Non-reducing SDS-PAGE of HypS and HypSC58S mutant proteins revealed that HypS is oxidized by NaOCl to disulphide-linked HypS dimers migrating at the size of 35 kDa, which are reversible with DTT **(A)**. HypSC58S protein is not sensitive to oxidation **(B)**. **(C)** The CD spectra of reduced and oxidized HypS proteins show a similar strong α-helical content and no major structural changes upon oxidation. **(D)** The structural model of HypS was generated using SWISS-MODEL (https://swissmodel.expasy.org/) and visualized with PyMol using the template of *M. tuberculosis* H37Rv Rv0880 (PDB code: 4YIF) [45]. Cys58 is located in the flexible loop between the α3 and α4 helices. **(E)** Model for redox-regulation of HypS in *M. smegmatis* in response to NaOCl stress. HypS senses NaOCl stress by Cys58-Cys58' intersubunit disulfide formation, leading to dissociation of HypS from its promoter and derepression of *hypO* transcription, which confers resistance to NaOCl and antibiotics.

To further investigate whether HypS undergoes structural changes in the secondary structural elements upon oxidation, we used CD spectroscopy in the far-UV range. Both reduced and oxidized HypS showed very similar far UV-CD spectra, containing a significant high α helical content **(Fig. 5C)**. This reflects the six α helices of the dimer interface and HTH motif, which are common in structures of MarR-type regulators [9, 10]. The lack of structural changes in the secondary structural elements upon HypS oxidation as revealed in the CD spectra confirms our predictions that Cys58 and Cys58' are likely positioned in close neighborhood and undergo disulfide bond formation without major conformational changes. In

conclusion, our results revealed that HypS is a redox-sensing repressor that senses NaOCl stress by intersubunit disulfide formation between Cys58 and Cys58' of both subunits of the HypS dimer, leading to inactivation of HypS and derepression of the *hypSO* operon **(Fig. 5E)**.

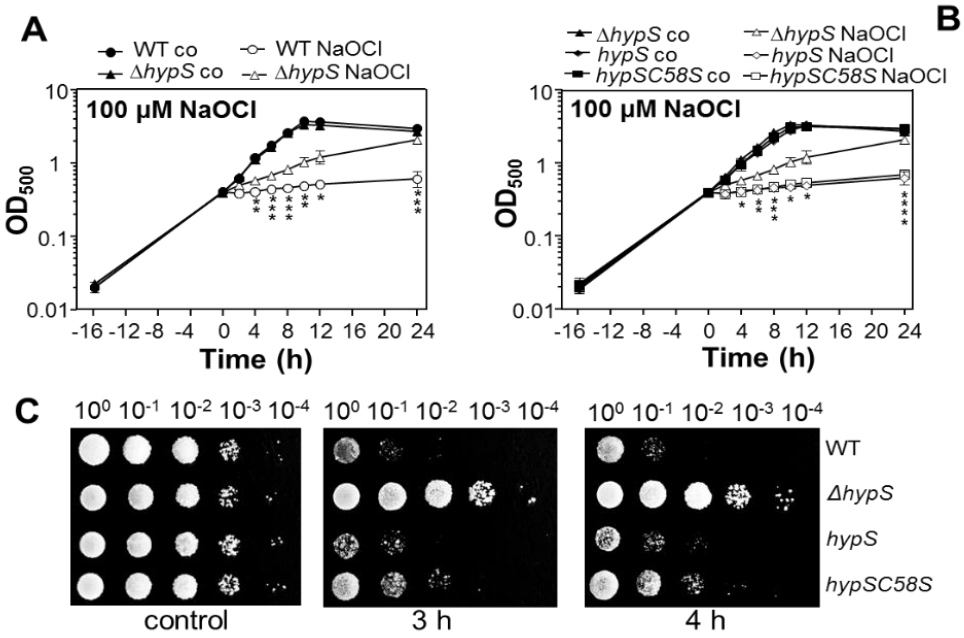

Figure 6. HypS confers resistance to NaOCl stress in *M. smegmatis.* Growth phenotypes **(A, B)** and survival assays **(C)** of the wild type (WT), *hypS* mutant, *hypS* and *hypSC58S* complemented strains before (control) and after exposure to sub-lethal concentration of 100 µM NaOCl at an OD_{500} of 0.4. The time point before NaOCl exposure was set to '0'. For the survival assay, 10 µl of serial dilutions were spotted after 3 and 4 h of NaOCl exposure onto LB agar plates with 0.05% Tween80. The NaOCl-resistant phenotype of the *hypS* mutant is reversed to wild type level by using plasmid-encoded *hypS*, but not in the *hypSC58S* complemented strain. The results are from 3 biological replicates. Error bars indicate the standard deviation (SD) and the statistics was calculated using a Student's unpaired two-tailed t-test by the GraphPad Prism software. Symbols are: $^{ns}p > 0.05$; *p < 0.05, **p ≤ 0.01, ***p ≤ 0.001, and ****p < 0.0001.

The HypS-controlled efflux pump HypO confers resistance to NaOCl and antibiotics. The redox-sensing MarR-type repressor HypS was shown to control the efflux pump HypO which could be involved in the oxidative stress defense and antibiotic resistance. Thus, we analyzed the phenotypes of the *hypS* mutant in comparison to the *hypS* and *hypSC58S* complemented strains under NaOCl stress and antibiotics treatments **(Fig. 6 and 7)**. The growth under control condition was similar for all strains, indicating that the *hypS* mutation did not affect the growth and fitness of *M. smegmatis*. However, the *hypS* mutant was more resistant to NaOCl stress and showed an improved growth with 100 µM NaOCl in comparison

to the NaOCl-sensitive wild type (**Fig. 6A)**. Complementation of the *hypS* mutant with plasmid-encoded *hypS* restored the NaOCl-sensitivity to wild type level **(Fig. 6B)**. Similarly, in survival assays the *hypS* mutant showed a strongly enhanced resistance under NaOCl stress relative to the wild type and to the *hypS* complemented strain (**Fig. 6C)**. However, the *hypSC58S* mutant was unable to complement the NaOCl resistant survival phenotype of the *hypS* mutant (**Fig. 6C)**. These results demonstrate that the HypS-controlled efflux pump functions as important mycobacterial defense mechanism under NaOCl stress. In addition, the conserved Cys58 was shown to be essential for redox-regulation of HypS under NaOCl stress to control HypO expression.

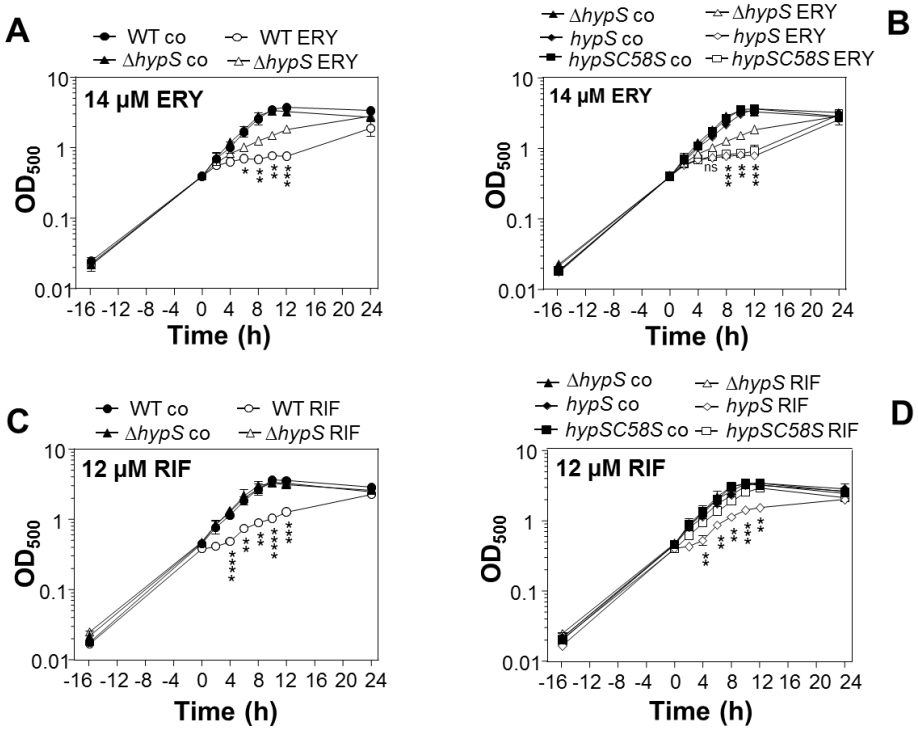

Fig. 7. The *hypS* mutant showed an increased resistance to the antibiotics rifampicin and erythromycin. Growth phenotype analyses of the wild type, *hypS* mutant*, hypS* and *hypSC58S* complemented strains were performed after exposure to sub-lethal concentrations of 14 µM erythromycin **(A, B),** 12 µM rifampicin **(C, D)** at an OD_{500} of 0.4. The time points of antibiotics treatment were set to '0'. Mean values and SD of three independent experiments are shown and *p*-values were calculated by the Student's unpaired two-tailed t-test by the graph prism software ($^{ns}p > 0.05$; *p < 0.05; **p < 0.01; ***p < 0.001; and ****p < 0.0001).

Multidrug efflux pumps are well-known antimicrobial resistance mechanisms. Thus, we used growth assays after rifampicin and erythromycin exposure to analyse if the HypS-controlled HypO transporter confers antimicrobial resistance in *M. smegmatis*. The *hypS*

mutant displayed an increased tolerance after treatment with sub-lethal doses of 12 µM rifampicin and 14 µM erythromycin in comparison to the sensitive wild type **(Fig. 7AC)**. The growth sensitivity of the wild type after rifampicin and erythromycin treatment could be restored in the *hypS* complemented strain **(Fig. 7BD)**. However, the *hypSC58S* mutant was unable to complement the rifampicin resistance of the *hypS* mutant to the sensitive wild type level **(Fig. 7BD)**. These results confirm that HypO functions as multidrug efflux pump and contributes to rifampicin and erythromycin resistance in *M. smegmatis*. The redox-sensing Cys58 functions might sense and respond to ROS which are perhaps generated under antibiotics treatment to up-regulate the HypO efflux pump expression. Taken together, our phenotype results clearly support the important role of the HypSO regulon in the mycobacterial oxidative stress defense and under antibiotics treatment.

DISCUSSION

In this work, we have characterized the function and regulatory mechanism of the novel redox-sensing MarR-type repressor HypS of *M. smegmatis*, which is conserved across mycobacteria including *Mtb* (Rv2327). HypS senses HOCl stress via its conserved Cys58 and regulates expression of the multidrug efflux pump HypO under HOCl stress. Based on the high conservation of the *hypSO* locus and of the regulatory promoter regions, the regulatory model and function of HypS should be similar also in *Mtb*. HypS was previously identified in the global redox proteomics approach OxICAT as highly oxidized exhibiting 42% increased oxidation at its single Cys58 under NaOCl stress [27]. DNA binding assays showed that HypS oxidation under NaOCl stress leads to its inactivation and dissociation of HypS from its promoter DNA. Mutation of Cys58 did not affect the DNA binding activity of HypS, but redox sensing of NaOCl was completely abolished. The role of Cys58 in redox-sensing was further confirmed in growth and survival assays under NaOCl stress, since the *hypSC58S* mutant was unable to restore the NaOCl susceptibility back to wild type level.

Using non-reducing SDS-PAGE, we could show that HypS is reversibly oxidized under NaOCl stress to form intersubunit disulfides between Cys58-Cys58’ in opposing subunits *in vitro*. Structural modelling revealed that Cys58 is located in close proximity to Cys58’ in the

adjacent subunit of the HypS dimer to allow for disulfide formation. HypS oxidation causes its dissociation from the *hypSO* operator *in vitro*, indicating that the DNA binding activity is inhibited in oxidized HypS protein probably due to structural changes in the wHTH motif. However, CD measurements did not reveal major structural changes upon HypS oxidation, suggesting local changes in the wHTH motifs which might lead to loss of DNA binding. Future crystal structure analyses will reveal the conformational changes of HypS upon oxidation.

Inhibition of the repressor activity of HypS due to thiol-oxidation causes derepression of the *hypO*-encoded multidrug efflux pump, which conferred resistance under NaOCl stress and antibiotic exposure, such as rifampicin and erythromycin. Many MarR family transcription factors with wHTH motifs, including the originally discovered MarR protein of *E. coli,* are known to sense ROS, RES and antibiotics due to thiol-oxidation of redox-sensing Cys residues [9, 10]. However, the regulatory mechanisms vary and have been classified in one- and two-Cys-type models based on the conserved MarR-family OhrR-repressor mechanistically and structurally characterized in *B. subtilis* and *Xanthomonas campestri* [9, 10, 17, 18, 23, 46-48]. The *B. subtilis* $OhrR_{Bs}$ is the prototype of a one-Cys-type repressor, which senses organic hydroperoxides (OHP) and NaOCl by thiol-oxidation to Cys-sulfenic acid that reacts further with the low molecular weight thiol bacillithiol to *S*-bacillithiolated OhrR protein [46, 49, 50]. *S*-bacillithiolation leads to inactivation of OhrR and transcriptional derepression of the *ohrA* peroxiredoxin gene.

In contrast, the two-Cys type OhrR protein of *X. campestris* was shown to sense OHP via intersubunit disulfide formation between the N-terminal redox-sensing Cys22 and C-terminal Cys127’ of opposing subunits of the OhrR dimer [23, 47, 48]. This two-Cys-type oxidation model was confirmed for other two-Cys-type MarR/DUF24-family regulators (HypR, YodB) of *B. subtilis* which are inactivated by intersubunit disulfide formation between N- and C-terminal Cys residues of adjacent subunits [17, 18]. However, the model for thiol-oxidation of the *M. smegmatis* HypS protein is different and revealed that MarR protein still can undergo intersubunit disulfide formation when the single Cys residues of both subunits are located in close proximities in the dimeric structure. This regulatory model of Cys17-Cys17’ intersubunit

disulfide formation was further revealed for the single Cys-type MarR/DU24-family regulator QorR which senses quinones and controls a quinone reductase in *Corynebacterium glutamicum* [17, 18, 51].

Apart from HypS, the MarR/OhrR-family repressor MosR of *Mtb* was previously characterized as redox-sensing repressor that senses and responds to H_2O_2 and OHP via Cys10-Cys12 intrasubunit disulfide formation in each subunit of the MosR dimer [24]. MosR negatively regulates expression of *rv1050* encoding an uncharacterized exported oxidoreductase which contributes to survival inside macrophages [24]. The *E. coli* MarR repressor was shown to be inactivated by many different ligands and antimicrobial compounds, such as salicylate, tetracycline, chloramphicol, norfloxacin, ampicillin, aromatic acid metabolites and lipophilic compounds (plumbagin, p-hydroxyenzoate, plumbagin, menadione) [7-10, 52]. In addition, *E. coli* MarR was recently shown to be redox-controlled in response to antibiotics, including norfloxacin and ampicillin [52]. The redox-sensing Cys80 of MarR is oxidized by intracellular Cu^{2+} leading to structural changes, dissociation of the MarR tetramer from its promoter DNA leading and derepression of the *marRAB* operon [52].

The MarR protein of *E. coli* controls a large regulon and confers multiple antimicrobial resistance in *E. coli* [53, 54]. HypS of *M. smegmatis* was shown to sense HOCl stress via the conserved Cys58 and controls the HypO efflux pump as main target which confers resistance to oxidative stress and the antibiotics erythromycin and rifampicin. The derepression of the *hypSO* operon in the *hypS* mutant was confirmed by RNA-seq transcriptomics and qRT PCR. In addition, the deletion of *hypS* resulted in upregulation of 27 genes of the SOS/LexA regulon, indicating a DNA-damage response. Among the LexA-regulon genes, *MSMEG_0827* was most highly up-regulated encoding another major facilitator superfamily protein as possible drug transporter. MSMEG_0827 could possibly further contribute to the antibiotics resistance phenotype observed in the *hypS* mutant. However, the conserved operator sequence was only detected upstream of the *hypSO* operon, not in any of the up-regulated LexA regulon genes, indicating no direct regulation of *lexA* or LexA-regulon genes by HypS.

In addition, we observed the down-regulation of the disulfide-stress-specific SigH and SigE regulons under basal conditions in the *hypS* mutant, which could be caused by the oxidative stress resistant phenotype of the *hypS* mutant. Activity of SigH is controlled by the redox-sensitive cognate anti sigma factor RshA (MSMEG_1915), which is inactivated by NaOCl stress due to thiol-oxidation, resulting in expression of the SigH regulon. Due to the resistance of the *hypS* mutant towards NaOCl stress, the RshA sigma factor could be more reduced and active as anti sigma factor to sequester SigH, leading to stronger repression of genes exclusively transcribed by SigH-containing RNAP. In support of this notion, the 5'-RNA-Seq data revealed that all SigH-dependently down-regulated genes in the *hypS* mutant are transcribed from a single TSS and have high basal levels in the wild type **(Table S8)**. It might be possible that down-regulation of SigH and SigE causes an increased DNA-damage response resulting in up-regulation of the observed LexA regulon genes.

We further analysed the phenotypes of the *hypS* mutant under NaOCl and antibiotics exposure. The *hypS* mutant was resistant to NaOCl and the antibiotics rifampicin and erythromycin, which could be restored back to wild type level in the *hypS* complemented strain. Since HypS controls the HypO efflux pump as major target, the resistance might be mediated by export of NaOCl and antibiotics through the efflux pump out of the cell. Similarly, the *Bacillus subtilis* YfmP repressor controls the multidrug efflux transporter YfmO protein which functions in the export of toxic metal ion, such as cadmium, cooper to avoid metal intoxification [55]. Since HypO shares 54% sequence identity to YfmO, we analyzed the phenotypes of the *M. smegmatis hypS* mutant under H_2O_2 and Cu^{2+} stress, but did not observe any defect in growth or survival (data not shown). Thus, the redox-sensing MarR-type regulator HypS seems to be specific to control HOCl and antimicrobial resistance through the HypO efflux pump involved in the export of HOCl and the antibiotics rifampicin and erythromycin in *M. smegmatis.* Of the eight annotated MarR proteins in *Mtb*, fours MarR-type regulators were shown to be implicated in drug resistance, including Rv0678, Rv0880 and Rv2887 [12-15]. Thus, the *Mtb* homologue Rv2327 might be also involved in HOCl and antimicrobial resistance by the control of the HypO homologous efflux pump which remains to be investigated in future studies.

ACKNOWLEDGEMENTS

We are grateful to Dorian Jamal Mikolajczak and Prof. Beate Koksch (Organic chemistry, FU Berlin) for support with CD spectrometry. We further wish to thank Susanne Gola and Kathleen Klaper for their support with construction of the *hypS* mutant. This work was supported by an European Research Council (ERC) Consolidator grant (GA 615585) MYCOTHIOLOME and grants from the Deutsche Forschungsgemeinschaft, Germany (AN746/4-1 and AN746/4-2) within the SPP1710 on “Thiol-based Redox switches”, by the Research Training Group GRK1947 (project C01), by the SFB973 (project C08) and the TR84 (project B06) to H.A.

AUTHOR DISCLOSURE STATEMENT

No competing financial interests exist.

LIST OF ABBREVIATIONS

CD	circular dichroism
EMSA	electrophoretic mobility shift assay
LB	Luria Bertani
OD_{500}	optical density at 500 nm
RCS	reactive chlorine species
RES	reactive electrophile species
ROS	reactive oxygen species
TSS	transcriptional start site
OHP	organic hydroperoxides
wHTH	winged helix-turn-helix

REFERENCES

[1] Global Tuberculosis Report 2019, Available at: https://www.who.int/tb/publications/global_report/en/ (2019).

[2] M. Berry, O.M. Kon, Multidrug- and extensively drug-resistant tuberculosis: an emerging threat, Eur Respir Rev 18(114) (2009) 195-7.

[3] T.R. Frieden, T. Sterling, A. Pablos-Mendez, J.O. Kilburn, G.M. Cauthen, S.W. Dooley, The emergence of drug-resistant tuberculosis in New York City, N Engl J Med 328(8) (1993) 521-6.

[4] R.C. Goldman, K.V. Plumley, B.E. Laughon, The evolution of extensively drug resistant tuberculosis (XDR-TB): history, status and issues for global control, Infect Disord Drug Targets 7(2) (2007) 73-91.

[5] Z. Udwadia, D. Vendoti, Totally drug-resistant tuberculosis (TDR-TB) in India: every dark cloud has a silver lining, J Epidemiol Community Health 67(6) (2013) 471-2.

[6] M.N. Alekshun, S.B. Levy, The mar regulon: multiple resistance to antibiotics and other toxic chemicals, Trends Microbiol 7(10) (1999) 410-3.

[7] M.N. Alekshun, S.B. Levy, Alteration of the repressor activity of MarR, the negative regulator of the *Escherichia coli* marRAB locus, by multiple chemicals *in vitro*, J Bacteriol 181(15) (1999) 4669-72.

[8] Z. Gong, H. Li, Y. Cai, A. Stojkoska, J. Xie, Biology of MarR family transcription factors and implications for targets of antibiotics against tuberculosis, J Cell Physiol 234(11) (2019) 19237-19248.

[9] D.K. Deochand, A. Grove, MarR family transcription factors: dynamic variations on a common scaffold, Crit Rev Biochem Mol Biol 52(6) (2017) 595-613.

[10] A. Grove, Regulation of metabolic pathways by MarR family transcription factors, Comput Struct Biotechnol J 15 (2017) 366-371.

[11] C. Healy, P. Golby, D.E. MacHugh, S.V. Gordon, The MarR family transcription factor Rv1404 coordinates adaptation of *Mycobacterium tuberculosis* to acid stress via controlled expression of Rv1405c, a virulence-associated methyltransferase, Tuberculosis (Edinb) 97 (2016) 154-62.

[12] A. Radhakrishnan, N. Kumar, C.C. Wright, T.H. Chou, M.L. Tringides, J.R. Bolla, H.T. Lei, K.R. Rajashankar, C.C. Su, G.E. Purdy, E.W. Yu, Crystal structure of the transcriptional regulator Rv0678 of *Mycobacterium tuberculosis*, J Biol Chem 289(23) (2014) 16526-40.

[13] E.J.R. Peterson, S. Ma, D.R. Sherman, N.S. Baliga, Network analysis identifies Rv0324 and Rv0880 as regulators of bedaquiline tolerance in *Mycobacterium tuberculosis*, Nat Microbiol 1(8) (2016) 16078-16078.

[14] T. Warrier, K. Kapilashrami, A. Argyrou, T.R. Ioerger, D. Little, K.C. Murphy, M. Nandakumar, S. Park, B. Gold, J. Mi, T. Zhang, E. Meiler, M. Rees, S. Somersan-Karakaya, E. Porras-De Francisco, M. Martinez-Hoyos, K. Burns-Huang, J. Roberts, Y. Ling, K.Y. Rhee, A. Mendoza-Losana, M. Luo, C.F. Nathan, N-methylation of a bactericidal compound as a resistance mechanism in *Mycobacterium tuberculosis*, Proc Natl Acad Sci U S A 113(31) (2016) E4523-30.

[15] K. Winglee, S. Lun, M. Pieroni, A. Kozikowski, W. Bishai, Mutation of Rv2887, a marR-like gene, confers *Mycobacterium tuberculosis* resistance to an imidazopyridine-based agent, Antimicrob Agents Chemother 59(11) (2015) 6873-81.

[16] Y.R. Gao, D.F. Li, J. Fleming, Y.F. Zhou, Y. Liu, J.Y. Deng, L. Zhou, J. Zhou, G.F. Zhu, X.E. Zhang, D.C. Wang, L.J. Bi, Structural analysis of the regulatory mechanism of MarR protein Rv2887 in *M. tuberculosis*, Sci Rep 7(1) (2017) 6471.

[17] M. Hillion, H. Antelmann, Thiol-based redox switches in prokaryotes, Biological chemistry 396(5) (2015) 415-44.

[18] H. Antelmann, J.D. Helmann, Thiol-based redox switches and gene regulation, Antioxid Redox Signal 14(6) (2011) 1049-63.

[19] P.R. Chen, T. Bae, W.A. Williams, E.M. Duguid, P.A. Rice, O. Schneewind, C. He, An oxidation-sensing mechanism is used by the global regulator MgrA in *Staphylococcus aureus*, Nat Chem Biol 2(11) (2006) 591-5.

[20] P.R. Chen, S. Nishida, C.B. Poor, A. Cheng, T. Bae, L. Kuechenmeister, P.M. Dunman, D. Missiakas, C. He, A new oxidative sensing and regulation pathway mediated by the MgrA homologue SarZ in *Staphylococcus aureus*, Mol Microbiol 71(1) (2009) 198-211.

[21] P.R. Chen, P. Brugarolas, C. He, Redox signaling in human pathogens, Antioxid Redox Signal 14(6) (2011) 1107-18.

[22] P. Chandrangsu, V.V. Loi, H. Antelmann, J.D. Helmann, The role of bacillithiol in Gram-positive Firmicutes, Antioxid Redox Signal (2017).

[23] M. Hong, M. Fuangthong, J.D. Helmann, R.G. Brennan, Structure of an OhrR-ohrA operator complex reveals the DNA binding mechanism of the MarR family, Mol Cell 20(1) (2005) 131-41.

[24] P. Brugarolas, F. Movahedzadeh, Y. Wang, N. Zhang, I.L. Bartek, Y.N. Gao, M.I. Voskuil, S.G. Franzblau, C. He, The oxidation-sensing regulator (MosR) is a new redox-dependent transcription factor in *Mycobacterium tuberculosis*, J Biol Chem 287(45) (2012) 37703-37712.

[25] H. Chen, C. Yi, J. Zhang, W. Zhang, Z. Ge, C.-G. Yang, C. He, Structural insight into the oxidation-sensing mechanism of the antibiotic resistance of regulator MexR, EMBO Rep 11(9) (2010) 685-690.

[26] H. Chen, J. Hu, P.R. Chen, L. Lan, Z. Li, L.M. Hicks, A.R. Dinner, C. He, The *Pseudomonas aeruginosa* multidrug efflux regulator MexR uses an oxidation-sensing mechanism, Proc Natl Acad Sci USA 105(36) (2008) 13586-91.

[27] M. Hillion, J. Bernhardt, T. Busche, M. Rossius, S. Maass, D. Becher, M. Rawat, M. Wirtz, R. Hell, C. Ruckert, J. Kalinowski, H. Antelmann, Monitoring global protein thiol-oxidation and protein *S*-mycothiolation in *Mycobacterium smegmatis* under hypochlorite stress, Sci Rep 7(1) (2017) 1195.

[28] M.J. Smeulders, J. Keer, R.A. Speight, H.D. Williams, Adaptation of *Mycobacterium smegmatis* to stationary phase, J. Bacteriol. 181(1) (1999) 270-283.

[29] R. Frampton, R.B. Aggio, S.G. Villas-Boas, V.L. Arcus, G.M. Cook, Toxin-antitoxin systems of *Mycobacterium smegmatis* are essential for cell survival, J Biol Chem 287(8) (2012) 5340-56.

[30] L.K. Hallak, K. Berger, R. Kaspar, A.R. Kwilas, F. Montanaro, M.E. Peeples, Efficient method for site-directed mutagenesis in large plasmids without subcloning, PLoS One 12(6) (2017) e0177788.

[31] J.C. van Kessel, L.J. Marinelli, G.F. Hatfull, Recombineering mycobacteria and their phages, Nat Rev Microbiol 6(11) (2008) 851-7.

[32] S. Gola, T. Munder, S. Casonato, R. Manganelli, M. Vicente, The essential role of SepF in mycobacterial division, Mol Microbiol 97(3) (2015) 560-76.

[33] R. Hilker, K.B. Stadermann, O. Schwengers, E. Anisiforov, S. Jaenicke, B. Weisshaar, T. Zimmermann, A. Goesmann, ReadXplorer 2-detailed read mapping analysis and visualization from one single source, Bioinformatics 32(24) (2016) 3702-3708.

[34] V.V. Loi, T. Busche, K. Tedin, J. Bernhardt, J. Wollenhaupt, N.T.T. Huyen, C. Weise, J. Kalinowski, M.C. Wahl, M. Fulde, H. Antelmann, Redox-sensing under hypochlorite stress and infection conditions by the Rrf2-family repressor HypR in *Staphylococcus aureus*, Antioxid Redox Signal 29(7) (2018) 615-636.

[35] M.I. Love, W. Huber, S. Anders, Moderated estimation of fold change and dispersion for RNA-seq data with DESeq2, Genome Biol 15(12) (2014) 550.

[36] F. Santos, S. Gómez-Manzo, E. Sierra-Palacios, A. González-Valdez, A. Castillo-Villanueva, H. Reyes-Vivas, J. Marcial-Quino, Purification, concentration and recovery of small fragments of DNA from Giardia lamblia and their use for other molecular techniques, MethodsX 4 (2017) 289-296.

[37] L. Zhang, W. Li, Z.G. He, DarR, a TetR-like transcriptional factor, is a cyclic di-AMP-responsive repressor in *Mycobacterium smegmatis*, J Biol Chem 288(5) (2013) 3085-96.

[38] T. Busche, R. Silar, M. Picmanova, M. Patek, J. Kalinowski, Transcriptional regulation of the operon encoding stress-responsive ECF sigma factor SigH and its anti-sigma factor RshA, and control of its regulatory network in *Corynebacterium glutamicum*, BMC Genomics 13 (2012) 445.

[39] S.S. Pao, I.T. Paulsen, M.H. Saier, Jr., Major facilitator superfamily, Microbiol Mol Biol Rev 62(1) (1998) 1-34.

[40] V.S. Reddy, M.A. Shlykov, R. Castillo, E.I. Sun, M.H. Saier, Jr., The major facilitator superfamily (MFS) revisited, FEBS J 279(11) (2012) 2022-35.

[41] A. Vastermark, M.H. Saier, Major Facilitator Superfamily (MFS) evolved without 3-transmembrane segment unit rearrangements, Proc Natl Acad Sci U S A 111(13) (2014) E1162-3.

[42] T.L. Bailey, M. Gribskov, Combining evidence using p-values: application to sequence homology searches, Bioinformatics (Oxford, England) 14(1) (1998) 48-54.

[43] S. Gupta, J.A. Stamatoyannopoulos, T.L. Bailey, W.S. Noble, Quantifying similarity between motifs, Genome Biology 8(2) (2007) R24.

[44] N. Agarwal, A.K. Tyagi, Mycobacterial transcriptional signals: requirements for recognition by RNA polymerase and optimal transcriptional activity, Nucleic Acids Research 34(15) (2006) 4245-4257.

[45] Y.R. Gao, N. Feng, T. Chen, D.F. Li, L.J. Bi, Structure of the MarR family protein Rv0880 from *Mycobacterium tuberculosis*, Acta Crystallogr F Struct Biol Commun 71(Pt 6) (2015) 741-745.

[46] J.W. Lee, S. Soonsanga, J.D. Helmann, A complex thiolate switch regulates the *Bacillus subtilis* organic peroxide sensor OhrR, Proc Natl Acad Sci U S A 104(21) (2007) 8743-8.

[47] R. Sukchawalit, S. Loprasert, S. Atichartpongkul, S. Mongkolsuk, Complex regulation of the organic hydroperoxide resistance gene (ohr) from *Xanthomonas* involves OhrR, a novel organic peroxide-inducible negative regulator, and posttranscriptional modifications, J Bacteriol 183(15) (2001) 4405-12.

[48] W. Panmanee, P. Vattanaviboon, L.B. Poole, S. Mongkolsuk, Novel organic hydroperoxide-sensing and responding mechanisms for OhrR, a major bacterial sensor and regulator of organic hydroperoxide stress, J Bacteriol 188(4) (2006) 1389-95.

[49] M. Fuangthong, S. Atichartpongkul, S. Mongkolsuk, J.D. Helmann, OhrR is a repressor of ohrA, a key organic hydroperoxide resistance determinant in Bacillus subtilis, J Bacteriol 183(14) (2001) 4134-41.

[50] B.K. Chi, K. Gronau, U. Mader, B. Hessling, D. Becher, H. Antelmann, S-bacillithiolation protects against hypochlorite stress in Bacillus subtilis as revealed by transcriptomics and redox proteomics, Mol Cell Proteomics 10(11) (2011) M111 009506.

[51] S. Ehira, H. Ogino, H. Teramoto, M. Inui, H. Yukawa, Regulation of quinone oxidoreductase by the redox-sensing transcriptional regulator QorR in Corynebacterium glutamicum, J Biol Chem 284(25) (2009) 16736-42.

[52] Z. Hao, H. Lou, R. Zhu, J. Zhu, D. Zhang, B.S. Zhao, S. Zeng, X. Chen, J. Chan, C. He, P.R. Chen, The multiple antibiotic resistance regulator MarR is a copper sensor in *Escherichia coli*, Nat Chem Biol 10(1) (2014) 21-8.

[53] P.F. Miller, M.C. Sulavik, Overlaps and parallels in the regulation of intrinsic multiple-antibiotic resistance in Escherichia coli, Mol Microbiol 21(3) (1996) 441-8.

[54] R.R. Ariza, S.P. Cohen, N. Bachhawat, S.B. Levy, B. Demple, Repressor mutations in the marRAB operon that activate oxidative stress genes and multiple antibiotic resistance in Escherichia coli, J Bacteriol 176(1) (1994) 143-8.

[55] A. Gaballa, M. Cao, J.D. Helmann, Two MerR homologues that affect copper induction of the *Bacillus subtilis* copZA operon, Microbiology 149(Pt 12) (2003) 3413-21.

Curriculum vitae

"For reasons of data protection, the curriculum vitae is not published in the electronic version "

"For reasons of data protection, the curriculum vitae is not published in the electronic version "

"For reasons of data protection, the curriculum vitae is not published in the electronic version "

Acknowledgements

I would like to express my deepest gratitude to my supervisor, Prof. Dr Haike Antelmann for giving me a golden opportunity to participate in the interesting projects. She enriched my knowledge in post-translational modification of redox proteins, regulation of transcriptional factors present in bacteria, and gave me with the chances to attend symposiums and conferences.

I acknowledge an European Research Council (ERC) Consolidator grant (GA 615585) MYCOTHIOLOME and grants from the Deutsche Forschungsgemeinschaft, Germany (AN746/4-1 and AN746/4-2) within the SPP1710 on "Thiol-based Redox switches", by the Research Training Group GRK1947 (project C01), by the SFB973 (project C08) and the TR84 (project B06) to H.A for the generous financial support.

I extend my gratitude to Dr. Vu Van Loi (Freie Universität Berlin), Dr. Tobias Busche and Prof. Dr Jörn Kalinowski (Center for Biotechnology-CeBiTec) for their continuous and unconditional supports through every state of the research.

Further, I would like to thank all our collaboration partners including Dr. Andreas Nerlich from Prof. Dr Andreas C. Hocke's group (Charité-UniversitätsmedizinBerlin) and Dr. Susanne Gola (Centro Nacional de Biotecnología–CSIC).

My special thanks also go to all colleagues and lab members at the Institut für Biologie-Mikrobiologie, Freie Universität Berlin for their encouragement, helpful discussions and taking care of last-minute orders. All the moments we have spent together inside and outside the Lab remains as never-to-be-forgotten.

I want to acknowledge Prof. Phi Quyet Tien (Institute for Biotechnology, Vietnam Academy of Science and Technology) and Dr. Khieu Thi Nhan (Vietnam Ministry of Education and Training), for inspiring me to pursue a doctorate.

Last but not least, my deep gratitude goes to my family who loves and supports me unconditionally.

Declaration

I hereby declare that this thesis is a result of my own research, and has not been submitted to Freie Universität Berlin or other institutions for purposes of gaining a degree. This thesis is original and written by myself under the supervision of Prof. Dr. Haike Antelmann, Institut für Biologie-Mikrobiologie, Freie Universität Berlin.

Berlin,…….

Quach Ngoc Tung